Elaboration of hierarchical host-guest nanoparticles

Iurii Antoniuk

UNIVERSITÉ PARIS-EST — Nano S3 — ÉCOLE DOCTORALE UNIVERSITÉ PARIS-EST Sciences, Ingénierie et Environnement

THÈSE DE DOCTORAT

Pour l'obtention du grade de

DOCTEUR DE L'UNIVERSITÉ PARIS-EST

Specialité Chimie et Sciences de Matériaux

Présentée par

Iurii ANTONIUK

Elaboration de nanoparticules auto-assemblées par interaction hôte-invité

Soutenue le 26 Mai 2016 devant le jury composé de

Pierre SCHAAF	Professeur, Université de Strasbourg	Examinateur (Pr. du jury)
Frederic HAPIOT	Professeur, Université d'Artois	Rapporteur
Dominique HOURDET	Professeur, Université Pierre et Marie Curie	Rapporteur
Imre VARGA	Assistant professor, Université Loránd Eötvös	Examinateur
Catherine AMIEL	Professeur, Université, Paris-Est Creteil	Directrice de thèse

Thèse préparée à
l'Institut de Chimie des Matériaux Paris-Est CNRS UMR 7182
au sein de l'équipe « Systèmes Polymères Complexes »
2-8 rue Henri Dunant, 94320

Acknowledgements

This PhD project has been realized within the frame of the NanoS3: Soft, Small, and Smart: Design, Assembly, and Dynamics of Novel Nanoparticles for Novel Industrial Applications, Marie Curie Initial Training Network and was funded by the European Union. Apart from working in the ICMPE I've had the opportunity to travel a lot, to pass a great deal of top-notch courses and training and, perhaps most importantly, meet some truly great people.

First, I would like to thank the members of my thesis committee, Pr. Frederic Hapiot, Pr. Dominique Hourdet, Pr. Pierre Schaaf and Asst. Pr. Imre Varga for accepting the challenge of going through this rather voluminous manuscript and giving their opinion about it.

I would like to express deep gratitude to my supervisor, Pr. Catherine Amiel. Thank you for the continuous guiding and support for more than 3 years of my PhD project and especially during the last couple of months of writing process, for your patience, kind-heartedness and knowledge.

My sincere thanks also go to Véronique Wintgens and Gisèle Volet for their large involvement in my PhD project, help in the lab and fruitful scientific discussions.

I would like to express my special appreciation and huge thanks to our scientific collaborators and partners. To Beatrice Plazzotta and Pr. Jan Skov Pedersen for truly introducing me to what the SAXS is and for accepting me in their lab in Aarhus University. To Daria Kaczmarek, Imre Varga and Attila Kardos for the preparation of pNIPAm microgels, for the exciting experiments we've done together, for having me in the lab for more than two months, for great time together, for nagy tej kave, Szimpla… well guys, I'm missing words here. My big thanks go to Jean-Michel Guignier for performing the cryo-TEM experiments and for his great sense of humor. I am thankful to Dr. Thorbjørn Nielsen for a great deal of useful advice on the synthesis of modified dextrans.

I'm using this opportunity to express my gratefulness and love to all the other Nano S3 PhD fellows: Akanksha, Amar, Beatrice, Céline, Jakob, Julia, Kathrin, Raymond, Joanna, Jing, Hongduo and Daria (once more my dear friend). It's amazing how we managed to become so close and

emphatic to each other during the brief periods of our meetings. The memories about the time spent with each of you are always on my mind, because those were the moments of treasure.

I would like to thank Clément ("I'm so happy to have you as my best friend"© Tommy Wiseau :), Gaelle, Céline Charbonneau, Cédric Lorthioir, Clémence Le Coeur, Julien Babinot and all the coworkers and labmates from the ICMPE for understanding my jokes and helping me both with the research and in everyday life.

Last but not least, a huge thanks to my family and friends back in Ukraine. Despite I haven't seen most of them for more than a year now, their support was strong and unceasing.

Finally, I have no doubt forgotten to mention at least a hundred of people whose support I'd greatly appreciated at different points of this PhD project. Well, it's only due to the intrinsic imperfectness of human (my) memory. I ask your pardon for this. Thank you.

Iurii

Table of contents

General introduction

Hierarchical self-assembly implies non-covalent organization of molecular, macromolecular or nanoscopic building blocks taking place over distinct, usually increasing, length scales in a bottom-up fashion with non-covalent interactions at larger length scales gradually decreasing in strength.[1] Although initially introduced to describe the organization of proteins and nucleic acids in living organisms, due to the rapid development of supramolecular chemistry in the last 20-30 years the concept of hierarchical self-assembly was extended to the area of artificial smart materials. Examples of such materials include metal-organic frameworks (MOFs) with double porosity[2], graphene-based hybrids for energy storage devices[3], complex nanostructures based on DNA block copolymers[4, 5] and a great variety of supramolecular hydrogels.[6, 7] Due to a number of advantages such as high flexibility, multifunctionality and structural responsivity to various external stimuli, artificial hierarchically organized systems might find applications as high performance catalysts[2], integrated parts of chemical sensors[8] or drug delivery vehicles. Driving forces used for their construction include, but are not limited to: electrostatic assembly, hydrogen bonding, van der Waals forces and molecular recognition also known as host-guest interactions.

Host-guest interactions arise as a product of non-polar van der Waals forces, hydrogen bonding and precise matching in size between a guest molecule and the internal cavity of a host molecule, the latter often being a macrocycle. As a result, they are usually characterized by higher specificity and controllability as opposed to simple electrostatic, hydrophobic or hydrogen interactions[9, 10, 11] and thus have been employed for construction of a number of sophisticated hierarchical materials.[6, 11, 12] A vast variety of both naturally derived and synthetic "host" macrocycles was described and used in supramolecular chemistry. Those include, but are not limited to: porphyrins[13], calixarenes[14], crown-ethers[15] and cryptands[16], pillarenes[17, 18] and cucurbiturils.[19] However, none of them is as well studied and widely applied as cyclodextrins (CDs).

CDs are naturally occurring cyclic oligosaccharides commonly composed of six, seven, or eight (α, β and γ-cyclodextrins respectively) D-glucose units connected by α-1,4-glucosidic linkages.[6, 20, 21] Besides their rich host-guest chemistry and easiness of modification, cyclodextrins also

show excellent biocompatibility.[9] Consequently, they are used in pharmaceutical industry as solubilizing agents, excipients and bioavailability enhancers for hydrophobic drugs.[22, 23, 24] So far, CDs are the only class of macrocycles approved by the Food and Drug Administration (FDA) for usage in food, personal care products and drug formulations.

In this PhD work we were aiming to develop new CD-containing polymer architectures with improved binding properties as well constructing hierarchically structured materials containing stimuli-responsive blocks such as poly(N-isopropylacrylamide) (pNIPAm) microgels along with βCD polymers.

This manuscript is composed of 4 chapters. First, a literature review describing the recent progress in the domain of CD-based hierarchical systems for biomedical application is presented. In the second chapter we will describe the synthetic route to new dextran-based host and guest polymers with flexible poly(ethylene glycol) (PEG) spacer between the polymer backbone and βCD or adamantyl (Ada) moieties respectively. Properties of the nanoparticles self-assembled from such polymers will be studied by a combination of small-angle X-ray scattering (SAXS) and light scattering techniques. In the third chapter we present the synthesis of a series of bifunctional (PEG, Ada)-grafted dextrans with a degree of substitution (DS) by 5000 g·mole^{-1} PEG grafts close to 20 mol.% and varying DS by Ada groups. We will discuss the impact of the DS on the affinity of (PEG, Ada)-grafted dextrans to β-cyclodextrin polymers in solution and on the surface. The fourth and last chapter is dedicated to the development of a non-covalent strategy of pNIPAm-based thermoresponsive microgels coating with a β-cyclodextrin polymers shell. We will investigate the possibility to sterically stabilize coated microgels with (PEG, Ada)-grafted dextrans described in the third chapter and to use them as building blocks for hierarchically structured supramolecular hydrogels crosslinked *via* host-guest interactions.

This PhD project has been carried out in the framework of **NanoS3: Soft, Small, and Smart:** Design, Assembly, and Dynamics of Novel Nanoparticles for Novel Industrial Applications, Marie Curie Initial Training Network, Grant agreement no.: 290251.

References

1. Choi, I. S.; Bowden, N.; Whitesides, G. M. Macroscopic, hierarchical, two-dimensional self-assembly. *Angew. Chem., Int. Ed.* **1999,** *38* (20), 3078-3081.
2. Furukawa, S.; Reboul, J.; Diring, S.; Sumida, K.; Kitagawa, S. Structuring of metal-organic frameworks at the mesoscopic/macroscopic scale. *Chem. Soc. Rev.* **2014,** *43* (16), 5700-5734.
3. Yin, S. Y.; Zhang, Y. Y.; Kong, J. H.; Zou, C. J.; Li, C. M.; Lu, X. H.; Ma, J.; Boey, F. Y. C.; Chen, X. D. Assembly of Graphene Sheets into Hierarchical Structures for High-Performance Energy Storage. *ACS Nano* **2011,** *5* (5), 3831-3838.
4. Chen, X. J.; Sanchez-Gaytan, B. L.; Hayik, S. E.; Fryd, M.; Wayland, B. B.; Park, S. J. Self-Assembled Hybrid Structures of DNA Block-Copolymers and Nanoparticles with Enhanced DNA Binding Properties. *Small* **2010,** *6* (20), 2256-2260.
5. Alemdaroglu, F. E.; Ding, K.; Berger, R.; Herrmann, A. DNA-Templated Synthesis in Three Dimensions: Introducing a Micellar Scaffold for Organic Reactions. *Angew. Chem., Int. Ed.* **2006,** *45* (25), 4206-4210.
6. Tan, S.; Ladewig, K.; Fu, Q.; Blencowe, A.; Qiao, G. G. Cyclodextrin-Based Supramolecular Assemblies and Hydrogels: Recent Advances and Future Perspectives. *Macromol. Rapid Commun.* **2014,** *35* (13), 1166-1184.
7. Liu, K. L.; Zhang, Z.; Li, J. Supramolecular hydrogels based on cyclodextrin–polymer polypseudorotaxanes: materials design and hydrogel properties. *Soft Matter* **2011,** *7* (24), 11290-11297.
8. Kreno, L. E.; Leong, K.; Farha, O. K.; Allendorf, M.; Van Duyne, R. P.; Hupp, J. T. Metal–organic framework materials as chemical sensors. *Chem. Rev.* **2011,** *112* (2), 1105-1125.
9. Qi, Z. H.; Schalley, C. A. Exploring Macrocycles in Functional Supramolecular Gels: From Stimuli Responsiveness to Systems Chemistry. *Acc. Chem. Res.* **2014,** *47* (7), 2222-2233.
10. Harada, A.; Takashima, Y.; Nakahata, M. Supramolecular Polymeric Materials via Cyclodextrin-Guest Interactions. *Acc. Chem. Res.* **2014,** *47* (7), 2128-2140.
11. Dong, S.; Zheng, B.; Wang, F.; Huang, F. Supramolecular polymers constructed from macrocycle-based host–guest molecular recognition motifs. *Acc. Chem. Res.* **2014,** *47* (7), 1982-1994.
12. Liao, X. J.; Chen, G. S.; Jiang, M. Hydrogels locked by molecular recognition aiming at responsiveness and functionality. *Polym. Chem.* **2013,** *4* (6), 1733-1745.
13. Ruthard, C.; Schmidt, M.; Gröhn, F. Porphyrin–Polymer Networks, Worms, and Nanorods: pH-triggerable Hierarchical Self-assembly. *Macromol. Rapid Commun.* **2011,** *32* (9-10), 706-711.
14. Bussolati, R.; Carrieri, P.; Secchi, A.; Arduini, A.; Credi, A.; Semeraro, M.; Venturi, M.; Silvi, S.; Velluto, D.; Zappacosta, R.; Fontana, A. Hierarchical self-assembly of amphiphilic calix 6 arene wheels and viologen axles in water. *Org. Biomol. Chem.* **2013,** *11* (35), 5944-5953.
15. Hui, J. K. H.; Frischmann, P. D.; Tso, C. H.; Michal, C. A.; MacLachlan, M. J. Spontaneous Hierarchical Assembly of Crown Ether-like Macrocycles into Nanofibers and Microfibers Induced by Alkali-Metal and Ammonium Salts. *Chem.-Eur. J.* **2010,** *16* (8), 2453-2460.
16. Wei, P. F.; Li, S. J.; Zhang, Y. Y.; Yu, Y. H.; Yan, X. Z. Responsive cross-linked supramolecular polymer network: hierarchical supramolecular polymerization driven by cryptand-based molecular recognition and metal coordination. *Polym. Chem.* **2014,** *5* (13), 3972-3976.

17. Tan, L. L.; Yang, Y. W. Molecular recognition and self-assembly of pillarenes. *Journal of Inclusion Phenomena and Macrocyclic Chemistry* **2015,** *81* (1-2), 13-33.
18. Zhou, Q. Z.; Jiang, H. J.; Chen, R.; Qiu, F. L.; Dai, G. L.; Han, D. M. A triply-responsive pillar 6 arene-based supramolecular amphiphile for tunable formation of vesicles and controlled release. *Chem. Commun.* **2014,** *50* (73), 10658-10660.
19. Kim, K. Mechanically interlocked molecules incorporating cucurbituril and their supramolecular assemblies. *Chem. Soc. Rev.* **2002,** *31* (2), 96-107.
20. Rekharsky, M. V.; Inoue, Y. Complexation thermodynamics of cyclodextrins. *Chem. Rev.* **1998,** *98* (5), 1875-1917.
21. Jie, K. C.; Zhou, Y. J.; Yao, Y.; Huang, F. H. Macrocyclic amphiphiles. *Chem. Soc. Rev.* **2015,** *44* (11), 3568-3587.
22. Brewster, M. E.; Loftsson, T. Cyclodextrins as pharmaccutical solubilizers. *Adv. Drug Delivery Rev.* **2007,** *59* (7), 645-666.
23. Loftsson, T.; Brewster, M. E. Pharmaceutical applications of cyclodextrins: basic science and product development. *J. Pharm. Pharmacol.* **2010,** *62* (11), 1607-1621.
24. Loftsson, T.; Brewster, M. E. Cyclodextrins as functional excipients: methods to enhance complexation efficiency. *J. Pharm. Sci.* **2012,** *101* (9), 3019-3032.

List of abbreviations

^{1}H-NMR – nuclear magnetic resonance of protons

2-PrOH – propan-2-ol

4-NC – 4-nitrophenyl chloroformate

4-NP - 4-nitrophenyl

AdaNCS – 1-adamantyl isothiocyanate

AdaTMA – 2-(1-adamantyl)ethyl trimethylammonium bromide

AHG – anhydroglucosidic ring

APS – ammonium persulfate

ATR – attenuated total reflection

AZT-TP – azidothymidine-triphosphate

BA – methylenbisacrylamide

βCD – β-cyclodextrin

CDs – cyclodextrins

CDV – cyclodextrin vesicles

cryo-TEM – cryogenic transmission electronic microscopy

CuAAC – copper(I)-catalyzed Huisgen azide-alkyne cycloaddition

DBCs – DNA block copolymers

DBTDL – dibutyltin dilaurate

DCC – dicyclohexylcarbodiimide

DCM - dichloromethane

DLS – dynamic light scattering

DMAP – 4-(dimethylamino)pyridine

DMSO-d_6 –dimethyl sulfoxide-d_6

DNA – deoxyribonucleic acid

DS – degree of substitution

DX microgels – doubly crosslinked microgels

EO – ethylene-oxide

EPR – enhanced permeability and retention effect

EtOAc – ethyl acetate

Fc – ferrocene

FDA – Food and Drug Administration

GMA – glycidyl methacrylate

GO – graphene oxide

GSH – glutathione

HA – hyaluronic acid

HSR – hypersensitivity reactions

ISA – ionic self-assembly

ITC – isothermal titration microcalorimetry

LbL – layer-by-layer

LC – liquid crystalline

LCST – lower critical solution temperature

MOF – metal-organic frameworks

MPS – mononuclear phagocyte system

MWCO – molecular weight cut-off

NDIR – nondispersive infrared

NOESY – nuclear Overhauser effect spectroscopy

NPs – nanoparticles

pAAc – poly(acrylic acid)

PAAm – polyacrylamide

PBS – phosphate-buffered saline

PCL – poly(ε-caprolactone)

PDDF – pair-distance distribution function

PE – polyelectrolyte

PEG – poly(ethylene glycol)

PEI – polyethylenimine

PEPO – poly(ethylene oxide-co-propylene oxide)

PhNCO – phenyl isocyanate

PhNCS – phenyl isothiocyanate

PHPMA – poly(N-hydroxypropylmethacrylamide

PIBMA – poly(isobutene-*alt*-maleic acid)

PILs – poly(ionic liquid)s

PLA – polylactic acid

PLGA – poly(lactide-co-glycolide)

pNIPAm – poly(N-isopropylacrylamide)

PPO – polypropylene oxide

PS – polystyrene

p*β*CD – poly-*β*-cyclodextrin

p*β*CDN+ – positively charged poly-*β*-cyclodextrin

RES – reticuloendothelial system

RI – refractive index

RNA – ribonucleic acid

SAMs – self-assembled monolayers

SAXS – small-angle X-ray scattering

SDS – sodium dodecyl sulfate

Si-MPs – mesoporous silica nanoparticles

siRNA – short interfering ribonucleic acid

SLS – static light scattering

SPR – surface plasmon resonance

SWNT – single-wall carbon nanotubes

TEM – transmission electron microscopy

TLC – thin layer chromatography

TMV –tobacco mosaic virus

TC – total carbon

TsCl – *p*-toluenesulfonyl chloride

VPT – volume phase transition

Chapter 1

Literature review:

Hierarchical self-assembly via cyclodextrin-mediated host-guest interactions

Table of contents

Introduction

The phenomenon of hierarchical self-assembly is traditionally defined as the non-covalent organization of molecules and macromolecules which takes places over distinct increasing length scales, whereby the non-covalent interactions at each subsequent length scale gradually decrease in strength.[1] Hierarchical self-assembly was one of the main nature's tools to ensure the life emergence ca. 4 billion years ago. In the last 20-30 years a fast development of the supramolecular chemistry area has occurred; the latter exploits weak non-covalent interactions, e.g. van der Waals forces and hydrogen bonds, to link molecules together. Given this, along with establishing deeper understanding of the processes taking place in nature, a lot of effort has been made to construct multi-level smart hierarchical systems, using synthetic and semisynthetic soft matter building blocks.

In the first part of this literature survey we will describe the general principles and scope of artificially constructed hierarchical materials. It will be followed by a discussion of the recent advances in the preparation and biomedical applications of cyclodextrin-based hierarchically structured systems, while dividing the latter into two distinct classes, i.e.: 1) supramolecular nanoparticles and related nanoscale systems; 2) host-guest mediated supramolecular hydrogels. Part of this work, entitled "Cyclodextrin-mediated hierarchical self-assembly and its potential in drug delivery applications", has been recently accepted as a review in the Journal of Pharmaceutical Sciences with minor corrections required.

1. Driving forces, building blocks and variety of architectures of hierarchically self-assembled systems

Hierarchical self-assembly might take place over a wide range of length scales and involves various types of interactions (usually non-covalent). Those include, but are not limited to: electrostatic interactions, hydrogen bonding and van der Waals forces. In addition to that, host-guest complexation and associations based on biological complementarity are often considered as two separate classes, though in fact they arise as a result of synergy between more basic interactions sterically arranged in a specific way. A classic example from nature illustrating the scope of length scales covered by hierarchical self-assembly is the formation of collagen fibers, represented in **Figure I.1**.

Three individual polypeptide chains built up of covalent amide bonds self-assemble into a triple helix, held together by intermolecular hydrogen bonds. The latter are 300 nm long and 1.5 nm in diameter and in a subsequent step self-assemble to produce elongated collagen microfibrils of 30 to 300 nm in diameter.[2, 3] Finally, the complex pattern of hydrogen bonds, van der Waals interactions and sparse disulfide bonds between cysteine residues leads to formation of cord-shaped collagen fibers about 1 to 20 microns in diameter.

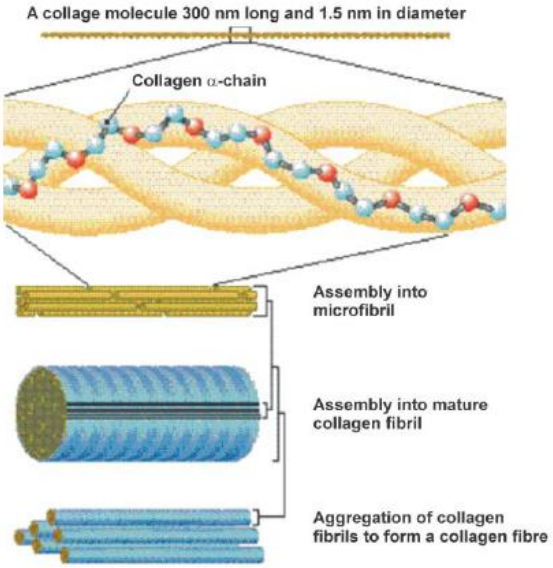

Figure I.1: Levels of hierarchical self-assembly of collagen. Reprinted from Elemans et al.[3]

1.1 Inorganic and hybrid hierarchically self-assembled materials

The construction elements used in hierarchical self-assembly are not limited to biopolymers and soft matter materials. There are a lot of examples of systems containing inorganic building blocks arranged in a specific way from nanometer to macroscopic length scales. Those are encountered both in living matter (e.g. human bone tissues and their mimics by biomineralization of hydroxyapatite with organic templates)[4, 5, 6] and in purely inorganic materials with double porosity.[7, 8] Given that these classes of hierarchically organized systems are out of the scope of the present work, a few examples will be given to highlight the recent advances.

In the field of zeolite catalysts considerable effort has been made to prepare hierarchical zeolites with dual micro/mesoporosity, as in so doing one can reduce diffusion limitations and enhance mass transport of substrate molecules, making the catalytic process faster and more

efficient.[9, 10, 11] The bottom-up methods to generate mesoporosity in intrinsically microporous synthetic zeolite were shown to allow for a better control over the pores parameters and rely either on precise tailoring of zeolites hydrothermal crystallization process[12] or on the usage of pore-forming templates, such as surfactant micelles.[13] The template-free methods are favorable in terms of avoiding of multistep synthesis and purification procedure. In a recent example Fan et al. have reported a facile one-step pathway to hierarchical ZSM-5 zeolites.[14] By carefully controlling the Si/Al ratio and the amount of base in the reaction mixture the self-assembling of microporous 30 nm precursor particles into 500 nm spherical aggregates was achieved, thus generating micro/mesoporosity of the final material (**Figure I.2**).

Two other classes of purely inorganic materials constructed via hierarchical self-assembly are environmental photocatalysts and active elements in photovoltaics. In the first case controlled hierarchical arrangement of the primary photocatalyst nanoparticles allows for more efficient mass transfer of organic pollutants[15, 16] while in the case of TiO_2-based photovoltaic cells it facilitates the interparticle transfer of photogenerated electrons.[17]

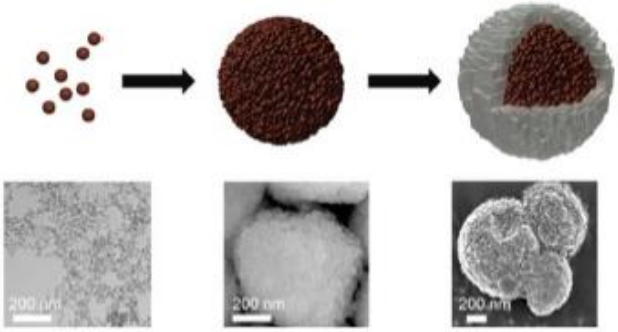

Figure I.2: Self-assembly of precursor zeolite nanoparticles into 500 nm beads with hierarchical micro/mesoporous internal structure. Reprinted from Wang et al.[14]

For instance, Zhang et al. have recently reported a facile procedure to obtain hierarchical flower-like bismuth tungstate (Bi_2WO_6) hollow microspheres which further integrated to form nanosheets.[15] Likewise hierarchical zeolites Bi_2WO_6 hollow microspheres were product of self-assembly of the initially formed nanoparticles (**Figure I.3**). Using this hierarchical architecture allowed to strongly improve the photocatalytic performance of Bi_2WO_6 in degradation of rhodamine B comparing to simple powder-like morphologies.

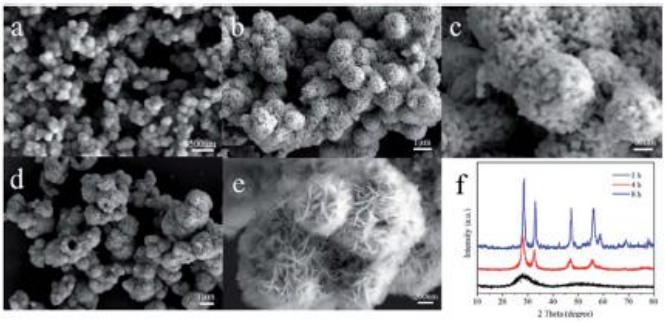

Figure I.3: Stages of growth of hierarchical flower-like bismuth tungstate (Bi_2WO_6) hollow microspheres visualized by SEM. Reprinted from Zhang et al.[15]

Due to the flexibility and variety of soft matter building blocks, during the last 2 decades a lot of effort has been dedicated to the development of hierarchical inorganic-organic hybrids which now constitute a vast class of materials. The most prominent examples include metal-organic frameworks with double porosity[18], graphene-based hybrids for energy storage devices[19] and self-healing hybrid hydrogels reinforced with inorganic nanoparticles.[20]

Metal-organic frameworks (MOF) are materials constructed via formation of coordination bonds between metal ions or clusters as nodes and organic ligands as spokes, possessing inherent microporous structure.[18] The wide choice of transition metals and molecular components allows for tuning of microspores size, shape and surface functionality. As in the case with microporous zeolites higher-order hierarchical structuring of MOF at meso/macroscopic leads to the synergy between the different length scales, thus boosting their performances as drug delivery vehicles[21, 22], catalysts[18] or integrated parts of chemical sensors.[23]

According to Furukawa et al. hierarchically structured MOF may be categorized into four groups depending on their dimensionality: (a) zero-dimensional (0D) architectures including hollow capsules or microspheres, (b) one-dimensional (1D) architectures such as nanorods or nanofibers, (c) two-dimensional (2D) architectures i.e. thin films, membranes or patterns, and (d) three-dimensional (3D) architectures that consist of extended in space systems (**Figure I.4**).[18] The synthetic strategies for hierarchical structuring of metal-organic frameworks rely both on adjusting of the primary MOF nanocrystals parameters and on spatial control over their secondary self-assembly and imply usage of hard templates (*macrostructural templating* with

e.g. inorganic NPs or nanofibers), soft templates (*molecular templating*) or reaction confinement in biphasic systems.

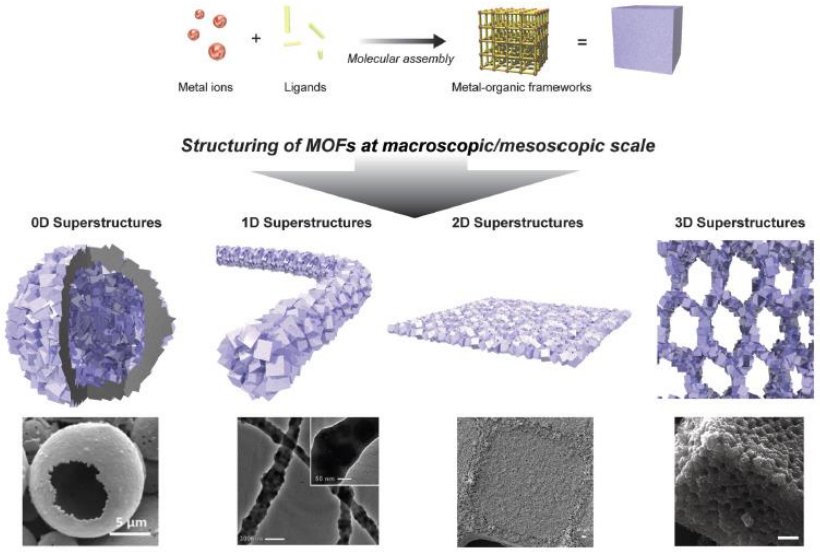

Figure I.4: Illustration of different dimensionalities of hierarchical structuring of MOF nanocrystals at meso/macroscale. Reprinted from Furukawa et al.[18]

Another recent example of inorganic-organic hierarchical hybrid comes from the field of high performance energy storage materials. Yin et al. have elaborated the procedure to assemble graphene sheets into macroporous honeycomb structure by using cationic surfactants as spacers between the neighboring graphene layers and water droplets as macroporous templates (**Figure I.5**).[19] Once again, bioinspired porous framework provided significantly decreased diffusion distances of lithium ions, making the prepared material promising for high performance Li-ion batteries.[24]

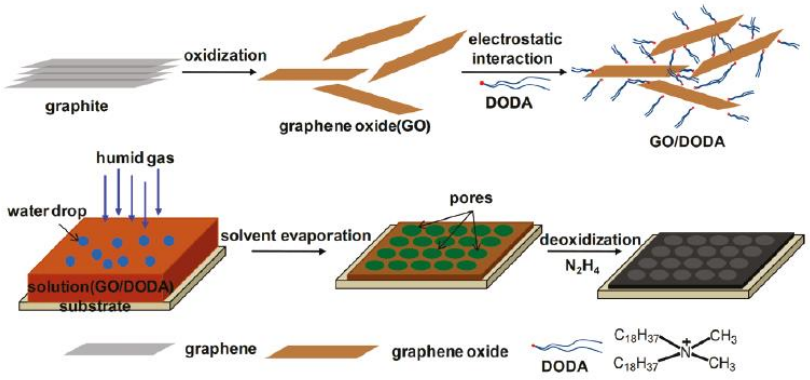

Figure I.5: Preparation of multi-layered honeycomb-shaped graphene for Li-ion energy storage devices. Reprinted from Yin et al.[19]

1.2 Soft matter hierarchically self-assembled materials

Biopolymers and soft matter in general are major construction materials in biological systems. The living matter being the main source of inspiration, there is no surprise that soft matter building blocks are prevalent in artificially prepared nanoarchitectures. Despite an immense variety and complexity of such systems created so far some basic classification appears to be possible.

Peptides and peptide-based polymeric materials outperform their synthetic counterparts in a number of parameters, such as: 1) multifunctionality/tunability, 2) adaptability/stimuli-responsiveness, 3) synthesis and processing under ambient and aqueous conditions, and 4) recyclability and biodegradability.[25] The chemical information encoded in peptide chains allows them to self-assemble across multiple length-scales in a modular, hierarchical fashion. Hence, during the last decade a lot of work has been dedicated to the preparation of hierarchically self-assembled nanoarchitectures constructed from peptide-based modular blocks tailored so as to increase the final material performance as scaffolds in regenerative medicine[26], templating vessels for biomineralization[27] and drug or gene delivery vehicles.[28, 29]

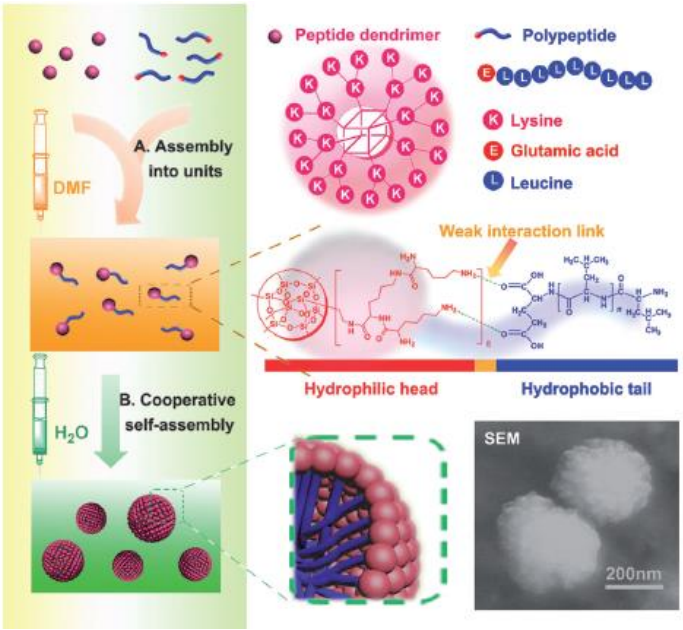

Figure I.6: Schematic illustration of the hierarchical self-assembly of poly(L-lysine) dendrimers and linear poly(L-leucine) into hierarchical peptidesomes. Reprinted from Xu et al.[29]

X. Xu and coworkers have successfully prepared biomimetic capsid-like nanoarchitectures of sub-micron size called peptidosomes.[29] They used a two-step strategy involving the formation of peptide amphiphiles via electrostatic interactions and/or hydrogen bonding between poly(L-lysine) dendrimers with polyhedral oligomeric silsesquioxane cores and hydrophobic linear poly(L-leucine)-based peptide as the first step. Upon nanoprecipitation from DMF in water peptide amphiphiles self-organized into stable peptidesomes (**Figure I.6**). The hierarchical peptidesomes exhibited high gene-transfection efficiency as non-viral gene vectors.

In another recent example interpeptide charge complementarity has been used to construct cage-within-cage Matryoshka-like architectures between two oppositely charged peptides of different sizes.[30] By carefully regulating ionic strength of the medium cage-within-cage structures were possible to obtain by two pathways: a) direct loading of intact capsid-like negatively charged enzyme lumazine synthase from *Aquifex aeolicus* bacteria (AaLS) with positively supercharged human ferritin; b) using positively supercharged human ferritin to template the self-assembly of negative AaLS capsid (**Figure I.7**). Moreover, three component Matryoshka-like structures loaded with iron NPs were prepared.

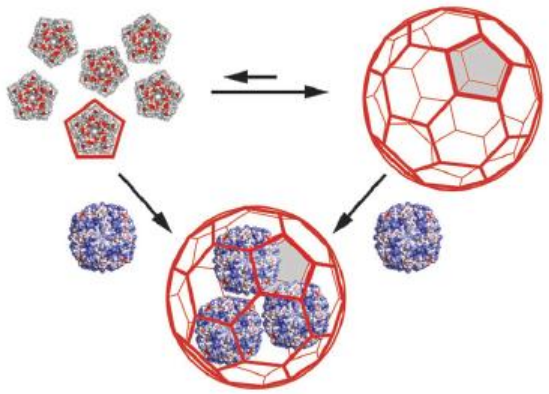

Figure I.7: Schematic illustration of the strategies for cage-within-cage peptide hierarchical structures preparation: a) direct loading of positively charged ferritin (blue) into intact negative AaLS capsids (red); ferritin-templated self-assembly of 13 AaLS fragments into closed-shell complexes. Reprinted from Beck et al.[30]

Another class of valuable building blocks for construction of hierarchical architectures is nucleic acids.[31, 32] Self-assembly properties of nucleic acids such as DNA and RNA are based on weak but specific hydrogen bonding between four distinct naturally occurring nucleotides. Artificial

modifications of nucleotide sequences allow hybridization of nucleic acids into secondary structures unknown in nature, e.g. tiles further self-propagating into 2-D lattices.[33] However this approach to construction of hierarchical nanomaterials is limited from practical point of view due to its complexity and time-consuming purification of cohesion blocks.[31]

Preparation of DNA block copolymers (DBCs), which combine nucleic acid strands as hydrophilic blocks with various hydrophobic synthetic polymers, proved to be a more robust and versatile way to exploit the patterning properties arising due to the DNA hybridization. Highly hydrophobic polymers such as polystyrene (PS)[34], polypropylene oxide (PPO)[35] or poly(butadiene)[36] were conjugated with DNA-oligonucleotides by solid phase synthesis in organic media. Likewise conventional amphiphilic block copolymers, when dissolved in water DBCs hydrophobically self-assemble into various nanometric architectures such as micelles[35], cylinders[37] or polymersomes[38] with DNA strands facing the aqueous medium. Their size and morphology can be tuned by adjusting the length of the DNA sequence and/or polymer molecular weight.

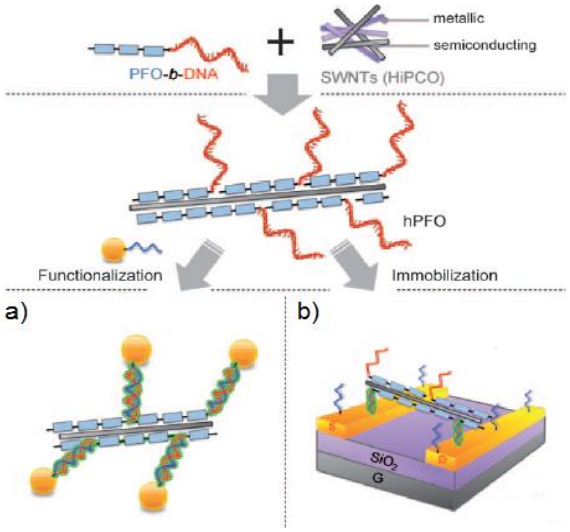

Figure I.8: Strategy for preparation of hierarchical nanohybrids via complementary hybridization between PPO-b-DNA – stabilized SWCNTs and DNA-modified Au NPs (a) or DNA-covered gold electrodes (b). Adapted from Kwak et al.[39]

The DNA corona on top of DBC-based nanostructures allows for their functionalization and extension with complementary nucleic acid strands attached to nanoparticles, drugs or dyes. Using this strategy various high-order hierarchical structures have been prepared. For instance,

Wang et al. have decorated nanocylinders self-assembled from amphiphilic DNA-dendron with complementary modified gold nanoparticles.[37] In another example even more complex superstructures were prepared: semiconductor single-walled carbon nanotubes (SWCNT) were first sterically stabilized with PPO-b-DNA copolymers and then attached via nucleic acid hybridization either to DNA-modifies gold NPs or DNA-covered gold electrodes (**Figure I.8**).[39]

A vast family of approaches to construct soft polymeric materials structured across multiple length scales is based on cooperative electrostatic interactions or simply **ionic self-assembly (ISA)** of polyelectrolytes (PE) with surfactants, amphiphilic block copolymers containing PE charge-carrying blocks[40] or polymeric ionic liquids.[41] A wide range of materials which are prepared by hierarchical ISA include: spanning liquid-crystalline (LC), porous, hybrid organic–inorganic[42], and electroactive materials.[40]

Ahmed et al. have described a pathway to hierarchically organized organic-metalorganic hybrids via combination of hydrophobic self-assembly of block copolymers (takes place on a length scale of 10-100 nm) and self-assembly between PE-amphiphilic surfactant.[43] They prepared polystyrene-b-poly(ferrocenylmethyl-(trimethylammoniumpropynylsilane)) DBCs of varying block ratios. Further, by synthetic variation of the block volume ratios, along with complexation of PE block with oppositely charged amphiphilic surfactants (hydrogenated or perfluorinated), which also changed the volume fractions in a predictable way; they ended up with a formation of long-range well-ordered phase structures, consisting of aligned cylinders of PS (with d-spacing of 35 nm) in a lamellar PFS–surfactant matrix extending over many micrometers (**Figure I.9**). In addition, by oxidative etching of polystyrene part thin metalorganic membranes with 34 nm holes were obtained.

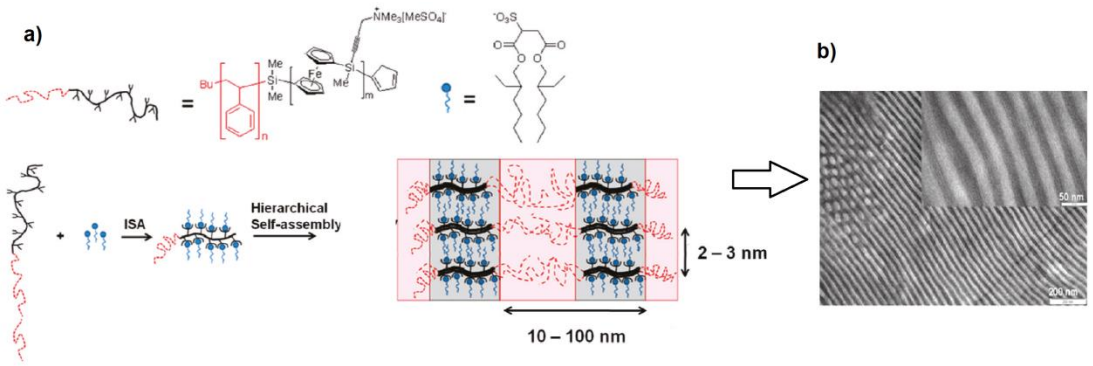

Figure I.9: Schematic representation of the formation of hierarchical organic-metalorganic nanoarchitectures via combination of ISA and hydrophobic self-assembly (a); their visualization by TEM (b). Adapted from Ahmed et al.[43]

Yuan et al. have explored the unique ability of poly(ionic liquid)s (PILs) based on 3-*n*-alkyl-1-vinylimidazolium bromide to self-assemble in one step during the polymerization process.[44] Upon varying the alkyl chain length from C12 to C18 for lower polymerization concentrations (50 g/L) they observed formation of multilamellar vesicular structures for shorter alkyl chains and unilamelar vesicles for C16-18 (**Figure I.10; a, b**). This was attributed to crystallinity in the longer alkyls' self-assembled layers and, thus, their lower bendability. At higher polymerization concentrations (100 g/L) the multilamellar PILs vesicles further self-organized into 1D-superstructure of nanoparticles with extended multilamellar substructure via synergy between electrostatic and hydrophobic interactions (**Figure I.10; c**); this higher level of hierarchy was not achieved in crystalline unilamelar vesicles.

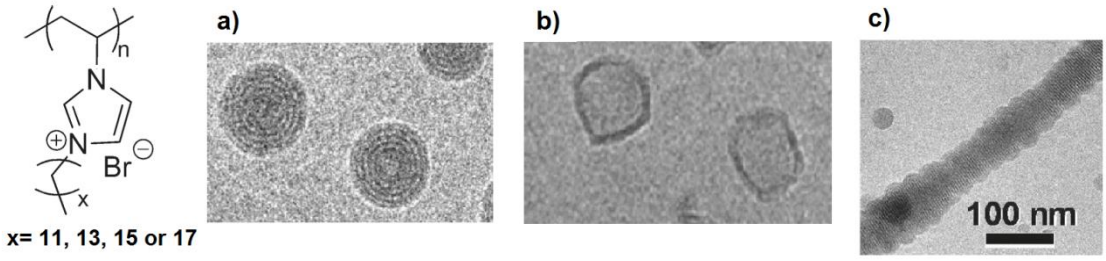

Figure I.10: Poly(ionic liquid)s nanoarchitectures on different length scales by varying the polymerization concentration and monomer architecture. Adapted from Yuan et al.[44]

2. Hierarchical self-assembly mediated by Host-guest interactions

Inclusion complexation, wherein usually macrocyclic "host" binds hydrophobic "guest" in a reversible manner constitutes a basis of a separate family of non-covalent interactions. Host-guest interactions arise as a result of synergy between non-polar van der Waals forces, hydrogen bonding and precise matching in size between the guest molecule and macrocycle hydrophobic internal cavity. The size and sterical requirements to the guests lead to the so-called "molecular recognition" phenomenon, and consequently to high specificity and controllability of host-guest interactions as opposed to their simple non-covalent counterparts used in supramolecular chemistry.[45, 46, 47] In addition to "molecular recognition" controlling tool, host-guest complexes formation and dissociation is sensitive to environmental changes such as temperature, light, mechanical pressure or competitive guests binding.[45] Due to these prominent features host-guest complexation was successfully applied in the construction of smart hierarchically structured architectures such as supramolecular polymers[47], molecular machines[48] and supramolecular responsive gels.[45, 49, 50]

A vast variety of both naturally derived and synthetic "host" macrocycles was described and used in supramolecular chemistry. Those include, but not limited to: porphyrins[51], calixarenes[52], crown-ethers[53] and cryptands[54], pillarenes[55, 56] and cucurbiturils.[57] In this account, however, we will limit our focus to cyclodextrins – without doubt the most widely exploited in supramolecular self-assembly class of macrocycles.

Cyclodextrins (CDs) are naturally occurring cyclic oligosaccharides commonly composed of six, seven, or eight (α, β and γ-cyclodextrins respectively) D-glucose units connected by α-1,4-glucosidic linkages.[49, 58, 59] Due to the intramolecular network of hydrogen bonds between the secondary hydroxyl groups of D-glucose, CDs assume a quite rigid toroidal shape. The primary hydroxyl groups are found on the narrower, primary face, of the resulting toroid, while the secondary hydroxyls are located on the wider, secondary face.[49, 58, 60] The exterior of the CDs cavities is polar due to the hydroxyl groups sticking out, while the interior is nonpolar due to the $–CH_2-$ groups and ether-like oxygens. Besides their rich host-guest chemistry and easiness of modification, cyclodextrins also show excellent biocompatibility.[45] So far, CDs are the only class of macrocycles approved by the Food and Drug Administration (FDA) for usage in food, personal care products and drug formulations. Some notable examples of their application include the

first siRNA delivery vehicles studied in humans, composed of βCD-based nanoassemblies containing RNA and sterically stabilized by PEG-Ada via host-guest interactions.[61] All these features make CDs indispensable building blocks for the construction of hierarchically structured systems with potential biomedical applications.

2.1 Nanoscale hierarchical systems based on cyclodextrins

2.1.1 Gene delivery systems

One of the most prominent directions in the biomedical application of cyclodextrin-based supramolecular systems is gene delivery. After a short period of popularity of the viral gene vectors in the early 90s, the associated risks and pitfalls of the latter such as toxicity, immunogenicity and difficulty of scale-up production quickly became obvious[62, 63]. Thus, in the last two decades a big deal of effort has been dedicated to the development of synthetic non-viral gene carriers, usually belonging to one of the following classes of compounds: cationic polymers[64] or cationic amphiphiles.[65, 66] In the presence of polyanionic nucleic acids these compounds undergo self-assembly into nanoscale particles, known as polyplexes and lipoplexes. In this way, the transported genetic material can be protected from the immune system response and targeted to the place of action in an organism[62]. However the transfection efficiency of such systems is usually inferior to that of viral carriers and because of their heavily charged nature they demonstrate high toxicity.[67]

To overcome the high charge-related issue, “steric stabilization” has been used as a means of protecting the positively charged surface of polyplexes and preventing their non-specific interactions with blood proteins. Carbohydrates and cyclodextrins in particular proved to be efficient sterical stabilizers of polyplexes due to the versatility of the benefits they bring: a) enhancement of the membrane adsorption of the polyplexes; b) protection from non-specific interactions; c) opportunity to further functionalize gene-carrying nanoparticles by exploiting the CD inclusion chemistry.

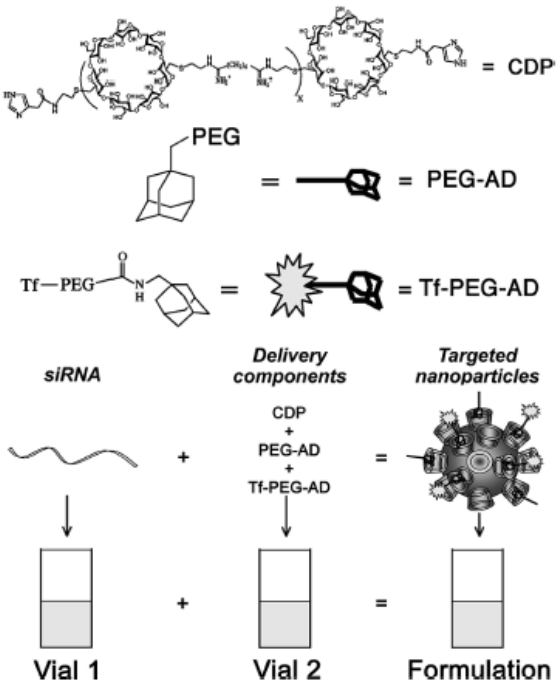

Figure I.11: Components and formulation principle of the siRNA targeted delivery system CALAA-01. The supramolecular host-guest complexes are first formed between linear βCDP and bifunctionalized Tf-PEG-Ada in the Vial 2; upon mixing with the siRNA (Vial) one they hierarchically self-assemble into sterically stabilized targeted nanoparticles. Adapted from Davis.[61]

The most successful examples using CDs for gene vectors formulations include the work of Mark E. Davis and coworkers. In the 1st step they prepared the so-called polyCDplexes – nanoparticles formed by electrostatic self-assembly between plasmid DNA and positively charged linear βCD-polymer (pβCD) and sterically shielded them from non-specific interactions and aggregation in the salty physiological medium by the inclusion of adamantane-modified poly(ethylene glycol) (Ada-PEG) into the superficial CD-cavities of the polyplexes.[68] They further developed the concept by using bifunctionalized Ada-PEG-Tg, additionally modified with active targeting agents (Tg). Thus, modification with galactosylated Ada-PEG-Gal selectively brings the pDNA-containing polyCDplexes to hepatocytes with overexpressed galactose membrane receptors.[69] When galactose is replaced by transferrin, the genetic material, in this case siRNA, is efficiently targeted to cancer cells characterized by upregulated transferrin receptors.[61, 70] The resulting four component transferrin-targeted formulation under the name CALAA-01 (**Figure I.11**) has been the first targeted delivery of siRNA tested in humans. The CALAA-01 nanoparticles

demonstrate similar to conventional PEI-based carriers siRNA transfection efficiency while being more selective to various cancer cell lines and far less toxic.[71, 72, 73]

In another example Park et al. proposed a way to spatially control CD-PEI DNA-polyplexes delivery by immobilizing them onto solid surfaces patterned with adamantyl groups.[74] Polyplex-forming PEI was modified with βCD moieties, ionically self-assembled with negatively charged pDNA and adsorbed onto Ada-modified gold surface via inclusion complexation (**Figure I.12**). Due to the multivalency of the HG-interactions between βCDs on a single nanoparticle and the surface-linked Ada-functions the binding strength was enhanced such that nanoparticles are not detached even at >10 000-fold concentrations of competitor monomeric βCD. The pDNA could be released from the surface on-demand by addition of polyanionic heparan sulfate which competitively disassembles the nanoparticles.

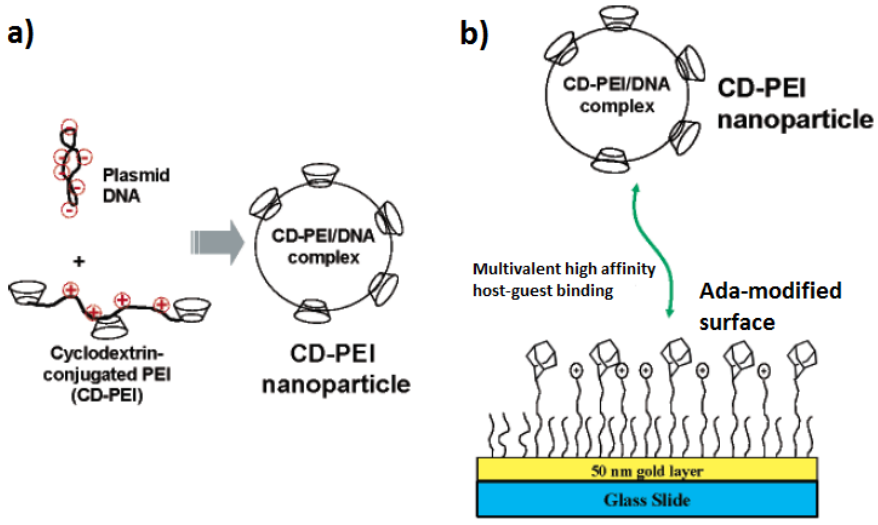

Figure I.12: a) Formulation of CD-PEI nanoparticles by condensation between plasmid DNA and positively charged βCD-grafted PEI; **b)** Immobilization of the resulting polyCDplexes onto Ada-modifies surface via multivalent inclusion interactions. Adapted from Park et al.[74]

Amiel's group developed a macromolecular DNA vector based on epichlorohydrin/βCD copolymer (pβCD).[75, 76, 77] Inclusion complexation between initially neutral pβCD and a series of amphiphilic cationic connectors, consisting of adamantane group, spacers with different chemical nature and length and a mono- or bicationic polar head, resulted in formation of reversible pseudo-polycation. The latter proved to hierarchically self-assemble to yield polyCDplexes (**Figure I.13**). The pβCD-based vector showed high gene transfection efficiency in

the experiments on HepG2 and HEK293 cell lines, as it was evidenced by luciferase protein activity monitoring. Interestingly, the imidazole-containing Ada6 connector (**Figure I.13; b**), though not able to compact DNA itself, when used in combination with cationic Ada5, proved to act as an efficient endosomal escape enhancer due to its "proton sponge" properties.[78] Moreover, the positive charge density of the vector and the polyCDplexes characteristics such as size and DNA compaction degree could be tuned by simple change of the connector/βCD molar ratio (**Figure I.13; c**).

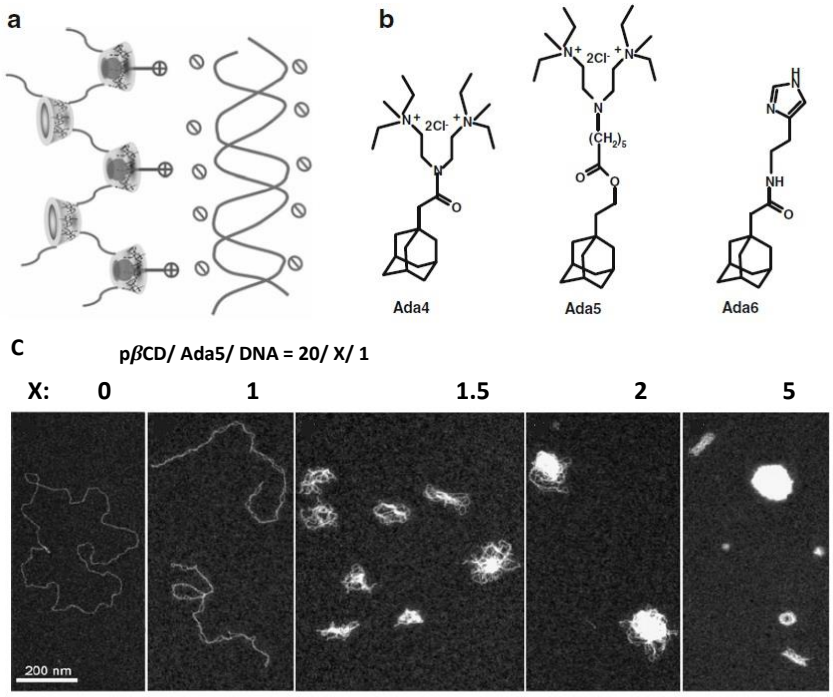

Figure I.13: **a)** Schematic illustration of the polyCDplexe hierarchical self-assembly between pβCD, cationic connector and DNA; **b)** Chemical structures of various Ada-connectors; TEM images illustrating the evolution of plasmid DNA compaction degree as a function of the amount of cationic connector Ada5 associated with prior to polyCDplexe formation (pβCD/Ada5/DNA = 20/X/1). The first image (X = 0) represents free pDNA in water. Adapted from Wintgens et al.[77]

Threading of cyclodextrins along the hydrophobic polymer chains or blocks, dubbed as *rotaxanation*, is widely known to endow the resulting supramolecular rotaxanes with higher hydrophilicity, flexibility and bioavailability.[46, 62, 79] An original way to exploit this property in gene delivery was introduced by Kissel and coworkers. They synthesized a new type of ternary copolymers by grafting PEG-b-poly(ε-caprolactone) (PCL) diblock copolymers onto branched PEI. The DNA polyplexes of such ternary copolymers demonstrated neutral surface ζ-potential and

enhanced, compared to PEI-b-PEG diblock copolymers, gene transfection efficiency.[80] However, at higher PCL block lengths and -PCL-b-PEG grafting densities the DNA binding rate and water-solubility of the resulting polyplexes was drastically decreased due to the PCL hydrophobicity and its hydrogen binding with positively charged PEI. The solution to this problem consisted in including the PCL block inside the α-cyclodextrin (α-CD) cavities.[81] Being able to form inclusion complexes with both PEG and PCL, α-CD end up threaded preferentially along the PCL block, making it more hydrophilic and preventing its association with PEI (**Figure I.14**). The resulting hierarchically structured polyplexes showed excellent stability, bioavailability and DNA transfection efficiency.

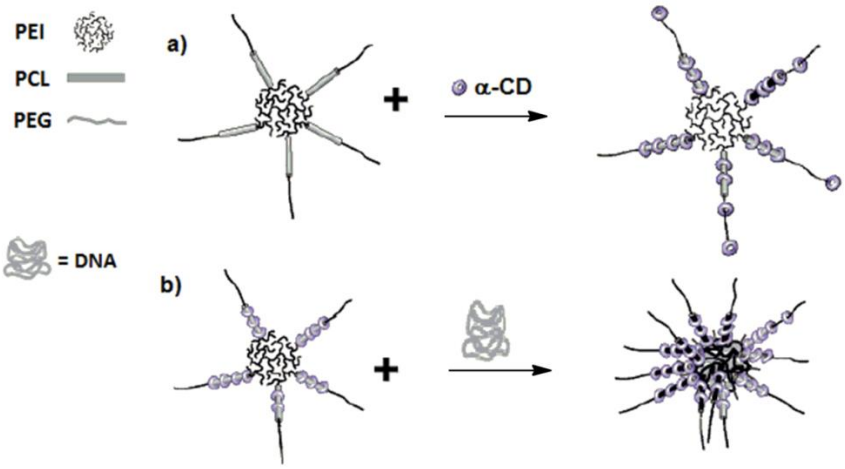

Figure I.14: Formulation of supramolecular gene vectors: **a)** Rotaxanation of the PCL block of the brPEI-PCL-PEG ternary copolymer by inclusion complexation with α-cyclodextrin; **b)** Formation of polyplexes via electrostatic association with DNA. Adapted from Shuai et al.[81]

In a number of recent studies CD-based hierarchical gene delivery systems with the so-called "biological stimuli-responsiveness" were reported.[82] For instance, intracellular milieu is known to be more reducible comparing to extracellular matrix due to its 100-fold higher concentration (2-10 mM) of glutathione (GSH) – thiol-containing antioxidant tripeptide.[82, 83] This considerable GSH concentration difference may be used to trigger rapid disassembly of gene delivery carriers, followed by the release of genetic material at the site of action. The strategy usually involves linking CD-containing moieties to nucleic acid-condensing cationic polymers *via* easily reducible disulfide S-S bond. The polymer responsible for sterical stabilization is modified with hydrophobic guest functions and linked to CD-containing gene vector *via* inclusion complexation

prior to polyplex formation. Once inside the cell, the protective guest polymer corona is removed by S-S bond reduction and the genetic material is released. This approach with βCD cationic star polymer as a host and adamantyl end-capped zwitterionic phosphorylcholine based polymer as a guest was successfully realized by Liu et al. for p53 anti-cancer gene delivery in MCF-7 cells.[84]

Within the same strategy Ping et al. reported a gene delivery carrier with redox-detachable PEG corona.[85] In their case S-S bond was introduced into the structure of Ada-ended PEG (Ada-SS-PEG) guest polymer. A host segment consisted of βCD-crosslinked low molecular weight PEI conjugated with a targeting peptide, able to condense DNA into 100-200 nm polyplexes. The formulation could be selectively delivered to carcinoma cells, followed by glutathione-induced PEG-corona detachment making the carried DNA available.

2.1.2 Various drug delivery-oriented nanoscale systems

Multivalent inclusion complexation between host polymers, modified with cyclodextrin moieties, and guest polymers, bearing hydrophobic groups, proved to be a powerful strategy to prepare supramolecular host-guest nanoparticles with interesting drug delivery profiles.[86, 87, 88] Amiel and coworkers have shown the importance to carefully control the physico-chemical properties of the utilized host-guest polymers such as molecular weight, substitution degree and chemical nature of the spacer; by doing so stable in aqueous medium nanoassemblies with tailorable sizes could be obtained without using toxic organic solvents and/or surfactants. Furthermore, free β-cyclodextrin cavities of the nanoassemblies were exploited to load them with hydrophobic drugs such as tamoxifen, which was showed to be released in a sustained manner. [89, 90] In order to make such polymeric nanoassemblies stable in salty physiological medium the same authors proposed a hierarchical strategy, which involves coating the nanoassemblies with a bifunctional dextran bearing adamantyl anchoring groups and hydrophilic “corona”-forming poly(ethylene oxide-co-propylene oxide) (PEPO) side chains to increase the steric repulsion between the nanoassemblies.[91]

M. Zan et al. have recently described a host-guest nanogels-based drug delivery system with dual pH-responsiveness.[92] They used random copolymers of two types: adamantyl (Ada)-benzoic imine-conjugated poly[poly(ethylene glycol) monomethyl ether methacrylate]-co-poly(2-hydroxyethyl methacrylate) (PPEGMA-co-PHEMA-Ada); doxorubicin (DOX)-hydrazone

and βcyclodextrin (βCD)-conjugated poly[N-(2-hydroxypropyl) methacrylamide]-co-poly(3-azidopropyl methacrylate) (PHPMAco-PPMA-DOX-CD) (**Figure I.15, a**). The 220 nm host-guest nanogels were obtained by dialysis of the mixture of PPEGMA-co-PHEMA-Ada and PHPMAco-PPMA-DOX-CD solutions in DMSO against phosphate-buffered saline (PBS) at pH 7.4. The benzoic imine linker between Ada and PPEGMA-co-PHEMA backbone can be cleaved at pH 6.5. As a result, nanogels undergo size reorganization when placed in a slightly acidic tumor cells microenvironment (**Figure I.15, b**).

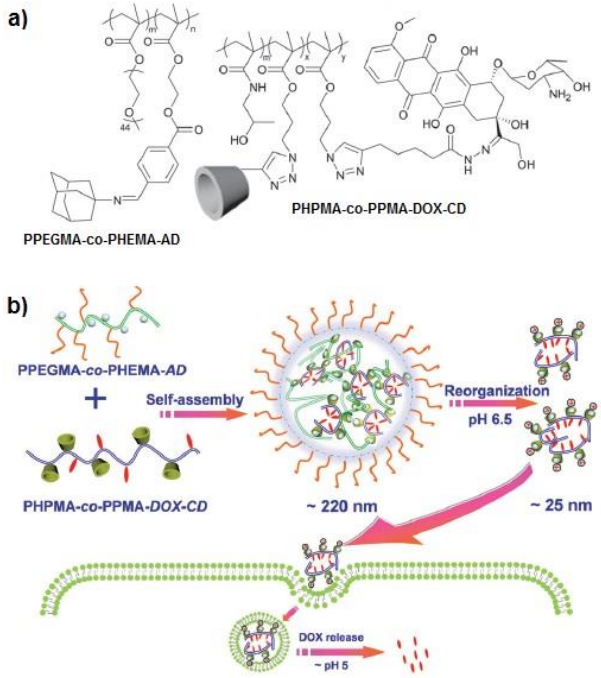

Figure I.15: a) Chemical structures of used guest (PPEGMA-co-PHEMA-AD) and host (PHPMAco-PPMA-DOX-CD) polymers with pH-sensitive AD-benzoic imine (cleaved at pH 6.5) and DOX-hydrazone (cleaved at pH 5) links respectively; **b)** Schematic illustration of the formation of host-guest self-assemblies and their dual pH-responsive rearrangement endo-lysosomal internalization and drug release. Adapted from Zan et al.[92]

The reorganized nanoparticles are much smaller (~25 nm) and able to penetrate deeper (>2 mm *vs.* 200 μm for large precursor NPs) inside the dense matrix of tumor tissue, herein mimicked by collagen hydrogel. Having slightly positive ζ-potential, the reorganized nanogels are internalized by the endolysosomes once inside the tumor cells. The hydrazone bonds used to link the DOX to the polymer backbone are further cleaved at pH 5, found in the endo-lysosomal

microenvironment, leading to the anticancer drug targeted sustained release (76.9% after 72h of incubation).

An example of hierarchical core-shell host-guest nanoparticles with promising drug delivery profile was reported by Ma and coworkers. They synthesized a hydrophilic-hydrophilic diblock copolymer comprising of a PEG block ($M_w \sim 5000$) and a polyaspartamide block ($M_w \sim 1500$), the latter carrying βCD units on the side chain (PEG-b-PCD).[93] This host copolymer was further used for self-assembly with various monomeric and polymeric hydrophobic guests, resulting in core shell nanoparticles with the sizes in the range 50-120 nm. For instance, when pyrene is inserted into the *β*CD, due to its large dimensions, a part of the molecule protrudes from the *β*CD cavities inducing a localized hydrophobicity in the polyaspartamide block. The resulting pseudo-amphiphilic copolymer further self-assembles into core-shell aggregates with the cores made up from βCD/pyrene complexes. By using negatively charged 1-adamantanecarboxylic acid in place of pyrene they obtained a pseudo-polyelectrolyte able to form core-shell micelles with positively charged PEI. In both cases hierarchical micelles are stabilized by hydrophilic PEG shell.

The concept was further extended by preparation of thermoresponsive nano-assemblies between PEG-b-PCD and poly(N-isopropylacrylamide) (PNIPAM), using the inclusion complexation interaction between the hydrophobic cavity of *β*CD and isopropyl group of PNIPAM.[94] The particle size of the assemblies was tunable and could be decreased by dropping off the temperature below the lower critical solution temperature (LCST) of PNIPAM or increased, by increasing the PNIPAM/PEG-b-PCD weight ratio. The subsequent release of a model hydrophobic drug study showed that the payload could be released in a sustained manner, and the release rate could be modulated *via* adjusting the temperature.

Zhuo et al. described simultaneously thermo- and pH-responsive doxorubicin delivery system. They used α-β cyclodextrin dimer to prepare amphiphilic supramolecular polymers *via* selective host-guest complexation of α-CD with phenyl (attached to the hydrophilic NIPAM-co-N-acroyloxysuccinimide (NAS) block) and of βCD with adamantane (linked to the hydrophobic PCL block) (**Figure I.16**). The resulting polymers showed well defined CMC lying between 0.15-0.30 mg/mL above which they hierarchically self-assemble into spherical core shell micelles.[95] The thermoresponsive (LCST = 38°C) NIPAM-co-NAS block was also modified with MPEG grafts ($M_n \sim 2000$) and targeting peptide sequences in a bottle-brush manner. Under normal physiological

conditions (pH ~ 7.4, T = 36.6 °C) the hierarchical micelles are stable and protected against immunogenic interactions. Upon reaching the solid tumor tissue with pH < 6.8 the PEG grafts are removed by the cleavage of benzoic imine bonds connecting them to the main chain and the micelles are internalized by the malignant cells. Furthermore, once the PEG grafts are gone the LCST of the hydrophilic block drops down to 35.5 °C which along with higher than normal (38 °C) temperature of cancer cells leads to the collapse of the micelles and release of the payload (doxorubicin).

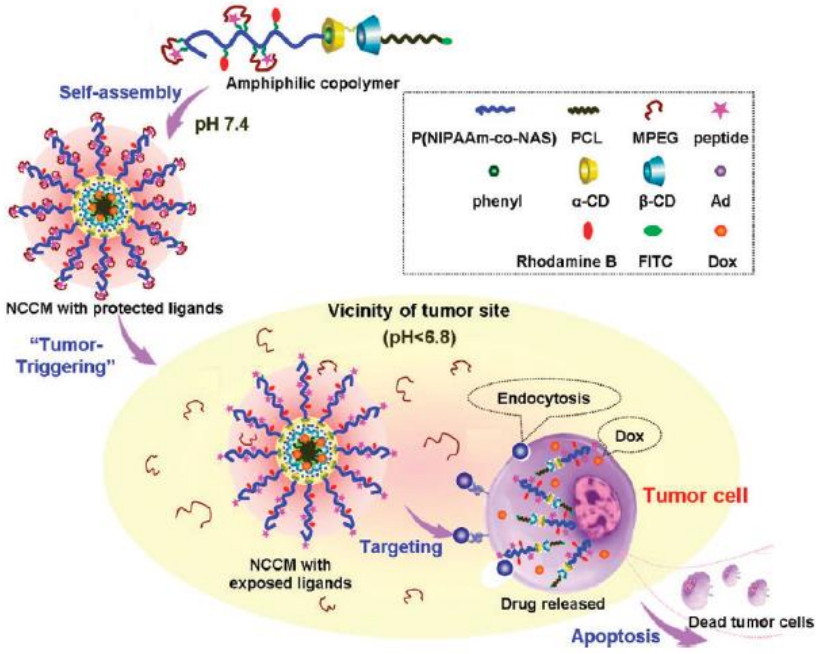

Figure I.16: Formation of hierarchical core-shell nanoparticles for delivery of doxorubicin with switchable tumor cell triggered targeting and release. Reproduced from Quan et al.[95]

Voltage-responsive cyclodextrin-containing hierarchical vesicles were also described and showed to have a high potential as controllable drug delivery vehicles by Yan et al.[96] In the first step they prepared an amphiphilic pseudo-copolymer by linking together ferrocene end-capped poly(ethylene oxide) (PEO-Fc) and poly(styrene)-β-cyclodextrin (PS-βCD) *via* inclusion complexation between Fc and βCD. Upon reaching the critical aggregation concentration ~0.28 mg/mL, PS-βCD/PEO-Fc hydrophobically self-assembles into ~102 nm hierarchical vesicles with the wall thickness ~19 nm. The loss of affinity to βCD in oxidized form of ferrocene (Fc^+) was exploited to achieve reversible assembly/disassembly of the vesicles by alternately exposing them to oxidative and reductive 1.5V voltages respectively.

The same group has further developed their system by using PNIPAM-βCD/PEO-Fc pseudo-copolymer, where PS-βCD was replaced by thermoresponsive PNIPAM-βCD as a host segment.[97] This way, *via* host-guest self-assembly they prepared a supramolecular amphiphile simultaneously containing redox (Fc) and temperature-sensitive elements (PNIPAM). Containing both redox (Fc) and temperature-sensitive elements (PNIPAM), the resulting micelles turned out to be dual-responsive, i.e. disassemble under the effects of oxidant (H_2O_2) or temperature *via* different mechanisms: (1) the oxidant induces dissociation of βCD-Fc, thus removing the PEO-Fc^+ protective shell from PNIPAM-βCD cores; (2) at temperatures below the LCST, the hydrophobic PNIPAM becomes hydrophilic, hence the hydrophobic core dissociates. The micelles were successfully loaded with doxorubicin and its release could be triggered by either of two stimuli.

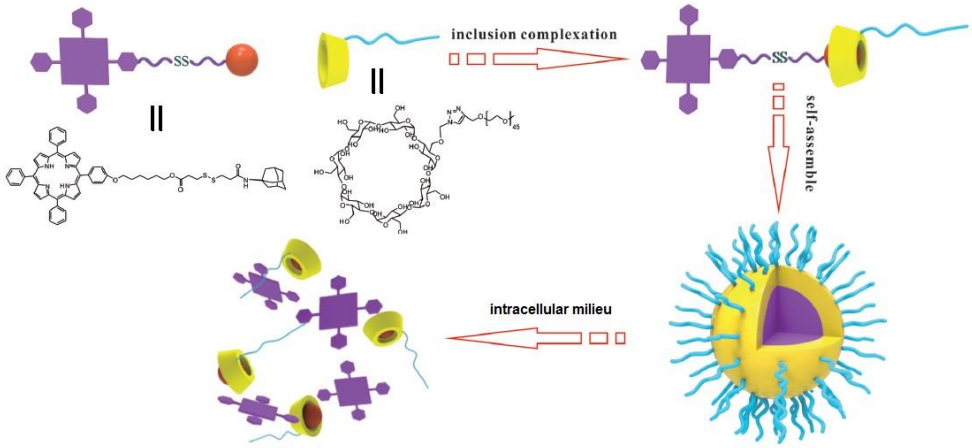

Figure I.17: Schematic representation of the formation and redox-triggered disassembly of the TPPC6-SS-Ada/PEG-βCD hierarchical micelles for photodynamic therapy. Adapted from Liu et al.[98]

Zhang and colleagues have recently described an example of hierarchically organized photodynamic therapy system taking advantage of βCD/adamantane inclusion complexation. Their strategy involved the preparation of a redox-responsive supramolecular amphiphile between the photosensitizer – adamantane-terminated porphyrin derivative bearing a disulfide bond (TPPC6-SS-Ada) and PEGylated βCD (PEG-βCD).[98] Akin to the previous two examples, the TPPC6-SS-Ada/PEG-β-CD pseudo-copolymer further self-assembles into hierarchical micelles in water (**Figure I.17**). The micelles proved to be efficiently up-taken by the MCF-7 malignant cells due to the Enhanced Permeability and Retention (EPR) effect. Moreover, given the presence of redox-sensitive S-S bonds the nanostructures demonstrate the aforementioned biological

responsiveness for gene transfection vectors, i.e. disassembly and the porphyrin photosensitizer payload release occur in a more reductive intracellular microenvironment.

To proceed with the topic of stimuli-responsive hierarchical nanostructures based on cyclodextrins, Ma et al. recently reported a simple way to supramolecular vesicles constructed *via* hydrophobic self-assembly of the amphiphilic βCD/tyrosine inclusion complex (**Figure I.18**).[99] The diameters of the vesicles range from 90 to 140 nm and their structure could be disrupted "on-demand" either by addition of a competitive guest, 1-hydroxyadamantane, or copper (II) ions. In the latter case Cu(II)-ions mechanism of action is based on their ability to form coordination complexes with tyrosine, thus preventing the inter-tyrosine hydrogen bonding, responsible for holding the vesicular membrane together. Triggered disassembly and nontoxicity of the developed vesicles makes them attractive for drug delivery applications.

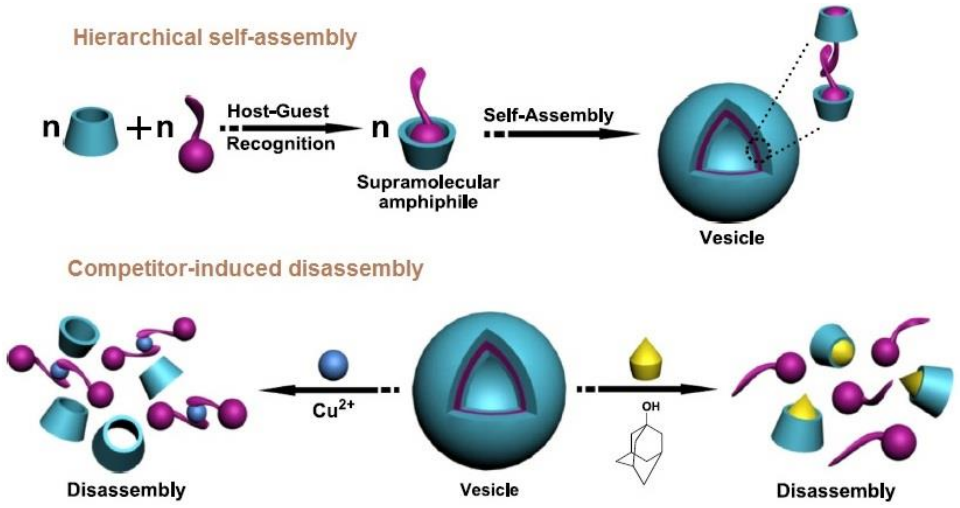

Figure I.18: Schematic illustration of the proposed mechanism of the hydrophobic self-assembly and competitor-induced disassembly of the βCD/tyrosine-based hierarchical vesicles. Reproduced from Ma et al.[99]

It has been shown that simultaneous delivery of chemotherapeutic drugs and apoptosis-inducing genetic material in tumor cells might increase the cancer treatment efficacy in a synergetic way. Several approaches to design such co-delivery systems *via* host-guest mediated "bricks and mortar" strategy were recently reported. The strategy comprises several key steps: 1) synthesis of hydrophobic pro-drugs by conjugation of either doxorubicin[100] or paclitaxel (PTX) [101] with adamantyl moiety; 2) inclusion of the pro-drugs into the βCDs linked to the positively

charged linear PEI (PEI-CD); 3) hierarchical electrostatic self-assembly of PEI-CD/Ada-DOX and PEI-CD/Ada-PTX with either apoptosis-encoding pDNA[100] or survivin shRNA[101] respectively (**Figure I.19**). For instance, in the case of PEI-CD/Ada-DOX/pDNA polyplexes stable sizes of ~230 nm in normal saline were achieved when nitrogen to phosphorus (N/P) ratio reached 25. They showed good *in vivo* doxorubicin retention ability. The cellular internalization of such co-delivery formulations occurred through endocytosis, followed by efficient endosomal escape due to the proton sponge effect of PEI. Usage of PEI-CD/Ada-DOX/pDNA allowed to decrease significantly the tumor growth rate in mice.[100]

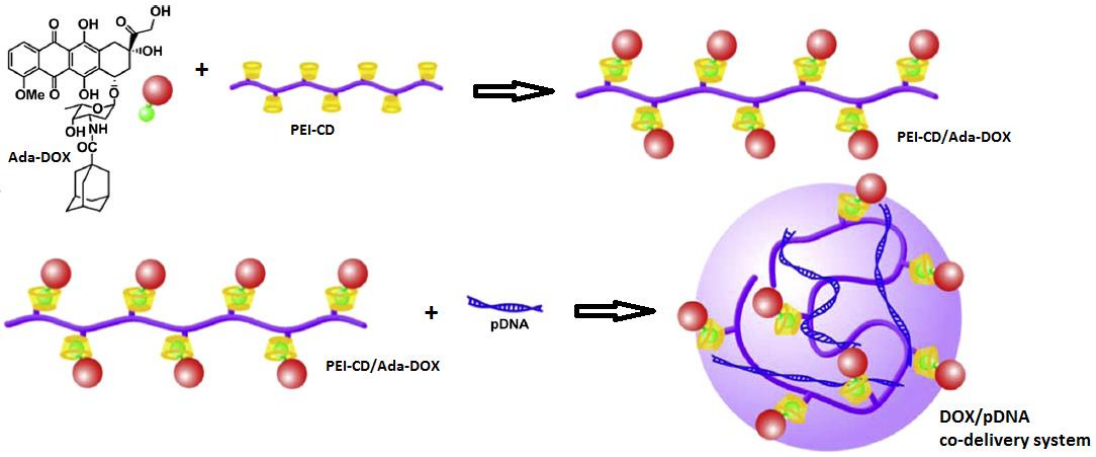

Figure I.19: Doxorubicin and apoptosis-inducing pDNA co-delivery system obtained *via* 2-step host-guest mediated hierarchical self-assembly. Adapted from Fan et al.[100]

Photothermal therapy for cancer treatment has been attracting a lot of attention over the past decades due to its providing a unique opportunity to spatially localize the cell damage effects to the irradiated region.[102, 103] Gold and other noble metal nanostructures as photothermal agents, allow to overcome limitations of organic-dye-based photothermal agents, such as low light absorption and undesired photobleaching.[104] However, the searched photophysical profiles are often found for large nanoparticles (> 100 nm), known for their unsatisfactory bioclearance (i.e., accumulation in the liver, spleen, and kidneys).[105] To solve this contradiction Wang et al. used aforementioned "bricks and mortar" approach to self-assemble size-controlled Au-supramolecular nanoparticles (Au-SNPs) from 2 nm Au colloids.[102] The Au-SNPs comprised three building blocks: Ada-grafted 2 nm Au colloids, CD-PEI, and Ada-PEG. By simply tuning the βCD/Ada mixing ratio between the Au colloids and CD-PEI they managed to obtain a series of Au-SNPs with variable sizes ranging between 40 and 118 nm (**Figure I.20**). The Au-SNPs

exhibited pronounced photothermal activity and selectivity as a result of the collective effects between associated Au colloids. Moreover, it was possible to thermally disassemble the Au-SNPs, thus allowing their in vivo bioclearance.

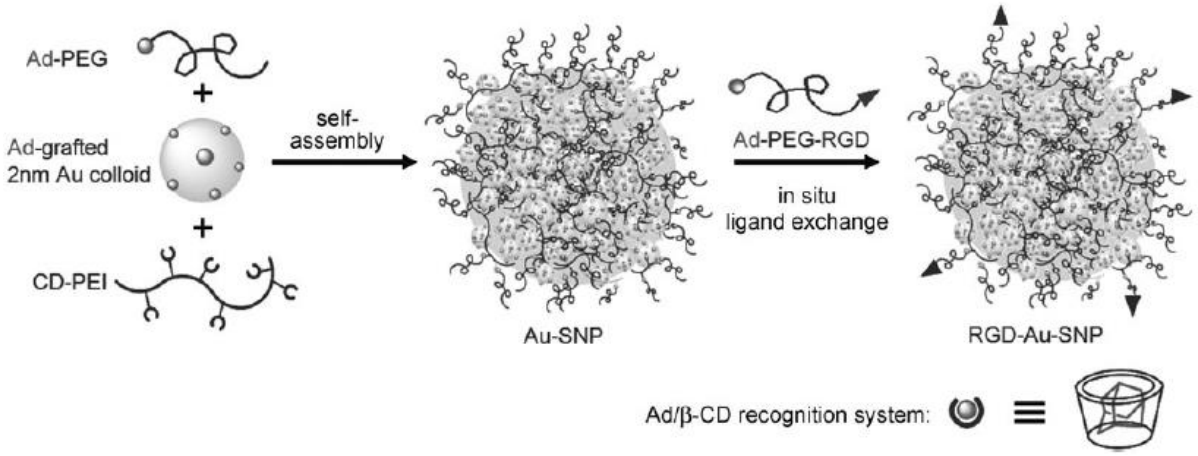

Figure I.20: Host-guest mediated "bricks and mortar" approach for the preparation of size-controlled gold supramolecular nanoparticles (Au-SNPs). Reproduced from Wang et al.[102]

In another recent example the "bricks and mortar" approach was employed to develop a magnetothermally responsive doxorubicin delivery/release system.[106] The SNPs in this case were composed of a fluorescently labeled anti-cancer DOX and the four other building blocks: Ada-grafted polyamidoamine dendrimers (Ada-PAMAM), βCD-grafted branched polyethylenimine (βCD-PEI), Ada-functionalized PEG (Ada-PEG), and 6 nm Ada-grafted $Zn_{0.4}Fe_{2.6}O_4$ superparamagnetic nanoparticles (Ada-MNP). The embedded Ad-MNP were used as built-in transformers converting radiofrequency external alternative magnetic field into heat, allowing for spatio-temporal controllability of *in vivo* DOX release from the nanoparticles.

Much effort is being made to prepare nanoscale supramolecular carriers where CDs play the role of the barrier, slowing down the release kinetics of loaded hydrophobic compounds. Thus, El Fagui et al. described core-shell nanoparticles composed of hydrophobic biodegradable polylactic acid (PLA) core and physically adsorbed β-cyclodextrin polymer (pβCD) shell.[107, 108] The PLA core could accommodate model hydrophobic compounds such as benzophenone[107] or triclosan[108] and the pβCD shell at the periphery ensured their sustained *in vitro* release and opened the pathway to additional functionalization of the particles with targeting agents, fluorescent labels etc. through inclusion complexation with free CD-cavities. Moreover, using

layer-by-layer (LbL) self-assembly technique, deposition of multiple (up to 6) alternate layers of oppositely charged pβCD on the PLA core was possible. It led to further improvement in the benzophenone release profile and demonstrated the potential of these nanoparticles as long-circulating drug carriers.[109]

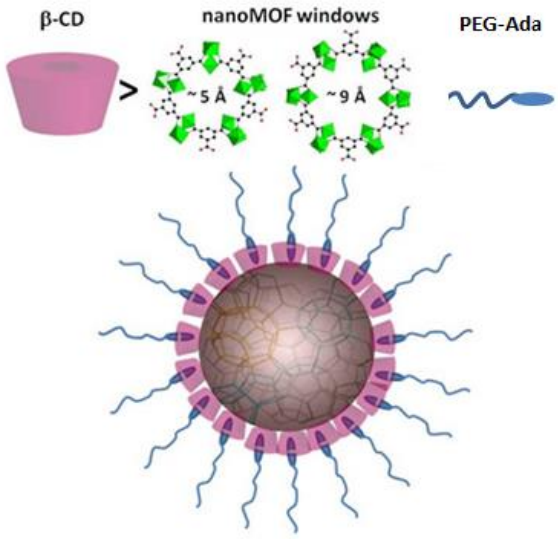

Figure I.21: Schematic illustration of the βCD-P-coated nanoMOF host-guest PEGylation strategy. Adapted from Agostoni et al.[110]

In yet another example by Agostoni et al. βCD-based shell formation was exploited to stabilize nanometric MOF (nanoMOF) in biological media and to establish a pathway for their further non-covalent functionalization with furtive PEG chains or targeting agents.[110] They prepared non-toxic mesoporous Fe(III) carboxylate nanoMOF built up from Fe(III) octahedra trimers and trimesate linkers (1,3,5-benzene tricartricarboxylate) that self-assemble to yield ~220 nm porous architectures delimited by large (29 Å) and small (24 Å) mesoporous cages. Antiretroviral hydrophilic drugs such as azidothymidine-triphosphate (AZT-TP) could be loaded inside the nanoMOF with high encapsulation efficiency (> 99%) due to their coordinate bonding with Fe(III) sites. Phosphate-bearing βCD (βCD-P) was further used to form a non-covalent bioavailable coating around the drug-loaded nanoMOF through the Fe(III)-phosphate interactions. Unlike their uncoated counterparts, βCD-P/nanoMOF demonstrated no signs of aggregation in water for more than 3 days and the coating proved to be stable under physiological simulated conditions (9.5 mM PBS, pH 7.4, 37°C) for 24 hours. Furthermore, βCD-P/nanoMOF could be endowed with "stealth" properties by the inclusion complexation of βCD-P

with Ada-modified 5000 Da PEG chains (**Figure I.21**). This PEGylation strategy also takes advantage of βCD-P as a "gatekeeper" which prevents MPEG-Ada from entering the 5 and 9 A˚ nanoMOF windows and interfering with the drug loading process.

2.2 Host-guest mediated supramolecular hydrogels

Hydrogels are cross-linked three-dimensional networks with porous structure made of various hydrophilic building blocks.[111] Due to their high water swellability and structural similarity to the human's body extracellular matrix, hydrogels have found a great deal of applications in a range of biomedical applications such as tissue engineering, regenerative medicine, storage and sustained release of therapeutics and smart chemical sensors.[49, 112, 113] Hydrogels may be divided into two main classes depending on the nature of the used cross-links: covalently cross-linked chemical gels and non-covalently constructed physical gels. In addition to their inherent stimuli-responsive nature[114], physical hydrogels possess a plethora of other advantageous features, e.g. compositional flexibility, tailorability and self-healing properties.[115, 116]

The introduction of cyclodextrins as structural units of both chemical and physical hydrogels proved to be beneficial given the ease and versatility of CD functionalization (*via* multiple primary and secondary hydroxyls), their high biocompatibility and the opportunity to exploit the cyclodextrin-hydrophobic guest inclusion chemistry.[117] In order to get a general insight into the advances in the domain of CD-containing hydrogels an interested reader is encouraged to refer to a recently published review by Tan et al.[49] Herein, though, we will concentrate on the most significant examples exploiting hierarchical self-assembly strategy to construct non-covalent CD-hydrogels with interesting biomedical profiles.

2.2.1 Hierarchical hydrogels formed from cyclodextrin-based polypseudorotaxanes

The first example of physical gel resulting from the non-covalent interactions between multiple CD-based polypseudorotaxanes (CD-PPRTX) was reported back in 1994 by Harada and coworkers.[118] In view of their thermoresponsive thixotropic properties and high biocompatibility, CD-PPRTX gels rapidly attracted a lot of interest as potential injectable drug delivery systems.[49, 119] The possibility to inject a drug-loaded hydrogel through a syringe allows minimizing the damage to living tissues as a result of the administration procedure.[120, 121] The CD-PPRTX hydrogels formation process is thought to proceed in a hierarchical manner and consist of two steps: 1) formation of CD-PPRTX as such, by threading multiple CDs along an

appropriate, typically PEO, polymer chain *via* inclusion complexation; 2) aggregation of CD-PPRTX due to the intermolecular hydrogen bonding between the threaded CDs and microcrystalline domains formation, the latter being able to hold the resulting 3D-network together (**Figure I.22**). Overwhelming majority of so far described CD-PPRTX gels are based on αCD/PEG inclusion complexation due to the perfect matching in size between the internal cavity of unmodified αCD and chain cross-section area of PEG.[122]

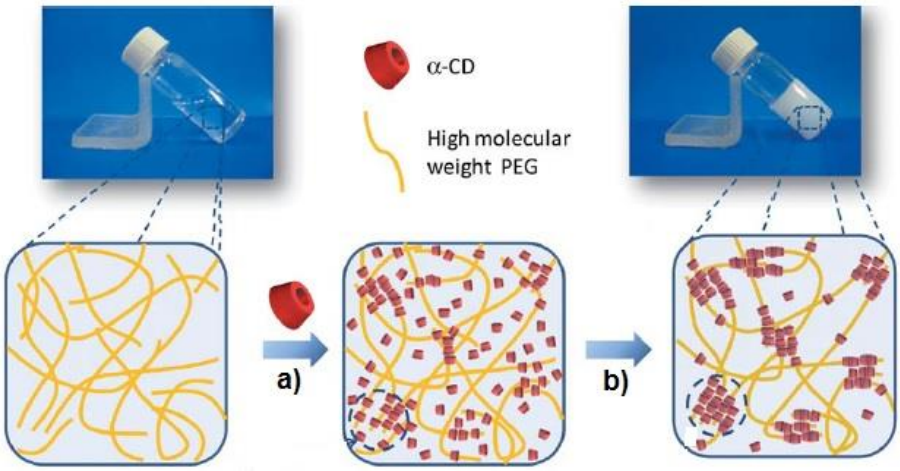

Figure I.22: Schematic illustration of the 2-step hierarchical CD-PPRTX gel formation mechanism: a) hydrophobically-driven inclusion of high molecular weight PEG chains into αCD; b) hydrogen bonding between the threaded αCD microcrystalline domains leading to gelation. Adapted from Liu et al.[122]

It was shown that relatively high PEG molecular weights (at least 10 kDa) are required to achieve the resulting hydrogel stability and long drug release terms.[122] However, being non-biodegradable, only PEG polymer chains or copolymer blocks with M_n below 5 kDa are efficiently eliminated from the body *via* renal clearance pathway. Moreover, the mechanical stability of CD-PPRTX gels is still unsatisfactory even when > 10 kDa PEG are used as guests. The typical solution to these problems consists in using linear, grafted or star-shaped copolymers consisting of PEG block with M_n around 5 kDa and higher molecular weight biodegradable polymer blocks such as polyesters, cationic polymers[123] or polypeptides instead of linear PEG. For instance, amphiphilic block copolymers containing 5 kDa PEG and either biodegradable polyester poly(3-hydroxybutyrate) (PHB, **Figure I.23**)[124], or PCL[125] were used as apolar blocks. The usage of biodegradable hydrophobic blocks was found to be doubly beneficial to the

mechanical properties of the gel due to: 1) removal of the restriction on the copolymer overall molecular weight, as long as PEG blocks are reasonably small; 2) additional physical cross-linking via poly(3-hydroxybutyrate) and PCL blocks hydrophobic microdomains formation. Furthermore, both CD-PPRTX hydrogels were non-cytotoxic, injectable through a small-diameter aperture and demonstrated a sustained *in vitro* release of fluorescein isothiocyanate-labeled dextran (dextran-FITC) model drug, which could last for more than 1 month, while a similar formulation derived from high molecular weight 35 kDa PEG survived only for 5 days.[124, 125]

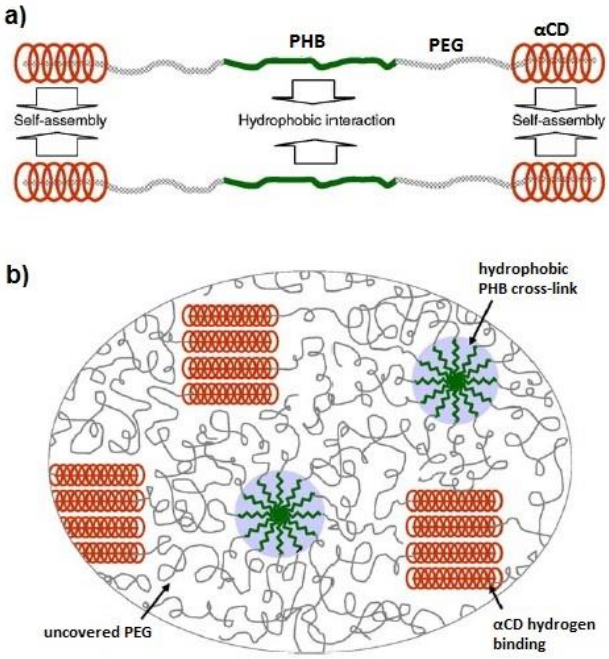

Figure I.23: Schematic illustration of the inclusion-driven formation of αCD/PEG-PHB-PEG polypseudorotaxane (**a**) and αCD/PEG-PHB-PEG-based doubly cross-linked hydrogel (**b**). Adapted from Li et al.[124]

In an attempt to produce stiffer CD-PPRTX hydrogels, while decreasing the total weight concentrations of the starting components, the researchers also used interpeptide hydrogen bonding as an additional associative force.[126, 127] For example Dong and coworkers demonstrated that usage of diblock copolymers containing PEG with molecular weight around 5 kDa and biodegradable polypeptide poly(L-glutamic acid) (PLG) leads to αCD-PPRTX hydrogels with remarkably high elastic storage modulus ($G' \sim 10^4$ Pa at 10 wt% vs. 10^3 Pa at 15 wt% for conventional amphiphilic hydrogels) and long loaded doxorubicin release times.[126] This gel strengthening phenomenon was ascribed to extra hydrogen bonding between the PLG blocks

under acidic pH and its synergy with polypseudorotaxane hydrogen bonds driven associations. In addition, the presence of polypeptide blocks endows the resulting hydrogels with pH-responsiveness.[126]

Following the same logic, PPRTX hydrogels were mechanically reinforced with various inorganic nanomaterials such as silica[128], silver nanoparticles[129] or multi-wall carbon nanotubes (MWCNT).[130] In this case the strategy usually involves physical or chemical anchoring of PEG or PEG-containing copolymers onto inorganic scaffolds prior to polypseudorotaxane formation, so that they play the role of additional network junctions.[122]

Li and colleagues used a αCD/PEG PPRTX-based hydrogel as a gene transfection system. They synthesized a series of biodegradable poly(ethylene glycol)-b-poly(ε-caprolactone)-b-poly[2-(dimethylamino)ethylmethacrylate] (MPEG-PCL-PDMAEMA) triblock copolymers, including positively charged PDMAEMA as a structural unit.[131] In the presence of plasmid DNA copolymers undergo a simultaneous micelle/polyplex formation process with the PCL blocks forming the hydrophobic core and the MPEG corona imparting sterical stability to the polyplexes (**Figure I.24**). Upon subsequent addition of 5 kDa MPEG and αCD a PPRTX forms leading to gelation of the system. Remarkably, the resulting hierarchical hydrogel possessed improved, comparing to conventional PPRTX hydrogels, mechanical properties due to the presence of two types of cross-links in the network, i.e. microcrystalline αCD domains and pDNA-containing polyplexes.

Yet another group of PPRTX hydrogels with recently demonstrated high biomedical potential are those based on αCD/poloxamer complexation. Poloxamers, also widely known as pluronics, are non-ionic triblock copolymers typically composed of central relatively hydrophobic poly(propylene oxide) (PPO) block and terminal hydrophilic PEO blocks (PEO-PPO-PEO).[132] Their high micelle formation capacity along with the ability of resulting micelles to hydrophobically self-organize into 3D-networks at increased temperatures made them popular as drug delivery vehicles.[132, 133] However, their application as injectable gels for sustained release goals is limited because of low mechanical stability and quick erosion from the injection sites event at increased body temperatures.[133] Alvarez-Lorenzo and coworkers have proposed to improve the rheological properties of poloxamers-based systems by pseudo-rotaxanation of PEO blocks of the latter with αCD. They developed syringeable gel formulations able to sustain the release of Vancomycin, an antimicrobial agent active against Gram-positive bacteria.[133] The formulations

contained 6.5 to 20% w/v of Poloxamer F127 and 0 to 9.7% of αCD. At the αCD content above 5% w/v fast gel formation was observed with G' exceeding G'' already at room temperature (~1×10^3 vs. 1×10^2 Pa at 10°C and 5% αCD). The moduli values could be increased at higher temperatures due to the hydrophobic associations between PPO blocks. The PPRTX gels were easily injectable, colloidaly stable for more than 2 months and provided sustained release of Vancomycin for several days.

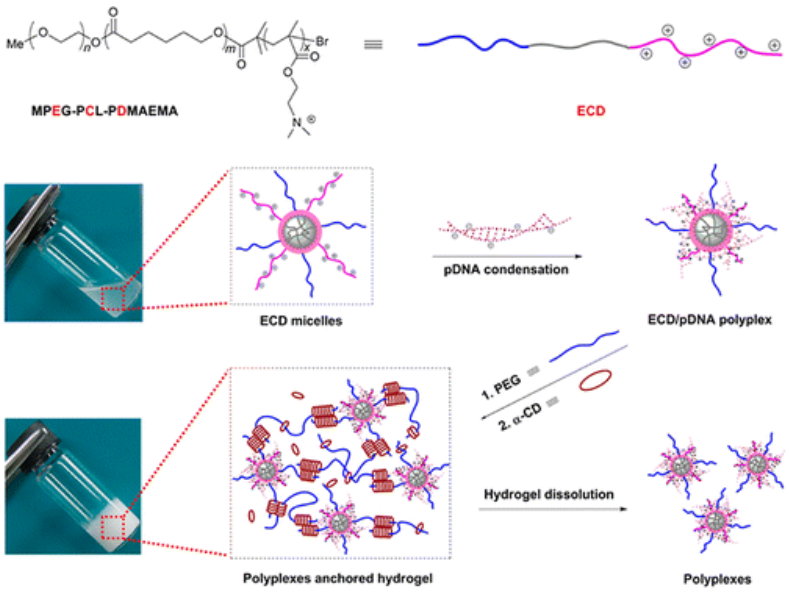

Figure I.24: Schematic illustration of the preparation of αCD/PEG PPRTX hierarchical hydrogels containing pDNA polyplexes for gene transfection and sustained release. Reproduced from Li et al.[131]

In spite of its advantages, simple Poloxamer/αCD system still suffers from quite weak consistency under the stress because of its shear-thinning and thixotropic properties. Recovery of the initial G' and G'' after syringe administration takes enough time to favor a rapid release of the drug before the hierarchical network is restructured. Therefore, the same research group has recently attempted to reinforce the Poloxamer/αCD system by addition of hydroxyethyl cellulose (HEC) as the third thickening component.[134] Such ternary systems were loaded with griseofulvin, a highly hydrophobic antifungal drug used for treatment of dermatophytosis. Due to the synergy between the Poloxamer-P123 and HEC apparent solubility of griseofulvin in water is significantly enhanced and αCD, being able to thread along both 2-hydroxy ethyl radicals of HEC and PEO blocks of poloxamer, prevents the formulation from phase separation.

The hierarchical hydrogel network is further established via physical cross-links between the PPRTX. The viscosity and storage moduli of such ternary Poloxamer/HEC/αCD PPRTX hydrogels at room temperature were higher than those of Poloxamer/αCD formulation, making the former easier to handle in topical treatment of dermatophytosis. Moreover, they demonstrate high biocompatibility and enable sustained release of griseofulvin for at least three weeks.

Poloxamines, a related to poloxamers family of copolymers composed of four arms of PEO-PPO blocks linked together through an ethylenediamine group, were recently reported to be the first group of synthetic polymers with osteoinductive ability.[135] Likewise poloxamers, they undergo a sol-gel transition at 37°C and appropriate pH and concentration conditions. Despite being injectable into bone degenerative defect sites, the resulting hydrogels lack in consistency and are not able to remain in the injection site long enough to provide a sustained release of auxiliary low molecular weight osteoblast growth-inducing agents. To overcome this limitation Simoes et al. prepared poloxamine/αCD PPRTX which were further hierarchically self-assembled into PPRTX hydrogels with high viscoelastic properties and low total weight concentration of the components, i.e. 20% w/v of poloxamer solely were required to undergo sol-gel transition at body temperature, while when 5-7% of αCD was introduced the gelation occurred at room temperature at as low as 2% of poloxamine.[136] Still being injectable poloxamine/αCD PPRTX were loaded with simvastatin, an agent inducing the differentiation of mesenchymal stem cells (MSCs) into osteoblasts. This allowed solubilizing, stabilizing and ensuring a sustained *in vitro* release of hydrophobic simvastatin at pH 7.4. Furthermore, the resulting formulation demonstrated high biocompatibility with both MSCs and osteoblasts and enhanced synergetic osteoinductive effect due to the simultaneous presence of poloxamine and simvastatin.

To summarize, despite the obviously high potential of PPRTX hydrogels as injectable sustained release systems, examples of real applications of these systems have only recently begun to emerge.[49, 125, 134, 136, 137] Thus, this field is expected to attire a great deal of researchers' attention in the years to come.

2.2.2 Cyclodextrin-based hierarchical hydrogels with external stimuli responsive properties

Besides CD/PEG PPRTX hydrogels, many examples of hierarchically organized physical gels with CD/guest inclusion complexation as one of the driving forces of the 3D-network formation have been reported. In addition to intrinsically high internal dynamics and self-healable properties[46],

these systems can also be imparted with stimuli responsiveness by introducing thermo-[114, 138], light-[139] or redox-sensitive[140] elements. In this way, reversible on-demand sol-gel transitions and payload release are achieved by simply alternating an appropriate external stimulus. In the following section we will look at some of the recent advances in the preparation of stimuli-responsive CD-based hierarchical hydrogels with attractive biomedical profiles.

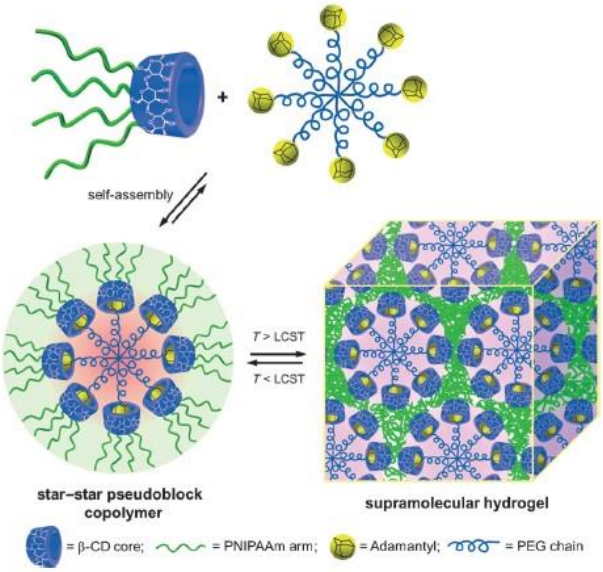

Figure I.25: Illustration of the "star-star" supramolecular complex formation via βCD/Ada inclusion complexation, followed by its temperature-triggered hierarchical hydrogelation. Reproduced from Zhang et al.[138]

For example, Zhang and coworkers described a so-called "star–star" supramolecular architecture obtained through a host-guest self-assembly between a star-shaped adamantyl-terminated 8-arm PEG and a star-shaped PNIPAM containing a βCD core (**Figure I.25**).[138] Being encircled by thermoresponsive corona, the star-star aggregate could be converted into a 3D hydrogel network by increasing the temperature above the LCST value of PNIPAM. Rheological studies showed a highly reversible and repeatable character of hydrogelation with G' reaching initial values (G'~ 100 Pa, G"~70 Pa) after up to 6 cycles of cooling to 25°C and heating back to 37°C. Furthermore, due to the low viscosity of the star-star complex solution at 25°C, authors suggested that therapeutic agents could be mixed with it and conveniently injected into the body. The subsequent temperature triggered *in vivo* hydrogelation is aimed to encapsulate and sustain the release of the therapeutic agents.

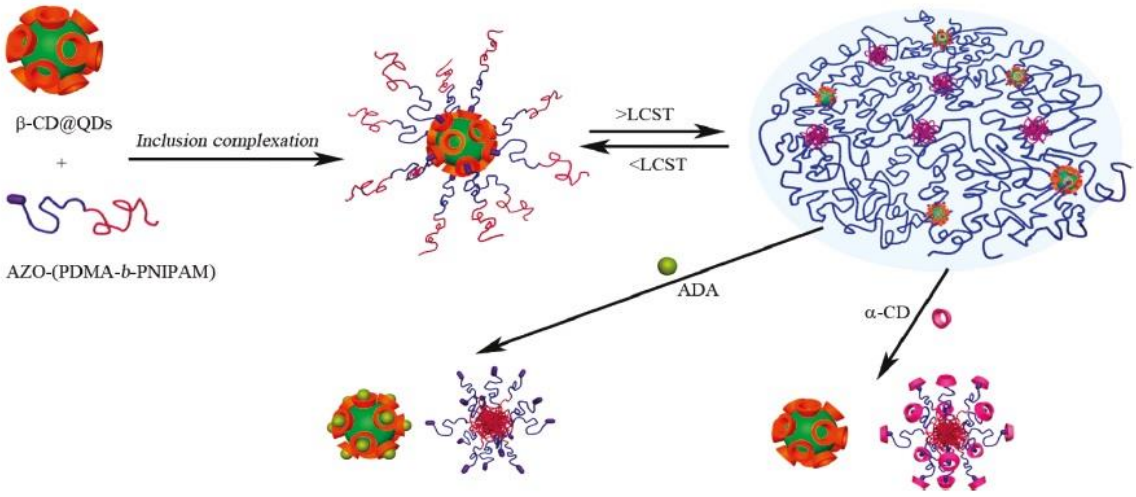

Figure I.26: Schematic illustration of the formation and temperature- or competitor triggered dissociation of QD-containing hierarchical hydrogels made of hybrid inclusion complexes (HIC). Reproduced from Liu et al.[114]

Applying a similar strategy, several years earlier, Ming Jiang and coworkers developed an approach to hybrid thermo-[114, 141] or dual stimuli-responsive[142] hierarchical hydrogels containing inorganic nanoobjects as supramolecular cross-linking points. The strategy involved covalent modification of inorganic nanomaterials such as graphene oxide (GO)[141] or CdS quantum dots (QD)[114, 142] with βCD, as the first step. Then, the resulting GO-βCD or QD-CD were self-assembled into hybrid inclusion complexes (HIC) with diblock copolymers containing a thermoresponsive PNIPAM block and poly-(N,N-dimethylacrylamide) (PDMA) block, the latter being end-modified with azobenzene[114, 141] or ferrocene[142] guest functions. The HIC superstructures were hierarchically and reversibly converted to hydrogels upon heating, while the LCST responsible for the sol-gel transition could be controlled by varying the ratio of degree of polymerization of PDMA to PNIPAM blocks (**Figure I.26**). In addition to temperature change, competitor binding[114, 141, 142] or Fc chemical oxidation to Fc^+ in the case of Fc-PDMA-b-PNIPAM[142] could be used to disrupt the 3D network and trigger the sol-gel transition. Moreover, the presence of inorganic nanomaterials in the hydrogels endowed them with improved rheological properties. Thus, for Fc-containing HIC at a concentration of 12.5 wt% the sol-gel crossover occurs at 40.5°C with G' reaching ~ 2000 Pa, indicating a strong gel formation.[142] The innate fluorescence of QD in such systems might be used as a visualization tool in biosensors elaboration.

A few examples of photo-responsive CD-based hierarchical hydrogels were reported in the past years. As it was mentioned, such systems are of particular interest in drug delivery applications due to their non-destructiveness, remote controllability and time-/site-specific features.[102, 143] A recent study by Chen et al. describes photo-switchable supramolecular hydrogel based on viruses, i.e. tobacco mosaic virus (TMV) and bacteriophage M13, as cross-linking points.[143] Thus, bacteriophage M13 - filamentous virus, 880 nm in length and 6.6 nm in diameter, consisting of a single-stranded DNA enclosed by hierarchically organized protein blocks, was covalently modified with βCDs. Its further inclusion complexation with azobenzene-grafted hyaluronan (HA-Azo) led to a hydrogel (**Figure I.27**).

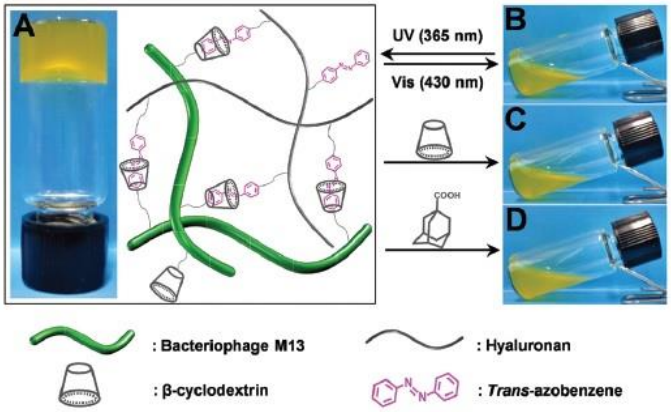

Figure I.27: Schematic illustration of the UV/Vis irradiation and competitor binding responsiveness of the bacteriophage M13-βCD/HA-Azo hierarchical hydrogel. Reproduced from Chen et al.[143]

Its sol-gel transitions can be induced by reversible *trans/cis* photoisomerization of azobenzene upon irradiation with UV light ($\lambda_{365\ nm}$) and visible light ($\lambda_{430\ nm}$). Furthermore, the hydrogel possessed low cytotoxicity and could be used for cells culturing.

A remarkable example of photocontrolled CD-hydrogel based on mesoporous silica nanoparticles (Si-MPs) was reported by Park et al.[139] Their system consisted of Si-MPs with 2 nm pores as a reservoir for guest molecules and βCD "gatekeeper" linked to the Si-MPs through a photocleavable o-nitrobenzyl ester linker acting as a nanovalve blocking the loaded molecules inside the silica pores. Loaded with a model fluorescent dye, calceine, Si-MPs were then used as building blocks to form physical hydrogels *via* molecular recognition-based interaction with six-arm poly(ethylene glycol)with dodecyl end groups (6-PEG-C12). The resulting hydrogel could be

switched to a sol either by addition of αCD as a competitive host or by UV irradiation induced photolysis of the o-nitrobenzyl ester linker. In the latter case the disruption of the gel network was accompanied by "on demand" release of the loaded calceine.

Finally, due to the sensibility of supramolecular CD/guest links to the presence of low molecular weight hosts or guests, in most cases CD-based hierarchical hydrogels are inherently chemically-responsive to competitor binding. To illustrate this concept, Ogoshi et al. prepared chemically-responsive hydrogel containing single-wall carbon nanotubes (SWNT). SWNT were first covered with pyrene-modified βCDs *via* π-π interaction. Then, the gel network was formed through host-guest interactions with poly(acrylic acid) modified with dodecyl groups and could be converted back to sol by simple addition of competitors such as 1-adamantane carboxylic acid Na-salt or αCD.[144] The same scientific group reported chemically-responsive supramolecular hydrogel made from a guest-modified monomeric βCDs.[115] In the first step, inclusion complexation between the βCD bearing hydrophobic 2,4,6-trinitrophenyl-6-amino-transcinnamoyl moieties yielded supramolecular fibrils, which were further self-assembled into physical hydrogel via hydrogen bonding. The gel-to-sol transition could be easily induced either by host-guest competitors or by urea, the latter acting as a denaturating agent, able to disrupt hydrogen bonds.

In a more recent example Himmelein and coworkers successfully used cyclodextrin vesicles (CDV) as multivalent 3D cross-linking points to prepare a chemically-responsive hydrogel.[116] The vesicles were hydrophobically self-assembled from synthetic βCD amphiphiles and their gelation was achieved by the interaction with adamantane-modified hydroxyethylcellulose (HEC-Ad) (**Figure I.28**). Once again, the gel network could be readily disrupted by the addition of competitors. Interestingly, the system showed shear-thinning/self-healing properties and was injectable through a syringe. This, as well as high content in free βCD cavities able to accommodate hydrophobic drugs, makes CDV-based hydrogel an interesting candidate for sustained release applications.

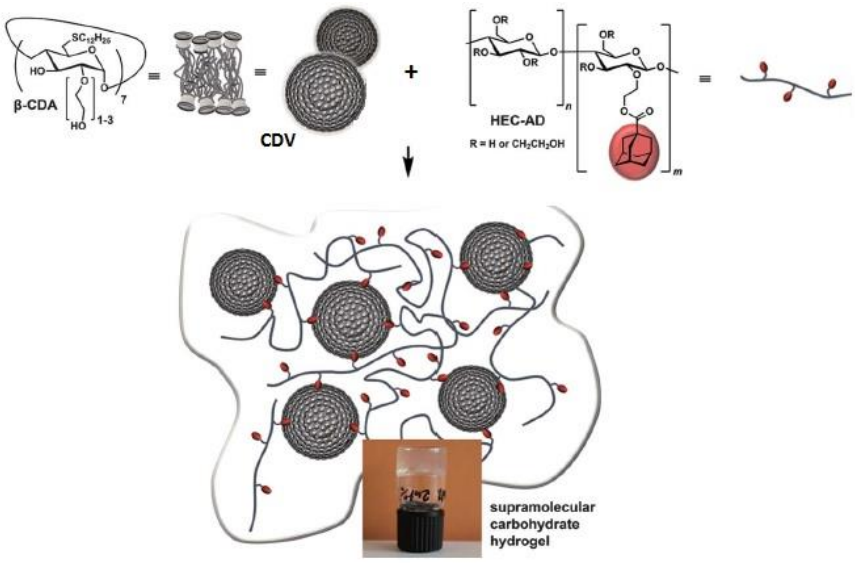

Figure I.28: Schematic illustration of the formation of hierarchical chemically-responsive hydrogels containing amphiphilic βCD supramolecular vesicles as cross-linking points. Adapted from Himmelein et al.[116]

At the same time, the drawback of chemically-responsive CD-based hydrogels comparing to their thermo-, redox- or photo-responsive counterparts lies in the irreversibility of the gel-to-sol transition in this case; i.e. the gel network becomes problematic to restore after the competitor addition, which is especially true when the manipulations are done *in vitro* or *in vivo*. Moreover, small synthetic competitors often might be toxic and non-biocompatible.

Conclusions

In summary, we have highlighted the basic principles and recent advances in the field of artificial hierarchically self-assembled materials. Their feature of being organized at multiple length scales through various types of interactions, allows triggering precise changes in the structure and physico-chemical properties of such systems by means of a wide range of external stimuli. On the other hand, high specificity and reversibility of the inclusion complexation of CDs with hydrophobic guest molecules makes CD-based interactions one of the most widely used tools to construct hierarchically organized materials. Moreover, the presence of CDs in their structure endows the resulting systems with such attractive properties as biocompatibility, mechanical self-healing, and easiness of further modification with targeting agents and/or

fluorescent labels and opportunity to include numerous hydrophobic drugs into free CD-cavities, thereby enhancing their solubility and bioavailability profiles.

Both nanoscale CD-based drug/gene delivery vehicles and macroscopic CD-based hydrogels with hierarchical structure for sustained release of actives were reported so far. However, to date, there are only a few examples of such systems being applied to address real-world clinical issues with most of the studies just conceptually proving the prospect of a system by doing routine *in vitro* tests. Nevertheless, as the field develops and more practical experience is gained, new efficient targeted delivery carriers and tissue engineering scaffolds based on CD-mediated hierarchical self-assembly are expected to make it to the biomedical market in the near future.

References

1. Choi, I. S.; Bowden, N.; Whitesides, G. M. Macroscopic, hierarchical, two-dimensional self-assembly. *Angew. Chem., Int. Ed.* **1999,** *38* (20), 3078-3081.
2. Ushiki, T. The three-dimensional ultrastructure of the collagen fibers, reticular fibers and elastic fibers: a review. *Kaibogaku zasshi. Journal of anatomy* **1992,** *67* (3), 186-99.
3. Elemans, J.; Rowan, A. E.; Nolte, R. J. M. Mastering molecular matter. Supramolecular architectures by hierarchical self-assembly. *J. Mater. Chem.* **2003,** *13* (11), 2661-2670.
4. Pouget, E.; Dujardin, E.; Cavalier, A.; Moreac, A.; Valery, C.; Marchi-Artzner, V.; Weiss, T.; Renault, A.; Paternostre, M.; Artzner, F. Hierarchical architectures by synergy between dynamical template self-assembly and biomineralization. *Nat. Mater.* **2007,** *6* (6), 434-439.
5. Arakaki, A.; Shimizu, K.; Oda, M.; Sakamoto, T.; Nishimura, T.; Kato, T. Biomineralization-inspired synthesis of functional organic/inorganic hybrid materials: organic molecular control of self-organization of hybrids. *Org. Biomol. Chem.* **2015,** *13* (4), 974-989.
6. Xia, Z.; Wei, M. Biomimetic fabrication of collagen-apatite scaffolds for bone tissue regeneration. *Journal of Biomaterials and Tissue Engineering* **2013,** *3* (4), 369-384.
7. Lee, J.-H. Gas sensors using hierarchical and hollow oxide nanostructures: overview. *Sensors and Actuators B: Chemical* **2009,** *140* (1), 319-336.
8. Yuan, Z.-Y.; Su, B.-L. Insights into hierarchically meso–macroporous structured materials. *J. Mater. Chem.* **2006,** *16* (7), 663-677.
9. Čejka, J.; Mintova, S. Perspectives of micro/mesoporous composites in catalysis. *Catalysis Reviews* **2007,** *49* (4), 457-509.
10. Perez-Ramirez, J.; Christensen, C. H.; Egeblad, K.; Christensen, C. H.; Groen, J. C. Hierarchical zeolites: enhanced utilisation of microporous crystals in catalysis by advances in materials design. *Chem. Soc. Rev.* **2008,** *37* (11), 2530-2542.
11. Parlett, C. M.; Wilson, K.; Lee, A. F. Hierarchical porous materials: catalytic applications. *Chem. Soc. Rev.* **2013,** *42* (9), 3876-3893.

12. Zhang, Z.; Han, Y.; Zhu, L.; Wang, R.; Yu, Y.; Qiu, S.; Zhao, D.; Xiao, F. S. Strongly acidic and high-temperature hydrothermally stable mesoporous aluminosilicates with ordered hexagonal structure. *Angew. Chem., Int. Ed.* **2001,** *40* (7), 1258-1262.
13. Choi, M.; Na, K.; Kim, J.; Sakamoto, Y.; Terasaki, O.; Ryoo, R. Stable single-unit-cell nanosheets of zeolite MFI as active and long-lived catalysts. *Nature* **2009,** *461* (7261), 246-249.
14. Wang, Z. P.; Li, C.; Cho, H. J.; Kung, S. C.; Snyder, M. A.; Fan, W. Direct, single-step synthesis of hierarchical zeolites without secondary templating. *J. Mater. Chem. A* **2015,** *3* (3), 1298-1305.
15. Zhang, P. G.; Zhang, J.; Xie, A. J.; Li, S. K.; Song, J. M.; Shen, Y. H. Hierarchical flower-like Bi2WO6 hollow microspheres: facile synthesis and excellent catalytic performance. *RSC Adv.* **2015,** *5* (29), 23080-23085.
16. Daghrir, R.; Drogui, P.; Robert, D. Modified TiO2 for environmental photocatalytic applications: a review. *Industrial & Engineering Chemistry Research* **2013,** *52* (10), 3581-3599.
17. Yao, H. Z.; Ma, J. W.; Mu, Y. N.; Chen, Y. L.; Su, S.; Lv, P.; Zhang, X. L.; Ding, D.; Fu, W. Y.; Yang, H. B. Hierarchical TiO2 nanoflowers/nanosheets array film: synthesis, growth mechanism and enhanced photoelectrochemical properties. *RSC Adv.* **2015,** *5* (9), 6429-6436.
18. Furukawa, S.; Reboul, J.; Diring, S.; Sumida, K.; Kitagawa, S. Structuring of metal-organic frameworks at the mesoscopic/macroscopic scale. *Chem. Soc. Rev.* **2014,** *43* (16), 5700-5734.
19. Yin, S. Y.; Zhang, Y. Y.; Kong, J. H.; Zou, C. J.; Li, C. M.; Lu, X. H.; Ma, J.; Boey, F. Y. C.; Chen, X. D. Assembly of Graphene Sheets into Hierarchical Structures for High-Performance Energy Storage. *ACS Nano* **2011,** *5* (5), 3831-3838.
20. Gerth, M.; Bohdan, M.; Fokkink, R.; Voets, I. K.; van der Gucht, J.; Sprakel, J. Supramolecular Assembly of Self-Healing Nanocomposite Hydrogels. *Macromol. Rapid Commun.* **2014,** *35* (24), 2065-2070.
21. Horcajada, P.; Gref, R.; Baati, T.; Allan, P. K.; Maurin, G.; Couvreur, P.; Férey, G.; Morris, R. E.; Serre, C. Metal–organic frameworks in biomedicine. *Chem. Rev.* **2011,** *112* (2), 1232-1268.
22. Anand, R.; Borghi, F.; Manoli, F.; Manet, I.; Agostoni, V.; Reschiglian, P.; Gref, R.; Monti, S. Host–Guest Interactions in Fe (III)-Trimesate MOF Nanoparticles Loaded with Doxorubicin. *The Journal of Physical Chemistry B* **2014,** *118* (29), 8532-8539.
23. Kreno, L. E.; Leong, K.; Farha, O. K.; Allendorf, M.; Van Duyne, R. P.; Hupp, J. T. Metal–organic framework materials as chemical sensors. *Chem. Rev.* **2011,** *112* (2), 1105-1125.
24. Bruce, P. G.; Scrosati, B.; Tarascon, J. M. Nanomaterials for rechargeable lithium batteries. *Angew. Chem., Int. Ed.* **2008,** *47* (16), 2930-2946.
25. Kushner, A. M.; Guan, Z. B. Modular Design in Natural and Biomimetic Soft Materials. *Angew. Chem., Int. Ed.* **2011,** *50* (39), 9026-9057.
26. Matson, J. B.; Stupp, S. I. Self-assembling peptide scaffolds for regenerative medicine. *Chem. Commun.* **2012,** *48* (1), 26-33.
27. Kang, Y. J.; Uchida, M.; Shin, H.-H.; Douglas, T.; Kang, S. Biomimetic FePt nanoparticle synthesis within Pyrococcus furiosus ferritins and their layer-by-layer formation. *Soft Matter* **2011,** *7* (23), 11078-11081.
28. Daemen, T.; de Mare, A.; Bungener, L.; de Jonge, J.; Huckriede, A.; Wilschut, J. Virosomes for antigen and DNA delivery. *Adv. Drug Delivery Rev.* **2005,** *57* (3), 451-463.
29. Xu, X. H.; Yuan, H.; Chang, J.; He, B.; Gu, Z. W. Cooperative Hierarchical Self-Assembly of Peptide Dendrimers and Linear Polypeptides into Nanoarchitectures Mimicking Viral Capsids. *Angew. Chem., Int. Ed.* **2012,** *51* (13), 3130-3133.

30. Beck, T.; Tetter, S.; Kunzle, M.; Hilvert, D. Construction of Matryoshka-Type Structures from Supercharged Protein Nanocages. *Angew. Chem., Int. Ed.* **2015,** *54* (3), 937-940.
31. Humenik, M.; Scheibel, T. Self-assembly of nucleic acids, silk and hybrid materials thereof. *J. Phys.-Condes. Matter* **2014,** *26* (50).
32. Rangnekar, A.; LaBean, T. H. Building DNA nanostructures for molecular computation, templated assembly, and biological applications. *Acc. Chem. Res.* **2014,** *47* (6), 1778-1788.
33. Saccà, B.; Niemeyer, C. M. Functionalization of DNA nanostructures with proteins. *Chem. Soc. Rev.* **2011,** *40* (12), 5910-5921.
34. Chen, X. J.; Sanchez-Gaytan, B. L.; Hayik, S. E.; Fryd, M.; Wayland, B. B.; Park, S. J. Self-Assembled Hybrid Structures of DNA Block-Copolymers and Nanoparticles with Enhanced DNA Binding Properties. *Small* **2010,** *6* (20), 2256-2260.
35. Alemdaroglu, F. E.; Ding, K.; Berger, R.; Herrmann, A. DNA-Templated Synthesis in Three Dimensions: Introducing a Micellar Scaffold for Organic Reactions. *Angew. Chem., Int. Ed.* **2006,** *45* (25), 4206-4210.
36. Teixeira Jr, F.; Rigler, P.; Vebert-Nardin, C. Nucleo-copolymers: oligonucleotide-based amphiphilic diblock copolymers. *Chem. Commun.* **2007,** (11), 1130-1132.
37. Wang, L.; Feng, Y.; Sun, Y.; Li, Z.; Yang, Z.; He, Y.-M.; Fan, Q.-H.; Liu, D. Amphiphilic DNA-dendron hybrid: a new building block for functional assemblies. *Soft Matter* **2011,** *7* (16), 7187-7190.
38. Albert, S. K.; Thelu, H. V. P.; Golla, M.; Krishnan, N.; Chaudhary, S.; Varghese, R. Self-Assembly of DNA–Oligo (p-phenylene-ethynylene) Hybrid Amphiphiles into Surface-Engineered Vesicles with Enhanced Emission. *Angew. Chem., Int. Ed.* **2014,** *53* (32), 8352-8357.
39. Kwak, M.; Gao, J.; Prusty, D. K.; Musser, A. J.; Markov, V. A.; Tombros, N.; Stuart, M. C.; Browne, W. R.; Boekema, E. J.; ten Brinke, G. DNA Block Copolymer Doing It All: From Selection to Self-Assembly of Semiconducting Carbon Nanotubes. *Angew. Chem.* **2011,** *123* (14), 3264-3268.
40. Faul, C. F. J. Ionic Self-Assembly for Functional Hierarchical Nanostructured Materials. *Acc. Chem. Res.* **2014,** *47* (12), 3428-3438.
41. Xu, W. N.; Ledin, P. A.; Shevchenko, V. V.; Tsukruk, V. V. Architecture, Assembly, and Emerging Applications of Branched Functional Polyelectrolytes and Poly(ionic liquid)s. *ACS Appl. Mater. Interfaces* **2015,** *7* (23), 12570-12596.
42. Zhang, T.; Brown, J.; Oakley, R. J.; Faul, C. F. Towards functional nanostructures: Ionic self-assembly of polyoxometalates and surfactants. *Current Opinion in Colloid & Interface Science* **2009,** *14* (2), 62-70.
43. Ahmed, R.; Patra, S. K.; Chabanne, L.; Faul, C. F.; Manners, I. Hierarchical Organometallic Materials: Self-Assembly of Organic–Organometallic Polyferrocenylsilane Block Polyelectrolyte–Surfactant Complexes in Bulk and in Thin Films. *Macromolecules* **2011,** *44* (23), 9324-9334.
44. Yuan, J.; Soll, S.; Drechsler, M.; Müller, A. H.; Antonietti, M. Self-assembly of poly (ionic liquid) s: polymerization, mesostructure formation, and directional alignment in one step. *J. Am. Chem. Soc.* **2011,** *133* (44), 17556-17559.
45. Qi, Z. H.; Schalley, C. A. Exploring Macrocycles in Functional Supramolecular Gels: From Stimuli Responsiveness to Systems Chemistry. *Acc. Chem. Res.* **2014,** *47* (7), 2222-2233.
46. Harada, A.; Takashima, Y.; Nakahata, M. Supramolecular Polymeric Materials via Cyclodextrin-Guest Interactions. *Acc. Chem. Res.* **2014,** *47* (7), 2128-2140.

47. Dong, S.; Zheng, B.; Wang, F.; Huang, F. Supramolecular polymers constructed from macrocycle-based host–guest molecular recognition motifs. *Acc. Chem. Res.* **2014,** *47* (7), 1982-1994.
48. Schalley, C. A.; Beizai, K.; Vögtle, F. On the way to rotaxane-based molecular motors: studies in molecular mobility and topological chirality. *Acc. Chem. Res.* **2001,** *34* (6), 465-476.
49. Tan, S.; Ladewig, K.; Fu, Q.; Blencowe, A.; Qiao, G. G. Cyclodextrin-Based Supramolecular Assemblies and Hydrogels: Recent Advances and Future Perspectives. *Macromol. Rapid Commun.* **2014,** *35* (13), 1166-1184.
50. Liao, X. J.; Chen, G. S.; Jiang, M. Hydrogels locked by molecular recognition aiming at responsiveness and functionality. *Polym. Chem.* **2013,** *4* (6), 1733-1745.
51. Ruthard, C.; Schmidt, M.; Gröhn, F. Porphyrin–Polymer Networks, Worms, and Nanorods: pH-triggerable Hierarchical Self-assembly. *Macromol. Rapid Commun.* **2011,** *32* (9-10), 706-711.
52. Bussolati, R.; Carrieri, P.; Secchi, A.; Arduini, A.; Credi, A.; Semeraro, M.; Venturi, M.; Silvi, S.; Velluto, D.; Zappacosta, R.; Fontana, A. Hierarchical self-assembly of amphiphilic calix 6 arene wheels and viologen axles in water. *Org. Biomol. Chem.* **2013,** *11* (35), 5944-5953.
53. Hui, J. K. H.; Frischmann, P. D.; Tso, C. H.; Michal, C. A.; MacLachlan, M. J. Spontaneous Hierarchical Assembly of Crown Ether-like Macrocycles into Nanofibers and Microfibers Induced by Alkali-Metal and Ammonium Salts. *Chem.-Eur. J.* **2010,** *16* (8), 2453-2460.
54. Wei, P. F.; Li, S. J.; Zhang, Y. Y.; Yu, Y. H.; Yan, X. Z. Responsive cross-linked supramolecular polymer network: hierarchical supramolecular polymerization driven by cryptand-based molecular recognition and metal coordination. *Polym. Chem.* **2014,** *5* (13), 3972-3976.
55. Tan, L. L.; Yang, Y. W. Molecular recognition and self-assembly of pillarenes. *Journal of Inclusion Phenomena and Macrocyclic Chemistry* **2015,** *81* (1-2), 13-33.
56. Zhou, Q. Z.; Jiang, H. J.; Chen, R.; Qiu, F. L.; Dai, G. L.; Han, D. M. A triply-responsive pillar 6 arene-based supramolecular amphiphile for tunable formation of vesicles and controlled release. *Chem. Commun.* **2014,** *50* (73), 10658-10660.
57. Kim, K. Mechanically interlocked molecules incorporating cucurbituril and their supramolecular assemblies. *Chem. Soc. Rev.* **2002,** *31* (2), 96-107.
58. Rekharsky, M. V.; Inoue, Y. Complexation thermodynamics of cyclodextrins. *Chem. Rev.* **1998,** *98* (5), 1875-1917.
59. Jie, K. C.; Zhou, Y. J.; Yao, Y.; Huang, F. H. Macrocyclic amphiphiles. *Chem. Soc. Rev.* **2015,** *44* (11), 3568-3587.
60. Khan, A. R.; Forgo, P.; Stine, K. J.; D'Souza, V. T. Methods for selective modifications of cyclodextrins. *Chem. Rev.* **1998,** *98* (5), 1977-1996.
61. Davis, M. E. The first targeted delivery of siRNA in humans via a self-assembling, cyclodextrin polymer-based nanoparticle: from concept to clinic. *Mol. Pharm.* **2009,** *6* (3), 659-668.
62. Mellet, C. O.; Fernández, J. M. G.; Benito, J. M. Cyclodextrin-based gene delivery systems. *Chem. Soc. Rev.* **2011,** *40* (3), 1586-1608.
63. Nayak, S.; Herzog, R. W. Progress and prospects: immune responses to viral vectors. *Gene therapy* **2010,** *17* (3), 295-304.
64. Park, T. G.; Jeong, J. H.; Kim, S. W. Current status of polymeric gene delivery systems. *Adv. Drug Delivery Rev.* **2006,** *58* (4), 467-486.

65. Li, W.; Szoka Jr, F. C. Lipid-based nanoparticles for nucleic acid delivery. *Pharm. Res.* **2007,** *24* (3), 438-449.
66. Srinivas, R.; Samanta, S.; Chaudhuri, A. Cationic amphiphiles: promising carriers of genetic materials in gene therapy. *Chem. Soc. Rev.* **2009,** *38* (12), 3326-3338.
67. Wagner, E. Strategies to improve DNA polyplexes for in vivo gene transfer: will “artificial viruses” be the answer? *Pharm. Res.* **2004,** *21* (1), 8-14.
68. Mishra, S.; Webster, P.; Davis, M. E. PEGylation significantly affects cellular uptake and intracellular trafficking of non-viral gene delivery particles. *European journal of cell biology* **2004,** *83* (3), 97-111.
69. Pun, S. H.; Davis, M. E. Development of a nonviral gene delivery vehicle for systemic application. *Bioconjugate Chem.* **2002,** *13* (3), 630-639.
70. Bartlett, D. W.; Davis, M. E. Physicochemical and biological characterization of targeted, nucleic acid-containing nanoparticles. *Bioconjugate Chem.* **2007,** *18* (2), 456-468.
71. Hu-Lieskovan, S.; Heidel, J. D.; Bartlett, D. W.; Davis, M. E.; Triche, T. J. Sequence-specific knockdown of EWS-FLI1 by targeted, nonviral delivery of small interfering RNA inhibits tumor growth in a murine model of metastatic Ewing's sarcoma. *Cancer research* **2005,** *65* (19), 8984-8992.
72. Heidel, J. D.; Yu, Z.; Liu, J. Y.-C.; Rele, S. M.; Liang, Y.; Zeidan, R. K.; Kornbrust, D. J.; Davis, M. E. Administration in non-human primates of escalating intravenous doses of targeted nanoparticles containing ribonucleotide reductase subunit M2 siRNA. *Proceedings of the National Academy of Sciences* **2007,** *104* (14), 5715-5721.
73. Davis, M. E.; Zuckerman, J. E.; Choi, C. H. J.; Seligson, D.; Tolcher, A.; Alabi, C. A.; Yen, Y.; Heidel, J. D.; Ribas, A. Evidence of RNAi in humans from systemically administered siRNA via targeted nanoparticles. *Nature* **2010,** *464* (7291), 1067-1070.
74. Park, I.-K.; Von Recum, H. A.; Jiang, S.; Pun, S. H. Supramolecular assembly of cyclodextrin-based nanoparticles on solid surfaces for gene delivery. *Langmuir* **2006,** *22* (20), 8478-8484.
75. Burckbuchler, V.; Wintgens, V.; Leborgne, C.; Lecomte, S.; Leygue, N.; Scherman, D.; Kichler, A.; Amiel, C. Development and characterization of new cyclodextrin polymer-based DNA delivery systems. *Bioconjugate Chem.* **2008,** *19* (12), 2311-2320.
76. Burckbuchler, V.; Wintgens, V.; Lecomte, S.; Percot, A.; Leborgne, C.; Danos, O.; Kichler, A.; Amiel, C. DNA compaction into new DNA vectors based on cyclodextrin polymer: Surface enhanced Raman spectroscopy characterization. *Biopolymers* **2006,** *81* (5), 360-370.
77. Wintgens, V.; Leborgne, C.; Baconnais, S.; Burckbuchler, V.; Le Cam, E.; Scherman, D.; Kichler, A.; Amiel, C. Smart DNA vectors based on cyclodextrin polymers: compaction and endosomal release. *Pharm. Res.* **2012,** *29* (2), 384-396.
78. Varkouhi, A. K.; Scholte, M.; Storm, G.; Haisma, H. J. Endosomal escape pathways for delivery of biologicals. *J. Controlled Release* **2011,** *151* (3), 220-228.
79. Wenz, G.; Han, B.-H.; Müller, A. Cyclodextrin rotaxanes and polyrotaxanes. *Chem. Rev.* **2006,** *106* (3), 782-817.
80. Shuai, X.; Merdan, T.; Unger, F.; Wittmar, M.; Kissel, T. Novel biodegradable ternary copolymers hy-PEI-g-PCL-b-PEG: synthesis, characterization, and potential as efficient nonviral gene delivery vectors. *Macromolecules* **2003,** *36* (15), 5751-5759.
81. Shuai, X.; Merdan, T.; Unger, F.; Kissel, T. Supramolecular gene delivery vectors showing enhanced transgene expression and good biocompatibility. *Bioconjugate Chem.* **2005,** *16* (2), 322-329.

82. Dan, Z.; Cao, H.; He, X.; Zeng, L.; Zou, L.; Shen, Q.; Zhang, Z. Biological stimuli-responsive cyclodextrin-based host–guest nanosystems for cancer therapy. *Int. J. Pharm.* **2015,** *483* (1), 63-68.
83. Hogg, P. J. Targeting allosteric disulphide bonds in cancer. *Nature Reviews Cancer* **2013,** *13* (6), 425-431.
84. Wen, Y.; Zhang, Z.; Li, J. Highly Efficient Multifunctional Supramolecular Gene Carrier System Self-Assembled from Redox-Sensitive and Zwitterionic Polymer Blocks. *Adv. Funct. Mater.* **2014,** *24* (25), 3874-3884.
85. Ping, Y.; Hu, Q.; Tang, G.; Li, J. FGFR-targeted gene delivery mediated by supramolecular assembly between β-cyclodextrin-crosslinked PEI and redox-sensitive PEG. *Biomaterials* **2013,** *34* (27), 6482-6494.
86. Gref, R.; Amiel, C.; Molinard, K.; Daoud-Mahammed, S.; Sébille, B.; Gillet, B.; Beloeil, J.-C.; Ringard, C.; Rosilio, V.; Poupaert, J. New self-assembled nanogels based on host–guest interactions: characterization and drug loading. *J. Controlled Release* **2006,** *111* (3), 316-324.
87. Daoud-Mahammed, S.; Couvreur, P.; Bouchemal, K.; Chéron, M.; Lebas, G.; Amiel, C.; Gref, R. Cyclodextrin and polysaccharide-based nanogels: entrapment of two hydrophobic molecules, benzophenone and tamoxifen. *Biomacromolecules* **2009,** *10* (3), 547-554.
88. Nielsen, T. T.; Amiel, C.; Duroux, L.; Larsen, K. L.; Städe, L. W.; Wimmer, R.; Wintgens, V. Formation of nanoparticles by cooperative inclusion between (S)-camptothecin-modified dextrans and β-cyclodextrin polymers. *Beilstein Journal of Organic Chemistry* **2015,** *11* (1), 147-154.
89. Layre, A.-M.; Wintgens, V.; Gosselet, N.-M.; Dalmas, F.; Amiel, C. Tuning the interactions in cyclodextrin polymer nanoassemblies. *Eur. Polym. J.* **2009,** *45* (11), 3016-3026.
90. Wintgens, V.; Nielsen, T. T.; Larsen, K. L.; Amiel, C. Size-Controlled Nanoassemblies Based on Cyclodextrin-Modified Dextrans. *Macromolecular Bioscience* **2011,** *11* (9), 1254-1263.
91. Wintgens, V.; Layre, A. M.; Hourdet, D.; Amiel, C. Cyclodextrin Polymer Nanoassemblies: Strategies for Stability Improvement. *Biomacromolecules* **2012,** *13* (2), 528-534.
92. Zan, M. H.; Li, J. J.; Luo, S. Z.; Ge, Z. S. Dual pH-triggered multistage drug delivery systems based on host-guest interaction-associated polymeric nanogels. *Chem. Commun.* **2014,** *50* (58), 7824-7827.
93. Zhang, J.; Ma, P. X. Polymeric core–shell assemblies mediated by host–guest interactions: Versatile nanocarriers for drug delivery. *Angew. Chem., Int. Ed.* **2009,** *48* (5), 964-968.
94. Zhang, J.; Feng, K.; Cuddihy, M.; Kotov, N. A.; Ma, P. X. Spontaneous formation of temperature-responsive assemblies by molecular recognition of a β-cyclodextrin-containing block copolymer and poly (N-isopropylacrylamide). *Soft Matter* **2010,** *6* (3), 610-617.
95. Quan, C.-Y.; Chen, J.-X.; Wang, H.-Y.; Li, C.; Chang, C.; Zhang, X.-Z.; Zhuo, R.-X. Core− shell nanosized assemblies mediated by the α− β cyclodextrin dimer with a tumor-triggered targeting property. *ACS Nano* **2010,** *4* (7), 4211-4219.
96. Yan, Q.; Yuan, J.; Cai, Z.; Xin, Y.; Kang, Y.; Yin, Y. Voltage-responsive vesicles based on orthogonal assembly of two homopolymers. *J. Am. Chem. Soc.* **2010,** *132* (27), 9268-9270.
97. Kang, Y.; Ma, Y.; Zhang, S.; Ding, L. S.; Li, B. J. Dual-Stimuli-Responsive Nanoassemblies as Tunable Releasing Carriers. *ACS Macro Lett.* **2015,** *4* (5), 543-547.
98. Liu, F.; Ma, Y. F.; Xu, L.; Liu, L. C.; Zhang, W. A. Redox-responsive supramolecular amphiphiles constructed via host-guest interactions for photodynamic therapy. *Biomater. Sci.* **2015,** *3* (8), 1218-1227.

99. Ma, M. F.; Xu, S. G.; Xing, P. Y.; Li, S. Y.; Chu, X. X.; Hao, A. Y. A multistimuli-responsive supramolecular vesicle constructed by cyclodextrins and tyrosine. *Colloid. Polym. Sci.* **2015,** *293* (3), 891-900.
100. Fan, H.; Hu, Q.-D.; Xu, F.-J.; Liang, W.-Q.; Tang, G.-P.; Yang, W.-T. In vivo treatment of tumors using host-guest conjugated nanoparticles functionalized with doxorubicin and therapeutic gene pTRAIL. *Biomaterials* **2012,** *33* (5), 1428-1436.
101. Hu, Q.; Li, W.; Hu, X.; Hu, Q.; Shen, J.; Jin, X.; Zhou, J.; Tang, G.; Chu, P. K. Synergistic treatment of ovarian cancer by co-delivery of survivin shRNA and paclitaxel via supramolecular micellar assembly. *Biomaterials* **2012,** *33* (27), 6580-6591.
102. Wang, S.; Chen, K. J.; Wu, T. H.; Wang, H.; Lin, W. Y.; Ohashi, M.; Chiou, P. Y.; Tseng, H. R. Photothermal effects of supramolecularly assembled gold nanoparticles for the targeted treatment of cancer cells. *Angew. Chem., Int. Ed.* **2010,** *49* (22), 3777-3781.
103. An, K.; Hyeon, T. Synthesis and biomedical applications of hollow nanostructures. *Nano Today* **2009,** *4* (4), 359-373.
104. Huang, X.; Jain, P. K.; El-Sayed, I. H.; El-Sayed, M. A. Plasmonic photothermal therapy (PPTT) using gold nanoparticles. *Lasers in medical science* **2008,** *23* (3), 217-228.
105. Nel, A. E.; Mädler, L.; Velegol, D.; Xia, T.; Hoek, E. M.; Somasundaran, P.; Klaessig, F.; Castranova, V.; Thompson, M. Understanding biophysicochemical interactions at the nano–bio interface. *Nat. Mater.* **2009,** *8* (7), 543-557.
106. Lee, J. H.; Chen, K. J.; Noh, S. H.; Garcia, M. A.; Wang, H.; Lin, W. Y.; Jeong, H.; Kong, B. J.; Stout, D. B.; Cheon, J. On-demand drug release system for in vivo cancer treatment through self-assembled magnetic nanoparticles. *Angew. Chem.* **2013,** *125* (16), 4480-4484.
107. El Fagui, A.; Amiel, C. PLA nanoparticles coated with a β-cyclodextrin polymer shell: preparation, characterization and release kinetics of a hydrophobic compound. *Int. J. Pharm.* **2012,** *436* (1), 644-651.
108. El Fagui, A.; Dubot, P.; Loftsson, T.; Amiel, C. Triclosan-loaded with high encapsulation efficiency into PLA nanoparticles coated with β-cyclodextrin polymer. *Journal of Inclusion Phenomena and Macrocyclic Chemistry* **2013,** *75* (3-4), 277-283.
109. El Fagui, A.; Wintgens, V.; Gaillet, C.; Dubot, P.; Amiel, C. Layer-by-Layer Coated PLA Nanoparticles with Oppositely Charged β-Cyclodextrin Polymer for Controlled Delivery of Lipophilic Molecules. *Macromol. Chem. Phys.* **2014,** *215* (6), 555-565.
110. Agostoni, V.; Horcajada, P.; Noiray, M.; Malanga, M.; Aykaç, A.; Jicsinszky, L.; Vargas-Berenguel, A.; Semiramoth, N.; Daoud-Mahammed, S.; Nicolas, V. A "green" strategy to construct non-covalent, stable and bioactive coatings on porous MOF nanoparticles. *Scientific reports* **2015,** *5*.
111. Lee, K. Y.; Mooney, D. J. Hydrogels for tissue engineering. *Chem. Rev.* **2001,** *101* (7), 1869-1880.
112. Balakrishnan, B.; Banerjee, R. Biopolymer-based hydrogels for cartilage tissue engineering. *Chem. Rev.* **2011,** *111* (8), 4453-4474.
113. Hoare, T. R.; Kohane, D. S. Hydrogels in drug delivery: progress and challenges. *Polymer* **2008,** *49* (8), 1993-2007.
114. Liu, J.; Chen, G.; Guo, M.; Jiang, M. Dual stimuli-responsive supramolecular hydrogel based on hybrid inclusion complex (HIC). *Macromolecules* **2010,** *43* (19), 8086-8093.
115. Deng, W.; Yamaguchi, H.; Takashima, Y.; Harada, A. A Chemical-Responsive Supramolecular Hydrogel from Modified Cyclodextrins. *Angew. Chem.* **2007,** *119* (27), 5236-5239.

116. Himmelein, S.; Lewe, V.; Stuart, M. C.; Ravoo, B. J. A carbohydrate-based hydrogel containing vesicles as responsive non-covalent cross-linkers. *Chem. Sci.* **2014,** *5* (3), 1054-1058.
117. Liao, X.; Chen, G.; Liu, X.; Chen, W.; Chen, F.; Jiang, M. Photoresponsive pseudopolyrotaxane hydrogels based on competition of host–guest interactions. *Angew. Chem.* **2010,** *122* (26), 4511-4515.
118. Li, J.; Harada, A.; Kamachi, M. Sol–gel transition during inclusion complex formation between α-cyclodextrin and high molecular weight poly (ethylene glycol) s in aqueous solution. *Polym. J.* **1994,** *26* (9), 1019-1026.
119. Li, J.; Ni, X.; Leong, K. W. Injectable drug-delivery systems based on supramolecular hydrogels formed by poly (ethylene oxide) s and α-cyclodextrin. *Journal of Biomedical Materials Research Part A* **2003,** *65* (2), 196-202.
120. Simoes, S. M. N.; Veiga, F.; Torres-Labandeira, J. J.; Ribeiro, A. C. F.; Concheiro, A.; Alvarez-Lorenzo, C. Syringeable Self-Assembled Cyclodextrin Gels for Drug Delivery. *Curr. Top. Med. Chem.* **2014,** *14* (4), 494-509.
121. Del Rosario, C.; Rodríguez-Évora, M.; Reyes, R.; Simões, S.; Concheiro, A.; Évora, C.; Alvarez-Lorenzo, C.; Delgado, A. Bone critical defect repair with poloxamine–cyclodextrin supramolecular gels. *Int. J. Pharm.* **2015,** *495* (1), 463-473.
122. Liu, K. L.; Zhang, Z.; Li, J. Supramolecular hydrogels based on cyclodextrin–polymer polypseudorotaxanes: materials design and hydrogel properties. *Soft Matter* **2011,** *7* (24), 11290-11297.
123. Choi, H. S.; Ooya, T.; Sasaki, S.; Yui, N.; Kurisawa, M.; Uyama, H.; Kobayashi, S. Spontaneous Change of Physical State from Hydrogels to Crystalline Precipitates during Poly-pseudorotaxane Formation. *ChemPhysChem* **2004,** *5* (9), 1431-1434.
124. Li, J.; Li, X.; Ni, X.; Wang, X.; Li, H.; Leong, K. W. Self-assembled supramolecular hydrogels formed by biodegradable PEO–PHB–PEO triblock copolymers and α-cyclodextrin for controlled drug delivery. *Biomaterials* **2006,** *27* (22), 4132-4140.
125. Wu, D. Q.; Wang, T.; Lu, B.; Xu, X. D.; Cheng, S. X.; Jiang, X. J.; Zhang, X. Z.; Zhuo, R. X. Fabrication of supramolecular hydrogels for drug delivery and stem cell encapsulation. *Langmuir* **2008,** *24* (18), 10306-10312.
126. Chen, Y.; Pang, X. H.; Dong, C. M. Dual Stimuli-Responsive Supramolecular Polypeptide-Based Hydrogel and Reverse Micellar Hydrogel Mediated by Host–Guest Chemistry. *Adv. Funct. Mater.* **2010,** *20* (4), 579-586.
127. Choi, H. S.; Yamamoto, K.; Ooya, T.; Yui, N. Synthesis of Poly (ε-lysine)-Grafted Dextrans and Their pH-and Thermosensitive Hydrogelation with Cyclodextrins. *ChemPhysChem* **2005,** *6* (6), 1081-1086.
128. Guo, M.; Jiang, M.; Pispas, S.; Yu, W.; Zhou, C. Supramolecular Hydrogels Made of End-Functionalized Low-Molecular-Weight PEG and α-Cyclodextrin and Their Hybridization with SiO2 Nanoparticles through Host− Guest Interaction. *Macromolecules* **2008,** *41* (24), 9744-9749.
129. Ma, D.; Xie, X.; Zhang, L. M. A novel route to in-situ incorporation of silver nanoparticles into supramolecular hydrogel networks. *J. Polym. Sci., Part B: Polym. Phys.* **2009,** *47* (7), 740-749.
130. Chen, Y.; Zhang, Y.-M.; Liu, Y. Multidimensional nanoarchitectures based on cyclodextrins. *Chem. Commun.* **2010,** *46* (31), 5622-5633.
131. Li, Z.; Yin, H.; Zhang, Z.; Liu, K. L.; Li, J. Supramolecular anchoring of DNA polyplexes in cyclodextrin-based polypseudorotaxane hydrogels for sustained gene delivery. *Biomacromolecules* **2012,** *13* (10), 3162-3172.

132. Gaucher, G.; Dufresne, M. H.; Sant, V. P.; Maysinger, D.; Leroux, J. C. Block copolymer micelles: preparation, characterization and application in drug delivery. *J. Controlled Release* **2005,** *109* (1-3), 169-188.
133. Simões, S.; Veiga, F.; Torres-Labandeira, J.; Ribeiro, A.; Sandez-Macho, M.; Concheiro, A.; Alvarez-Lorenzo, C. Syringeable Pluronic–α-cyclodextrin supramolecular gels for sustained delivery of vancomycin. *Eur. J. Pharm. Biopharm.* **2012,** *80* (1), 103-112.
134. Marcos, X.; Pérez-Casas, S.; Llovo, J.; Concheiro, A.; Alvarez-Lorenzo, C. Poloxamer-hydroxyethyl cellulose-α-cyclodextrin supramolecular gels for sustained release of griseofulvin. *Int. J. Pharm.* **2016**.
135. Rey-Rico, A.; Silva, M.; Couceiro, J.; Concheiro, A.; Alvarez-Lorenzo, C. Osteogenic efficiency of in situ gelling poloxamine systems with and without bone morphogenetic protein-2. *Eur Cell Mater* **2011,** *21* (4), 317-340.
136. Simões, S.; Veiga, F.; Torres-Labandeira, J. J.; Ribeiro, A. C. F.; Concheiro, A.; Alvarez-Lorenzo, C. Poloxamine–cyclodextrin–simvastatin supramolecular systems promote osteoblast differentiation of mesenchymal stem cells. *Macromolecular Bioscience* **2013,** *13* (6), 723-734.
137. Hashim, I. I. A.; Higashi, T.; Anno, T.; Motoyama, K.; Abd-ElGawad, A.-E. H.; El-Shabouri, M. H.; Borg, T. M.; Arima, H. Potential use of γ-cyclodextrin polypseudorotaxane hydrogels as an injectable sustained release system for insulin. *Int. J. Pharm.* **2010,** *392* (1), 83-91.
138. Zhang, Z. X.; Liu, K. L.; Li, J. A thermoresponsive hydrogel formed from a star–star supramolecular architecture. *Angew. Chem.* **2013,** *125* (24), 6300-6304.
139. Park, C.; Lee, K.; Kim, C. Photoresponsive Cyclodextrin-Covered Nanocontainers and Their Sol-Gel Transition Induced by Molecular Recognition. *Angew. Chem.* **2009,** *121* (7), 1301-1304.
140. Bruns, C. J.; Fujita, D.; Hoshino, M.; Sato, S.; Stoddart, J. F.; Fujita, M. Emergent Ion-Gated Binding of Cationic Host-Guest Complexes within Cationic M12L24 Molecular Flasks. *J. Am. Chem. Soc.* **2014,** *136* (34), 12027-12034.
141. Liu, J.; Chen, G.; Jiang, M. Supramolecular hybrid hydrogels from noncovalently functionalized graphene with block copolymers. *Macromolecules* **2011,** *44* (19), 7682-7691.
142. Du, P.; Liu, J.; Chen, G.; Jiang, M. Dual responsive supramolecular hydrogel with electrochemical activity. *Langmuir* **2011,** *27* (15), 9602-9608.
143. Chen, L. M.; Zhao, X.; Lin, Y.; Su, Z. H.; Wang, Q. Dual stimuli-responsive supramolecular hydrogel of bionanoparticles and hyaluronan. *Polym. Chem.* **2014,** *5* (23), 6754-6760.
144. Ogoshi, T.; Takashima, Y.; Yamaguchi, H.; Harada, A. Chemically-responsive sol-gel transition of supramolecular single-walled carbon nanotubes (SWNTs) hydrogel made by hybrids of SWNTs and cyclodextrins. *J. Am. Chem. Soc.* **2007,** *129* (16), 4878-4879.

Chapter 2

Host-guest polymers with hydrophilic poly(ethylene glycol) spacer, their inclusion properties and self-assembly in water

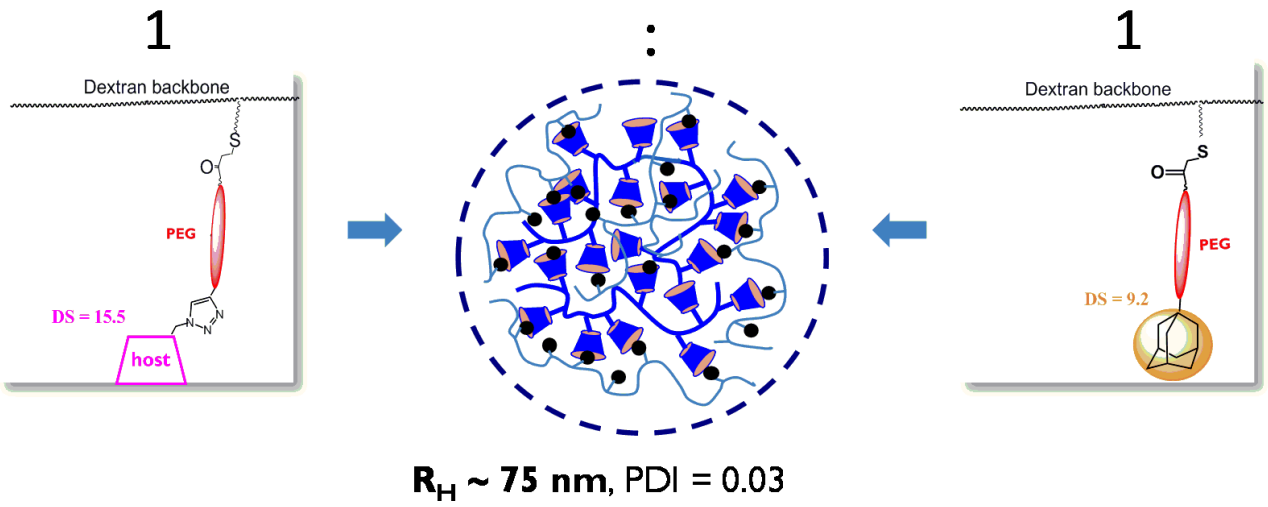

R_H ~ 75 nm, PDI = 0.03

Table of contents

Introduction

The focus of this chapter lies on the synthesis of dextran-based host and guest polymers with hydrophilic poly(ethylene glycol) (PEG) spacers and the study of host-guest nanoassemblies formed between them.

Cyclodextrins have proven to be beneficial in solving a number of food and pharmaceutical industries issues, such as formulation of poorly water-soluble drugs[1], masking odors[2] and several other purposes. Indeed, the inclusion of "guest" hydrophobic actives into the hydrophobic interior of the CD cavities usually allows to increase their apparent solubility[3], chemical stability and bioavailability.[1, 4] Given this, in the last years the researches are oriented toward the elaboration of colloidal or nanoscale carrier systems containing CDs, most usually based on cyclodextrin polymers (CD-polymers).[5] Such systems combine the advantages of CDs and polymers such as nanoscale size[6] and the possibility to assemble in the polymeric structure several functional elements, providing them with additional useful properties.[7] For instance, active targeting agents, fluorescent labels, “stealth” and stimuli-responsive blocks can be introduced in resulting nanocarrier structure.

Among the polymers used for drug delivery purposes, biopolymers and polysaccharides in particular are especially attractive. This is due to their biocompatibility, biodegradability and high content of easily modified hydroxyl groups. In recent years a handful of polysaccharide based CD-polymers were synthesized by various approaches such as βCD-linked chitosan by carbodiimide-mediated amidation[8] or hyaluronic acid[9] and dextran[10, 11] CD-polymers via reductive amination. Pendant CD moieties in such polymers were shown to preserve the conformation and good complexing characteristics of native cyclodextrins.[8, 12]

On the other hand, in the last years “click” chemistry has become an increasingly popular approach in organic and polymer synthesis. It involves the use of a bunch of effective, selective and adaptive to a wide range of functional groups, reactions.[13] Copper (I) catalyzed Huisgen azide-alkyne cycloaddition (CuAAC)[14, 15] and thiol-ene click chemistry[16, 17] appear to be by far the most prominent among them. CuAAC “click” chemistry has been already used for the synthesis of βCD-grafted polymethacrylates[18] and linear dextran-βCD polymers.[12] Linear dextran-βCD polymers have shown excellent, compared with the branched pβCD, binding properties. When

mixed in water media with their adamantane-grafted counterparts, dextran-βCD yield spherical nanoassemblies with controlled size. The latter, however, were found to lose their colloidal stability upon salt addition.[19] Being inspired by these examples, we were seeking to further advance the properties of both "host" and "guest" polymers by introducing the flexible hydrophilic spacer between the polymer backbone and βCD or adamantyl moieties.

We choose the thiolated dextran as a water-soluble, biocompatible backbone which is modified with bifunctional short PEG-acrylates by means of thiol-Michael addition click chemistry. Depending on the omega-end functionalization of PEG-acrylate, grafted dextrans bearing either hydrophobic adamantyl functions (guest polymer) or terminal alkynes are obtained. Further "clicking" of 6-monodeoxy-6-monoazido-βCD to the alkyne terminated dextran-*g*-PEG copolymer by copper(I)-catalyzed azide-alkyne cycloaddition is used to obtain βCD-bearing host counterpart. The binding properties of the polymers are studied in solution by isothermal titration microcalorimetry (ITC) and on the gold surface by surface plasmon resonance (SPR). The formation of host-guest nanoparticles upon mixing the host and guest counterparts' solutions in water is further studied by dynamic light scattering (DLS), static light scattering (SLS) and small-angle X-ray scattering (SAXS). The impact of the presence of the hydrophilic PEG spacer between the dextran backbone and the host/guest functions is estimated by comparing their binding properties with those of previously described dextran-based host-guest polymers with short hydrophobic spacers.[19]

Part of the work described in this chapter has been published in the Journal of Inclusion Phenomena and Macrocyclic Chemistry in 2014.[20]

1. Synthesis of the host-guest polymers with hydrophilic PEG spacer

1.1 General synthetic strategy

To prepare the rather complex aimed structures our strategy relied on modular synthetic design, involving thiolated 40 kDa dextran as a synthetic platform to obtain both host and guest polymers and orthogonal highly selective "click" reactions such as thiol-Michael addition click chemistry and copper(I)-catalyzed azide-alkyne dipolar cycloaddition (**Figure II.1**).

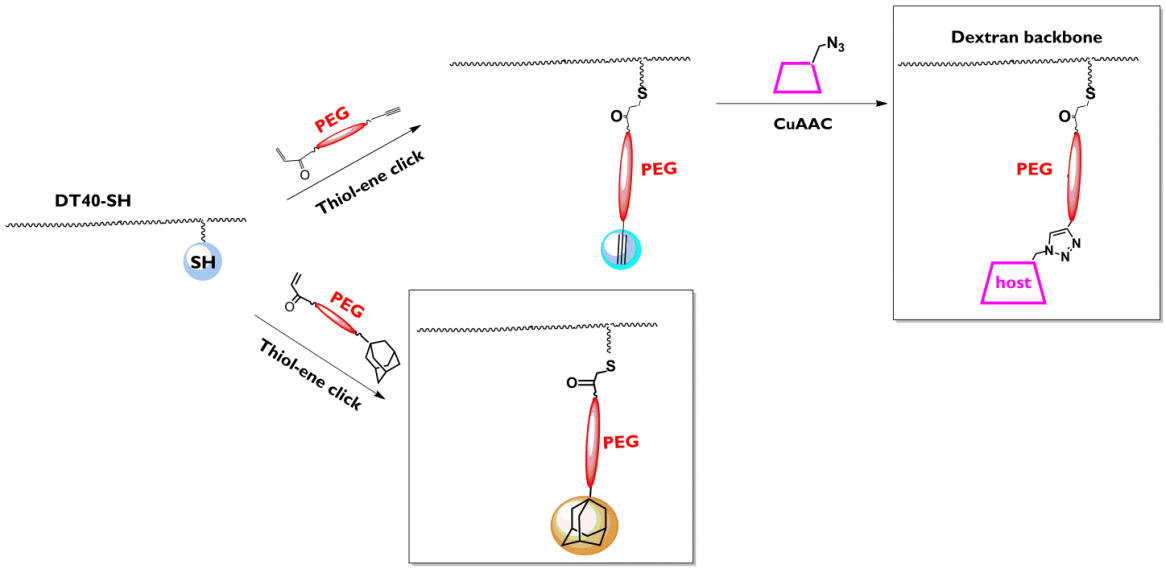

Figure II.1: Strategy of modular synthesis of dextran-based polymers with hydrophilic PEG spacer.

1.2 Synthesis of thiolated dextrans (DT40-SH)

The thiolation of dextran was chosen due to the vast synthetic possibilities provided by –SH groups. In this work it was used to graft monosubstituted short PEG chains bearing electron deficient C=C bonds using rapid and efficient thiol-ene "click" chemistry approach.[16] Thiol functionalized dextrans were obtained using the 2-step procedure reported by Hiemstra et al (**Scheme II.1**).[21] It consists in previous activation of the hydroxyl groups of dextran with 4-nitrophenyl chloroformate (4-NC) and its subsequent nucleophilic substitution with excess of cysteamine. By varying the amount of 4-NC in the first stage, a series of 4-NC activated dextrans with degrees of substitution (DS) varying from 9 to 25% were obtained (**Figure II.3**). The details of the synthetic procedures for all the described products may be found in the Experimental section.

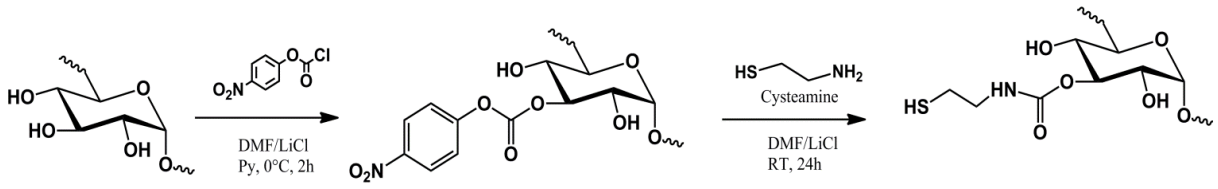

Scheme II.1: Reaction scheme representing the 2-step synthesis of thiolated dextran (DT40-SH).[21]

The DS values were obtained from ^{1}H-NMR in DMSO-d_6 by comparing the sum of the integrals of the 4-nitrophenyl (4-NP) aromatic protons (7.55 and 8.33 ppm) and the massive of the anomeric and 3 hydroxyl protons of dextran (4H) at 4.4-5.3 ppm (**Figure II.2**).

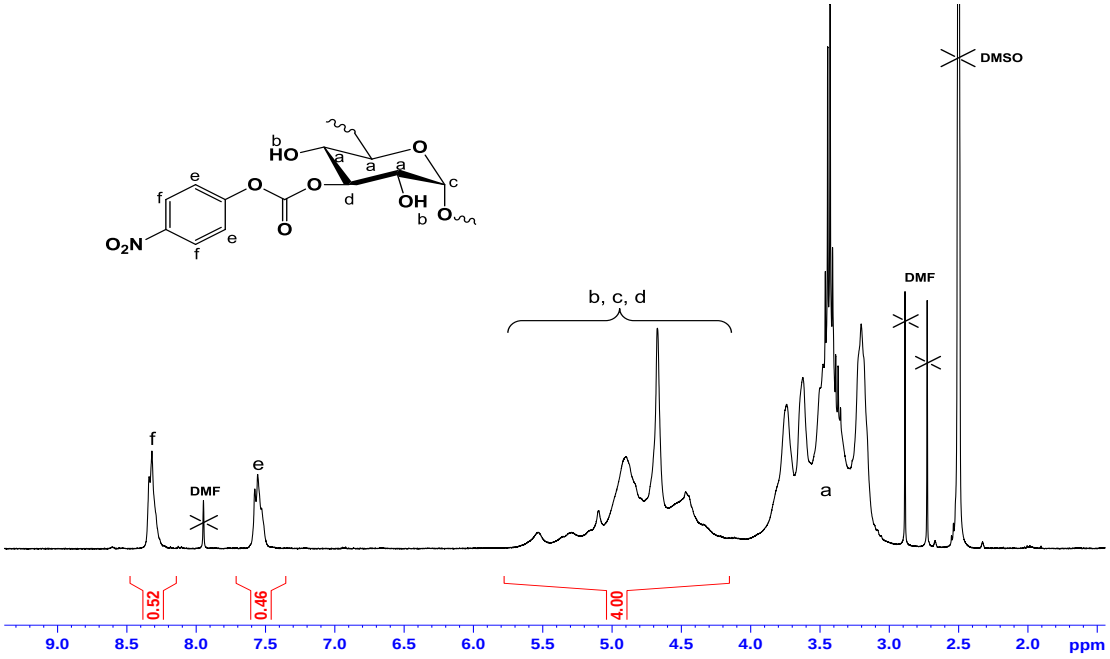

Figure II.2: ^{1}H-NMR spectrum (DMSO, 400 MHz) of DT40-4NC (DS_{4NC} = 24.5 mol.%). Traces of DMF are complicated to remove completely. However, it doesn't interfere with accuracy of DS determination and is used as a reaction medium in the next step.

The required [4-NC]/[AHG] (AHG – anhydroglucosidic ring) ratios were typically slightly higher than one given in the original article (0.56 for DS 15%).[22] As can be seen from the graph (**Figure II.3**), when going below the 0.3 ratio only negligible quantities of grafted 4-NP were found.

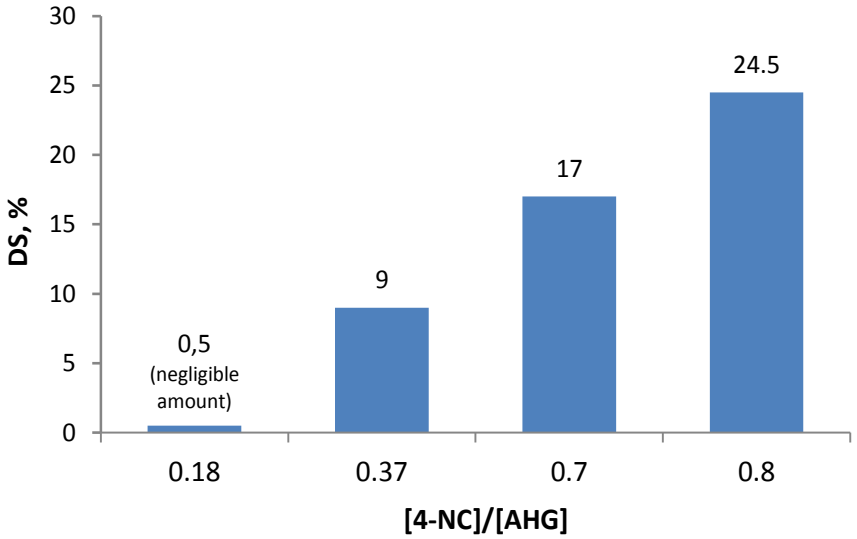

Figure II.3: Influence of the 4-NC/AHG ratio on the degree of substitution of 4-NC activated dextrans.

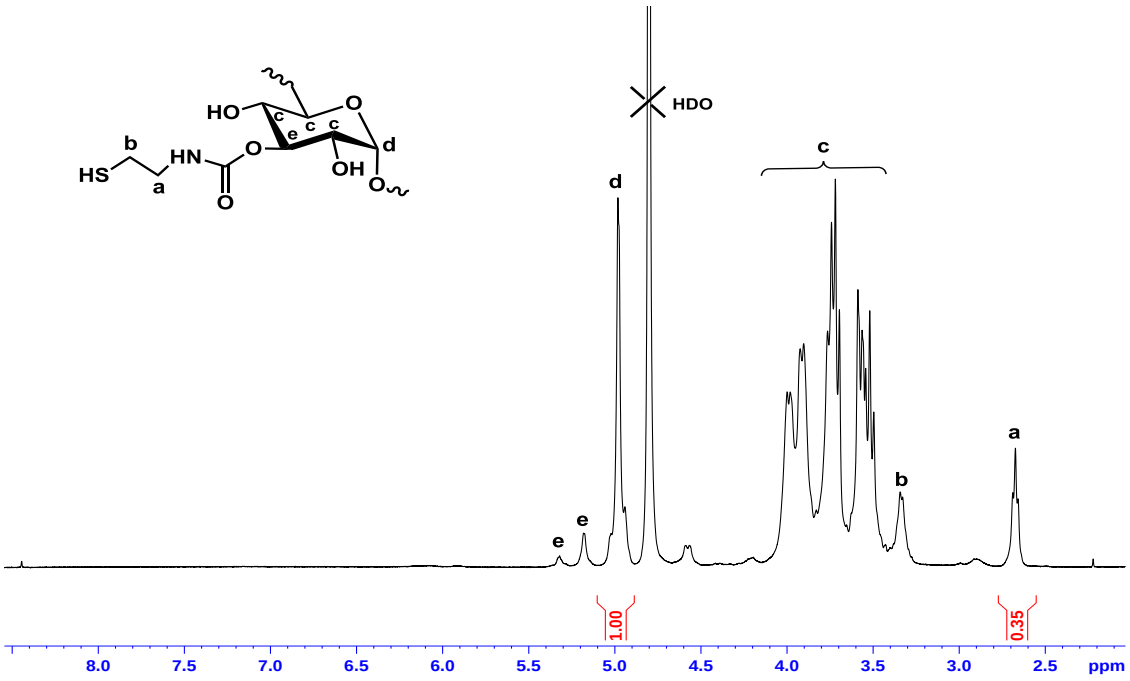

Figure II.4: ^{1}H-NMR spectrum (D_2O, 400 MHz) of thiolated dextran (DT40-SH, DS= 17.5 mol.%).

The subsequent nucleophilic substitution of 4-NP with an excess of cysteamine leads to Dext-SH. The final product purification implied the addition of reducing agent - dithioerythritol and following ultrafiltration under inert atmosphere in order to destroy and prevent the reformation of any disulfide S-S bonds. The DS of thiolated dextrans were calculated from ^{1}H-NMR in D_2O by

comparing the integrals of the well-resolved -CH_2- groups of grafted cysteamine (2.66 ppm) with the anomeric proton of dextran. The products were obtained with the yields of ca. 80% and an example of ^{1}H-NMR spectrum of DT40-SH bearing 17.5 mol.% of thiols, is shown in **Figure II.4**.

1.3 Synthesis of host polymers with hydrophilic PEG spacer (DT40-*g*-PEG-βCD)

The synthetic pathway to host polymers with PEG spacer implied preparation of hetero-bifunctionalized poly(ethylene glycol) acrylate bearing terminal alkyne (PEG-acryloyl-5-hexynoate) and 6-monodeoxy-6-monoazido-βCD (βCD-N_3) synthetic modules at the first stage. In the following step PEG-acryloyl-5-hexynoate is grafted to DT40-SH by means nucleophile-mediated thiol-Michael chemistry. Finally DT40-g-PEG-βCD is obtained by copper(I)-catalyzed 1,3-dipolar cycloaddition "click" reaction between DT40-g-PEG-hex-5-ynoate and βCD-N_3.

1.3.1 Steglich esterification of poly(ethylene glycol) acrylate with 5-hexynoic acid

Short poly (ethylene glycol) acrylate (Mn ~ 375, n = 9-10) was coupled with 5-hexynoic acid via mild Steglich esterification using dicyclohexylcarbodiimide (DCC) as a coupling agent and 4-(dimethylamino)pyridine (DMAP) as a catalyst (**Scheme II.2**).[23]

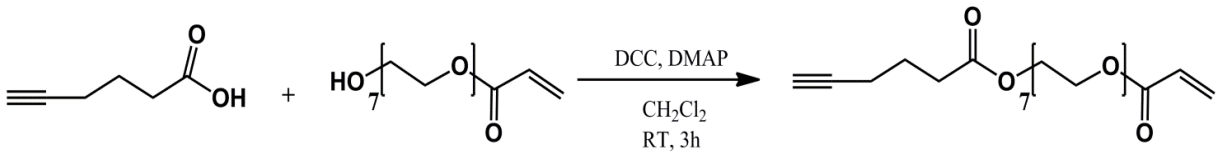

Scheme II.2: Synthesis of PEG-acryloyl-5-hexynoate by Steglich esterification.

The terminal –OH groups of PEG-acrylate were fully converted as evidenced by the ^{1}H-NMR data: emergence of a new triplet at 4.18 ppm corresponding to the -CH_2- group of PEG adjacent to grafted 5-hexynoate was observed; the latter has equal integral intensity with the triplet at 4.30 ppm belonging to the -CH_2- of PEG adjacent to acrylate (**Figure II.5**).

The obtained bifunctional PEG-acryloyl-5-hexynoate was used in the next step without extensive purification from the slight excess of 5-hexynoic acid, the latter being non-active in thiol-Michael addition reaction.

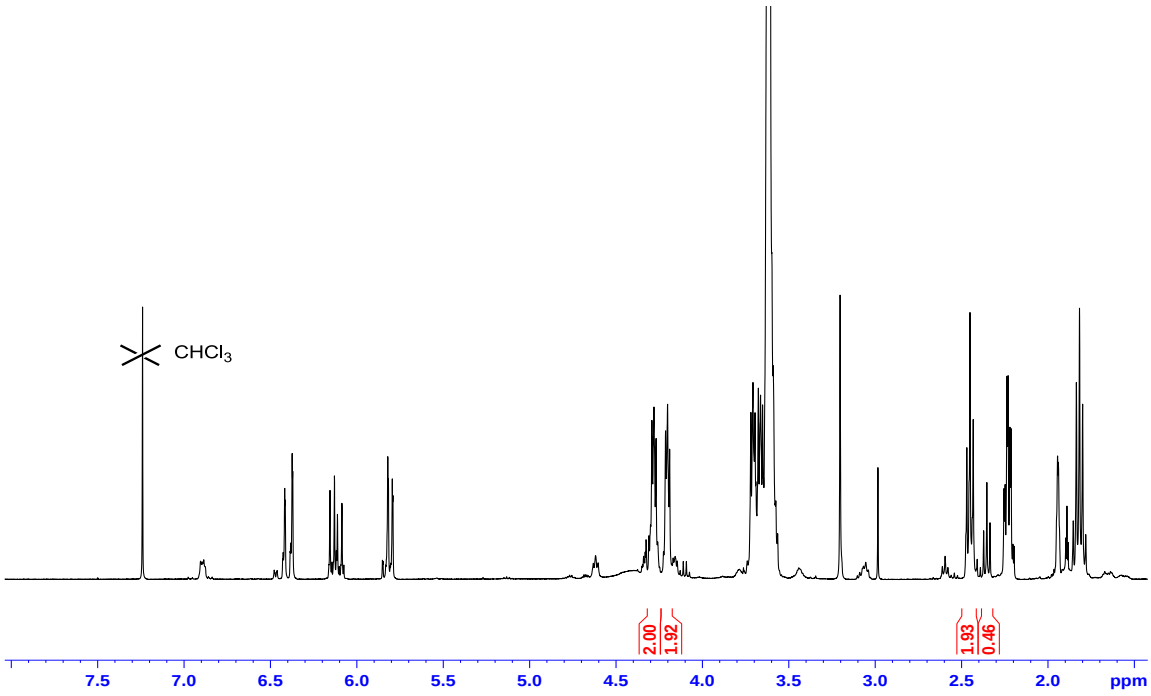

Figure II.5: ^{1}H-NMR spectrum ($CDCl_3$, 400 MHz) of PEG-acryloyl-5-hexynoate. The signal of -CH_2- of 5-hexynoic acid in the α-position to the carbonyl is shifted from 2.38 to 2.47 ppm once it's coupled to PEG. The signal at 2.38 ppm on the spectrum corresponds to the excess of 5-hexynoic acid.

1.3.2 Nucleophile-mediated thiol-Michael click of DT40-SH and PEG-acryloyl-5-hexynoate

In the next step PEG-acryloyl-5-hexynoate was attached to DT40-SH by means of nucleophile-mediated thiol-ene click chemistry.

The reactions of thiols with carbon-carbon double bonds have been attracting a lot of researchers' attention during the last decades due to the fact that they meet most of the requirements to the so-called "click" reactions conceptualized by B. Sharpless et al. in 2001: a) high yields with by-products (if any) that are removable by nonchromatographic processes, b) regioselectivity, c) insensitivity to oxygen or water, d) mild, solventless (or aqueous) reaction conditions, e) orthogonality with other common organic synthesis reactions, and f) amenability to a wide variety of readily available starting compounds.[24, 25]

Two main types of thiol-ene click reactions are commonly distinguished: thiol-ene free-radical addition to electron-rich carbon–carbon double bonds, and the catalyzed thiol Michael addition to electron-deficient carbon-carbon double bonds (**Scheme II.3**).

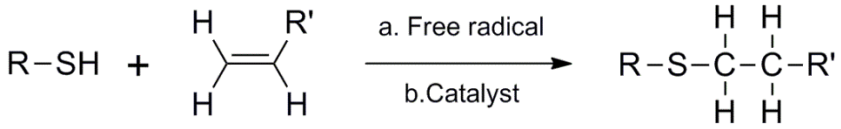

Scheme II.3: General thiol-ene couplings via: a) free radical and b) Michael addition processes. Adapted from Hoyle and Bowman.[25]

The suitability of thiol and C=C substrates for either free radical-mediated or Michael reactions is defined by their molecular structure with the general tendency for electron-deficient carbon-carbon double bonds and electron-rich thiols to be more active in Michael additions and reverse situation for free radical reactions. Given the commercial availability of monosubstituted short PEG acrylate bearing electron-deficient terminal C=C bonds, the latter had been used for preparation of bifunctional PEG-acryloyl-5-hexynoate in the previous step and defined our choice of Michael addition pathway for the preparation of alkyne-terminated DT40-g-PEG-hex-5-ynoate (**Scheme II.4**).

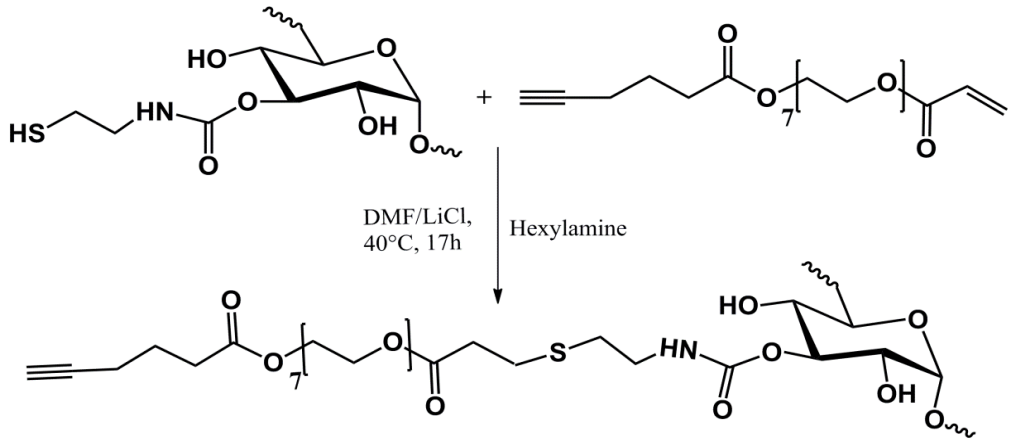

Scheme II.4: Synthesis of dextran grafted with alkyne-terminated 375 Da PEG chains - DT40-g-PEG-hex-5-ynoate via nucleophile-mediated thiol-Michael addition to the acrylate C=C bonds.

The concept of nucleophile-mediated thiol-Michael addition was introduced by Chan, Hoyle et al. in 2010.[16] It was demonstrated that primary and secondary aliphatic amines and especially phosphines, despite their lower comparing to tertiary amines basicity, provide dramatically increased rates of model reaction of hexyl acrylate and hexanethiol.[26] Based on this, authors concluded that, contrary to the accepted belief, the hydrothiolation process is mediated by nucleophilic addition of primary amine (or phosphine) to the activated C=C bond instead of

being simply catalyzed by base. They also proposed the assumed mechanism of the process (**Scheme II.5**).

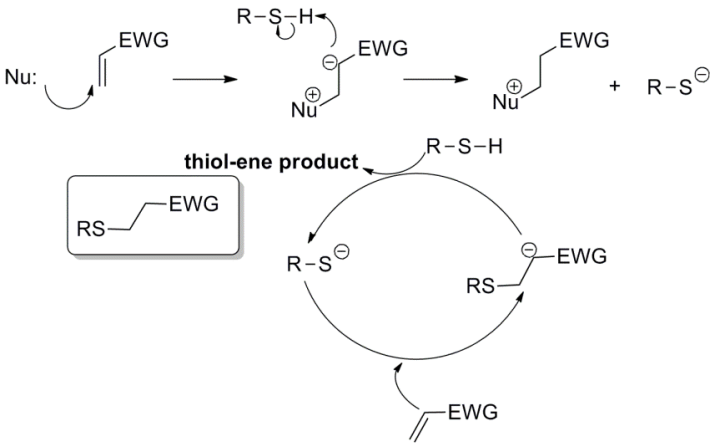

Scheme II.5: Assumed mechanism of the nucleophile-mediated hydrothiolation of an activated C=C bond (EWG stands for electron withdrawing group). Adapted from Hoyle et al.[16]

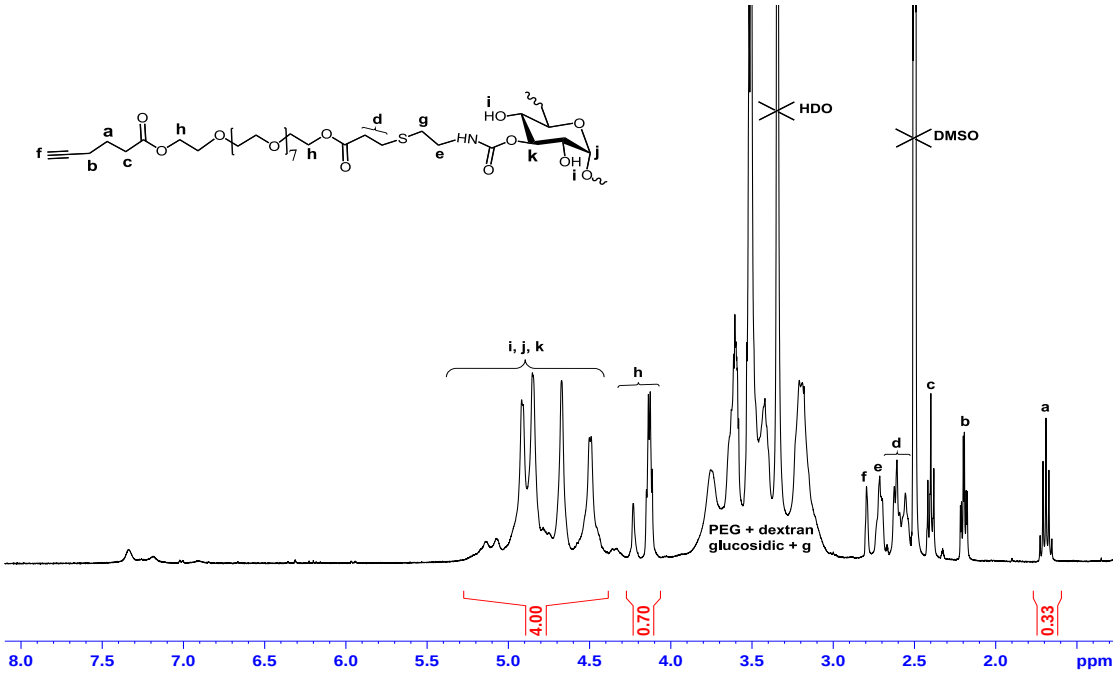

Figure II.6: ^{1}H-NMR spectrum (DMSO-d_6, 400 MHz) of DT40-g-PEG-hex-5-ynoate (DS= 16.2 mol.%). The signals at 4.20-4.30 ppm correspond to -CH_2- protons of PEG adjacent to -O-CO- groups of acrylate and 5-hexynoate.

Thus, the initial thiol-ene click trials were performed in water with hexylamine as nucleophilic catalyst and proved to be failed: no or negligible quantities of PEG-acryloyl-5-hexynoate were

"clicked" to the DT40-17SH (DS = 17 mol.%) backbone. Given the above, DMF was applied as an alternative of water, leading to dramatic improvements in the reaction profile. Nearly quantitative conversions of -SH groups were observed both for unmodified PEG methyl ether acrylate and for PEG-acryloyl-5-hexynoate within reasonable time (~24h) under mild conditions.

The DS of DT40-g-PEG-hex-5-ynoate was calculated from ^{1}H-NMR in DMSO-d_6 by comparing the integrals of βCH_2- of 5-hexynoic acid moiety at 1.69 ppm with the massive of the anomeric and 3 hydroxyl protons of dextran (4H) at 4.4-5.3 ppm (**Figure II.6**). The conversion was as high as 96%.

1.3.3 Synthesis of 6-Monodeoxy-6-monoazido-βCD (βCD-N_3)

Monosubstituted at primary side βCD-N_3 was prepared via slightly modified version of a two-step procedure found in literature (**Scheme II.6**).[12, 27]

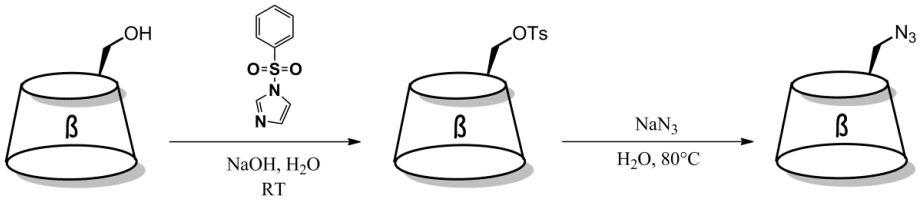

Scheme II.6: Reaction route for the azide-substituted βCD (βCD-N_3)

Monotosylated, selectively on the primary side, βCD (βCD-OTs) was synthesized using 1-(p-toluenesulfonyl)imidazole which was reported to give better, compared to *p*-toluenesulfonyl chloride (TsCl), results.[27] The low content of disubstituted product was achieved at the cost of relatively low yield (23%) and controlled by thin layer chromatography (TLC). In the second step the obtained βCD-OTs was converted into azide-substituted βCD (βCD-N_3) with a yield of 84% by reaction with the excess of NaN_3 in water media. The βCD-N_3 was characterized by ^{1}H-NMR (**Figure II.7**) and FTIR (**Figure II.8**).

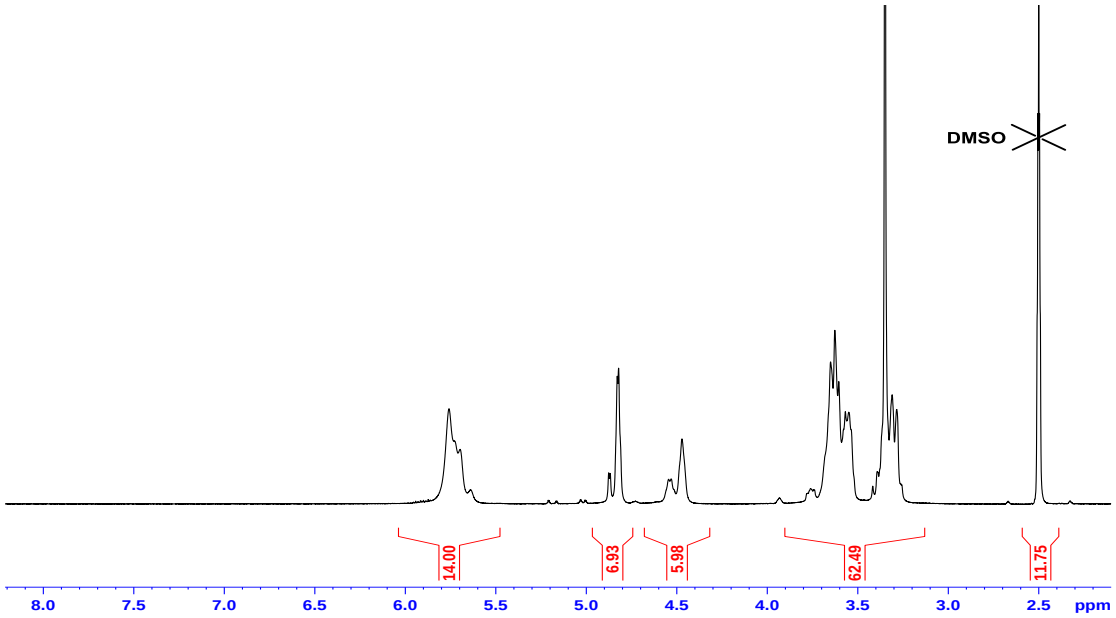

Figure II.7: ^{1}H-NMR spectrum ($DMSOd_6$, 400 MHz) of 6-monodeoxy-6-monoazido-βCD (βCD-N_3).

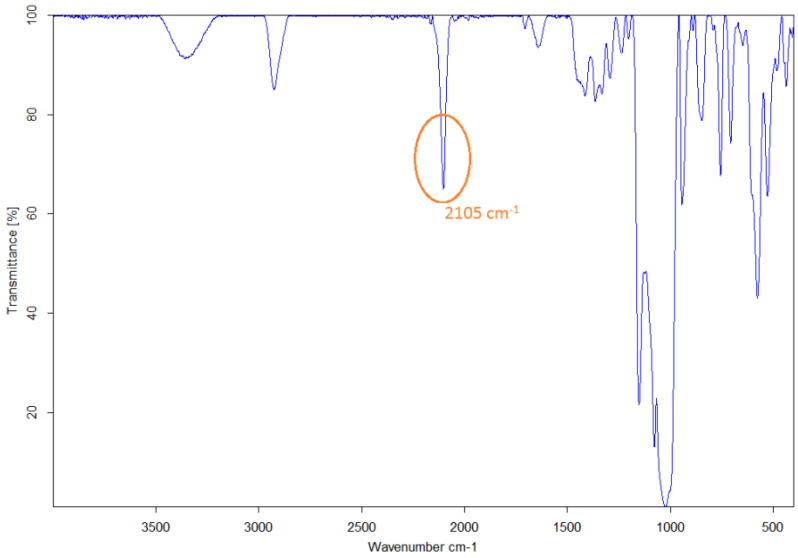

Figure II.8: IR-spectrum of mono-(O-6-deoxy-6-azido)-βcyclodextrin (βCD-N_3) showing the single peak at 2105 cm^{-1} corresponding to the grafted azides.

1.3.4 Synthesis of DT40-g-PEG-βCD by copper(I)-catalyzed azide-alkyne cycloaddition

To "click" βCD-N_3 to alkyne terminated DT40-g-PEG-hex-5-ynoate, Cu(I)-catalyzed azide-alkyne cycloaddition (CuAAC) in pure water or water-DMSO 1:1 mixtures with $CuSO_4$/Na-Asc as a catalytic system was tested first.

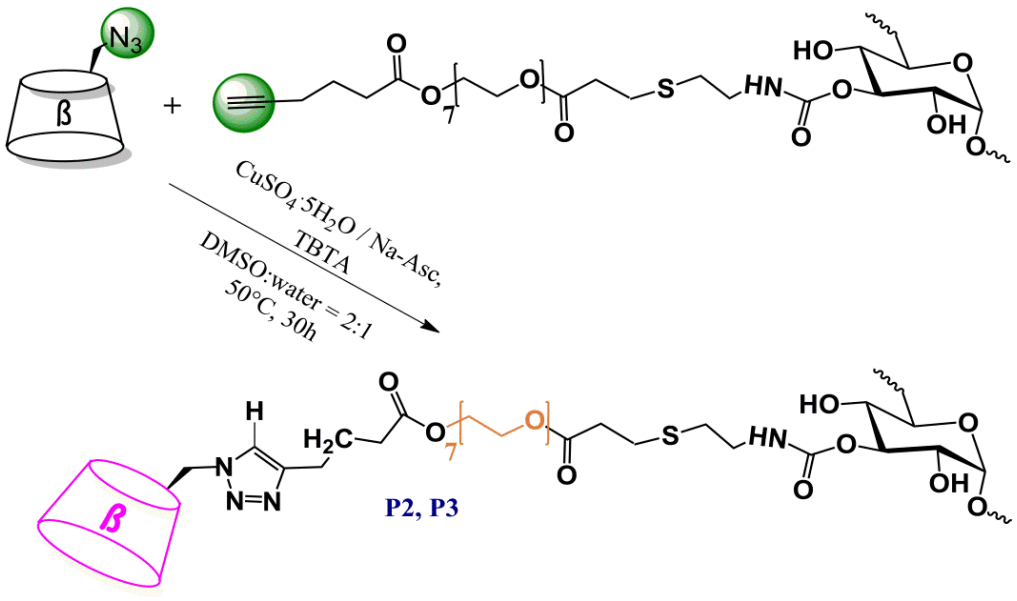

Scheme II.7: Synthesis of host polymer (DT40-g-PEG-βCD) by CuAAC with $CuSO_4$/Na-Asc+TBTA catalytic system.

The reaction mixtures were typically stirred at 50°C for 24h, purified by dialysis and freeze-dried. The βCD content of the obtained products was calculated from the ^{1}H-NMR in DMSO-d_6 by comparing the integrals of triazole proton at 7.79 ppm with the overlap of dextran and βCD anomeric and primary hydroxyl protons at 4.4-5.3 ppm. Namely, the integral value corresponding to the triazole proton (x), originating from the grafted βCD moiety, was defined as unity by calibration ($x = 1$). Then, the massive at 4.4-5.3 ppm contains 13 protons originating from the grafted moiety (7 anomeric and 6 primary hydroxyl $\rightarrow 13x$) and 4 protons originating from the dextran backbone ($4y$) (**Figure II.9-II.10**). The integral value corresponding to 1 proton from the dextran backbone (y) is obtained by subtracting 13 from the total integral value of the massive and dividing the residue by 4. Finally, the DS_{CD}(NMR) was calculated as the x/y ratio.

The obtained values turned out to be not more than 25% of the theoretical ones (**P0** in the **Table II.1**). In addition, a significant part of 5-hexynoate was not consumed as it is obvious from the splitting of the 5-hexynoate βCH_2- protons at 1.6-1.9 ppm (**Figure II.9**). This failure might be related to two principal reasons: a) oxidation of non-stabilized Cu(I)-catalyst; b) alkyne cross-coupling by Glaser, Straus or Erlington mechanisms.[15] The latter possibility appears probable, as in several cases of CuAAC carried out in DMSO partially gelly products were formed.

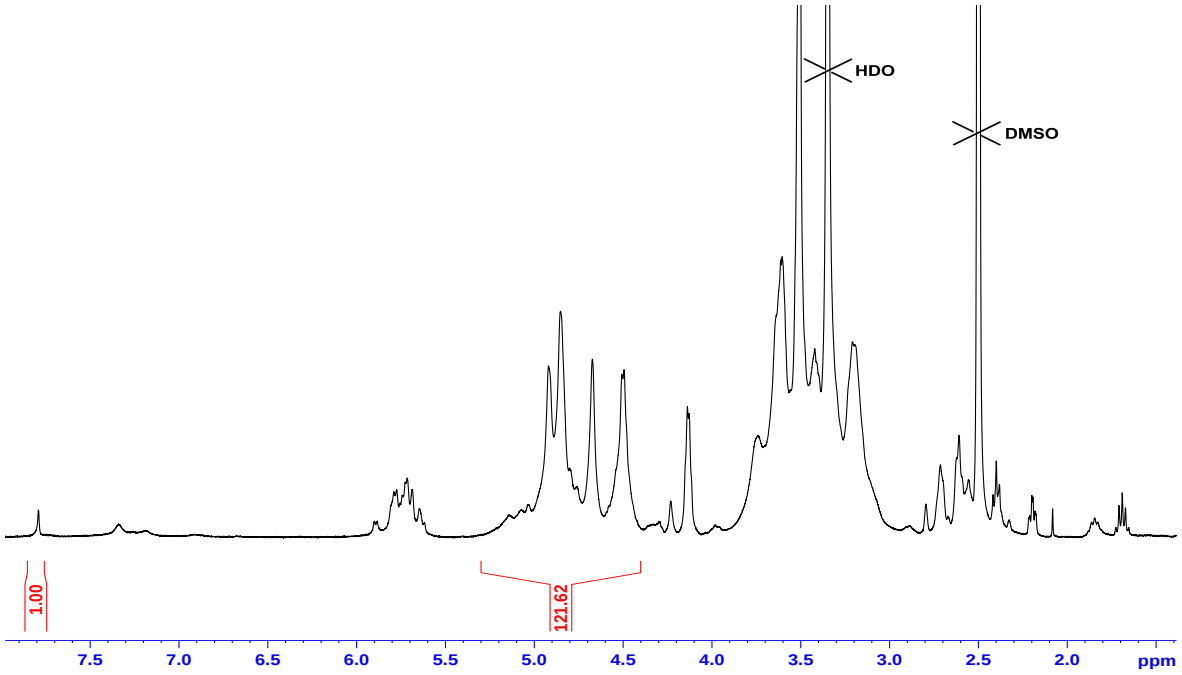

Figure II.9: ^{1}H-NMR spectrum (DMSO-d_6, 400 MHz) of DT40-g-PEG-βCD (DS_{CD} = 3.7mol.%) prepared by CuAAC in pure water without TBTA (**P0**). Redoubling of β-CH_2- protons of 5-hexynoate at 1.6-1.9 ppm is clearly observed.

Polytriazoles, and especially TBTA, were reported to lead to significant improvements in Huisgen cycloadditions on alkyne scaffolds when used as Cu(I)-stabilizing ligands.[12] Given this, the latter was synthesized following the previously described two-step procedure[28] and used in the next step. Regarding the rather hydrophobic character of TBTA, $Cu(MeCN)_4PF_6$/Na-Asc as a new catalytic system and pure DMSO as a reaction medium were applied. Despite being higher compared to **P0**, the DS_{CD} of the obtained product (**P1**) was still much lower than expected from the DS_{alkyne} of the starting DT40-g-PEG-Hex-5-ynoate (**Table II.1**). The βCD content could also be found from the ITC data using the approach described in greater detail in the 2.2 section of this chapter. Assuming the DS_{CD} determined by NMR correct, one should calculate the binding stoichiometry, *n*, between the grafted βCD and the titrant, 2-(1-adamantyl)ethyl trimethylammonium bromide (AdaTMA). Ideally the latter should equal to unity and DS_{CD}(ITC) = DS_{CD}(NMR). However, due to adsorbed water, inevitably present in freeze-dried polymer samples (~10-15 wt.%), the experimental *n* value, and consequently the resulting DS_{CD} are slightly lower than those obtained by NMR. As one can see, the ITC experiment confirmed the incompleteness of alkynes conversion for **P1** click assay (**Table II.1**).

Water was shown to be the most favorable solvent for CuAAC and tends to be used where appropriate regarding the solubility of the reaction components.[14, 15] Based on this we went back to the initially applied $CuSO_4$/NaAsc catalytic system, while using TBTA and DMSO/water 2:1 mixture as a reaction medium (**Scheme II.7**). ^{1}H-NMR spectra of the products obtained by this approach (**P2**, **P3** in **Table II.1**) showed complete disappearance of the peaks of terminal alkyne and -CH_2- in β-position to carbonyl of "unclicked" 5-hexynoate (at 2.79 and 1.69 ppm respectively) (**Figure II.10**). However, the apparent grafted amounts of βCD were still lower than theoretical (~ 84%), which must be related to: **a)** inaccuracies in phase calibration and baseline correction of the saturated spectra leading to overestimation of the integrals in the middle chemical shift range; **b)** alkyne cross-coupling still occurring to some extent due to higher reactivity of the triple bonds at the end of flexible PEG spacers.

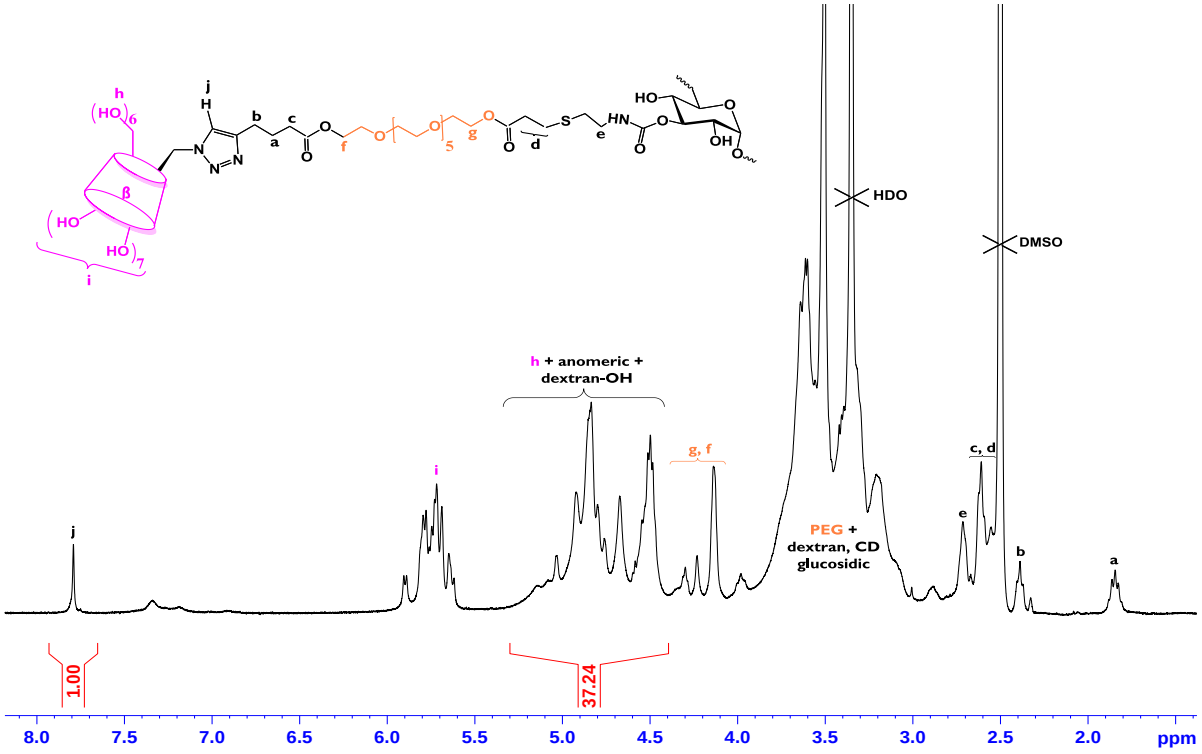

Figure II.10: ^{1}H-NMR spectrum (DMSO-d_6, 400 MHz) of DT40-g-PEG-βCD (DS_{CD} = 16.5 mol.%, **P3** in **Table II.1**).

Once again, the DS_{CD} of successful **P2** and **P3** samples deduced from ITC measurements are slightly lower than those obtained by NMR due to the adsorbed water contained in the freeze-dried products (**Table II.1**). The **P2** and **P3** polymers are relatively well soluble in water (s = 15

g/L) while both **P0** and **P1**, which contain residual terminal alkynes, have shown limited solubility in water (gel formation at concentrations higher than 10 g/L).

Table II.1. Characteristics of DT40-g-PEG-βCD polymers prepared by CuAAC with different catalytic systems

Entry	Catalytic system	DS_{alkyne} (NMR), mol.%	DS_{CD} (NMR), mol.%	DS_{CD} (ITC), mol.%	Alkyne to CD conversion, %	Yield, %
P0	$CuSO_4$/Na-Asc, water	14.5	3.7	-	25.5	61
P1	$Cu(MeCN)_4PF_6$/Na-Asc+TBTA, DMSO	15.5	11.2	9.5	72.2	63
P2	$CuSO_4$/Na-Asc+TBTA, DMSO/water = 2:1	15.5	13.4	11.3	86.4	85
P3	$CuSO_4$/Na-Asc+TBTA, DMSO/water = 2:1	19.5	16.5	14.3	84.6	81

An inversion phenomenon of β-cyclodextrin dimers prepared by CuAAC was recently described by Menuel et al.[29] In particular, it was found that triazole-substituted on the primary side glucopyranose units undergo a spontaneous 360° rotation in water (**Figure II.11**). As a result, part of the spacers end up being deeply included inside one of the βCD cavities. Thereby, the latter become no longer available for inclusion complexation.

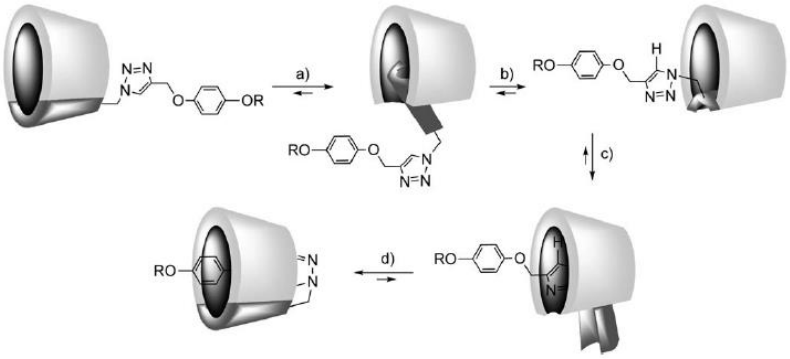

Figure II.11: Schematic illustration of the substituted glucopyranose inversion process for the case of *para*-isomer. Reprinted from Menuel et al.[29]

Furthermore, it was demonstrated that the extent of the inversion in water is strongly influenced by the nature of the bridge (or spacer) between the βCD cavities.[30] Thus, increased

proportions of dimers with only one out of two βCDs available were found in the cases where long and/or hydrophobic spacers had been used.

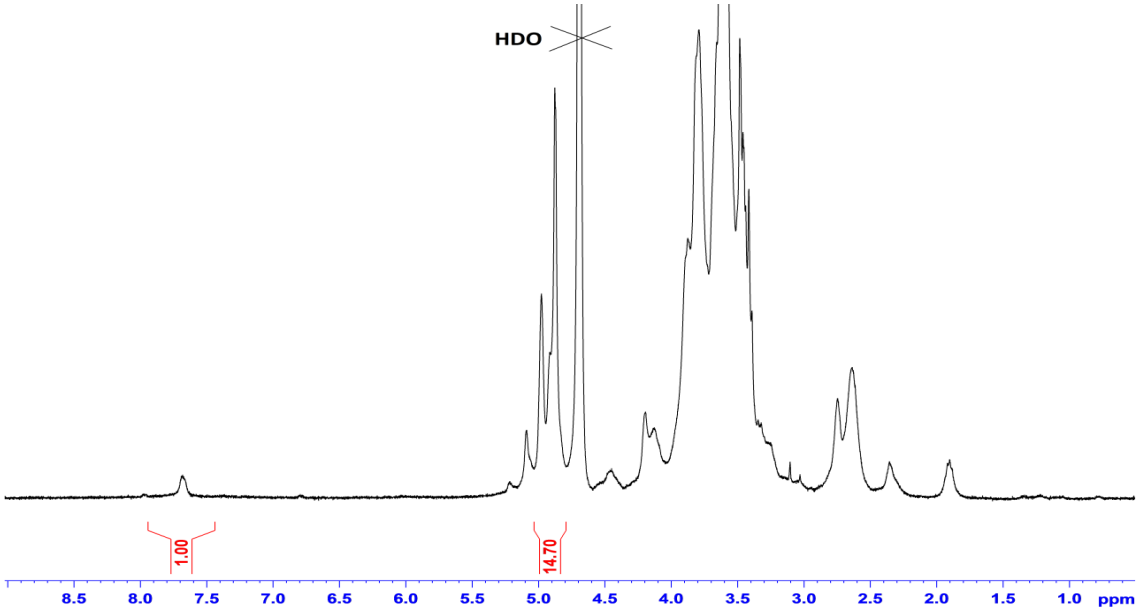

Figure II.12: ^{1}H-NMR spectrum (D_2O, 400 MHz) of DT40-g-PEG-βCD (**P2**). A single triazole proton signal is observed at 7.70 ppm.

Given the structure of prepared polymers, containing relatively long PEG spacers with 1,2,3-triazoles adjacent to primary face, the grafted βCD in DT40-g-PEG-βCD are likely to undergo inversion. However, we were not able to find a direct experimental confirmation of this. Only one, though quite broadened, singlet of triazole protons at 7.70 ppm, is observed in a 1D NMR spectrum of **P2** recorded in D_2O (**Figure II.12**). At the same time, emergence of distinct secondary singlets, corresponding to the triazole protons included in the βCD cavities, could be detected for the dimers undergoing inversion.[29] Nor could we detect any reliable cross-peaks between the triazole protons and inner anomeric protons of βCD in the 2D NOESY spectrum of **P2**.

The failure of our attempts to find the confirmation of the inversion phenomenon is most likely related to the polymeric structure of the investigated product, leading to lower sensitivity and intrinsic peak broadening in water, thus making separate triazole proton signals undistinguishable.

1.4 Synthesis of guest polymers with hydrophilic PEG spacer (DT40-g-PEG-Ada)

Hydrophobically modified with adamantyl groups (Ada) guest polymers were prepared following the similar, as in the case with their host counterparts, strategy. Briefly, monosubstituted poly(ethylene glycol) acrylate was functionalized directly with Ada-groups by esterification and subsequently grafted to DT40-SH by nucleophile-mediated thiol-Michael chemistry.

1.4.1 Synthesis of hetero-bifunctionalized PEG-acrylate-Ada

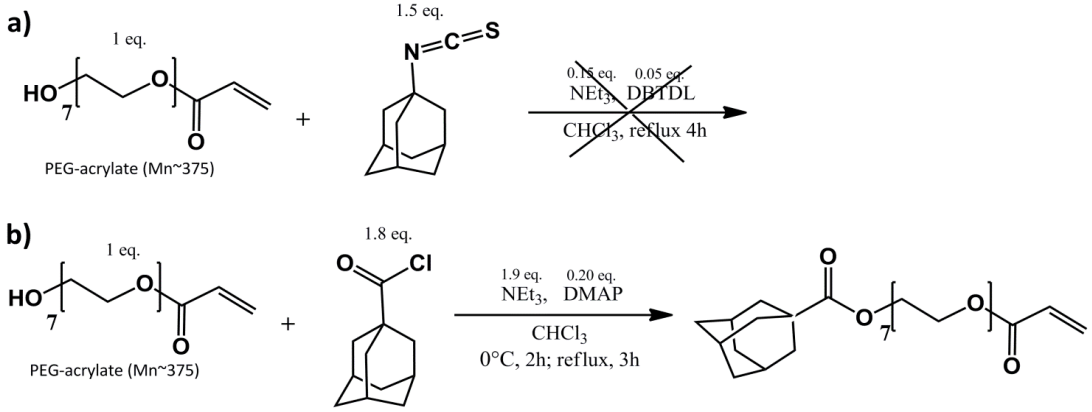

Scheme II.8: Synthesis of PEG-acrylate-Ada: a) by DBTDL-catalyzed isothiocyanate-alcohol reaction; (b) DMAP-catalyzed esterification with 1-adamantanecarbonyl chloride.

To modify PEG-acrylate with adamantyl groups, dibutyltin dilaurate (DBTDL)-catalyzed isothiocyanate-alcohol coupling was tested first. 1-Adamantyl isothiocyanate (AdaNCS) was chosen instead of its counterpart isocyanate because of its lower moisture-sensitivity and easiness of handling. Surprisingly, the reaction didn't work in this case: no detectable amount of Ada-NCS was coupled to PEG-acrylate after 4h of refluxing in $CHCl_3$ (**Scheme II.8, a**). It was evidenced from the ^{1}H-NMR spectrum of the product, where a single triplet at 4.25 ppm, corresponding to the terminal -CH_2- group of PEG adjacent to acrylate, was detected (**Figure II.13, a**).

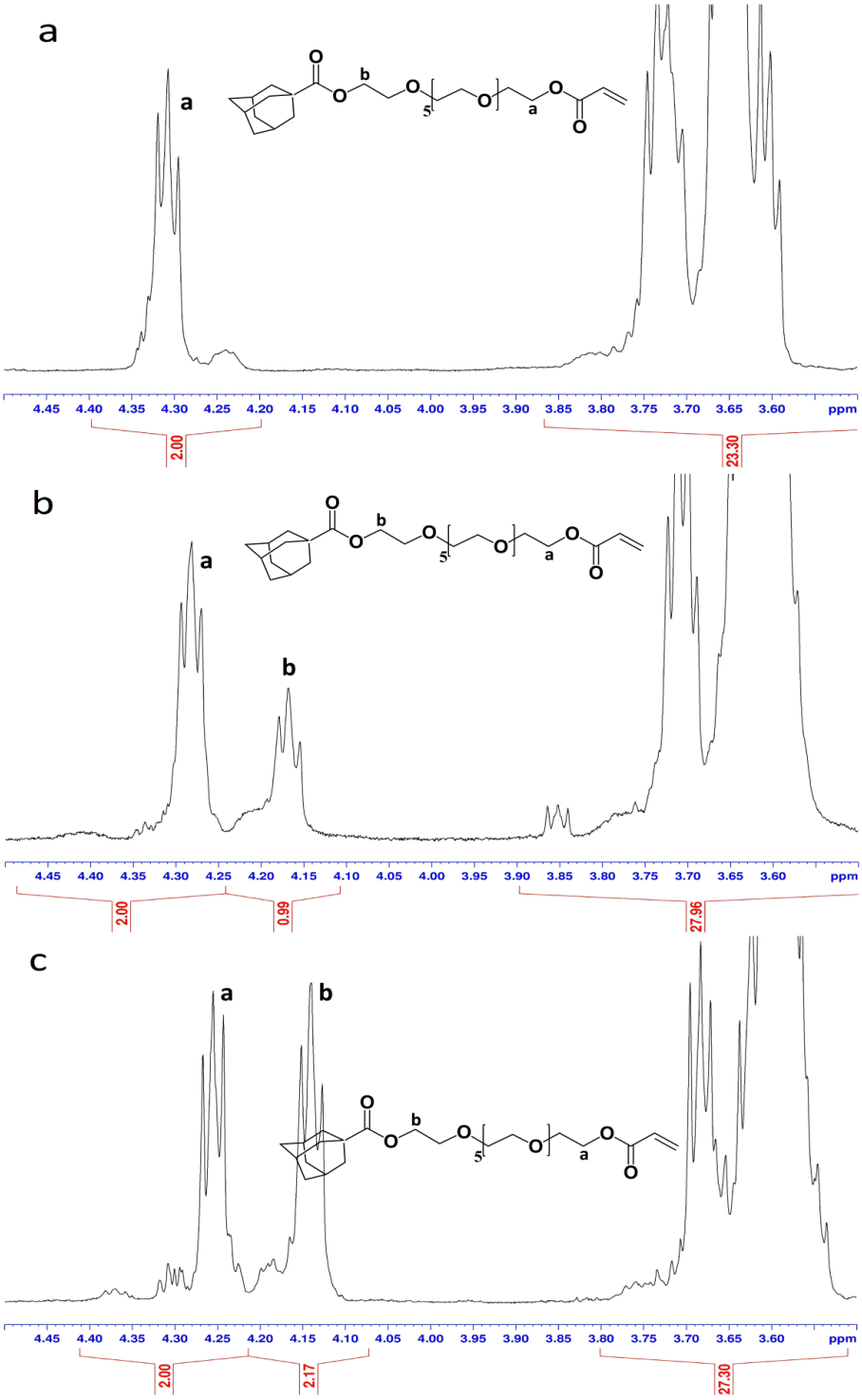

Figure II.13: ^{1}H-NMR spectra ($CDCl_3$, 400 MHz) of the products of PEG-acrylate modification via: **a)** DBTDL-catalyzed coupling with Ada-NCS; **b)** DMAP-catalyzed esterification with 1-adamantanecarbonyl chloride (3h reflux in $CHCl_3$); **c)** DMAP-catalyzed esterification with 1-adamantanecarbonyl chloride (2h at 0°C + 3h reflux in $CHCl_3$).

Some controversial data on isothiocyanate-hydroxyl group reactivity profile are found in literature. Thus, de Belder et al. described successful modification of dextran by fluorescein-isothiocyanate in the presence of DBTDL and pyridine in DMSO[31]; at the same time in a more recent example Wiberg et al. have reported much lower reactivity of phenyl isothiocyanate (PhNCS) comparing to phenyl isocyanate (PhNCO) in the reaction with cyclohexanol catalyzed by a tertiary amine in dichloromethane (DCM) – no product formation was observed even after 24h of stirring at room temperature in the case of PhNCS.[32] In our case the failure might be due to the relatively low effective concentration of the alcohol groups at the ends of bulky PEG chains; indeed, a second order dependence of the rate of the reaction on the alcohol concentration was found in the work of Wiberg et al.[32]

Given the above, in the next step we tested the 4-dimethylaminopyridine (DMAP)-catalyzed esterification of PEG-acrylate with 1-adamantanecarbonyl chloride in $CHCl_3$ (**Scheme II.8, b**). Significantly improved results were achieved after refluxing the reaction mixture with catalytic amounts of DMAP and pyridine for 3h: emergence of a new triplet at 4.17 ppm corresponding to the -CH_2- group of PEG adjacent to grafted 1-adamantanecarbonyl was observed in the ^{1}H-NMR spectrum of the product (**Figure II.13, b**). However, its integral was only 50% of the expected value, indicating non-completeness of the reaction. Conducting the reaction at 0°C at the initial stage for 2h before switching to reflux proved to solve this problem - the integrals of the triplets at 4.15 and 4.25 ppm were quasi-equivalent, indicating the completeness of PEG-acrylate -OH groups' modification with Ada (**Figure II.13, c**).

1.4.2 Synthesis of DT40-g-PEG-Ada guest polymers

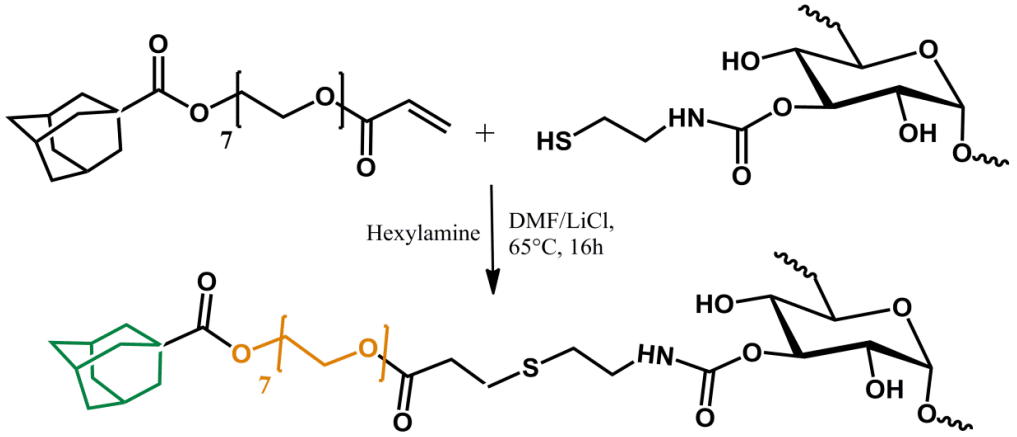

Scheme II.9: Synthesis of DT40-PEG-Ada by nucleophile-mediated thiol-Michael addition.

Likewise DT40-g-PEG-hex-5-ynoate, DT40-g-PEG-Ada was prepared by nucleophile-mediated thiol-Michael addition of bifunctional PEG-acrylate-Ada to the thiolated dextrans with different degrees of substitution (**Scheme II.9**). From 2 to 3 equivalents of PEG-acrylate-Ada with respect to thiols and reaction temperatures up to 65°C were required to reach the completeness of grafting. The DS_{Ada} of the products were obtained from ^{1}H-NMR in D_2O by comparing the integral of the ensemble of grafted Ada groups at 1.50-2.00 ppm (15H) with that of the anomeric proton of dextran (1H) (**Figure II.14**). The obtained polymers were water-soluble both at the DS (Ada) 5.1 and 10.5 mol. %. However, it should be noted that the values of DS (Ada) were lower (78-84%) compared to DS (SH) of the starting dextrans (**Table II.2**). At the same time the totality of -SH appear to be consumed given the quantitative grafting of PEG part (integral of 4H adjacent to clicked acrylate and 1-adamantyl chloride at 4.0-4.3 ppm in **Figure II.14**) and good water-solubility and, hence, non-cross-linked nature of the polymers. A possible explanation of this might be a partial hydrolysis of the ester bonds during the synthesis and purification by dialysis and, once again, uncertainties in the integration of oversaturated ^{1}H-NMR spectra (**Figure II.14**).

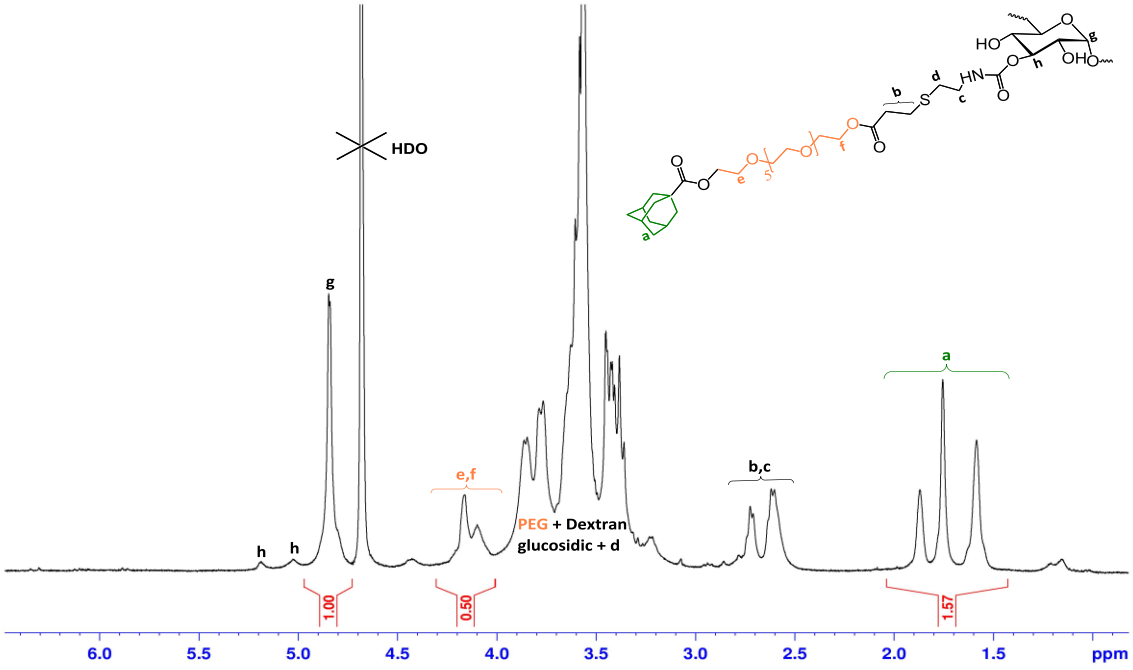

Figure II.14: ^{1}H-NMR spectrum (D_2O, 400 MHz) of DT40-g-PEG-Ada (DS_{CD} = 10.5 mol. %).

Table II.2. Degree of substitution and yields of DT40-g-PEG-Ada polymers

Compound	DS (-SH), mol.%	DS (Ada), mol.%	-SH to Ada conversion, %	Yield, %
DT40-g-PEG-Ada1	6.5	5.1	78.5	81
DT40-g-PEG-Ada2	12.5	10.5	84.0	84

2. Binding properties of host-guest polymers with hydrophilic PEG spacers

The binding properties of the polymers were investigated by ITC and SPR, aiming to compare them to those with short hydrophobic spacers and gain insight into the influence of the flexible hydrophilic PEG spacer.

2.1 Guest polymers - DT40-gPEG-Ada

2.1.1 Isothermal titration microcalorimetry studies

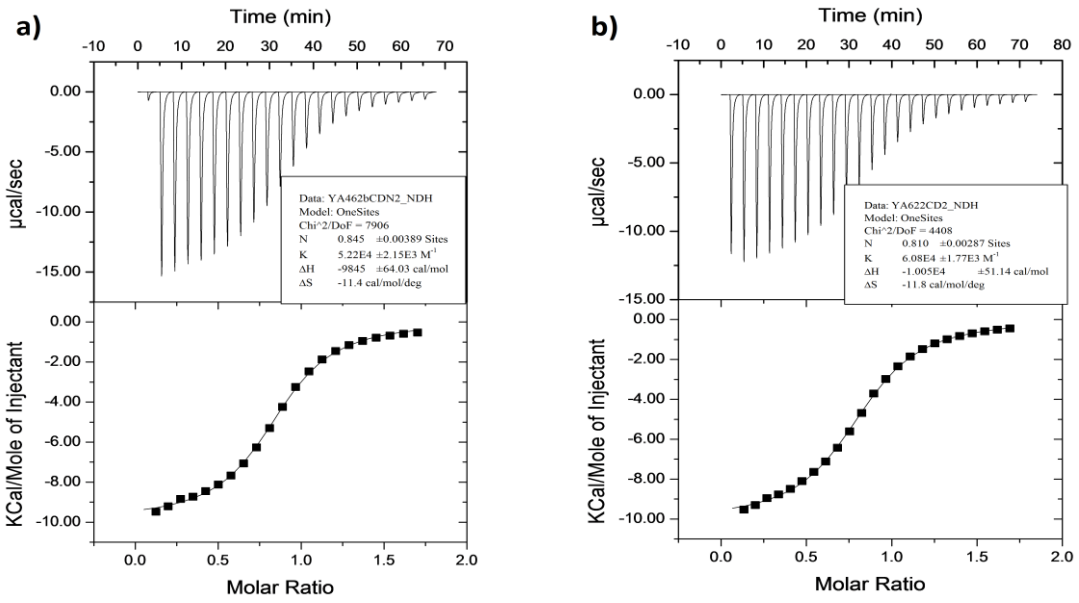

Figure II.15: ITC enthalpograms characterizing the interactions of βCD as monomeric hosts with DT40-g-PEG-Ada1 (**a**, 5.1 mol.% Ada) and DT40-g-PEG-Ada2 (**b**, 10.5 mol.% Ada) as hosts. Upper panel: amounts of heat released upon successive injection of 15 µL aliquots of βCD (5 mM) into solutions of DT40-g-PEG-Ada (0.5 mM in Ada). Bottom panel: integrated heat data, giving a differential binding curve which was fitted to a standard single-site binding model.

The ability of the DT40-g-PEG-Ada guest polymers to form inclusion complexes in solution was evaluated by ITC. According to the literature data, spherically shaped adamantane residues have a radius of ca. 3.6 Å, thus corresponding almost ideally to the dimensions of the βCD internal cavity (being approximately 3.3 and 3.0 Å).[33] The polymers were dissolved in pure water (C_{Ada} = $5.0 \cdot 10^{-4}$ M) and titrated with the solution of native βCD (C_{CD} = $5.0 \cdot 10^{-3}$ M); all the corresponding technical details may be found in the Experimental section. The interactions between the polymers and βCD are pronouncedly exothermic with the $|\Delta H|$ values as high as 39-42 kJ·mole^{-1}. The complex formation in this case is clearly enthalpy driven considering that entropy factor takes negative values (*TΔS* in **Table II.3**; **Figure II.15**). Large negative enthalpy changes may be attributed to strong Van der Waals interactions that arise due to the precise matching in size and shape between adamantane and βCD moieties.

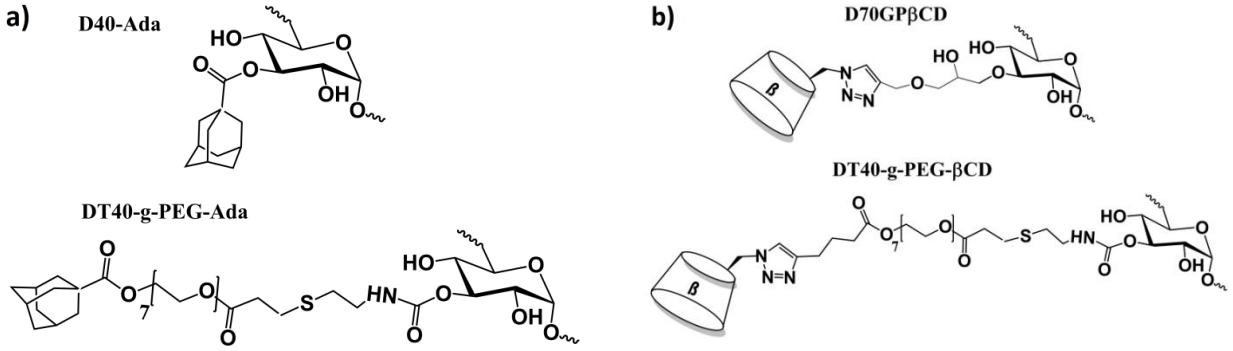

Figure II.16: Structural comparison of the investigated host (**a**) and guest (**b**) polymers.

Comparing the values of the binding constants (K_a in **Table II.3**) of DT40-g-PEG-Ada with those of the previously described Ada-substituted dextrans with adamantyl groups attached directly to the backbone via ester bond (**Figure II.16a**),[19] one can clearly see the beneficial impact of the PEG spacer on Ada groups' availability. It leads to an average 5-fold increase of K_a in polymers with close DS values (**Table II.3**). Interestingly, the gain in Gibbs free energy (ΔG) comes from less negative values of entropy factor *TΔS* for the guest polymers with PEG spacer, whereas both types of polymers show very similar large $|\Delta H|$ of interaction with βCD. This gain in entropy for DT40-g-PEG-Ada is most likely due to the enhanced mobility of the Ada-groups located at the end of the flexible PEG spacers.

Table II.3. Thermodynamic parameters of inclusion complexes formation of βCD with DT40-g-PEG-Ada and with the Ada-substituted dextrans with short spacers (DT40Ada)[19]

Polymer	DS^{NMR} (Ada), mol.%	K_a, L·mole^{-1}	ΔH, kJ·mole^{-1}	TΔS, kJ·mole^{-1}	ΔG, kJ·mole^{-1}
DT40-g-PEG-Ada1	5.1	$5.22 \cdot 10^4$	-41.2	-14.2	-27.0
DT40-g-PEG-Ada2	10.5	$6.08 \cdot 10^4$	-42.1	-14.7	-27.4
DT40Ada6	6.6	$1.16 \cdot 10^4$	-39.4	-16.2	-23.2
DT40Ada9	8.8	$1.14 \cdot 10^4$	-41.1	-17.9	-23.1

2.1.2 Surface plasmon resonance studies

To evaluate binding properties of the guest polymers on the surface, an SPR adsorption experiment was performed. Quaternary-ammonia modified branched βCD-polymer (pβCDN+; 58.2 wt.% of βCD; 1.62 positive charges per βCD) was used as an anchor to deposit on the golden surface of the sensor. The pβCDN+ was prepared according to the previously described procedure[34, 35] and its structural formula is given in **Figure II.17**.

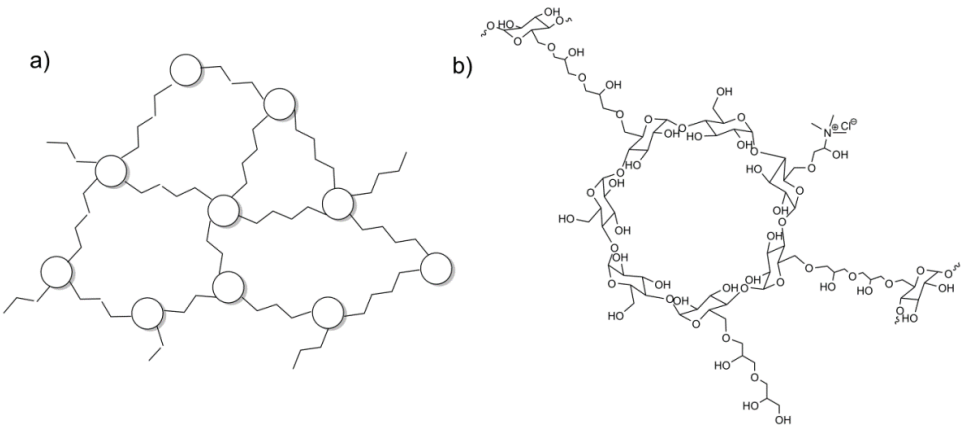

Figure II.17: Schematic representation (**a**) and chemical structure (**b**) of pβCDN+.

Due to the physical adsorption of pβCDN+, driven by non-specific and electrostatic interactions between the polymer molecules and gold, the refractive index (RI) probed by the SPR sensor in the vicinity of the surface is increasing (expressed as ΔRI_1 in **Figure II.18**). Typically 3 injections of 2 g/L pβCDN+ solutions were enough to reach the plateau in RI, indicating the surface

saturation, as shown in the first part of the sensorgram in **Figure II.19**. The sharp peaks in the sensogram observed at the moments of pβCDN+ injections correspond to sodium chloride, the polymer being dissolved in 0.5 M NaCl solution.

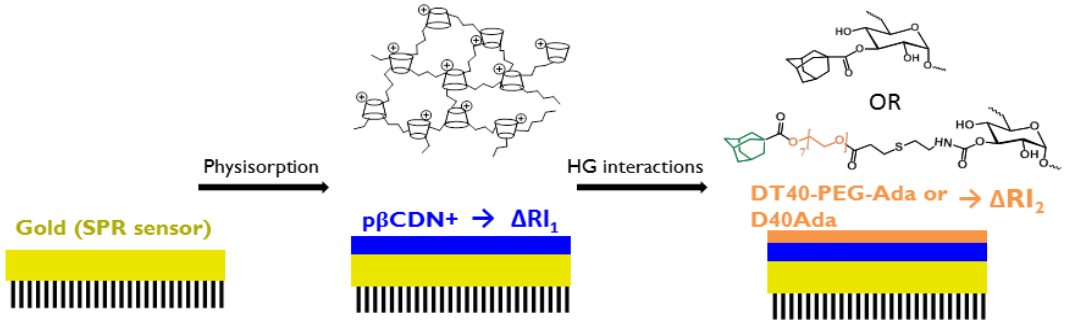

Figure II.18: Schematic representation of an SPR experiment for evaluation of D40Ada and DT40-gPEG-Ada binding properties on the surface (HG stands for host-guest interactions).

In the next step the solutions of investigated guest polymers DT40Ada9 (DS = 8.8 mol.%) and DT40-g-PEG-Ada2 (DS = 10.5 mol.%) at 1 g/L were flowed over the gold/ pβCDN+ surface in two parallel experiments. The changes in RI due to the deposition of the 2nd layer were detected by the SPR sensor as ΔRI_2 (**Figure II.18, 19**).

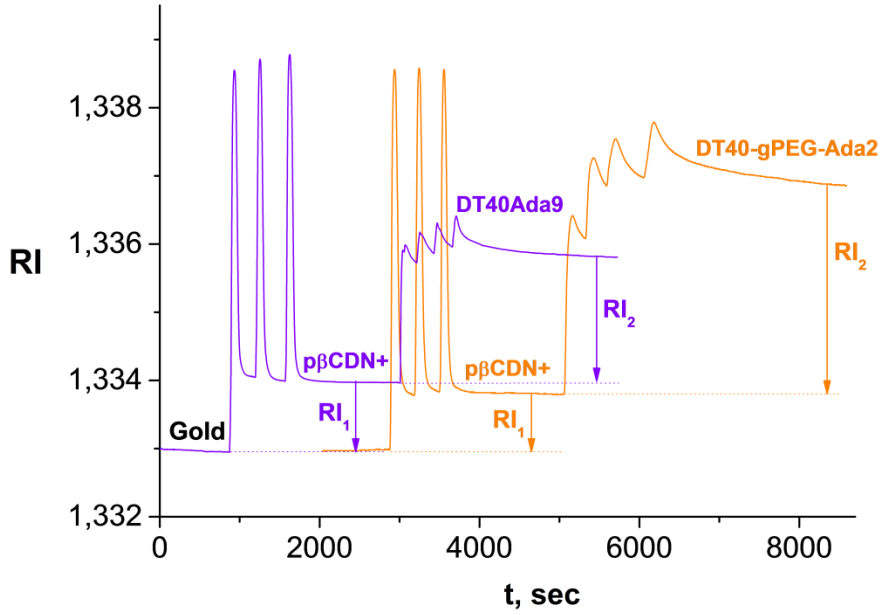

Figure II.19: SPR sensograms of the host-guest driven adsorption of D40Ada9 and DT40-gPEG-Ada2 on top of gold/ pβCDN+ bilayers.

As explained in greater detail in the Experimental section, from the refractive index variation data one may estimate the adsorbed amounts of the polymers (Q_{ads}), provided that their differential refractive indices (*dn/dc*) are known.[36] And that is by using the equation below:

$$Q_{ads} = \frac{\Delta RI \cdot l_d}{2m \cdot (dn/dc)_{pol}} \qquad \textbf{(II.1)}$$

where l_d is the depth of penetration of the evanescent electromagnetic field (typically 25-50% of the probing light wavelength); for this experiment it was roughly estimated as 37% (310.8 nm).[37] We assumed l_d to be constant upon each subsequent polymer adsorption, given the low density of highly hydrated layers and their thickness being much lower than 310.8 nm. The calibration coefficient *m* of the sensor was estimated as 1. For simplicity the *dn/dc* of the polymers was considered equal to that of dextran and native βCD (0.145 mL/g), given the proximity of the latter with the *dn/dc* of PEG (0.135 mL/g), according to the American Polymer Standards Corporation data (http://www.ampolymer.com/dn-dcValues.html).

The Q_{ads} values calculated in this way (**Table II.4**) were comparable to those found by Amiel and Wintgens for alkyl- and adamantyl-substituted poly(N-isopropylacrylamide)s (pNIPAm) adsorption on neutral pβCD layers.[37]

Difficulty was encountered in achieving exactly equal adsorbed amounts of the anchor pβCDN+ layer (ΔRI_1) for further parallel experiments with D40Ada9 and DT40-gPEG-Ada2; in addition, the studied polymers are characterized by a significant difference in DS (**Table II.3**). Given this, the most correct approach to compare their binding efficiencies should imply calculation of the number of βCD and adamantyl moieties per unit area in the 1st and 2nd adsorbed layers respectively. From the Q_{ads} [mg/m^2] of the polymers and the weight percentage (wt%) of βCD or adamantyl groups in them one can determine the Q_{ads} and number of moles of βCD/Ada groups. Then, using the Avogadro constant (N_A), the number of βCD/Ada groups per unit area can be estimated. The results of these calculations are reported in **Table II.4**. In agreement with the ITC data, considerably stronger interactions arise between pβCDN+ and the guest polymer with PEG spacer, as it might be concluded analyzing the Ada/CD ratios in the deposited bilayers.

Table II.4. Comparison of the binding efficiency of D40Ada9 and DT40-gPEG-Ada2 with respect to a positively charged cross-linked βCD-polymer (pβCDN+)

Experiment	Adsorbed layer	ΔRI, 10^3·a.u.	Q_{ads}, mg/m^2	N(CD, Ada)/m^2	Ada/CD ratio
no PEG spacer	pβCDN+	1.02	1.09	$3.76 \cdot 10^{17}$	1.58
	D40Ada9	1.85	1.98	$5.94 \cdot 10^{17}$	
PEG spacer	pβCDN+	0.86	0.92	$3.17 \cdot 10^{17}$	2.85
	DT40-gPEG-Ada2	3.08	3.30	$9.05 \cdot 10^{17}$	

2.2 Host polymers - DT40-gPEG-βCD

2.2.1 Isothermal titration microcalorimetry studies

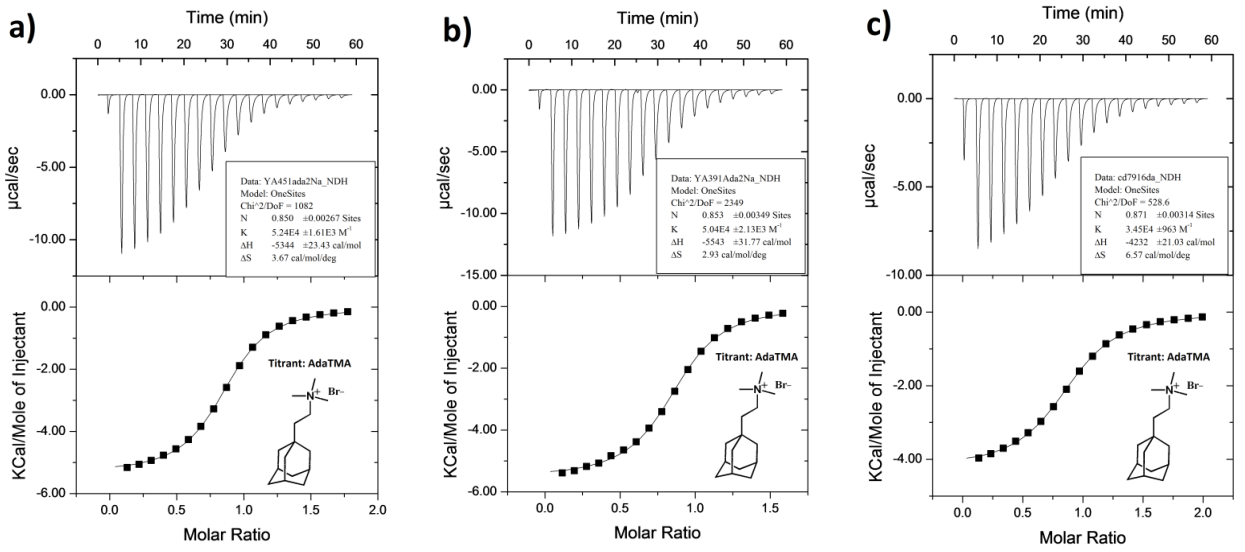

Figure II.20: ITC enthalpograms characterizing the interactions between AdaTMA as monomeric guest and different DT40-g-PEG-βCD as hosts: a) **P1**; b) **P2**; c) **P3**. Upper panel: amounts of heat released upon successive injection of 15 µL aliquots of AdaTMA (5 mM) into solutions of DT40-g-PEG-βCD (0.5 mM in βCD), both dissolved in 0.1 mol·L^{-1} NaCl. Bottom panel: integrated heat data, giving a differential binding curve which was fit to a standard single-site binding model.

Thermodynamic parameters of the inclusion complexation between DT40-g-PEG-βCD and model adamantane derivative, 2-(1-adamantyl) ethyl trimethylammonium bromide (AdaTMA), were studied by ITC. The polymers were dissolved in 0.1M NaCl solution in order to screen any

electrostatic repulsion between already included charged guests along the same chain. The interactions between the species are strongly exothermic, as expected for a complex formation between βCD cavities and an adamantyl derivative (**Figure II.20**).

The $|\Delta H|$ values are of 17-23 kJ·mole^{-1} and the complex formation is overall enthalpy driven (**Table II.5**). However, the gain in entropy factor due to the presence of flexible PEG spacer for DT40-g-PEG-βCD is even more pronounced than for the guest polymers described in the previous section. Indeed, the *TΔS* of DT40-g-PEG-βCD acquire positive values (3.6-8.2 kJ ·mole^{-1}) (**Table II.5**). In contrast, slightly negative values of *TΔS* are observed all the same for native βCD[38], epichlorhydrin pβCD[38] and linear dextran-βCD polymers.[12] The binding constants (K_a) are of 5.04·10^4 (**P2**) and 3.45·10^4 L·mole^{-1} (**P3**), which is significantly higher than for epichlorhydrin pβCD (~1·10^4 L·mole^{-1}) but, yet, lower than those of previously reported by our group linear dextran-βCD polymers (DT70GPβCD) with βCD linked to dextran via short ether bond (ca. 1-2·10^5 L·mole^{-1}, **Table II.5**).[12] Comparison of the structural formulas of the investigated polymers is shown in **Figure II.16, b**. This finding was surprising given the nature of flexible hydrophilic spacers which were supposed to increase the availability of βCD moieties.

Table II.5. Thermodynamic parameters of inclusion complexes formation of AdaTMA with DT40-g-PEG-βCD and with the host polymers with short hydrophobic spacers (DT70GPβCD)[12]

Polymer	DS^{NMR} (CD), mol.%	n	K_a, L·mole^{-1}	ΔH, kJ·mole^{-1}	TΔS, kJ·mole^{-1}	ΔG, kJ·mole^{-1}
DT40-g-PEG-βCD (P1)	11.2	0.85	5.24·10^4	-22.4	4.6	-27
DT40-g-PEG-βCD (P2)	13.4	0.85	5.04·10^4	-23.2	3.6	-26.8
DT40-g-PEG-βCD (P3)	16.5	0.87	3.45·10^4	-17.7	8.2	-25.9
DT70GPβCD5	12.7	0.85	2.05·10^5	-31.9	-1.3	-30.6
DT70GPβCD6	16.8	0.82	1.90·10^5	-31.9	-1.4	-30.5

2.2.2 Surface plasmon resonance studies

To verify the unexpected results described above, in the next step we looked into the binding properties of the host polymers of different types on the surface. The SPR binding experiments

were structured in a more complex way compared to the one utilized for the guest polymers. Namely, the same quaternary-ammonia modified pβCDN+ (**Figure II.17**) was used as the 1st layer to saturate the gold surface of the sensor. Its deposition resulted in an increase of the measured refractive index ΔRI_1.

A layer of the guest polymer with PEG spacer (DT40-g-PEG-Ada, DS = 10.5 mol.%) was then adsorbed on top of pβCDN+ layer via host-guest interactions, resulting in a 2nd increase in refractive index (ΔRI_2 in **Figure II.21**).

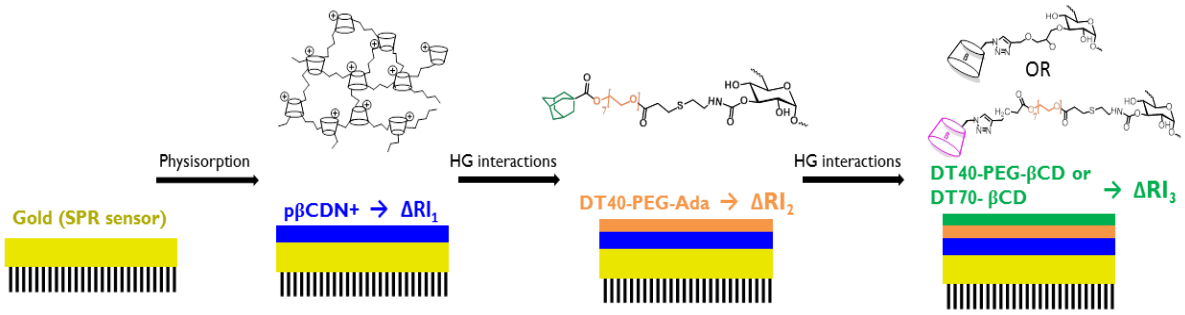

Figure II.21: Schematic representation of an SPR experiment for evaluation of DT70GPβCD8 and DT40-gPEG-βCD binding properties on the surface.

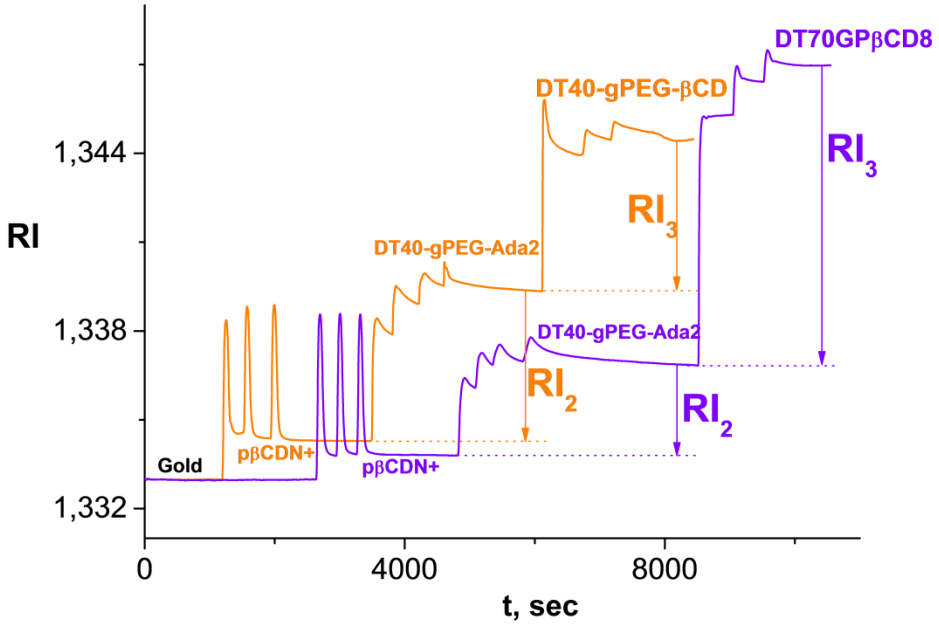

Figure II.22: SPR sensograms of the host-guest driven adsorption of DT70GPβCD8 and DT40-gPEG-βCD on top of gold/ pβCDN+/ DT40-g-PEG-Ada multilayers.

Finally, to compare the strength of host-guest interactions between DT40-g-PEG-Ada and either DT70GPβCD8 (DS = 26.2 mol.%) or DT40-gPEG-βCD (**P3**, DS = 16.5 mol.%), the solutions of host polymers with equal mass concentrations (1 g/L) were flowed over the surface of gold/ pβCDN+/ DT40-g-PEG-Ada in two parallel experiments. The changes in RI due to the deposition of the 3rd layer were detected by the SPR sensor as ΔRI_3 in this case (**Figure II.21,22**).

As in the previous case, the adsorbed amounts of the polymers Q_{ads} were calculated using the equation **(II.1)**, assuming the evanescent field penetration depth l_d to be 310.8 nm and *dn/dc* equal to 0.145 mL/g for all investigated polymers. Based on Q_{ads}, the numbers of βCD- and Ada-moieties the in the 3rd and the 2nd adsorbed layers respectively (**Figure II.21**) were calculated. The results are reported in **Table II.6**. The CD/Ada molar ratio drops from 4.13 to 0.75 for DT70GPβCD8 and DT40-gPEG-βCD respectively, indicating higher binding efficiency for the host polymer with no PEG spacer. As in the case of the guest polymers, this result is coherent with the ITC data.

However, in the case of DT70GPβCD8, highly substituted (26 mol.%) by bulky βCD groups, one should also consider the sterical hindrance factor. Due to the local rigidity of DT70GPβCD8, after formation of the initial interpolymer host-guest links, the βCD in their vicinity can be restricted from approaching the surface. Saturation of the adamantyl surface sites should thus result in thicker adsorbed layers. In this case, the same number of free Ada binding sites on the surface is occupied by a higher number of DT70GPβCD8 molecules, leading to higher polymer coverage (Q_{ads}) and CD/Ada ratios (4:1). On the other hand, for DT40-gPEG-βCD with lower DS (16.5 mol.%) and with βCDs being more loosely attached to the backbone *via* PEG spacer, the host polymer local rigidity should be much lower. There should be much less hindrance toward linking neighboring βCDs on surface sites. As a matter of fact, in this case association tends to occur close to the stoichiometrical 1:1 CD/Ada ratio. These remarks show that the discussion of the adsorption mechanism of the host and guest polymers is quite complex, given that they involve multivalent interactions with several opposing effects. For instance, high substitution degree should favor cooperative interactions with a zip fastener mechanism leading to stoichiometric host/guest association. However, high substitution ratio can at the same time lead to increased local rigidity and anticooperativity.

Table II.6. Comparison of the binding efficiency of DT70GPβCD8 and DT40-gPEG-βCD with respect to guest polymer (DT40-g-PEG-Ada) surface layer by SPR

Experiment	Adsorbed layer	ΔRI, 10^3·a.u.	Q_{ads}, mg/m^2	N(Ada or CD)/m^2	CD/Ada molar ratio
no PEG spacer	DT40-g-PEG-Ada	3.12	3.28	$0.90 \cdot 10^{18}$	4.13
	DT70GPβCD8	10.12	10.86	$3.70 \cdot 10^{18}$	
PEG spacer	DT40-g-PEG-Ada	5.11	5.50	$1.51 \cdot 10^{18}$	0.75
	DT40-gPEG-βCD	5.14	5.46	$1.13 \cdot 10^{18}$	

Thus, the ITC and SPR studies of DT40-gPEG-βCD and DT40-gPEG-Ada show that the initial strategy of rendering the host and guest moieties more accessible for inclusion complexation by grafting them to a polymer backbone through flexible hydrophilic PEG spacer works in a desired way in the case of Ada-substituted guest polymers but proves to be less successful in the case of their βCD-substituted host counterparts.

3. Nanoassemblies prepared from host-guest polymers with hydrophilic PEG spacers

During the last decade size-controlled host-guest nanoassemblies based on cyclodextrin-modified polymers were reported in our group.[19, 39, 40] These had been obtained by simply mixing in pure water hydrophobically substituted (with alkyl chains or adamantyl groups) dextrans with either βCD-epichlorohydrin branched copolymers[39, 40, 41] or βCD-substituted linear dextrans with short spacers between the backbone and grafted βCD-groups[19]. Regarding their excellent biocompatibility profile together with avoiding the use of organic solvents and surfactants during the preparation stage, promising drug delivery applications of the host-guest nanoassemblies (HG nanoassemblies) were considered. However, they are characterized by a number of limitations, such as low stability over long periods of time and fast aggregation upon addition of salt.

One of the goals to prepare host and guest polymers with hydrophilic PEG spacer was to understand how the presence of the latter might affect the mobility and accessibility of grafted

Ada and βCD groups in order to address the mentioned drawbacks of the existing HG nanoassemblies. Thus, in the following part of the chapter we will focus on self-assembly of DT40-gPEG-βCD and DT40-gPEG-Ada in water. The obtained nanoassemblies will be characterized by various techniques, such as dynamic light scattering (DLS), small-angle X-ray scattering (SAXS) and static light scattering (SLS). Their size, structure and stability will be compared with those of the HG nanoassemblies prepared from the polymers with no PEG spacers and mixed nanoparticles where either host or guest polymer with PEG spacer is used.

3.1 Size and stability of HG-nanoassemblies by DLS

Interpolymer host-guest interactions, when sufficiently large in strength, might lead to associative phase separations in a certain concentration range of the components.[42] The cohesion of the polymers happens in a "zip fastener" manner due to the establishment of numerous inclusion complexes between the hydrophobic groups (alkyl, Ada) and the βCD cavities acting as physical crosslinks between the chains of the two polymers.

To achieve the associative phase separation and formation of HG-nanoassemblies between DT40-gPEG-βCD and DT40-gPEG-Ada we worked with the stock polymer solutions at fixed Ada groups and βCD molar concentrations ($2.5\text{-}5.0\cdot10^{-4}$ mole$\cdot$L^{-1}). Thus, different βCD/Ada molar ratios were achieved by simply varying the volumes of the stock solutions during the mixing process. The total polymer concentrations in the resulting nanoassemblies typically lied in the range of 0.50-1.36 g/L.

In the first experiment freshly prepared solutions of DT40-gPEG-βCD (**P3**, DS = 16.5 mol.%) and DT40-gPEG-Ada2 (DS = 10.5 mol.%) were mixed while varying βCD/Ada molar ratios (**Table II.7**). Surprisingly, with a slight excess of Ada groups and, even at equimolar ratios, formation of large, rapidly growing aggregates was observed (**Figure II.23, a**). This resulted in a fast drop of scattering intensity, caused by associative phase separation and precipitation (**Figure II.23, b**). However, when excess of βCD with respect to Ada was used the resulting nanoassemblies were smaller and more stable. At the same time, the experimental data for other types of HG nanoassemblies indicate that equimolar βCD/Ada ratios typically lead to the best results, which is explained by the opportunity to form the maximal number of physical links between the polymer chains in this case.[19, 40]

Table II.7. Hydrodynamic diameters of the nanoassemblies obtained from the freshly prepared DT40-gPEG-βCD (16.5 mol.%) and DT40-gPEG-Ada2 (10.5 mol.%) stock solutions

βCD/ Ada	C(host), g/L	C(guest), g/L	C_{tot}, g/L	D_h, nm			PDI			CR** (10^{-3}, kpcs)		
				5 min	5d	11d	5 min	5d	11d	5 min	5d	11d
1:1	0.38	0.30	0.68	249	503	pr.	0.05	0.01	pr.	52	16	pr.
1:2	0.23	0.36	0.59	1000	pr.*	pr.	1	pr.	pr.	17	pr.	pr.
2:1	0.46	0.18	0.64	146	305	401	0.05	0.09	0.10	111	30	15
3:1	0.57	0.15	0.72	139	295	330	0.06	0.04	0.01	92	29	23
4:1	0.61	0.12	0.73	128	266	334	0.05	0.11	0.06	59	28	20

*pr. – precipitation; ** - count rate.

3.1.1 Effect of the stock solutions aging

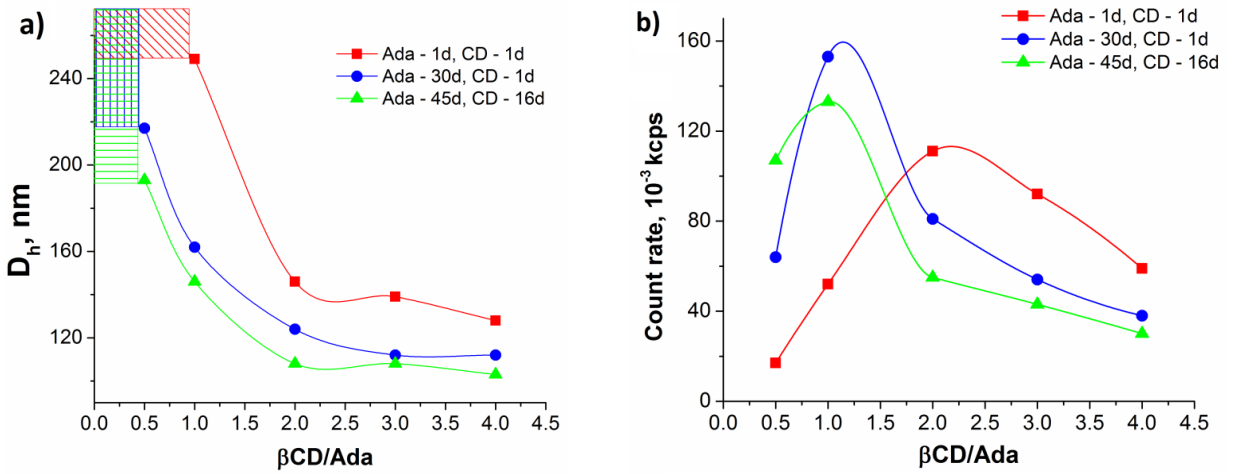

Figure II.23: Hydrodynamic diameters (**a**) and scattered intensity count rates (**b**) of the freshly prepared HG nanoassemblies prepared from DT40-gPEG-Ada2 (Ada) and DT40-gPEG-βCD (CD) solutions stored for different periods of time. Patterned area corresponds to precipitation region.

On the other hand, it was noticed that when the guest polymer solution used for self-assembly is stored for longer periods of time, nanoparticles with better characteristics are obtained. Given that, the DT40-gPEG-Ada2 stock solution was aged for 30 days at 4°C and used for analogue self-assembly experiment with freshly prepared DT40-gPEG-βCD solution. The results reported in **Table II.8** show a significant decrease in hydrodynamic diameters and improved stability of the resulting nanoassemblies for all βCD/Ada molar ratios. Moreover, the maximum

in the scattered light intensity is observed for βCD/Ada = 1:1 in this case, which should be related to both the higher particle number and increase of their compactness (**Figure II.23, b**).

Despite nanoassemblies with the lowest average D_h are still obtained for the βCD/Ada ratios higher than 2:1, their polydispersity is considerably increased comparing to those prepared at equimolar ratios (**Table II.8**).

Interestingly, aging of the host polymer stock solution along with the guest leads to further, though much less pronounced, decrease in D_h (green curve in **Figure II.23, a**). In this case the most efficient nanoassemblies formation was observed, once again, at equimolar βCD/Ada ratio as evidenced by the maximum position in the scattered light intensity (green curve in **Figure II.23, b**). However, the absolute scattering intensity at maximum is slightly lower comparing to the experiment where non-aged host polymer solution was used. It might be due to a partial degradation of the dextran polymers during the extended periods of storage.

Table II.8. Hydrodynamic diameters of the nanoassemblies obtained by mixing of freshly prepared DT40-gPEG-βCD (16.5 mol.%) and aged for 30 days DT40-gPEG-Ada2 (10.5 mol.%) stock solutions

βCD/ Ada	**C(host), g/L**	**C(guest), g/L**	**C_{tot}, g/L**	**D_h, nm**			**PDI**			**CR (10^{-3}, kpcs)**		
				5min	**5d**	**11d**	**5min**	**5d**	**11d**	**5min**	**5d**	**11d**
1:1	0.38	0.30	0.68	162	251	313	0.02	0.01	0.11	153	56	28
1:2	0.23	0.36	0.59	217	708	pr.*	0.02	0.21**	pr.	64	22	pr.
2:1	0.46	0.18	0.64	124	236	275	0.07	0.03	0.02	81	73	29
3:1	0.57	0.15	0.72	112	223	234	0.10	0.05	0.01	54	55	35
4:1	0.61	0.12	0.73	112	211	224	0.14	0.07	0.06	38	51	32

*- precipitated, **- 2nd generation of large aggregates is emerged

3.1.2 Nanoassemblies stability by DLS

After 5 days of storing the difference between the HG nanoassemblies prepared from the fresh and aged polymer solutions becomes even more apparent both in terms of their sizes and stability (**Figure II.24**). At the same time, the distinction between the cases when only DT40-gPEG-Ada2 or both stock solutions were aged is levelled off; the nanoparticles show similar D_h

over the whole range of βCD/Ada ratios (**Figure II.24a**). Oddly enough, the maximum in the scattered light intensity was shifted towards βCD/Ada = 2:1 molar ratio, indicating that an excess of βCD is still required to favor the long-term stability of the nanoassemblies (**Figure II.24b**).

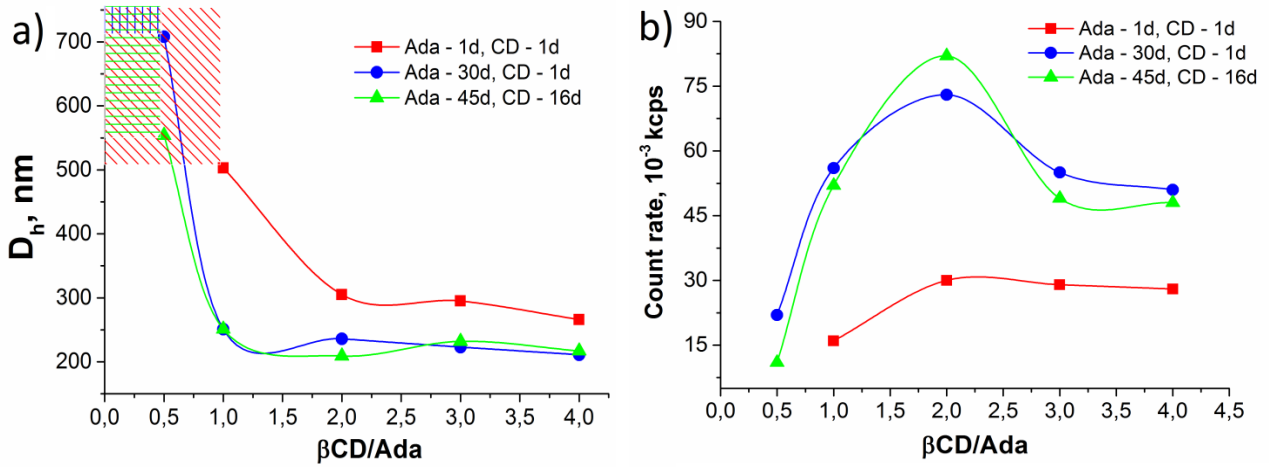

Figure II.24: Hydrodynamic diameters (**a**) and scattered intensity count rates (**b**) of the HG nanoassemblies stored for 5 days, prepared from DT40-gPEG-Ada2 (Ada) and DT40-gPEG-βCD (CD) solutions stored for different periods of time.

3.1.3 Minimal required DT40-gPEG-Ada2 aging time

Based on the results above, it was concluded that the time of storage of the guest polymer stock solutions happens to be an important parameter influencing the properties of the resulting nanoparticles. Hence, in the next step we wondered how long it should be stored before reproducible nanoassemblies' sizes might be obtained. To figure it out, continuously aged DT40-gPEG-Ada2 stock solutions were used for nanoassemblies' formation with freshly prepared host polymer solutions at two different total concentrations. As shown in **Figure II.25**, it takes between 18 to 33 days and, unexpectedly, the stable particle sizes are obtained faster for higher C_{tot} of the polymers (**Figure II.25b**).

One possible cause of the observed phenomenon could be the polymer inter- or intra-polymer association into transient hydrophobic agglomerates, as it was previously observed by Ravoo et al. for Ada-substituted poly(isobutene-*alt*-maleic acid) (PIBMA).[43] If the latter is true, to ensure the interaction with the host polymer, the agglomerates would require to be disrupted either by aging or by addition of the excess of βCD groups with respect to adamantanes.

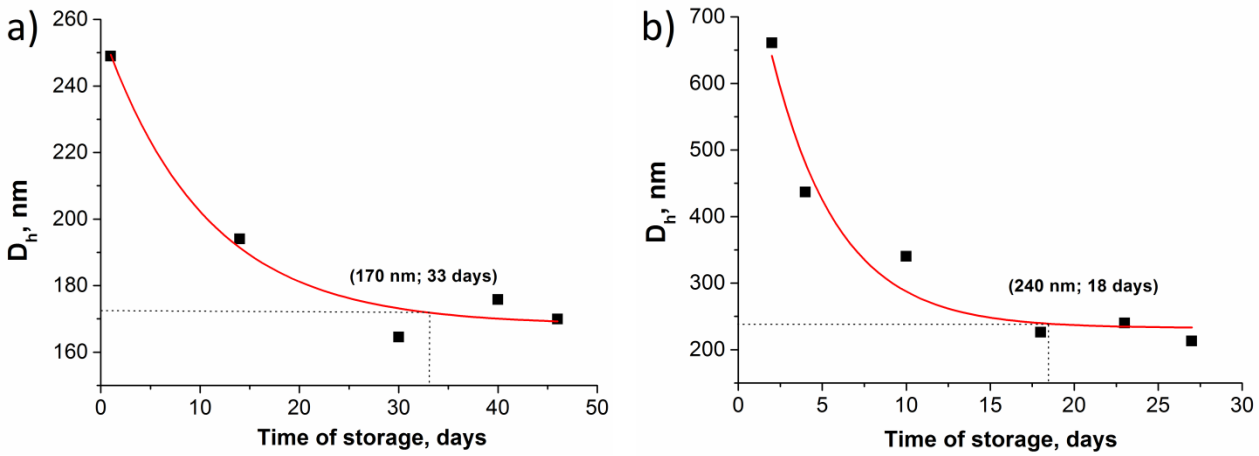

Figure II.25: Hydrodynamic diameters of the HG nanoassemblies stored for 5 days, prepared from fresh host polymer and continuously aged guest polymer stock solutions at C_{tot} of the polymers: **a)** 0.68 g/L, **b)** 1.36 g/L (βCD/Ada = 1:1). The experimental data points fitted to the 1st order exponential decay function.

3.1.4 Control experiment with βCD aiming to disrupt hydrophobic Ada-conglomerates in fresh DT40-gPEG-Ada2 solutions

In order to further verify the hypothesis of the PEG-Ada grafts hydrophobic association, a control experiment with monomeric βCD was conducted. Various amounts of native βCD (up to βCD^{mon}/Ada molar ratio 4:1) were added to fresh DT40-gPEG-Ada2 stock solution one day before the mixing with the host polymer. Then, the nanoassemblies were prepared at equimolar βCD^{pol}/Ada ratio and 1.36 g/L C_{tot} of the polymers. In this way any hydrophobic aggregation was aimed to be suppressed. The formed guest polymer-βCD^{mon} complexes are in turn expected to be destroyed after the addition of the host polymer due to the higher strength of interpolymer cooperative host-guest interactions. The results of the experiment are depicted in **Figure II.26**. One clearly observes a maximum in D_h of the nanoassemblies at βCD^{mon}/Ada = 1:1, correlating with the precipitation phenomenon, expressed as a drop in scattering intensity. Most likely the presence of βCD^{mon} leads to a competition with βCD^{pol} for available Ada-groups and affects the growth mechanism of the nanoparticles. This, in turn, leads to coalescence of more loose interpolymer complexes into larger aggregates. Thus, the method of monomeric βCD addition is not applicable to the preparation of the nanoassemblies as it influences the nanoassemblies' growth mechanism.

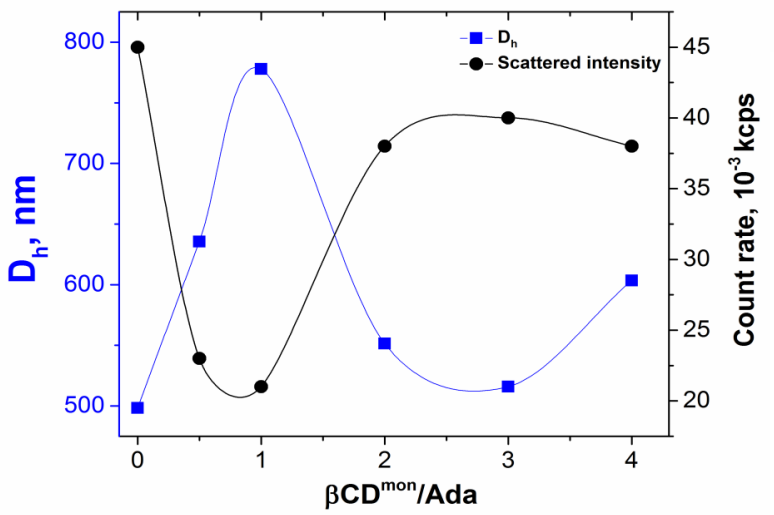

Figure II.26: Hydrodynamic diameters and scattered intensity count rates of the HG nanoassemblies prepared from DT40-gPEG-Ada2 preliminary incubated for 24h with various amounts of monomeric βCD (βCD^{mon}). C_{tot} of the polymers 1.36 g/L, βCD/Ada = 1:1.

3.2 SAXS and SLS investigation of the individual polymers and HG-nanoassemblies of different types

The SAXS measurements of the individual HG polymers of different types and nanoassemblies prepared from them were done using the laboratory instrument at Aarhus University (Denmark) in collaboration with our colleagues Beatrice Plazzotta and Prof. Jan Skov Pedersen. The SAXS data were complemented by SLS experiments performed at University of Maine with the kind support from Dr. Céline Charbonneau and Dr. Taco Nicolai.

R_g/R_H [a]	Topology	Morphology
0.775	Homogeneous sphere	Spherical micelles
1	Hollow sphere	Polymersomes
>1	Extended Structure	Cylinders

[a] Determined by a combination of DLS and SLS /SAXS

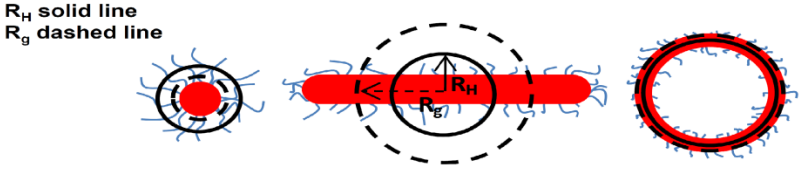

Figure II.27: Determination of the particles morphology by combining of the SAXS and DLS data. Adapted from Patterson et al.[44]

Some basic characteristics of the individual polymers and the nanoparticles, such as radius of gyration (R_g) and molecular weight, might be determined using SAXS and SLS.[45, 46] One may also draw information on the shape of the scatterers in a model-free way, by combining the SAXS (or SLS) data with the DLS and calculating the R_g/R_H ratios (**Figure II.27**).[44]

However, more definite conclusions on the nano-objects shape, internal structure and aggregation state can be made by fitting the SAXS data to different structural models.[47, 48] The typical values of scattering vector lengths q covered in SAXS lay in the range 0.003-0.35 $Å^{-1}$. According to the Fourier transformation sampling theorem, it means that the maximum overall size, that can be determined by SAXS is ~100 nm.[48] As described in the previous section, host-guest nanoassemblies typically surpass this size limit, depending on mass concentration, βCD/Ada molar ratio etc. Hence, for the proper modelling of SAXS data for such bulky nano-objects it is often beneficial to use complementarity between SAXS and SLS, the latter giving the opportunity to extend the range of available q down to 0.00035 $Å^{-1}$.[48]

The theoretical background on SAXS and static light scattering, as well as the details on the experimental set-up can be found in the Experimental Section.

3.2.1 Individual host- and guest polymers

The results of SLS experiments for the individual host-guest polymers with various structures are represented in **Figure II.28a**. The weight concentrations were chosen so that to keep a constant $C_{CD(Ada)}$ value ($5 \cdot 10^{-4}$ M) and lie in the range of 1.2-1.9 g/L.

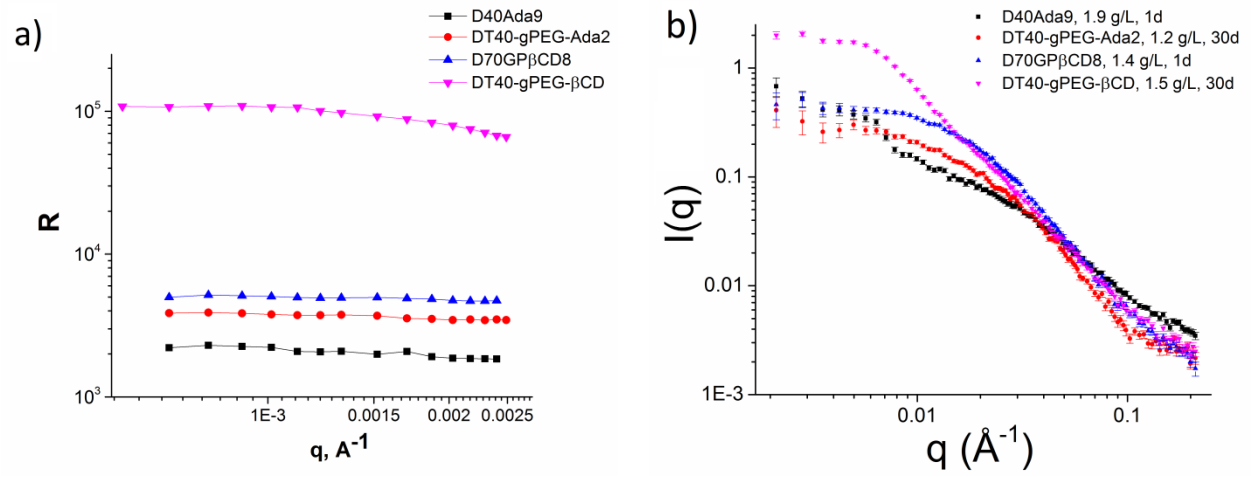

Figure II.28: a) Rayleigh ratios angular dependency ($R(q)$) by SLS and **b)** SAXS scattering curves for the individual host and guest polymers without PEG spacer and with hydrophilic PEG spacer (samples with the same concentrations and times of storage were used for both kinds of experiments).

At comparable weight concentrations DT40-gPEG-βCD sample scatters much more than the other polymers in the whole range of q (**Figure II.28, a**). Radii of gyration and molecular weights of the polymers were determined using the Guinier approximation, based on the equation:

$$R(q) = KCM \cdot \exp\left(-\frac{1}{3}q^2R_g^2\right) \qquad \textbf{(II.2)}$$

where K is the optical constant (the details on the K calculation may be found in the Experimental section), C – concentration of the sample [g/mL], M –molecular weight [g/mole]. The exponential part in the expression (**II.2**) is the Guinier approximation for $P(q)$ – SLS form factor.[46] Taking the logarithm on both sides of (**II.2**) and subsequent plotting the Rayleigh ration $R(q)$ as a function of q^2 leads to a straight line with a slope coefficient $a = -\frac{1}{3}R_g^2$ and an intercept with the y-axis equal to $\ln(KCM)$. This procedure also provides a simple way to calculate the molecular weight, without the need for determination the partial specific volumes of the polymers required for the M_w determination from SAXS data.

The DLS experiments performed in parallel with SLS showed the presence of two populations of scatterers in the solutions of all polymers with the 1st one corresponding to the individual polymer molecules (R_H = 6-12 nm in **Table II.9**) and the 2nd one to the aggregates or cross-linked

polymers (R_H ca. 100 nm). However, converting the DLS data into Size-Volume distributions using the Mie theory showed that the bigger scatterers typically constitute not more than 0.5 Vol.% for all polymers but for DT40-gPEG-βCD, where their amount is one order of magnitude higher (5 Vol.%). Given this, before the determination of R_g of DT40-gPEG-βCD, the SLS data were treated so as to eliminate the contribution from the slow relaxation mode (bigger scatterers) to the scattering intensity at all q-values. Nevertheless, the obtained R_g were a way higher than the R_H of the 1st peak in DLS for all the polymers (**Table II.9**), indicating that the impact of aggregation and/or cross-linking on the SLS results is still substantial and difficult to fully get rid of.

Though the obtained M_w are considerably higher than the theoretical ones for all investigated polymers (**Table II.9**), the most drastic discrepancy was found, once again, for DT40-gPEG-βCD (4908 kDa instead of expected 116 kDa), which is consistent with the DLS results.

Table II.9. Characteristics of different types of host-guest polymers determined by light scattering (SLS + DLS); the theoretical M_w are given in brackets; R_H were measured at a single angle (173°) using a Zetasizer Nano-ZS and SLS measurements were performed at university of Maine with a multi-angle light scattering apparatus.

Polymer	C, g/L	Time of storage, days	R_g, nm (SLS)	M_w, 10^{-3} g·mole^{-1} (SLS)	R_H, nm		Volume, %	
					1 peak	2 peak	1 peak	2 peak
DT40Ada9	1.9	1	41.0	78 (44)	5.3	81.8	99.9	0.1
DT40-gPEG-Ada2	1.2	30	45.3	221 (62)	9.9	106.3	99.3	0.7
	1.2	1			9.6	103.3	99.7	0.3
	5.0	1			13.7	>1000	99.9	0.1
DT70GPβCD8	1.4	1	26.4	244 (130)	12.0	128.1	99.7	0.3
DT40-gPEG-βCD	1.5	30	52.2*	4907 (116)	8.8	81.4	94.6	5.4
	1.5	1			9.2	80.6	94.9	5.1
	0.75	30			9.1	81.1	94.7	5.3
DT40-g-PEG-hex-5-ynoate	1.5	2	-		13.6	103.9	99.5	0.5

* - experimental data were treated so as to eliminate the contribution from bigger scatterers

An analogous trend was found in the SAXS data for the individual polymers (**Figure II.28b**). The first thing to notice while analyzing the low-q range of the curves is a considerably higher scattering intensity for the host polymer with PEG spacer comparing to the other polymers. Two ways to obtain their R_g were used: a) the construction of Guinier plots; b) analysis of the pair-distance distribution functions (PDDF) obtained *via* inverse Fourier-transformation of the oscillating part of the form factor in the middle-q range (described in detail in the Experimental section). Both ways of calculation lead to twice as high R_g values for DT40-gPEG-βCD compared to its PEG-containing guest counterpart (DT40-gPEG-Ada2) and host polymer without PEG spacer (DT70GPβCD8), as reported in **Table II.10**. Comparably high R_g obtained for the guest polymer with no PEG spacer (DT40Ada9) might be explained by the partial aggregation occurring in the solution of this hydrophobically modified polymer.

Table II.10. Radii of gyration R_g of different types of host-guest polymers determined from the SAXS data by two methods, Guinier plots construction and PDDF analysis.

Polymer	C, g/L	Time of storage, days	R_g, nm (Guinier)	R_g, nm (PDDF)
DT40Ada9	1.9	1	17.8	24.0
DT40-gPEG-Ada2	1.2	30	6.9	10.1
	1.2	1	15.2	13.3
	5.0	1	21.9	23.7
DT70GPβCD8	1.4	1	6.8	9.3
DT40-gPEG-βCD	1.5	30	21.5	18.8
	1.5	1	20.5	19.4
	0.75	30	21.0	19.8

Interestingly, for the guest polymers with PEG spacer, differences in the SAXS scattering patterns were observed upon changing the concentration and time of storage of the solutions (**Figure II.29**). For instance, the R_g values for the freshly prepared DT40-gPEG-Ada2 are 1.3 to 2.2 times higher than for the solution stored for 30 days (estimated by PDDF and Guinier plot construction respectively). This result supports the validity of the assumption of Ada-groups being partially aggregated in freshly prepared DT40-gPEG-Ada solutions. It is, however, not fully

confirmed by the DLS data, where similar hydrodynamic radii R_H and volume percentages are found for the fresh and aged solutions of DT40-gPEG-Ada2 (**Table II.9**)

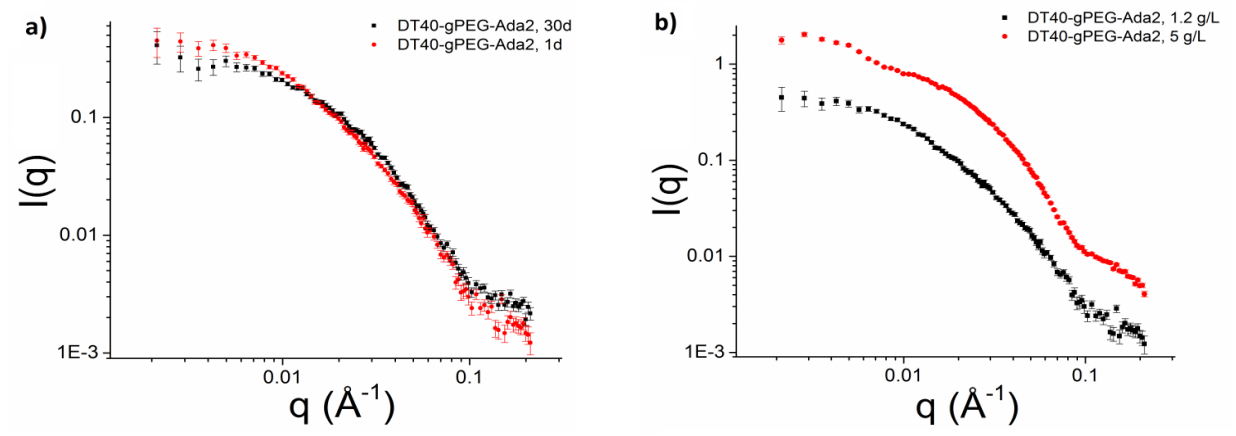

Figure II.29: SAXS scattering curves of the DT40-g-PEG-Ada2 (DS_{CD} = 10.5 mol.%) solutions as a function of: **a)** time of storage (both at 1.2 g/L); **b)** concentration (both solutions 1 day after preparation).

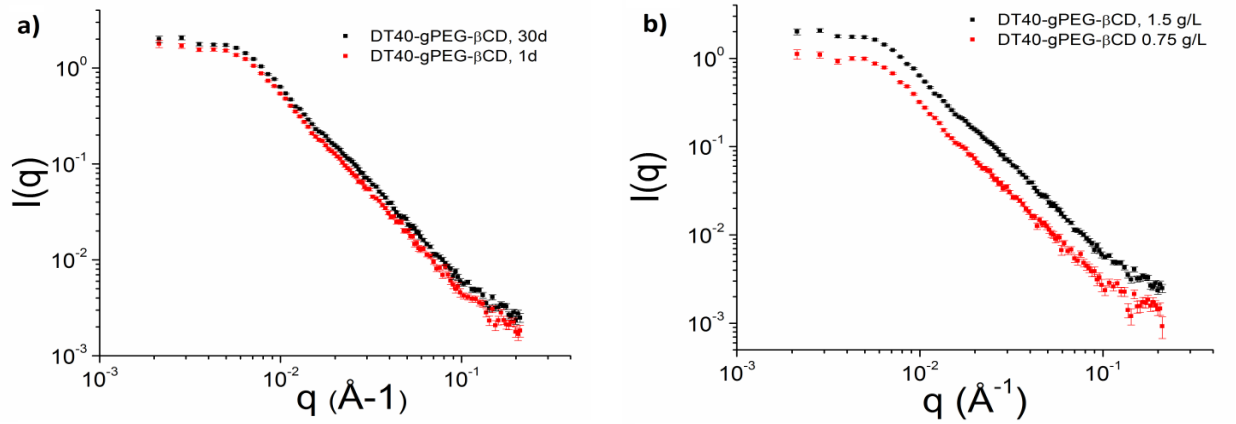

Figure II.30: SAXS scattering curves of the DT40-g-PEG-βCD (DS_{CD} = 16.5 mol.%) solutions as a function of: **a)** time of storage (both at 1.5 g/L); **b)** concentration (both solutions 1 day after preparation). The scaling factor between the two dataset on the right is coherent with the concentration difference.

On the other hand, the SAXS scattering patterns of the DT40-gPEG-βCD solutions are not influenced by the concentration or the time of storage (**Table II.10; Figure II.30**). The latter might indicate that their increased R_g are rather due to the partial cross-linking of the polymer than due to the aggregation processes. Moreover, the cross-linking appears to occur during the

last CuAAC-involving stage of synthesis, as the alkyne-modified DT40-g-PEG-hex-5-ynoate – the precursors of DT40-gPEG-βCD, contain only 0.5 Vol.% of bulky scatterers (**Table II.9**).

To get a deeper insight into the state of the polymers in solution we performed a modelling of the SAXS data, using the formalism of Svaneborg and Pedersen[49]; the details on the models used are provided in the Experimental section. The form factors $P_{arm}(q)$ of most polymers could be modelled as comb-like structures (**Figure II.31a**). Each polymer chain was considered as consisting of N basic subunits with the form factors $P_{sub}(q)$, the structure of which is schematically given in **Figure II.31c**. The X indicates the point, for which the scattering amplitude is calculated, L_s is the length of the grafted side-chain and l corresponds to the length of the main chain per one comb-like graft. The value of l was a fixed parameter of the fit and had been determined from the NMR data on the PEG-X or βCD side-chain grafting density. When constructing the larger structure, the substructure is connected at the ends of the red chain. All data were modelled assuming theta solvent conditions.

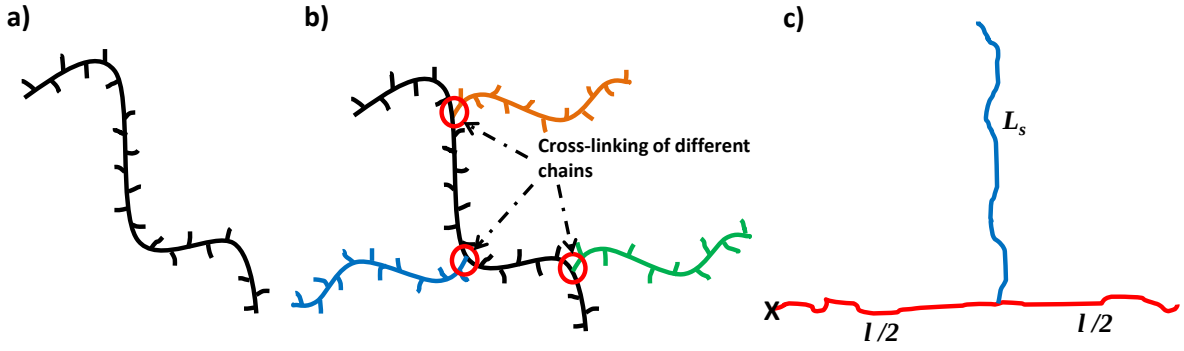

Figure II.31: Schematic representations of **a)** a comb-like polymer chain; **b)** a star-like structure with 4 comb-like arms (DT40-gPEG-βCD); **c)** the basic subunit (form factor$P_{sub}(q)$) of a comb-like polymer chain (form factor$P_{arm}(q)$). Derivation of the mathematical expressions for $P_{sub}(q)$ and $P_{arm}(q)$ can be found in the Experimental section.

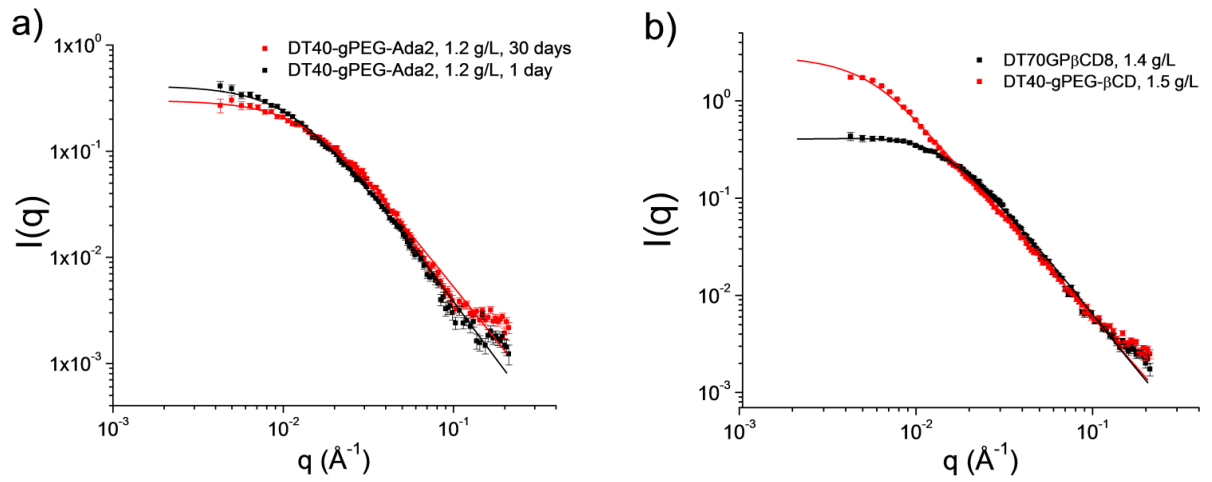

Figure II.32: Experimental SAXS data (symbols) and best fits (lines) for: **a)** guest polymers with the PEG spacer aged for different periods of time (comb-like model); **b)** host polymers with and without PEG spacer, both aged for 30 days (comb-like model for DT70GPβCD8, star of comb-like chains model for DT40-gPEG-βCD).

Table II.11. Information on the models used to fit the experimental SAXS data and the size and structure parameters obtained for the individual host-guest polymers.

Polymer	χ^2	Structure	Number of Branches	R_g, nm (Model)	R_g, nm (Guinier)
DT40-gPEG-βCD 1.5 g/L aged	2.9	Star of comb-like chains	4	19.1±0.7	21.5
DT40-gPEG-βCD 0.75 g/L aged	1.6	Star of comb-like chains	4	19.0±0.1	21.0
DT40-gPEG-βCD 1.5 g/L fresh	1.8	Star of comb-like chains	4	18.7±0.4	20.5
DT40-gPEG-Ada2 1.2 g/L aged	1.9	Comb-like	-	10 ± 2	6.9
DT40-gPEG-Ada2 1.2 g/L fresh	2.5	Comb-like	-	13.3±0.2	15.2
DT70GPβCD8 1.4 g/L fresh	1.1	Comb-like	-	9.3±0.5	6.8

However, in the case of DT40-gPEG-βCD, which shows clear signs of cross-linking, the data could be successfully modelled as star-like structure with 4 comb-like arms (**Figure II.31b, 32b**). This

might possibly display only the local structure and the polymer can form a more extended network on a larger scale.

The quality of a fit may be estimated from the Chi-square (χ^2) parameter which is equal to 1 when a perfect model is chosen.[49] The proximity of the χ^2 values to unity (**Table II.11**) indicates that the applied models are appropriate for describing the studied host-guest polymers. Furthermore, the R_g values derived from modelling are in a very good agreement with those obtained by Guinier approximation and inverse Fourier transformation of the scattering curves (**Table II.10**).

3.2.2 Host-guest nanoparticles of different types

Host-guest nanoassemblies of various compositions were prepared by mixing the solutions of individual polymers at equimolar βCD/Ada ratio and $C_{CD/Ada}$ = $5 \cdot 10^{-4}$ M (aged for 30 days in the case of the polymers with PEG-spacer). At the first stage we collected the scattering data for lower q range by performing SLS experiments (**Figure II.33**).

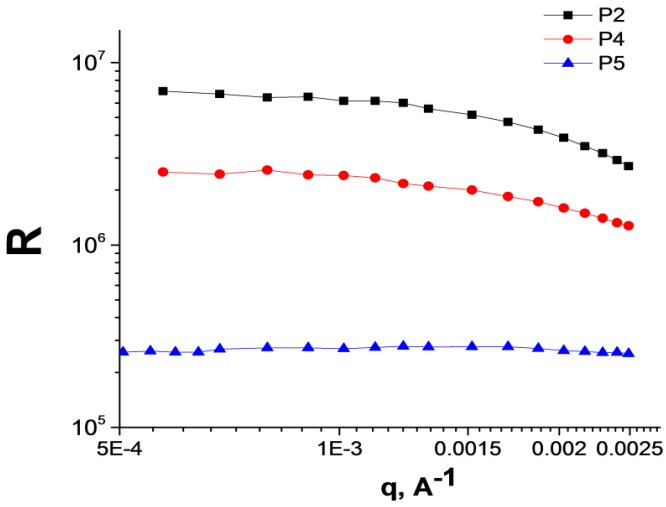

Figure II.33: Rayleigh ratios angular dependency ($R(q)$) for the HG-nanoassemblies of different compositions (**Table II.12**).

From the SLS-data, sizes (R_g) and molecular weights of the HG-nanoassemblies were calculated using the Guinier approximation, in a way similar to that described in previous section for individual polymers (**Table II.12**). DLS experiments on the same samples were conducted in parallel. Due to the high scattering intensity from the nanoassemblies, we didn't detect any

impact from aggregates or/and cross-linked molecules as it was the case with the individual polymers. In the "R_H-intensity" and "R_H-volume" distributions single peak was observed for all types of nanoassemblies. By combining the SLS and DLS data we could estimate the R_g/R_H ratios which turn up to lie in the range 0.54-0.59 (**Table II.12**). It is significantly lower than 0.775 – the indicated in literature criterion for homogenous sphere.[44] The disparity between the R_g and R_H, might be related to non-uniform radial density distribution in highly water-swollen polysaccharide-based HG-nanoassemblies. Thus, a lot of loosely attached pending polymer chains should be present on the nanoparticles surface.

Table II.12. Characteristics of different types of host-guest nanoassemblies determined by light scattering (SLS + DLS).

Code	Components	C_{tot}, g/L	Way of mixing	R_g, nm (SLS)	M_w, 10^{-6}g·mole^{-1} (SLS)	R_H, nm	R_g/R_H
P2	DT70GPβCD8; DT40Ada9	1.65	stirring	63.2	283	116.4	0.54
P4	DT40-gPEG-βCD; DT40-gPEG-Ada2	1.35	stirring	60.7	128	107.1	0.57
P5	DT70GPβCD8; DT40-gPEG-Ada2	1.30	stirring	30.7	15	52.0	0.59
P6	DT40-gPEG-βCD; DT40Ada9	1.70	stirring	-*		97.5	-

* - negative slope in Guinier plot, R_g determination is not possible.

Interestingly, despite a little difference in R_g, nanoassemblies prepared from the polymers without PEG spacers (**P2**) have significantly higher molecular weight than PEG-spacer containing ones (**P4**, **Table II.12**). This might be a proof of a higher chain packing density in **P2**, as the result of stronger interpolymer interactions. On the other hand, the "mixed" particles (**P5**) show drastically lower both R_g and M_w values. Assuming dense packing in the case of **P2**, (without PEG spacer), M_w should vary as R_g^3, meaning that a decrease of R_g by a factor of 2.06 should result in 8.74 times lower M_w. Comparing **P2** and **P5**, the observed M_w decrease is more than

twice larger (19), in agreement with the assumption that the packing density is lower in the mixed system than in the system without PEG spacer.

HG nanoassemblies for the SAXS investigation were prepared at the same as for SLS $C_{CD/Ada}$ = $5 \cdot 10^{-4}$ M and equimolar βCD/Ada ratio. The obtained scattering patterns for different types of nanoassemblies are reported in **Figure II.34**.

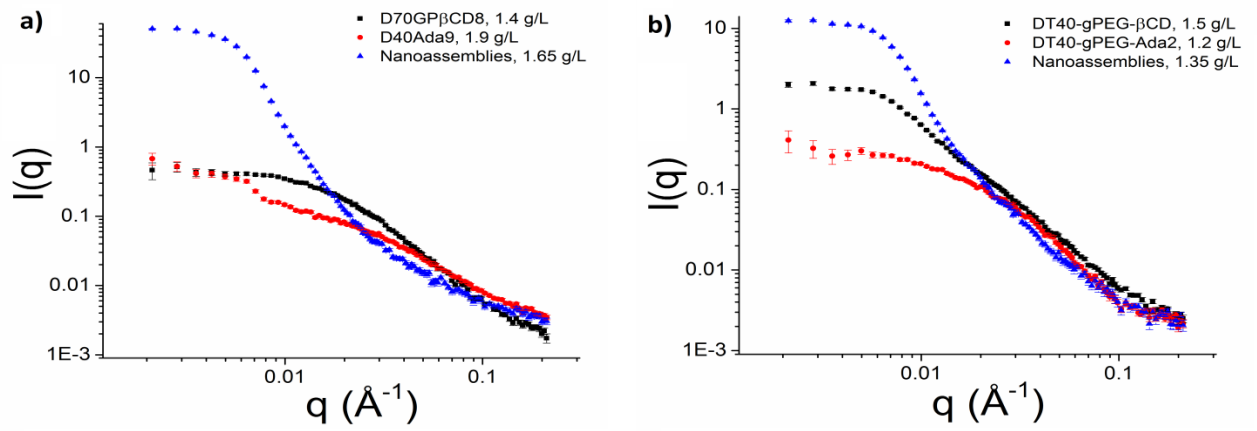

Figure II.34: SAXS scattering patterns representing the formation of HG-nanoassemblies between the polymers without (**a**) and with (**b**) hydrophilic PEG spacer ($C_{CD/Ada} = 5 \cdot 10^{-4}$ M).

Two ways of nanoassemblies' formulation were tested: **a)** diffusion-controlled formulation when the solutions of the host-guest polymers were successively injected directly into the SAXS measurement capillary shortly before the data acquisition; **b)** preliminary preparation by vigorous stirring of the individual polymers mixtures at 800 rpm. Remarkably, no differences in the obtained SAXS scattering patterns were found (**Figure II.35**) for either kind of HG nanoassemblies. It's an indication of the fast kinetics of interpolymer interaction, arising due to the high interpolymer affinity.

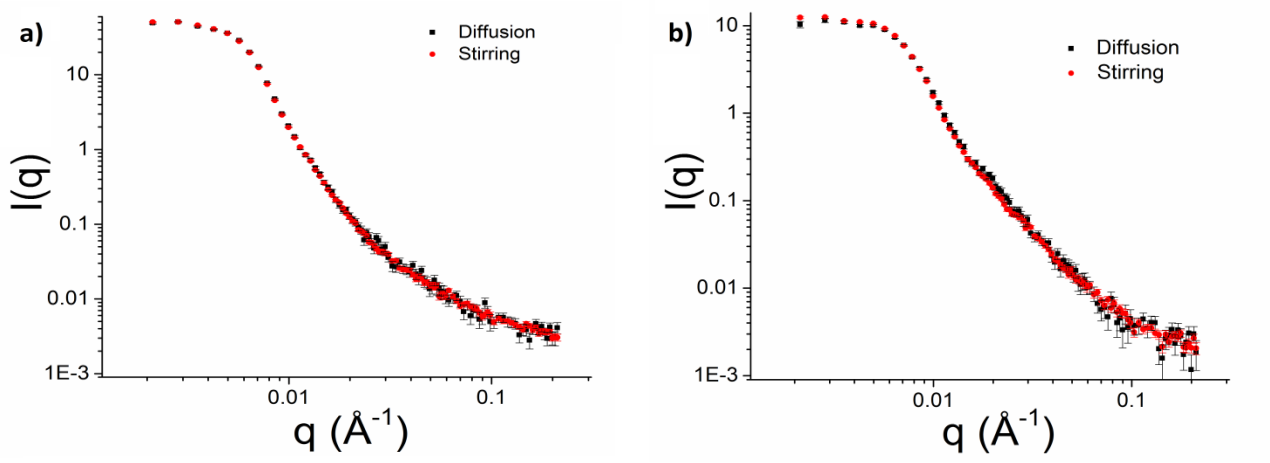

Figure II.35: SAXS scattering patterns of the HG-nanoassemblies between the polymers without (**a**) and with (**b**) hydrophilic PEG spacer prepared in the different ways, i.e. either by diffusion-driven mixing of the polymers in the SAXS measuring capillary (red curves) or by preliminary vigorous stirring of the polymer solutions at 800 rpm (black curves).

Table II.13. Radii of gyration R_g of different types of host-guest nanoassemblies determined by SAXS.

Code	Components	C_{tot}, g/L	Way of mixing	R_g, nm (Guinier)	R_g, nm (PDDF)	R_H, nm	R_g^{Guin}/R_H
P1	DT70GPβCD8; D40Ada9	1.65	diffusion	36.1	31.4	116.0	0.31
P2	DT70GPβCD8; D40Ada9	1.65	stirring	36.1	32.0	116.4	0.31
P3	DT40-gPEG-βCD; DT40-gPEG-Ada2	1.35	diffusion	24.9	24.9	105.5	0.24
P4	DT40-gPEG-βCD; DT40-gPEG-Ada2	1.35	stirring	27.8	26.1	107.1	0.26
P5	DT70GPβCD8; DT40-gPEG-Ada2	1.30	stirring	23.1	21.4	52.0	0.44
P6	DT40-gPEG-βCD; D40Ada9	1.70	stirring	32.7	31.0	97.5	0.34

As in the case of individual polymers, the R_g estimations by two approaches (i.e. Guinier plots and PDDF) were generally in good agreement (**Table II.13**). The nanoassemblies prepared from the polymers with PEG spacer (**P3**, **P4** in **Table II.13**) appear to be slightly smaller both in terms of R_g and hydrodynamic radius R_H compared to their PEG-free counterparts (**P1**, **P2**).

Unfortunately, no definitive conclusions on the nanoassemblies shape could be made based on the R_g/R_H ratios derived from the SAXS data. Indeed, they lie in the range of 0.24-0.41 for all investigated cases (**Table II.13**), which is much lower than the previously mentioned criterion for hard homogeneous sphere. In addition to the reasons given above for SLS, that is a non-uniform density distribution in the particles, this disparity can be also related to the fact that the hydrodynamic diameters of the nanoassemblies are considerably higher than 100 nm – the size corresponding to the q_{min} limit of SAXS.

The modelling was performed by fitting the SAXS scattering data for the nanoassemblies using a model developed by Stieger, Richtering, Pedersen, and Lindner[50] for pNIPAm microgel particles. The internal structure of the nanoassemblies, resulting from the host and guest polymer associations, could be related to the one of a hydrogel with a correlation length ξ_l. The nanoassemblies are thus modelled by a polydisperse spherical form factor and a Lorentzian term was introduced to account for the fluctuations of the gel network. Due to the relative low concentrations of the samples the structure factor was neglected while fitting the data. The mathematical description of the model used is provided in the Experimental section. The parameters deduced from the fits using this model are thus: R_g, radius of gyration of the nanoassemblies; σ_{poly}, their polydispersity index and ξ_l – correlation length of the network inside the nanoassemblies.

Despite a certain shift towards higher R_g values, most of the nanoparticle features derived from the modeling were consistent with those obtained by the Guinier approximation and PDDF analysis (**Table II.14**). Namely, the nanoparticles composed of DT70GPβCD8 and DT40Ada9 are bigger than those produced from their PEG-containing counterparts (**Figure II.36a**). When host polymer with PEG spacer (DT40-gPEG-βCD) and guest polymer without PEG spacer (DT40Ada9) are used, the R_g of the resulting mixed nanoparticles (**P6**) is roughly an average of those of **P2** and **P4** (**Table II.14**). At the same time, the "inversed" mixed nanoparticles self-assembled from

DT70GPβCD8 and DT40-gPEG-Ada2 proved to be the smallest ones with R_g~ 28 nm (**P5**). No difference was found between the nanoparticles prepared by stirring and by diffusion.

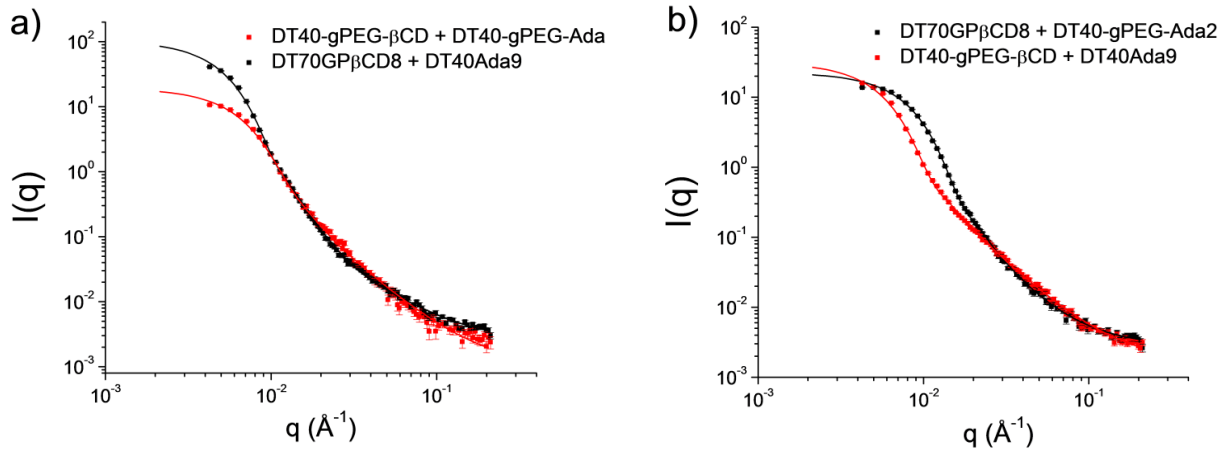

Figure II.36: Experimental SAXS data (symbols) and best fits to a polydisperse spherical form factor model (lines): **a)** nanoparticles made of the polymers with and without the PEG spacer; **b)** mixed nanoparticles of two types. The corresponding R_g and other parameters are given in **Table II.14**.

Table II.14. Modelling of the SAXS data for various HG-nanoparticles to a polydisperse spherical form factor model.

Code	Components	Way of mixing	R_g, nm (Model)	R_g, nm (Guinier)	σ_{poly}	ξ_I, nm	χ^2
P1	DT70GPβCD8+ DT40Ada9	Diffusion	45.4 ± 0.04	36.1	0.188 ±0.003	2.4±0.3	5.8
P2	DT70GPβCD8+ DT40Ada9	Stirring	44.9 ± 0.4	36.1	0.187 ±0.003	2.1±0.3	5.7
P3	DT40-gPEG-βCD + DT40-gPEG-Ada2	Diffusion	35.1 ± 0.1	24.9	0.207 ±0.004	16.7±0.3	4.0
P4	DT40-gPEG-βCD + DT40-gPEG-Ada2	Stirring	35.3 ± 0.5	27.8	0.182 ±0.003	16.9±0.9	3.9
P5	DT70GPβCD8 + DT40-gPEG-Ada2	Stirring	28.4 ± 0.2	23.1	0.182 ±0.002	4.6±0.2	4.6
P6	DT40-gPEG-βCD + DT40Ada9	Stirring	42.6 ± 0.4	32.7	0.187 ±0.005	10.5±0.2	3.0

Contemporary theories of semidilute/concentrated polymer solutions and swollen polymer gel networks define correlation length (ξ_I in **Table II.14**) as the radius of a volume inside which

intramolecular effects are dominant and beyond which intermolecular effects prevail.[51] For instance, the SAXS-derived correlation length values were used to estimate the size of the inhomogeneities in the structure of thermosensitive pNIPAm microgels; the results were consistent with those obtained by cryo-TEM.[52] In our case, the substitution of DT40Ada9 (**P2**) by the guest polymer with PEG spacer DT40-gPEG-Ada2 (**P5**) leads to a moderate increase in correlation length from 2.1 to 4.6 nm (**Table II.14**), which is coherent with the less compact structure of **P5** evidenced by the SLS data (**Table II.12**). In the case of "mixed" particles containing host polymer with PEG spacer (**P6**) the increase of ξ_l is much more pronounced, i.e. from 2.1 to 10.5 nm. Finally, the nanoassemblies composed of both guest and host polymers with PEG spacer (**P4**) show the highest correlation length of 16.9 nm. The results clearly demonstrate the impact of the PEG spacers on the internal structure of the nanoassemblies. The more PEG spacers are used, the less compact are the internal structures, as evidenced by the values of correlation lengths (samples **P3**, **P4** and **P6** in **Table II.14**).

To summarize, by the combination of SLS/DLS and SAXS modelling we proved that the nature of the individual host-guest polymers has a strong impact on the size and internal structure of the resulting HG nanoassemblies. The nanoassemblies composed of the polymers with PEG spacer have lower sizes and significantly lower compactness comparing to their PEG-free counterparts, as evidenced by their large correlation length values. At the same time, all types of nanoassemblies appear to have non-uniform radial density distribution with denser cores and pending polymer chains at the periphery.

Conclusions

In this chapter, we have proposed a synthetic pathway to novel type of host-guest polymers with hydrophilic PEG spacer. It relies on the use of thiol-substituted dextrans as a unique platform, which is subsequently transformed into either PEG-βCD grafted host or PEG-Ada grafted guest polymers *via* combination of nucleophile-mediated thiol-click and CuAAC reactions.

The polymers were characterized by NMR, light scattering techniques and SAXS. We performed modelling of the SAXS data for various types of host and guest polymers. All of them except DT40-gPEG-βCD show comb-like structure in water solutions. The latter could be modelled as a

star-like structure composed of at least 4 comb-like branches. It might serve as an indication that cross-linking of the alkyne-modified dextran scaffolds takes place during the CuAAC stage of the synthesis. It can be related to the fact that alkynes in DT40-g-PEG-hex-5-ynoate precursor, being located at the ends of flexible PEG chains, are more likely to approach each other and undergo acetylenic cross-coupling.

The binding properties of the host and guest polymers in solution and on solid surface were studied by ITC and SPR respectively and compared to those of previously reported βCD- and Ada-substituted dextrans with short hydrophobic spacers. The latter was done with the aim of understanding the impact of flexible PEG on the availability of grafted groups for the inclusion complexes formation. Both ITC and SPR results were coherent, indicating a significant improvement of the binding properties of DT40-gPEG-Ada compared to DT40Ada (5-fold increase of the affinity constant K_a for comparable substitution degrees). On the other hand, the presence of PEG spacer proved to be less beneficial in the case of host polymers, where DT40-gPEG-βCD showed in average 4 times lower K_a than those of DT70GPβCD.

At the next stage we investigated the formation of nanoassemblies between various types of host-guest polymers by combination of light scattering and SAXS. The nanoassemblies were formed spontaneously upon mixing the host and guest polymer solutions and we found that their structure was not influenced by the mixing process. The low values obtained for the R_g/R_h ratio (<0.55) were interpreted as the result of non-uniform radial density distribution, i.e. with denser core and looser periphery parts.

In order to get insight into the internal structure of the nanoassemblies, we used a simplified model of spherical gel-like particles with uniform density distribution, characterized by a R_g and a correlation length ξ_l. The nature of individual polymers proved to have a significant influence on the size and internal organization of the nanoassemblies. In general, particles containing DT40-gPEG-βCD are smaller and have less compact structure (larger ξ_l) than those containing DT70GPβCD. The same effect, though to a much lesser extent, holds true for the particles composed of DT40-gPEG-Ada as a guest polymer.

The obtained results contribute to design of host-guest polymers with improved properties, i.e. polymers capable of self-assembling into more stable, biodegradable nanoparticles with "stealth" properties and attractive drug delivery profiles.

Experimental section

Materials and reagents

Pyridine (99.9%, anhydrous), 4-nitrophenyl chloroformate (4-NC, 96%), cysteamine (98+ %), N,N'-dimethylformamide (DMF, 99.8%, anhydrous), 5-hexynoic acid (97%), dibutyltin dilaurate (DBTDL, 95%), N,N'-dicyclohexylcarbodiimide (DCC, 99%), trimethylamine (≥99%), tripropargylamine (98%), tetrakis(acetonitrile)copper(I)tetrafluoroborate ($Cu(MeCN)_4PF_6$, 97%), 1-adamantyl isothiocyanate (99%), and dithioerythritol (99+ %) were purchased from Sigma-Aldrich (Saint Quentin Fallavier, France) and used as received. p-Toluenesulfonyl chloride (98%), imidazole (99%), ammonium chloride (NH_4Cl, 98+ %), sodium azide (99%), L-ascorbic acid sodium salt (99%), benzyl bromide (99%), 1-adamantanecarbonyl chloride (95%) and 2,6-lutidine (98+ %) were purchased from Alfa Aesar and used as received. Hexylamine (99%) and sodium hydroxide (98+ %, anhydrous pellets) were purchased from Acros Organics and used as received. Copper(II)sulfate pentahydrate ($CuSO_4 \cdot 5H_2O$, 99+ %) and 4-(dimethylamino)pyridine (DMAP, 98+ %) were purchased from Fluka and used as received. β-cyclodextrin (βCD) was a gift from Roquette Company (France) and was used as received.

Dextran (DT40, M_w 4.3×10^4 g mol^{-1}, PDI =1.5, Amersham Pharmacia Sweden) and lithium chloride (Alfa Aesar) were dried overnight in vacuum at 95°C prior to use. Poly(ethylene glycol) acrylate (M_n 375 g mol^{-1}, Sigma Aldrich) was dried overnight in vacuum at room temperature before use. Dichloromethane (DCM) was distilled from calcium hydride prior to use.

1-(p-Toluenesulfonyl)imidazole[27], benzyl azide[53], 2-(1-adamantyl) ethyl trimethyl ammonium bromide (AdaTMA)[54] and tris[(1-benzyl-1H-1,2,3-triazol-4-yl)methyl]amine (TBTA)[28] were synthesized using the literature data. Monoazidated on the primary side βCD (βCD-N_3) was prepared using a previously reported 2-stage procedure, which may be found elsewhere.[12, 27]

Methods and instrumentation

NMR spectroscopy: NMR analyses were performed in D_2O or DMSO-d_6, unless other is indicated, on a Bruker Avance II Ultrashield Plus 400 MHz NMR spectrometer. ^{1}H-NMR spectra were calibrated using the residual signals of D_2O, DMSO-d_6 or $CDCl_3$ as the reference signals.

Thin layer chromatography (TLC): TLC experiments were carried out using Silica gel 60 F_{254} TLC plates with 0.2 mm silica gel and 2-PrOH/H_2O/EtOAc/$NH_4OH_{(c)}$ as a mobile phase and visualized with 5% H_2SO_4 in ethanol.

Fourier transform infrared spectroscopy (FT-IR): FT-IR spectra were recorded on a Bruker Tensor 27 FT-IR spectrometer in the attenuated total reflection (ATR) mode using 32 or 64 scans at a resolution of 4 wavenumbers.

Ultrafiltration: Ultrafiltration was carried out under N_2 atmosphere using Amicon equipment and regenerated cellulose membranes with MWCO 10,000.

Dialysis: Dialysis was performed using Spectra/Por molecular porous tubing with MWCO 6,000-8,000.

Freeze-drying: Solutions of the water-soluble polymers typically purified by ultrafiltration or dialysis were freeze-dried on CHRIST ALPHA 1-2 LD plus lyophilizator.

Isothermal titration microcalorimetry: ITC measurements were performed using a MicroCal VPITC microcalorimeter. In each titration, injections of 15 µL of concentrated AdaTMA or βCD solutions (both at $5 \cdot 10^{-3}$ mol $\cdot L^{-1}$ in 0.1 mol $\cdot L^{-1}$ NaCl and in pure water respectively) were added from the computer controlled 295 µL microsyringe at an interval of 180 s into the cell (V= 1.4569 mL) containing the investigated polymer solution ($5 \cdot 10^{-4}$ mol $\cdot L^{-1}$of βCD or Ada groups) while stirring at 450 rpm. The temperature was fixed at 25°C. The raw experimental data are obtained as the amount of heat produced per second following each injection of titrant as a function of time. Integration of the heat flow peaks by the instrument software (after taking into account heat of dilution) provides the amount of heat produced per injection. The experimental data were fitted with a theoretical titration curve using the instrument software with a model assuming a 1:1 stoichiometry for the adamantyl/βCD complex. The enthalpy

change, $|\Delta H|$, the association constant, K_a, and the overall stoichiometry, n, were the adjustable parameters.

Dynamic light scattering: The mean hydrodynamic diameter and the polydispersity index (PdI) of the nanoassemblies were determined by dynamic light scattering (DLS) using a Zetasizer Nano ZS (Model ZEN3500) Malvern Instrument equipped with a He–Ne laser (λ = 633 nm, scattering angle 173°). Individual polymer solutions in water were filtered using 0.40 μm regenerated cellulose syringe filters prior to measurements and/or nanoassemblies preparation. Each investigated sample was measured fifteen times for ten seconds at 25°C.

In DLS, a sample containing a suspension of colloidal particles in solution is irradiated by a laser beam. The laser light which hits particles is scattered in all directions. The scattering intensity shows time-dependent fluctuations as a result of the particles undergoing Brownian motions in the irradiated volume. The fluctuation rate is related to the size of the particles: the smaller the particles, the quicker they will move causing higher fluctuation rates. By the means of special equipment, digital autocorrelators, quantitative information can be derived from the intensity fluctuations. It is represented by so-called intensity autocorrelation function:

$$G(\tau) = B + A\sum \exp(-2q^2 D\tau) \qquad \textbf{(II.3)}$$

where B – baseline at infinite time, A – amplitude (or intercept), D-diffusion coefficient, τ – correlator delay time, q – scattering vector,

$$q = \frac{4\pi n}{\lambda} \cdot \sin(\theta) \qquad \textbf{(II.4)}$$

where λ – laser wavelength, n – dispersant refractive index and 2θ is the detection angle. By fitting the autocorrelation function with a suitable algorithm one can determine the diffusion coefficient D. The hydrodynamic radius R_h can be then calculated using the Stokes-Einstein equation:

$$R_h = \frac{k_b T}{6\pi\eta D} \qquad \textbf{(II.5)}$$

where T is the temperature, η is the viscosity of the solvent and k_b is the Boltzmann constant ($1.23 \cdot 10^{-23}$ J/K).

If determined the solution has a rather narrow Gaussian-like distribution of sizes, Cumulants analysis of the data is appropriate; the latter determines the mean size (Z-average) and PdI values of the particles. If more than single exponential decay rates are observed (as it was the case for the individual polymers, **Table II.9**), the autocorrelation function is treated by Distribution analysis which relies on non-negative least squares (NNLS) algorithm and calculates the distribution of sizes by their scattering intensity. Finally, the Size-Intensity distribution might be converted into Size-Volume distribution by a built-in software, which applies Mie theory.[55]

Static light scattering: SLS measurements were done using an ALV-CGS3system operating with a vertically polarized laser with wavelength λ = 632 nm. Individual polymer solutions in water used for SLS measurements or for nanoassemblies formation were filtered with a 0.40 μm syringe filters prior to use. The measurements were done at 20°C over a wide range of scattering wave vectors q (0.00046-0.00249 $Å^{-1}$). The normalized electric field autocorrelation functions ($g_1(t)$) obtained from the multi-angle DLS measurements were analyzed in terms of a relaxation time (τ) distribution using the REPES routine[56]: $g_1(t) = \int A(\tau)\exp(-t/\tau)\, d\tau$.

For individual polymers, in addition to fast relaxation mode (short τ) we observed a slow relaxation mode (longer τ), which was particularly the case for the host polymer with the PEG spacer (DT40-gPEG-βCD). The slow relaxation mode has two possible origins. The first, trivially, is the presence of spurious big scatterers problematic to remove by filtration. The second origin consists in possible partial aggregation of the polymers or/and cross-linking issues. Hence, in the case of DT40-gPEG-βCD for the construction of Rayleigh ratio dependency on q and R_g determination we were considering only fast relaxation mode by eliminating the slow mode contribution to the scattering intensity determined from multi-angle DLS.

To establish the values of the detector constants an absolute calibration with toluene was used.[46] The Rayleigh ratios ($R(q)$) for different scattering angles were calculated based on the scattering intensity:

$$R(q) = \frac{I_s(q) \cdot r^2}{I_0 \cdot V_s(q)} \qquad \textbf{(II.6)}$$

where $I_s(q)$the intensity of the scattered light is measured at the scattering wave vector q, I_0 is the intensity of the used laser, $V_s(q)$ is the scattering volume and r is the distance from the

scattering volume to the detector. Rayleigh ratio may be expressed through the Guinier approximation of the form factor:

$$R(q) = KCM \cdot \exp\left(-\frac{1}{3}q^2R_g^2\right) \quad \textbf{(II.2)}$$

where K is the optical contrast constant, C – concentration of the sample [g/mL], M –molecular weight [g/mole]. The exponent part in the expression (**II.2**) is the Guinier approximation for the form factor of a scatterer$P(q) = \exp\left(-\frac{1}{3}q^2R_g^2\right)$.[46] Taking the logarithm on both sides of (**II.2**) and subsequent plotting the Rayleigh ration $R(q)$ as a function of q^2 leads to a straight line with a slope coefficient $a = -\frac{1}{3}R_g^2$ and an intercept with the y-axis equal to $\ln(KCM)$. The optical contrast constant was calculated according to the equation:

$$K = \frac{4\pi^2 n_0^2 (dn/dC)^2}{N_A \lambda_0^4} \quad \textbf{(II.7)}$$

where n_0 is the refractive index of the solvent, λ_0 is the wavelength of the laser beam in vacuum, $N_A$is the Avogadro number and dn/dC the differential refractive index increment of the dissolved molecules. We were using dn/dC = 0.145 mL·g^{-1} reported as the average value for most polysaccharides.[46]

Small-angle X-ray scattering, General: SAXS data were recorded at a wavelength of 1.54 Å, on a flux and background optimized camera from Bruker AXS.[57] The instrument uses a rotating Cu anode as a source and is equipped with Montel multilayer optics, and a home-built (J.S. Pedersen, Aarhus University) compact "scatterless" slit is placed before the samples, which were measured in quartz capillaries of 2 mm diameter. A so-called low-q instrumental setup with 1061 mm sample-to-detector distance was applied. Individual polymer solutions in water used for SLS measurements or for nanoassemblies formation were filtered with a 0.40 μm syringe filters prior to use. In the case of HG nanoassemblies two ways of formulation were investigated: a) successive injection of the host and guest polymer solutions into the capillary while keeping the βCD/Ada = 1:1; b) injection of the nanoassemblies, preliminary formulated by stirring the mixture of the polymers at 800 rpm. The acquisition time for the data was 1800 s. All the measurements were performed at 25°C. Individual polymer and particle scattering patterns were obtained by subtracting from the raw curves the background from Milli-Q water measured

at the same conditions. The initial data treatment was performed using the SUPERSAXS program package (C. L. P. Oliveira and J. S. Pedersen, unpublished) using Milli-Q water as a standard.[58]

The scattering intensity patterns of the investigated polymer and nanoassemblies in aqueous solutions were recorded as functions of "length of the scattering vector" q. As the resolution range for typical SAXS set-ups lies in the range from 1 to 100 nm, the usage of modified low-q set-up with increased sample-to-detector distance was required to match the experimental parameters with the large sizes of the HG nanoassemblies (> 100 nm in terms of D_h). In this way the q_{min} of 0.0038 Å^{-1} was achieved. According to the Fourier transformation sampling theorem, information is lost for sizes larger than π/q_{min} [48], thus indicating that the R_{max} in the experiments discussed below was of 82.6 nm. According to the SAXS theory, the scattering intensity of an ensemble of monodisperse particles is:

$$\Delta I(q) = N \cdot I_0(\Delta\rho)^2 \cdot V_1^2 \cdot P(q) \cdot S(q) \qquad \textbf{(II.8)}$$

where N – number of the particles, $\Delta\rho$ – the difference in electron density between the particles and the matrix (water), I_0 – primary X-ray beam intensity, V_1 – volume of the particle, $P(q)$ – form factor and $S(q)$ – structure factor of the particle. The latter carries information about particle-particle interactions and in cases of dilute systems might be treated as $S(q) = 1$.[59] All the components of the equation (3) except the $P(q)$ and $S(q)$ are independent of scattering angle and might be treated as a constant, which leads to a simplified version of the equation:

$$\Delta I(q) = K \cdot P(q) \cdot S(q) \qquad \textbf{(II.9)}$$

The form factor $P(q)$ bears information on the shape and the internal density distribution of the particles. At small angles any form factor can be approximated by a Gaussian curve and the curvature of the latter is defined by the overall size of the scatterers, according to Guinier[45, 60]:

$$\Delta I(q) = I(0) \cdot e^{-(R_g^2 q^2/3)} \qquad \textbf{(II.10)}$$

where $I(0)$ is the extrapolated zero-angle intensity and R_g is the so-called radius of gyration. $P(q)$ is equal to $\Delta I(q)/I(0)$. Unlike $P(q)$, the radius of gyration is model-independent and contains no information on the shape or structure of the nanoparticles. However, if these parameters could be assumed, like it is the case with the host-guest nanoparticles (spherical

with approximately homogenous internal density distribution), the R_g can be used for calculation of the particle dimensions. For instance, the average radius of compact spherical particles is known to be:

$$R = R_g \cdot \sqrt{\frac{5}{3}} \qquad \textbf{(II.11)}$$

The first way to obtain the R_g values consists in constructing a so-called Guinier plot where the natural logarithm of the intensity $\ln I(q)$ is plotted versus q^2:

$$\ln\Delta I(q) = \ln I(0) - \frac{R_g^2 q^2}{3} \qquad \textbf{(II.12)}$$

The R_g is obtained from the slope of the straight-line fit to the Guinier plot, which is equal to $-\frac{R_g^2}{3}$. As it was mentioned above, the plot should be constructed using the data points from the low q range, where $qR_g < 1$ criterion holds.

The alternative approach to the calculation of R_g from the SAXS data relies upon the Fourier-transformation of the oscillating part of the form factor in the middle-q range, based on the equation:

$$P(q) = 4\pi \int_0^\infty p(r) \frac{\sin(qr)}{qr} dr \qquad \textbf{(II.13)}$$

The resulting curve $p(r)$ is a so-called "pair-distance distribution function" or PDDF and is essentially a histogram of distances that could be found inside the scatterer. Parameters such as the particle maximal dimension and R_g might be then evaluated from a PDDF-curve.[61]

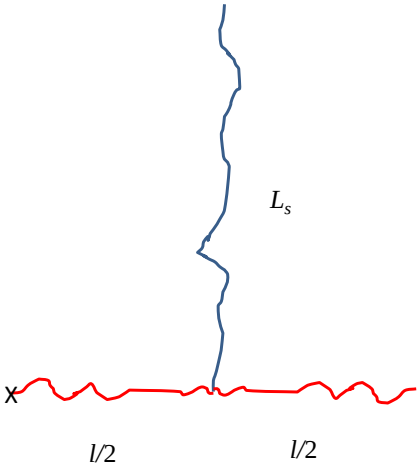

SAXS data modelling: *a) Form factor for comb-like polymers and for stars with comb-like structured arms of Gaussian chains*

We use the formalism of Svaneborg and Pedersen[49] and by this reproduce the results of Casassa and Berry[62] during the

derivation. The basic substructure and the contour length of the cub chains are given in the figure. The X indicates the point for which the scattering amplitude is calculated. When constructing the larger structure, the substructure is connected at the ends of the red chain.

The form factor of the subunit is:

$$P_{sub}(q) = l^2 P_D(q,l) + L_s^2 P_D(q,L_s) + 2lL_s A\left(q,\frac{l}{2}\right) A(q,L_s) \qquad \textbf{(II.14)}$$

where

$$P_D(q,l) = \frac{2(\exp(-x) - 1 + x)}{x^2} \qquad \textbf{(II.15)}$$

with $x = q^2 bl/6$, where q is the modulus of the scattering vector and b is the Kuhn length.

Furthermore:

$$A(q,l) = \frac{(1 - \exp(-x))}{x} \qquad \textbf{(II.16)}$$

The amplitude calculated with respect to X is:

$$A_X(q) = \left(\frac{l}{2}\right) A\left(q,\frac{l}{2}\right) + \Psi(q,l/2)\left((l/2)A\left(q,\frac{l}{2}\right) + L_s A(q,L_s)\right) \qquad \textbf{(II.17)}$$

where:

$$\Psi(q,l) = \exp(-x) \qquad \textbf{(II.18)}$$

For a chain or arm consisting of N substructures (one comb-like) one has, according to Svaneborg and Pedersen[49]:

$$P_{arm}(q) = \frac{1}{N} P_{sub}(q,l) + 2\,\frac{1}{N^2}\frac{\Psi(q,l)^N - N\,\Psi(q,l) + N - 1}{(\Psi(q,l) - 1)^2} A_X(q)^2 \qquad \textbf{(II.19)}$$

Similarly, the scattering amplitude from the end point is:

$$A_{arm}(q) = \frac{1}{N}\frac{\Psi(q,l)^N - 1}{\Psi(q,l) - 1} A_X(q) \qquad \textbf{(II.20)}$$

These last two expressions can now be combined in the star form factor[63] for a structure with f arms:

$$P_{star}(q) = P_{arm}(q, l) + (f - 1)A_{arm}(q)^2 \quad \textbf{(II.21)}$$

b) Form factor for gel-like spherical particles

The particles were fitted with a polydisperse spherical form factor with a Lorentzian function added, similar to the form factor used by Stieger, Richtering, Pedersen, and Lindner.[50] The Lorentzian term accounts for the fluctuations of the polymer network:

$$I(q) = I_{sph}(q) + I_{fluct}(q) \quad \textbf{(II.22)}$$

with $I_{sph}(q)$ equal to:

$$I_{sph}(q) = N \cdot (\Delta\rho)^2 \cdot F(q, \langle R\rangle, \sigma_{poly}) \cdot S(q, \langle R\rangle) \quad \textbf{(II.23)}$$

$\Delta\rho$ is the difference in electron density between the nanoparticles and the solvent, N denotes the number density of the nanoparticles. Due to the relatively low concentrations of the samples the structure factor $S(q, \langle R\rangle$ was approximated to 1 while fitting the data.

The form factor F is expressed as:

$$F(q,\langle R\rangle,\sigma_{poly}) = \int_0^\infty D_{\text{int}}(R,\langle R\rangle,\sigma_{poly})\,\Phi(qR)^2\,dR \quad \textbf{(II.24)}$$

Where $\langle R\rangle$ is the average size, σ_{poly} is the relative polydispersity, $D_{\text{int}}(R,\langle R\rangle,\sigma_{poly})$ is the intensity size distribution and:

$$\Phi(x) = \left(\frac{3[\sin(x) - x\cos(x)]}{(x)^3}\right) \quad \textbf{(II.25)}$$

The intensity size distribution is related to the number size distribution $D_n(R,\langle R\rangle,\sigma_{poly})$ by:

$$D_{\text{int}}(R,\langle R\rangle,\sigma_{poly}) = V^2 D_n(R,\langle R\rangle,\sigma_{poly}) \quad \textbf{(II.26)}$$

where *V* is the volume of the particle with radius *R*. A Gaussian function was used for the intensity size distribution:

$$D_{\text{int}}(R,\langle R\rangle,\sigma_{poly})=\frac{1}{\sqrt{2\pi\sigma_{poly}{}^{2}\langle R\rangle^{2}}}\exp\left(-\frac{(R-\langle R\rangle)^{2}}{2\,\sigma_{poly}{}^{2}\langle R\rangle^{2}}\right) \qquad \textbf{(II.27)}$$

The fluctuation term, $I_{fluct}(q)$, is a lorentzain:

$$I_{fluct}(q)=\frac{I_{fluct}(0)}{1+\xi^{2}q^{2}} \qquad \textbf{(II.28)}$$

where ξ is a correlation length.

Surface plasmon resonance: SPR measurements were carried out with a Spreeta SPR-EVM-BT from Texas Instruments. The light of an infrared light-emitting diode (LED; λ = 840 nm) reaches the sensor surface at a range of angles above the critical angle. A reflectivity-versus-angle spectrum is obtained, and an apparent refractive index (RI) is derived from it by the Spreeta software. The sensor surface is a gold layer (ca. 50 nm). In the case of adsorption on the golden surface the RI changes provide information on the adsorbed layer parameters. The sensor is integrated in a flow cell and the measurements were carried out at 23 °C using a continuous water flow (3 mL/h) which was delivered by a syringe pump (Kd Scientific), and a Rheodyne injection valve to switch to the sample solution.

The sensor surface was cleaned with a 4 % CrO_3 solution in water and rinsed with MeOH before each experiment. After settling the sensor into the flow cell, an in-situ cleaning was performed with one injection (0.1 mL) of a solution of 0.1 M NaOH and 1 % Triton X-100 in water followed by 3 injections (0.1 mL) of 10 % EtOH in water. The sensor was calibrated in pure water, assuming a RI value of 1.33300, and the RI variations after the different polymer injections were monitored as a function of time.

After the cleaning and calibration the adsorption experiments were performed as follows. Three to four consecutive injections of 0.1 mL of pβCDN+ in 0.5 M NaCl (at 2 g/L) were carried out to saturate the gold surface of the sensor. This was followed by 3-4 consecutive injections (0.1 mL) of the host-guest polymers of different types (1 g/L). Then the ΔRI_2 and ΔRI_2 were measured as

the deviations of refractive index due to the 2nd and 3rd layer deposition respectively 20 min after the first injections.

From the values of *Δ*RI the adsorbed amounts of the polymers may be estimated based on the following equation [36]:

$$\Delta RI = m\left(n_{pol} - n_s\right)\left[1 - exp\left(-2d_{pol}/l_d\right)\right] \quad \textbf{(II.29)}$$

where n_s and n_{pol} are refractive indexes of the solvent and the polymer respectively, d_{pol} is the thickness of deposited polymer layer and l_d is the depth of penetration of the evanescent electromagnetic field (typically 25-50% of the probing light wavelength). In the present work it was roughly estimated as 37% (310.8 nm), according to the literature data.[36, 37] We assumed l_d to be constant upon each subsequent polymer adsorption, given the low density of highly hydrated layers and their thickness being much lower than 310.8 nm. The calibration coefficient *m* of the sensor was estimated at 1.

Since $d_{pol} \ll l_d$, *Δ*RI is directly proportional to the layer thickness and the equation (1) may be rewritten as:

$$\Delta RI = m\left(n_{pol} - n_s\right)\left(2d_{pol}/l_d\right) \quad \textbf{(II.30)}$$

The deposited polymer being highly swollen with the solvent leads $n_{pol} \sim n_s$ which means that:

$$n_{pol} - n_s = C_{surf}(dn/dc)_{pol} = (dn/dc)_{pol} \cdot (Q_{ads}/d_{pol}) \quad \textbf{(II.31)}$$

where C_{surf} is the surface concentration and Q_{ads} is the adsorbed amount of the polymer; dn/dc is the RI increment of the polymer with respect to water. In this work it was assumed as 0.145 mL/g for both pβCDN+ and dextran-based host-guest polymers[37]. Combining (**II.28**) and (**II.29**) one obtains already mentioned in the main part equation (1) to calculate the adsorbed amounts:

$$Q_{ads} = \frac{\Delta RI \cdot l_d}{2m \cdot (dn/dc)_{pol}} \quad \textbf{(II.1)}$$

Synthetic procedures

Thiolated Dextran (DT40-SH): In the first stage the dextran hydroxyl groups were activated with 4-NC.[22] Typically dextran (4.0 g, 24.6 mmol of AHG) was dissolved in 120 ml of anhydrous DMF containing 2 w/v% of LiCl at 90°C, under vigorous stirring. The reaction mixture was cooled to 0°C and pyridine (1.5 ml, 20 mmol, molar ratio pyridine/AHG = 0.81) was added to the solution followed by 4-NC (3.47 g, 17.2 mmol). The reaction mixture was stirred at 0°C for 2h, precipitated twice in cold EtOH, washed with 1:1 mixture of EtOH/Et_2O and dried in vacuum overnight at 56°C yielding a white solid (m = 4.06g). DS (from ^{1}H-NMR = 17%). ^{1}H-NMR (DMSO-d_6) δ = 3.0-4.0 (m, dextran glucosidic protons), 4.45, 4.78 and 4.90 (s, dextran hydroxyl protons), 4.67 (s, anomeric proton), 5.29 and 5.53 (s, glucosidic protons at positions bearing nitrophenyl substituents), 7.55 and 8.33 (dd, 2H, aromatic protons).

4-NC activated dextran (4.0 g, 21 mmol of AHG, 3.6 mmol of 4-NC) was dissolved in 35 ml of DMF containing 2 w/v% of LiCl at 55°C. Cysteamine (2.2 g, 28.5 mmol) was dissolved in 50 ml of DMF by warming the solution to 40°C and continuously blowing Argon through it. The solution of cysteamine was added drop wise to the solution of 4-NC activated dextran previously cooled to room temperature. The reaction mixture was stirred at room temperature under argon for 24h, precipitated in cold EtOH and washed with ethanol. The resulting white solid was redissolved in 250 ml of water. Dithioerythritol (0.26 g, 1.7 mmol) was added in order to reduce the disulfide bonds, possibly formed during the reaction. The solution was purified by ultrafiltration (MWCO 10000) against degassed distilled water under nitrogen and finally the product was recovered by freeze drying (m = 3.08 g, 82%). DS (from ^{1}H-NMR = 17%). ^{1}H-NMR (D_2O) δ = 2.66 (t, 2H, NHCH_2), 3.32 (d, 2H, CH_2SH), 3.4-4.1 (m, dextran glucosidic protons), 4.97 (s, anomeric proton), 5.17 and 5.31 (s, glucosidic protons at positions bearing thiol groups).

PEG-acryloyl-5-hexynoate: 5-hexynoic acid (0.69 ml, 6.2 mmol) was dissolved in 15 ml of DCM. A catalytic amount of DMAP (87 mg, 0.72 mmol) was added followed by PEG acrylate (1.60 ml, 4.8 mmol). The solution was cooled until 3-4°C and DCC (1.09 g, 5.3 mmol) was added as a solid. The reaction mixture was stirred at 3°C under argon for 3h and then at room temperature overnight. The formed N,N´-dicyclohexylurea was filtered off through a sintered glass funnel. After removing the DCM under reduced pressure the obtained product was dried under vacuum and used in the next step without purification. ^{1}H-NMR ($CDCl_3$) δ = 1.82 (quin, 2H, hexynoic-

CH_2), 1.94 (t, 1H, C ≡C*H*), 2.23 (td, 2H, hexynoic-CH_2), 2.45 (t, 2H, hexynoic-CH_2), 3.56-3.64 (m, -C*H*$_2$- PEG), 3.66 (t, 2H, C*H*$_2$$CH_2$O-hexynoate), 3.71 (t, 2H, C*H*$_2$$CH_2$O-acrylate), 4.20 (t, 2H, CH_2C*H*$_2$O-hexynoate), 4.28 (t, 2H, CH_2C*H*$_2$O-acrylate), 5.82 (m, 1H, C*H*=CH_2), 6.12 and 6.42 (m, 2H, CH=C*H*$_2$).

DT40-g-PEG-hex-5-ynoate: Thiolated DT40-SH (1.4 g, 1.33 mmol of -SH groups) and lithium chloride (0.45 g, 10.6 mmol) were dissolved in 22 ml of DMF at 50°C while bubbling the solution with argon. The temperature was lowered to 35°C and the 0.4M solution of PEG-acryloyl-5-hexynoate in DMF (6.6 ml, 2.26 mmol) was added to the reaction mixture dropwise followed by hexylamine (60 µl, 0.65 mmol). The reaction was stirred at 35°C for 35h under atmosphere of argon. Finally DMF was evaporated under reduced pressure; the obtained product was redissolved in approximately 50 ml of water and dialyzed against pure water for 3 days. The alkyne terminated grafted copolymer (DT40-g-PEG-hex-5-ynoate) was isolated by freeze drying (m = 1.49 g). DS (from ^{1}H-NMR = 16%). ^{1}H-NMR (DMSO-d_6) δ = 1.69 (quin, 2H, hexynoic-CH_2), 2.20 (td, 2H, hexynoic-CH_2), 2.40 (t, 2H, hexynoic-CH_2), 2.52-2.66 (m, 4H, CC*H*$_2$C*H*$_2$S-clicked acrylate), 2.71 (t, 2H, NHC*H*$_2$), 2.79 (s, 1H, C ≡C*H*), 2.98-3.96 (m, C*H*$_2$SH with dextran glucosidic and PEG main chain protons, overlapped with HDO), 4.06-4.28 (m, 4H, CH_2C*H*$_2$O-hexynoate and CH_2C*H*$_2$O-acrylate), 4.67 (s, anomeric proton), 4.50, 4.85 and 4.91 (m, dextran hydroxyl protons), 5.07 and 5.14 (s, glucosidic protons at substituted positions).

6A-O-p-toluenesulfonyl-βcyclodextrin: *β*CD (25.9 g, 22.5 mmol) was dissolved in 60 ml of water by warming under vigorous stirring. The temperature was lowered to 25°C and finely ground 1-(p-toluenesulfonyl)imidazole (20 g, 90.1 mmol) was added to the solution. The reaction mixture was stirred for 2h hours at room temperature. Sodium hydroxide (11.7 g, 293 mmol) in 32 ml of water was added over 15 min. The reaction mixture was left under stirring for another 15 min and filtered through a sintered-glass funnel in a flask charged with NH_4Cl (31.3 g, 585 mmol). The mixture which gets turbid almost immediately after the complete dissolving of NH_4Cl was concentrated to approximately 3/5 of the initial volume by blowing the air over its surface. The obtained precipitate was filtered off and washed two times with 65 ml of ice cold water and 130 ml of acetone. After drying in vacuum the product was purified by dissolving it in 10 ml of DMSO and precipitation in 140 ml of water. In the following step the product was dissolved in 100 ml of boiling water and cooled in an ice bath. Finally the formed precipitate was filtered off,

washed with 30 ml of water and 60 ml of acetone and isolated by drying in vacuum overnight at 60°C, over P_2O_5. The TLC of the obtained 6A-O-p-toluenesulfonyl-βcyclodextrin (βCD-OTs) showed no residual native βCD and bitosylated product. Yield: 6.54 g (22.6%). ^{1}H-NMR (DMSO-d_6) δ = 2.43 (s, 3H), 3.17-3.42 (m, overlapped with HDO), 3.40-3.76 (m, 28H), 4.15-4.58 (m, 6H), 4.75-4.92 (m, 7H), 5.56-5.93 (m, 14H), 7.43 (d, 2H), 7.75 (d, 2H).

Mono-(O-6-deoxy-6-azido)-βcyclodextrin: βCD-OTs (3.5 g, 2.71mmol) was dissolved in 30 ml of water by warming it to 85°C under vigorous stirring. Excess of sodium azide (2.65 g, 40.7 mmol) was added to the solution and the reaction was stirred at 80°C for 60h. The mixture was precipitated in 320 ml of acetone, filtrated and the product was isolated by drying at 65°C in vacuum. To obtain the pure mono-(O-6-deoxy-6-azido)-βcyclodextrin (βCD-N_3) precipitations in acetone were proceeded until the IR spectrum showed no peak from free sodium azide at 2138 cm^{-1} (**Figure II.8**). Yield: 2.64 g (84.1%). ^{1}H-NMR (DMSO-d_6) δ = 3.21-3.45 (m, overlapped with HDO), 3.49-3.84 (m, 28H), 4.38-4.60 (m, 6H), 4.75-4.93 (m, 7H), 5.56-5.93 (m, 14H).

DT40-g-PEG-βCD: *$CuSO_4$/Na-Asc path.* DT40-g-PEG-hex-5-ynoate (0.2 g, 0.13 mmol of terminal alkynes), βCD-N_3 (0.264 g, 0.23 mmol) and TBTA (0.014 g, 0.026 mmol) were dissolved in 30 ml of preliminary degassed DMSO/water 2:1. The mixture was heated to 50°C while continuously flushing argon through it. After the sodium ascorbate (400 µl of 20 g/L solution, 0.04 mmol) and $CuSO_4 \cdot 5H_2O$ (320 µl of 10 g/L solution, 0.013 mmol) were added, the solution was degassed by bubbling argon under sonication. After stirring at 50°C for 30h the reaction mixture was precipitated in acetone. The precipitate was then washed twice with acetone, dissolved in water and dialyzed against water for 3 days. The βCD terminated Dextran-PEG grafted copolymers (DT40-g-PEG-βCD) were isolated by freeze drying (m = 0.255 g, **P2**). ^{1}H-NMR (DMSO-d_6) δ = 1.85 (quin, 2H, hexynoic-CH_2), 2.39 (t, 2H, hexynoic-CH_2), 2.52-2.66 (m, 4H+2H, CC*H2*C*H2*S-clicked acrylate and hexynoic-CH_2, partly overlapped with DMSO), 2.72 (s, 2H, NHC*H_2*), 2.98-3.91 (m, dextran and βCD glucosidic and PEG main chain protons, overlapped with HDO), 4.07-4.34 (m, 4H, CH_2CH_2O-hexynoate and CH_2CH_2O-acrylate), 4.38-5.30 (m, dextran and βCD anomeric protons + dextran -OH and βCD primary -OH), 5.52-5.97 (m, 14H, βCD-$OH^{2,3}$), 7.79 (s, 1H, triazole).

TBTA: Tris-(benzyltriazolylmethyl)amine or TBTA was prepared using the original procedure reported by Valery V. Fokin and coworkers (**Scheme II.10**).[28]

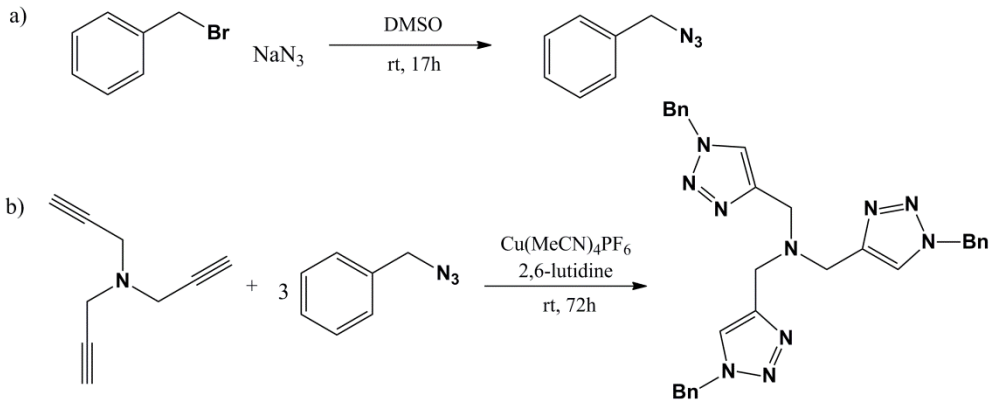

Scheme 10: Two-step synthesis of TBTA – Cu(I)-stabilizing ligand.

a) Sodium azide (6.69 g, 102.9 mmol) was dissolved in 220 ml of DMSO. The solution was dried with molecular sieves, warmed at 25°C and purged with Argon. Benzyl bromide (16 g, 93.5 mmol) was added and the reaction mixture was left under stirring for 17h. The reaction was stopped by adding 800 mL of water while cooling off the reaction flask on ice bath. The resulting DMSO-water mixture was extracted 3 times with 220 mL of Et_2O and the combined Et_2O fractions were washed with brine and water. The benzyl azide was isolated as greenish oil by evaporation of Et_2O under reduced pressure and drying in vacuum for 2h. ^{1}H-NMR ($CDCl_3$) δ = 4.33 (s, 2H, -CH_2-), 7.29-7.41 (m, 5H, aromatic).

b) Tripropargylamine (1.97 g, 15.0 mmol) was dissolved in acetonitrile (20 mL) and treated sequentially with benzyl azide (9.0 g, 67.6 mmol), 2,6-lutidine (1.61 g, 15.0 mmol), and $Cu(MeCN)_4PF_6$ (1.3 mol % with respect to total alkyne units). Upon the addition of the copper salt, the reaction mixture warmed and was cooled down on ice bath. After 72h of stirring at room temperature, white crystalline solid precipitated from the reaction mixture. Filtration and washing with cold acetonitrile yielded fine needle-like crystals of tris-(benzyltriazolylmethyl)amine (4.11 g, 52%). Further used analytically pure sample was obtained by recrystallization of TBTA (2 g) from a hot 1:1 tert-butyl alcohol/water mixture (80 mL), followed by filtration, washing with water (2×40 mL) and drying in vacuum overnight. ^{1}H-NMR ($CDCl_3$) δ = 3.72 (s, 6H, N-CH_2-triazole), 5.50 (s, 6H, Ph-CH_2-), 7.26 (m, 6H, aromatic), 7.34 (m, 9H, aromatic), 7.69 (s, 3H, triazole) (**Figure II.37**).

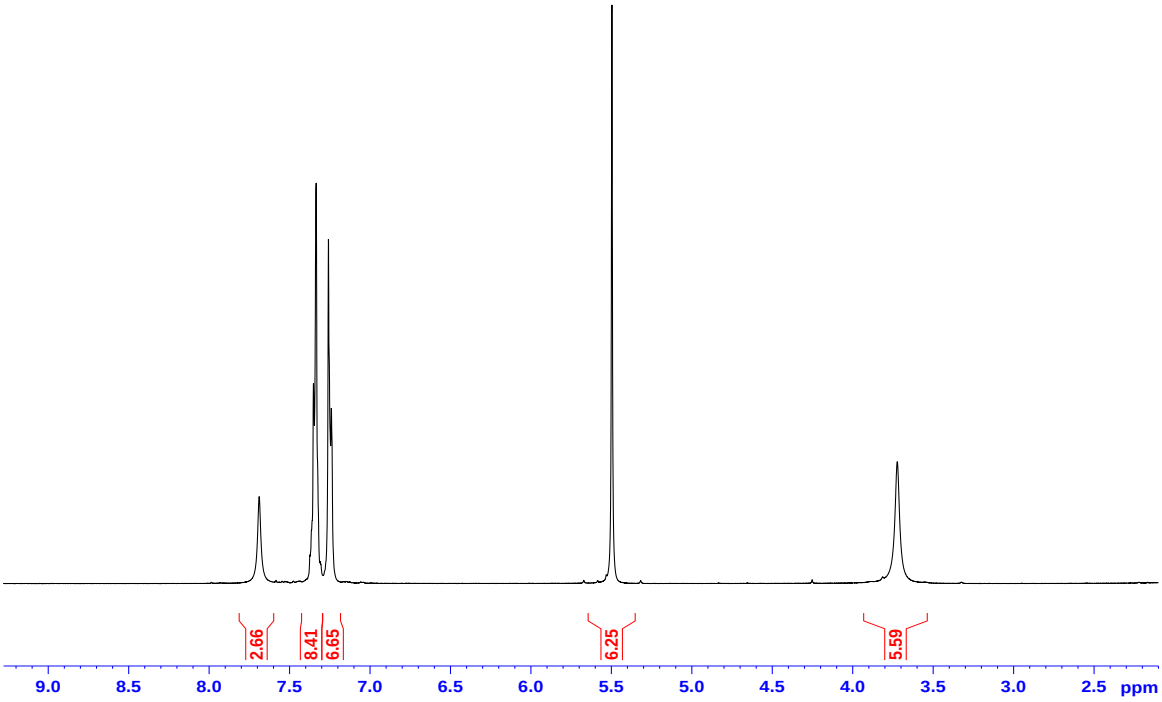

Figure II.37: ^{1}H-NMR spectrum ($CDCl_3$, 400 MHz) of tris-(benzyltriazolylmethyl)amine (TBTA) prepared according to the original procedure.[28]

PEG-acrylate-Ada: PEG-acrylate with M_n~ 375 (0.27 ml, 0.8 mmol) was dissolved in 12 ml of $CHCl_3$. A catalytic amount of DMAP (20 mg, 0.16 mmol) and NEt_3 were added and the solution was cooled to 2-3°C on ice bath followed by addition of 1-adamantanecarbonyl chloride (0.286g, 1.44 mmol) as solid. The reaction mixture was then left under stirring at 2-3°C for 2h, allowed to warm to room temperature and subsequently refluxed for 3h. After evaporation of the solvent under reduced pressure the product was dissolved in 25 mL of 1:1 water-acetone mixture and stirred for 3h at 45°C to destroy the excess of 1-adamantanecarbonyl chloride. The solvents were removed by evaporation under reduced pressure and drying in vacuum. The resulting PEG-acrylate-Ada was isolated as white solid and used in the next step without purification. ^{1}H-NMR ($CDCl_3$) δ = 1.36 (t, 6H, Ada), 1.66 (m, 6H, Ada), 1.83 (s, 3H, Ada), 3.56-3.74 (m, -C*H*$_2$- PEG), 4.14 (t, 2H, -C*H*$_2$O-CO-Ada), 4.25 (t, 2H, -C*H*$_2$O-acrylate), 5.76 (m, 1H, C*H*=CH_2), 6.09 and 6.38 (m, 2H, CH=C*H*$_2$).

DT40-g-PEG-Ada: Thiolated DT40-SH with DS = 12.5 mol.% (0.38 g, 0.28 mmol of -SH groups) and lithium chloride (0.30 g, 7.1 mmol) were dissolved in 15 ml of DMF at 50°C while bubbling the solution with argon. The temperature was lowered to 35°C and PEG-acrylate-Ada (0.430 g,

0.8 mmol) solution in 15 mL of DMF was added to the reaction mixture followed by hexylamine (152 µl, 1.02 mmol). After stirring at 65°C under argon for 16h, the reaction mixture was precipitated in 420 mL of Et_2O, washed twice with Et_2O on a sintered-glass funnel, redissolved and dialyzed against pure water for 5 days. The adamantyl-grafted guest copolymer (here DT40-g-PEG-Ada2) was isolated by freeze drying (m = 0.42 g). DS (from ^{1}H-NMR = 10.5 mol.%). ^{1}H-NMR (D_2O) δ = 1.58 (s, 6H, Ada), 1.75 (s, 6H, Ada), 1.88 (s, 3H, Ada), 2.42-2.85 (m: 4H, -C*H*$_2$C*H*$_2$S-clicked acrylate + 2H, NHC*H*$_2$), 3.02-4.02 (m, C*H*$_2$SH with dextran glucosidic and PEG main chain protons, overlapped with HDO), 4.03-4.30 (m, 4H, CH_2C*H*$_2$O-CO-Ada and CH_2C*H*$_2$O-acrylate), 4.87 (s, anomeric proton), 5.02 and 5.19 (s, glucosidic protons at substituted positions).

References

1. Uekama, K.; Hirayama, F.; Irie, T. Cyclodextrin drug carrier systems. *Chem. Rev.* **1998,** *98* (5), 2045-2076.
2. Drewnowski, A.; Gomez-Carneros, C. Bitter taste, phytonutrients, and the consumer: a review. *Am. J. Clin. Nutr.* **2000,** *72* (6), 1424-1435.
3. Brewster, M. E.; Loftsson, T. Cyclodextrins as pharmaccutical solubilizers. *Adv. Drug Delivery Rev.* **2007,** *59* (7), 645-666.
4. Loftsson, T.; Duchene, D. Cyclodextrins and their pharmaceutical applications. *Int. J. Pharm.* **2007,** *329* (1-2), 1-11.
5. Wintgens, V.; Layre, A. M.; Hourdet, D.; Amiel, C. Cyclodextrin Polymer Nanoassemblies: Strategies for Stability Improvement. *Biomacromolecules* **2012,** *13* (2), 528-534.
6. Maeda, H.; Bharate, G. Y.; Daruwalla, J. Polymeric drugs for efficient tumor-targeted drug delivery based on EPR-effect. *Eur. J. Pharm. Biopharm.* **2009,** *71* (3), 409-419.
7. Lutz, J. F. 1,3-dipolar cycloadditions of azides and alkynes: A universal ligation tool in polymer and materials science. *Angew. Chem., Int. Ed.* **2007,** *46* (7), 1018-1025.
8. Auzely-Velty, R.; Rinaudo, M. Chitosan derivatives bearing pendant cyclodextrin cavities: Synthesis and inclusion performance. *Macromolecules* **2001,** *34* (11), 3574-3580.
9. Charlot, A.; Auzely-Velty, R. Synthesis of novel supramolecular assemblies based on hyaluronic acid derivatives bearing bivalent beta-cyclodextrin and adamantane moieties. *Macromolecules* **2007,** *40* (4), 1147-1158.
10. Ramirez, H. L.; Valdivia, A.; Cao, R.; Fragoso, A.; Labandeira, J. J. T.; Banos, M.; Villalonga, R. Preparation of beta-cyclodextrin-dextran polymers and their use as supramolecular carrier systems for naproxen. *Polym. Bull.* **2007,** *59* (5), 597-605.
11. Fernández, M.; Villalonga, M. L.; Caballero, J.; Fragoso, A.; Cao, R.; Villalonga, R. Effects of β-cyclodextrin–dextran polymer on stability properties of trypsin. *Biotechnol. Bioeng.* **2003,** *83* (6), 743-747.
12. Nielsen, T. T.; Wintgens, V.; Amiel, C.; Wimmer, R.; Larsen, K. L. Facile Synthesis of beta-Cyclodextrin-Dextran Polymers by "Click" Chemistry. *Biomacromolecules* **2010,** *11* (7), 1710-1715.

13. Moses, J. E.; Moorhouse, A. D. The growing applications of click chemistry. *Chem. Soc. Rev.* **2007,** *36* (8), 1249-1262.
14. Rostovtsev, V. V.; Green, L. G.; Fokin, V. V.; Sharpless, K. B. A stepwise Huisgen cycloaddition process: Copper(I)-catalyzed regioselective "ligation" of azides and terminal alkynes. *Angew. Chem., Int. Ed.* **2002,** *41* (14), 2596-2599.
15. Bock, V. D.; Hiemstra, H.; van Maarseveen, J. H. Cu-I-catalyzed alkyne-azide "click" cycloadditions from a mechanistic and synthetic perspective. *Eur. J. Org. Chem.* **2006,** (1), 51-68.
16. Hoyle, C. E.; Lowe, A. B.; Bowman, C. N. Thiol-click chemistry: a multifaceted toolbox for small molecule and polymer synthesis. *Chem. Soc. Rev.* **2010,** *39* (4), 1355-1387.
17. Heggli, M.; Tirelli, N.; Zisch, A.; Hubbell, J. A. Michael-type addition as a tool for surface functionalization. *Bioconjugate Chem.* **2003,** *14* (5), 967-973.
18. Munteanu, M.; Choi, S.; Ritter, H. Cyclodextrin Methacrylate via Microwave-Assisted Click Reaction. *Macromolecules* **2008,** *41* (24), 9619-9623.
19. Wintgens, V.; Nielsen, T. T.; Larsen, K. L.; Amiel, C. Size-Controlled Nanoassemblies Based on Cyclodextrin-Modified Dextrans. *Macromolecular Bioscience* **2011,** *11* (9), 1254-1263.
20. Antoniuk, I.; Volet, G.; Wintgens, V.; Amiel, C. Synthesis of a new dextran-PEG-b-cyclodextrin host polymer using ‘‘Click’’ chemistry. *Journal of Inclusion Phenomena and Macrocyclic Chemistry* **2014,** *80*, 93-100.
21. Hiemstra, C.; van der Aa, L. J.; Zhong, Z. Y.; Dijkstra, P. J.; Feijen, J. Rapidly in situ-forming degradable hydrogels from dextran thiols through michael addition. *Biomacromolecules* **2007,** *8* (5), 1548-1556.
22. Ramirez, J. C.; Sanchezchaves, M.; Arranz, F. DEXTRAN FUNCTIONALIZED BY 4-NITROPHENYL CARBONATE GROUPS - AMINOLYSIS REACTIONS. *Angew. Makromol. Chem.* **1995,** *225*, 123-130.
23. Neises, B.; Steglich, W. Simple Method for the Esterification of Carboxylic Acids. *Angew. Chem., Int. Ed.* **1978,** *17* (7), 522-524.
24. Kolb, H. C.; Finn, M.; Sharpless, K. B. Click chemistry: diverse chemical function from a few good reactions. *Angew. Chem., Int. Ed.* **2001,** *40* (11), 2004-2021.
25. Hoyle, C. E.; Bowman, C. N. Thiol–ene click chemistry. *Angew. Chem., Int. Ed.* **2010,** *49* (9), 1540-1573.
26. Chan, J. W.; Hoyle, C. E.; Lowe, A. B.; Bowman, M. Nucleophile-Initiated Thiol-Michael Reactions: Effect of Organocatalyst, Thiol, and Ene. *Macromolecules* **2010,** *43* (15), 6381-6388.
27. Byun, H.-S.; Zhong, N.; Bittman, R. 6A-O-p-TOLUENESULFONYL-β-CYCLODEXTRIN. *Org. Synth.* **2004,** *10*, 690-692.
28. Chan, T. R.; Hilgraf, R.; Sharpless, K. B.; Fokin, V. V. Polytriazoles as copper(I)-stabilizing ligands in catalysis. *Org. Lett.* **2004,** *6* (17), 2853-2855.
29. Menuel, S.; Azaroual, N.; Landy, D.; Six, N.; Hapiot, F.; Monflier, E. Unusual Inversion Phenomenon of β-Cyclodextrin Dimers in Water. *Chemistry–A European Journal* **2011,** *17* (14), 3949-3955.
30. Potier, J.; Menuel, S.; Azaroual, N.; Monflier, E.; Hapiot, F. Limits of the Inversion Phenomenon in Triazolyl-Substituted β-Cyclodextrin Dimers. *Eur. J. Org. Chem.* **2014,** *2014* (7), 1547-1556.
31. De Belder, A.; Granath, K. Preparation and properties of fluorescein-labelled dextrans. *Carbohydr. Res.* **1973,** *30* (2), 375-378.

32. Wiberg, K. B.; Wang, Y.-g.; Miller, S. J.; Puchlopek, A. L.; Bailey, W. F.; Fair, J. D. Disparate Behavior of Carbonyl and Thiocarbonyl Compounds: Acyl Chlorides vs Thiocarbonyl Chlorides and Isocyanates vs Isothiocyanates. *The Journal of organic chemistry* **2009,** *74* (10), 3659-3664.
33. Carrazana, J.; Jover, A.; Meijide, F.; Soto, V. H.; Vázquez Tato, J. Complexation of adamantyl compounds by β-cyclodextrin and monoaminoderivatives. *The Journal of Physical Chemistry B* **2005,** *109* (19), 9719-9726.
34. Renard, E.; Deratani, A.; Volet, G.; Sebille, B. Preparation and characterization of water soluble high molecular weight beta-cyclodextrin-epichlorohydrin polymers. *Eur. Polym. J.* **1997,** *33* (1), 49-57.
35. Blomberg, E.; Kumpulainen, A.; David, C.; Amiel, C. Polymer bilayer formation due to specific interactions between beta-cyclodextrin and adamantane: A surface force study. *Langmuir* **2004,** *20* (24), 10449-10454.
36. Jung, L. S.; Campbell, C. T.; Chinowsky, T. M.; Mar, M. N.; Yee, S. S. Quantitative interpretation of the response of surface plasmon resonance sensors to adsorbed films. *Langmuir* **1998,** *14* (19), 5636-5648.
37. Wintgens, V.; Amiel, C. Surface plasmon resonance study of the interaction of a beta-cyclodextrin polymer and hydrophobically modified poly(N-isopropylacrylamide). *Langmuir* **2005,** *21* (24), 11455-11461.
38. Wintgens, V.; Daoud-Mahammed, S.; Gref, R.; Bouteiller, L.; Amiel, C. Aqueous polysaccharide associations mediated by beta-cyclodextrin polymers. *Biomacromolecules* **2008,** *9* (5), 1434-1442.
39. Daoud-Mahammed, S.; Couvreur, P.; Bouchemal, K.; Chéron, M.; Lebas, G.; Amiel, C.; Gref, R. Cyclodextrin and polysaccharide-based nanogels: entrapment of two hydrophobic molecules, benzophenone and tamoxifen. *Biomacromolecules* **2009,** *10* (3), 547-554.
40. Daoud-Mahammed, S.; Ringard-Lefebvre, C.; Razzouq, N.; Rosilio, V.; Gillet, B.; Couvreur, P.; Amiel, C.; Gref, R. Spontaneous association of hydrophobized dextran and poly-β-cyclodextrin into nanoassemblies.: Formation and interaction with a hydrophobic drug. *J. Colloid Interface Sci.* **2007,** *307* (1), 83-93.
41. Gref, R.; Amiel, C.; Molinard, K.; Daoud-Mahammed, S.; Sébille, B.; Gillet, B.; Beloeil, J.-C.; Ringard, C.; Rosilio, V.; Poupaert, J. New self-assembled nanogels based on host–guest interactions: characterization and drug loading. *J. Controlled Release* **2006,** *111* (3), 316-324.
42. Wintgens, V.; Daoud-Mahammed, S.; Gref, R.; Bouteiller, L.; Amiel, C. Aqueous polysaccharide associations mediated by β-cyclodextrin polymers. *Biomacromolecules* **2008,** *9* (5), 1434-1442.
43. Ravoo, B. J.; Jacquier, J. C.; Wenz, G. Molecular recognition of polymers by cyclodextrin vesicles. *Angew. Chem., Int. Ed.* **2003,** *42* (18), 2066-2070.
44. Patterson, J. P.; Robin, M. P.; Chassenieux, C.; Colombani, O.; O'Reilly, R. K. The analysis of solution self-assembled polymeric nanomaterials. *Chem. Soc. Rev.* **2014,** *43* (8), 2412-2425.
45. Schnablegger, H.; Singh, Y. The SAXS guide: getting acquainted with the principles. *Anton Paar GmbH* **2013,** *2*.
46. Øgendal, L. Light Scattering. **2013**.
47. Plazzotta, B.; Fegyver, E.; Mészáros, R.; Pedersen, J. S. Anisometric Polyelectrolyte/Mixed Surfactant Nanoassemblies Formed by the Association of Poly (diallyldimethylammonium chloride) with Sodium Dodecyl Sulfate and Dodecyl Maltoside. *Langmuir* **2015,** *31* (26), 7242-7250.

48. Jensen, G. V.; Shi, Q.; Hernansanz, M. J.; Oliveira, C. L.; Deen, G. R.; Almdal, K.; Pedersen, J. S. Structure of PEP–PEO block copolymer micelles: exploiting the complementarity of small-angle X-ray scattering and static light scattering. *J. Appl. Crystallogr.* **2011,** *44* (3), 473-482.
49. Svaneborg, C.; Pedersen, J. S. A formalism for scattering of complex composite structures. I. Applications to branched structures of asymmetric sub-units. *The Journal of chemical physics* **2012,** *136* (10), 104105.
50. Stieger, M.; Richtering, W.; Pedersen, J. S.; Lindner, P. Small-angle neutron scattering study of structural changes in temperature sensitive microgel colloids. *The Journal of chemical physics* **2004,** *120* (13), 6197-6206.
51. Davidson, N. S.; Richards, R. W.; Maconnachie, A. Determination of correlation lengths in swollen polymer networks by small-angle neutron scattering. *Macromolecules* **1986,** *19* (2), 434-441.
52. Lyon, L. A.; Serpe, M. J. *Hydrogel micro and nanoparticles*; John Wiley & Sons2012.
53. Alvarez, S. G.; Alvarez, M. T. A practical procedure for the synthesis of alkyl azides at ambient temperature in dimethyl sulfoxide in high purity and yield. *Synthesis-Stuttgart* **1997,** (4), 413-414.
54. Burckbuchler, V.; Wintgens, V.; Lecomte, S.; Percot, A.; Leborgne, C.; Danos, O.; Kichler, A.; Amiel, C. DNA compaction into new DNA vectors based on cyclodextrin polymer: Surface enhanced Raman spectroscopy characterization. *Biopolymers* **2006,** *81* (5), 360-370.
55. Instruments, M. Dynamic light scattering: an introduction in 30 minutes. *Technical Note Malvern, MRK656-01* **2012**, 1-8.
56. Brown, W. *Dynamic light scattering: the method and some applications*; Oxford University Press, USA1993; Vol. 49.
57. Plazzotta, B.; Dai, J.; Behrens, M. A.; Furó, I.; Pedersen, J. S. Core Freezing and Size Segregation in Surfactant Core–Shell Micelles. *The Journal of Physical Chemistry B* **2015,** *119* (33), 10798-10806.
58. Orthaber, D.; Bergmann, A.; Glatter, O. SAXS experiments on absolute scale with Kratky systems using water as a secondary standard. *J. Appl. Crystallogr.* **2000,** *33* (2), 218-225.
59. Glatter, O.; Kratky, O. Small angle scattering. Academic Press: New York, 1982.
60. Guimer, A.; Fournet, G. Small angle scattering of X-rays. *J. Wiley & Sons, New York* **1955**.
61. Glatter, O. A new method for the evaluation of small-angle scattering data. *J. Appl. Crystallogr.* **1977,** *10* (5), 415-421.
62. Casassa, E. F.; Berry, G. C. Angular distribution of intensity of Rayleigh scattering from comblike branched molecules. *Journal of Polymer Science Part A-2: Polymer Physics* **1966,** *4* (6), 881-897.
63. Benoit, H. On the effect of branching and polydispersity on the angular distribution of the light scattered by gaussian coils. *Journal of Polymer Science* **1953,** *11* (5), 507-510.

Chapter 3

Bifunctionalized dextrans for surface PEGylation via multivalent host-guest interactions

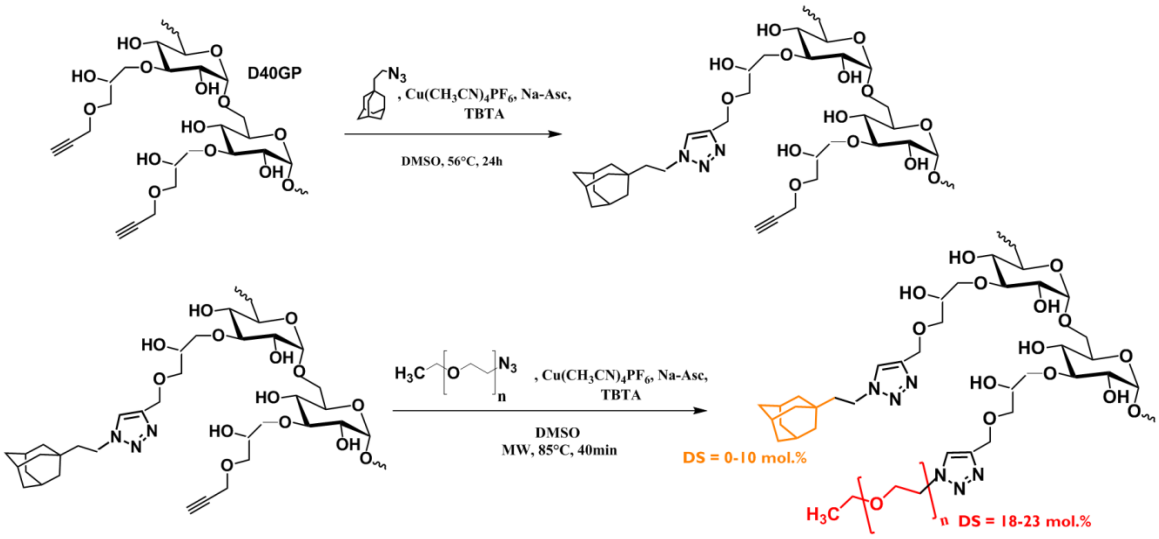

Table of contents

Introduction

a. PEG and PEGylation. General information

Nowadays, poly(ethylene glycol) (PEG) is by far the most commonly used non-ionic hydrophilic polymer in cosmetic and health care industries.[1, 2] The most basic advantageous properties of PEG include:

- Easiness of preparation of polymers with a wide range of molar masses, from 400 $g \cdot mole^{-1}$ up 4000 $kg \cdot mole^{-1}$ and higher
- The most common way of PEG synthesis, i.e. anionic polymerization of ethylene oxide allows preparing PEGs with the polydispersity indexes (PDIs) as low as 1.01[1]; this feature is of high importance in biomedical applications to gain the reproducibility of the bioavailability and immunogenicity profiles of PEG-containing formulations
- PEG has an amphiphilic character, i.e. shows a high solubility both in water and in organic solvents; the latter leads to easiness of its end-modifications with various hydrophobic functionalities, such as targeting groups, fluorescent labels etc.
- Very low toxicity (LD_{50} = 50 $g \cdot kg^{-1}$ body weight for oral administration in mice and guinea pigs)

The covalent or non-covalent coupling of drugs or drug-containing nanoscale carriers with PEG is referred to as PEGylation. The first coupling of PEG to a protein was reported back in the 1970s by Abuchowski et al., and the resulting PEGylated albumin exhibited improved pharmacokinetic profile, i.e. non-immunogenicity and increased blood circulation time from 12h to 48h.[3] Since then, a great number of PEG conjugates with proteins, polypeptides, DNA, RNA and small molecule therapeutics were found to show significantly improved, as compared to non-PEGylated formulations, performances, with some of them getting the FDA approval and reaching the market. As for 2011, there was nine FDA-approved PEGylated protein drugs already on the market and much more on the last stages of clinical trials.[4] In the case of such PEG-drug conjugates there are a few main reasons behind the beneficial impact of PEG:

- Increase of their molar mass leads to reduced rates of kidney excretion and results in a prolonged blood circulation time of the drug. For this reason proteins and small

molecule drugs are usually coupled with relatively high molecular mass PEGs (20-50 kg·mole^{-1})

- Due to the high flexibility of PEG chains, the latter exist in a form of so-called "conformational cloud"[1], its polymer chains experience fast transitions between a large number of possible conformations in water. "Conformational cloud" creates an effect of sterical hindrance on the surface of a PEGylated drug carrier, thus preventing their enzymatic cleavage, as well as opsonization by blood proteins[5] and uptake by reticuloendothelial system (RES)[6, 7] This phenomenon is also known as "stealth" effect.
- In the case of charged nanomedicines such as PEI-based gene carriers, PEGylation allows shielding their positive charges, thereby diminishing non-specific interactions with blood components and reducing toxicity[8, 9]

The initial works describing the PEGylation of nanoparticulate drug carriers date back to the beginning of 1990s. At the first stage, PEG brush layers were attached to liposomes, which resulted in sterical stabilization and increased blood circulation times of the latter.[10] Further, in 1994, Gref et al. reported reduced rates of liver clearance for poly(lactide-co-glycolide) (PLGA) nanospheres coated with 20 kg·mole^{-1} PEG.[11] These early studies became the basis for the development of the only FDA-approved particulate drug delivery system on the market – Doxil/Caelyx, composed of PEGylated liposomes loaded with anticancer doxorubicin.[1] Beneficial impact of PEG coating on the nanoscale drug carriers is due to the similar reasons as those listed above for protein-, gene- and small molecule-based drugs. In the case of intravenous administration PEGylated nanocarriers are sterically stabilized against aggregation and uptake by the blood mononuclear phagocyte system (MPS)[7, 12, 13]; PEG "corona" leads to higher apparent sizes, thus increasing the efficiency of nanocarriers accumulation in cancer and/or inflamed tissues due to the enhanced permeability and retention effect (EPR). Altogether these effects allow for lower frequencies of administration and decreased payloads of drugs in nanoparticulate carriers, which in turn improves the life quality of the patients. It should be noted that lower PEG molar masses (1-5 kg·mole^{-1}) are typically used for modification of nanoparticles, as compared to proteins and small molecules. This is explained by the possibility of linking multiple PEG grafts to a single nanoparticle, thus still significantly increasing its molar mass and hydrodynamic diameter.[2] In addition, after the therapeutic function of a nanocarrier is

completed 1-5 kg·mole^{-1} PEGs can be much easily excreted from the body though the renal clearance.

Besides all the aforementioned positive qualities of PEG, its biomedical use can also be associated with a number of drawbacks and unfavorable effects.[1, 14] For instance, PEGylated liposomal carriers such as Doxil/Caelyx were reported to provoke immunogenic hypersensitivity reactions (HSR) that can provoke an anaphylactic shock in up to 25% of patients.[15] However, to date there is no clear evidence as to whether the HSR is caused by PEG alone or by a complex combination of several factors. The second important drawback of PEG consists in its non-biodegradability. Therefore, the highest molar mass appropriate for *in vivo* applications cannot exceed the renal clearance threshold, the latter being around 60 kg·mole^{-1}(corresponds to hydrodynamic radius of 3.5 nm).[5, 16, 17] In several studies researchers observed accelerated blood clearance of PEGylated nanomedicines occurring after repeated administrations.[18, 19] Though the mechanism behind it is not fully understood, it was suggested that anti-PEG antibodies might be formed in spleen. Finally, as compared to polymers with carbon backbone, PEG is more susceptible to undergo peroxide-mediated degradation at increased temperatures and under stress, leading to formation of toxic byproducts.[1]

The PEGylation might be achieved using both covalent and non-covalent modification methods. To date, covalent PEGylation techniques are more numerous and usually rely either on preparation of PEG-containing block copolymers with subsequent drug-loaded polymeric micelles formation[13] or on covalent post-modification of small molecule drugs, proteins or nanocarriers.[16, 20, 21] For solid NPs, such as gold, thiol-chemistry is the classic approach for PEGylation, where a sulfhydryl-capped PEG chain adheres to the gold surface.[2]

Non-covalent techniques are more commonly used for PEGylation of nanoparticulate carriers and include: coating the hydrophobic nanoparticle surface with lipid-PEG conjugates (was applied for stabilization of single-walled carbon nanotubes)[22]; simple inclusion of lipid-PEG conjugates in the lipid mixture during the preparation of liposomal systems[23]; formation of coordination complexes between Ni^{2+} or Cu^{2+} chelate-functionalized PEGs and nitrogen of histidine side chains in a protein[24]; physical adsorption by “host-guest” interactions.[25, 26, 27] Non-covalent approach can avoid some important shortcomings of covalent PEGylation such as

decrease of activity in case of protein-based drugs and tedious purification steps that decrease the yield of the final product.

b. βCD host-guest chemistry and PEGylation

During the last two decades a high number of researches were aiming at diminishing the phenomenon of initial "burst release" of actives from nanoscale drug delivery carriers.[28] Along with superficial cross-linking, adsorption or impregnation of drug carriers with CD-containing materials was found to be an efficient strategy to address this issue. For instance, Quaglia et al. found that co-encapsulation of hydroxypropyl-βCD into PLGA microspheres leads to a significant decrease of the initial "burst" of loaded insulin.[29] El Fagui and Amiel reported a procedure of benzophenone-loaded polylactic acid (PLA) nanoparticles coating with neutral epichlorohydrin-crosslinked poly-βCD and showed it beneficial impact on the kinetic profile of benzophenone release, governed by the inclusion complexation of the latter with the βCDs in the shell of the nanocarriers.[30] In a more recent example membrane fusion between liposomes and cyclodextrin vesicles was exploited to prepare hybrid assemblies composed of liposomal core covered with layers of βCD amphiphiles.[31] Yet another way of introducing βCD in nanoscale drug carriers consists in assembling βCD polymers with "guest"- labeled amphiphilic copolymers. [32, 33]

Although a number of works has already reported host-guest anchoring of PEG chains onto β-cyclodextrin containing surfaces[9, 25], to the best of our knowledge, only few studies of the multivalence effect, when multiple poly(ethylene oxide-co-propylene oxide) (PEPO) grafts and guest groups were attached to a polymer backbone, on the PEGylation efficiency have been done so far.[34] Cooperative character of multivalent host-guest interactions leads to strong interpolymer binding, which might be successfully exploited for the construction of various supramolecular architectures. For instance, Dubacheva et al.[35] used ferrocene (Fc)-guest and βCD-host derivatives of the same polymer, poly(N-hydroxypropylmethacrylamide (PHPMA), to construct polymeric multilayer films with no limitation of the number of layer-by-layer (LbL) deposition steps. More recently, the same researchers observed a phenomenon of so-called "superselectivity" in the multivalent interactions between self-assembled monolayers (SAMs) functionalized with the Fc-guest and hyaluronic acid (HA) modified with βCDs.[36] It implies that the surface density of bound macromolecules increases faster than linearly with the density of surface binding sites. In this work we present a possible path for combination of the benefits of

PEGylation and βCD-containing materials. We report a synthesis of novel (PEG, Ada)-grafted dextrans, prepared by copper-catalyzed azide-alkyne cycloaddition (CuAAC). These bifunctionalized "guest" polymers are bearing various amounts of 5000 g/mol PEG chains and hydrophobic adamantyl (Ada) groups at the same time. The ability of (PEG, Ada)-grafted dextrans to form inclusion complexes in solution and on surface with native βCD and βCD-polymers are investigated with the purpose of their further use for facile PEGylation of interfaces and nanoparticles via multivalent host-guest interactions.

This work has been published as an original article in Carbohydrate Polymers in 2015.[37]

1. Synthesis of PEGylated guest polymers - D40-*X*GP-*Y*Ada-*Z*PEG

Copper-catalyzed azide-alkyne cycloaddition (CuAAC) was chosen as an efficient tool to couple both adamantyl and MeOPEG moieties to the dextran backbone.[38, 39] Azide-substituted adamantane derivatives, azide-terminated MeOPEG and alkyne-substituted dextrans were chosen as building blocks for CuAAC.

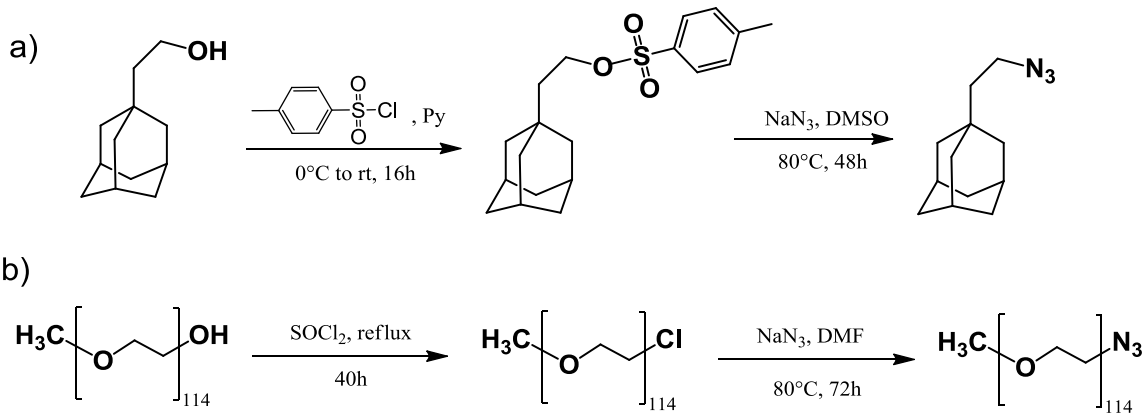

Scheme III.1: Reaction scheme for the synthesis of 1-adamantaneethylazide (a) and MeOPEG-N_3 (b).

Azide-substituted adamantane derivative (Ada-N_3, **Scheme III.1a**) was prepared according to the modified 2-step procedure used by Suzuki et al.[40] It involves tosylation of 1-adamantaneethanol in pyridine, followed by nucleophilic substitution with NaN_3 in DMSO. It should be noted that the obtained 1-adamantaneethyltosylate was not exposed to tedious column chromatography purification and after filtration on silica pad it contained some traces of native 1-

adamantaneethanol. However, it was not a problem due to its inability to react with NaN_3 in DMSO during the second step.

Azide-terminated MeOPEG (MeOPEG-N_3) was synthesized by a two-step procedure (**Scheme III.1b**). The terminal hydroxyls of PEG were first converted to chlorides with $SOCl_2$, according to a previously described method.[41] The chlorides were subsequently converted into azides by S_N2 substitution with an excess of NaN_3 in DMF. During the purification stage washing with water proved to be crucial for the full elimination of unreacted NaN_3.

Dextran with a molecular weight of 40 000 g·mole^{-1} was modified with alkynes using the basic epoxide opening of glycidyl propargyl ether in water, according to the procedure described in literature (Experimental section, **Scheme III.2**).[42] Choice of the ether bond was made considering its hydrolytic stability and a relatively long resulting spacer between the dextran backbone and grafted alkynes. The latter proved to be important for the preservation of good inclusion properties of subsequently grafted host-guest functions. The ^{1}H-NMR spectra of the resulting polymers (D40-GP) in D_2O show a well-separated singlet of terminal alkyne protons at 2.90 ppm (**Figure III.1**).

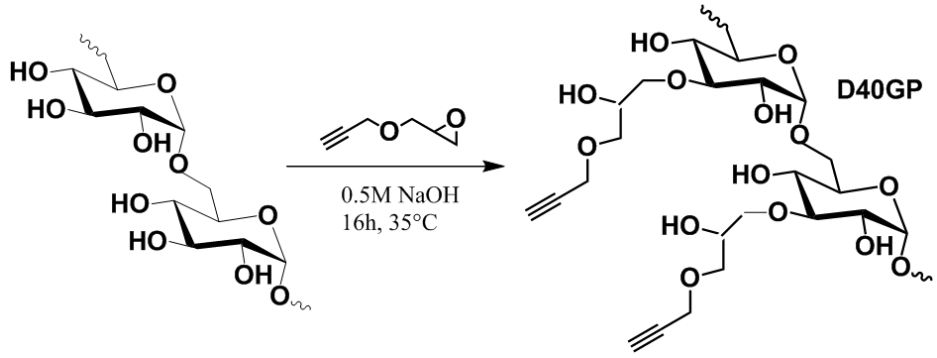

Scheme III.2: Synthesis of terminal alkyne-substituted dextrans (D40-GP).

At the next stage, D40-GP-Ada-PEG with various DS were prepared by one-pot CuAAC (**Scheme III.3**). Pure DMSO as a solvent and Cu(MeCN)$_4$PF$_6$ /Na-Asc as a catalytic system were chosen because of the poor solubility of Ada-N_3 in water. A Cu(I)-stabilizing polytriazole ligand TBTA was applied to prevent any undesirable acetylenic cross-couplings often encountered when dealing with alkyne polymeric scaffolds.[42, 43, 44]

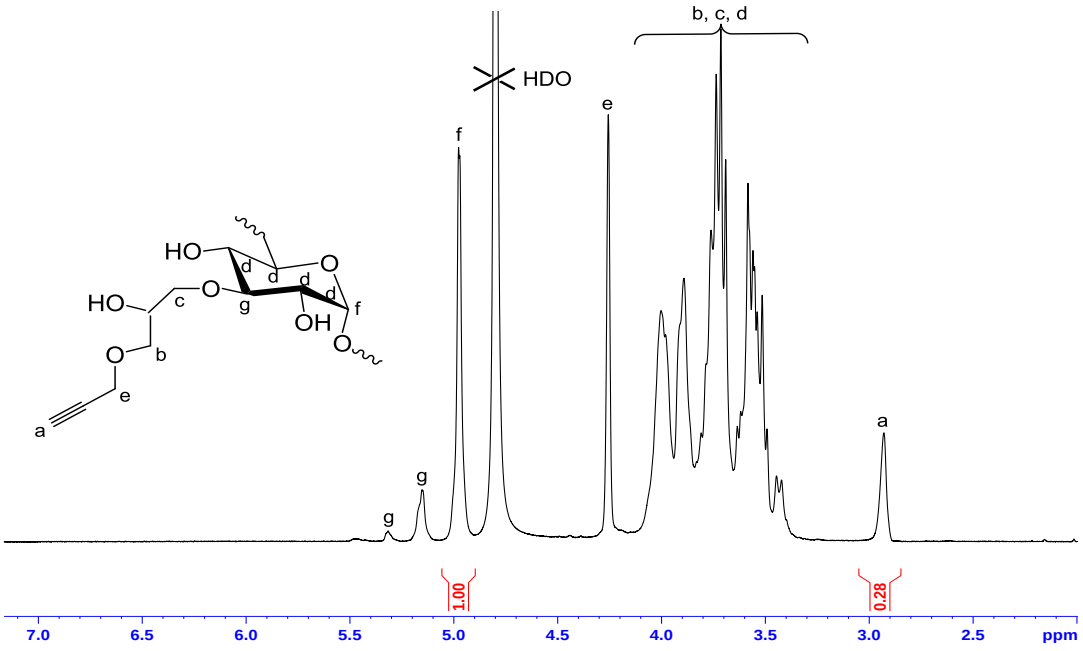

Figure III.1: ^{1}H-NMR spectrum of alkyne-modified dextran D40-28GP in D_2O.

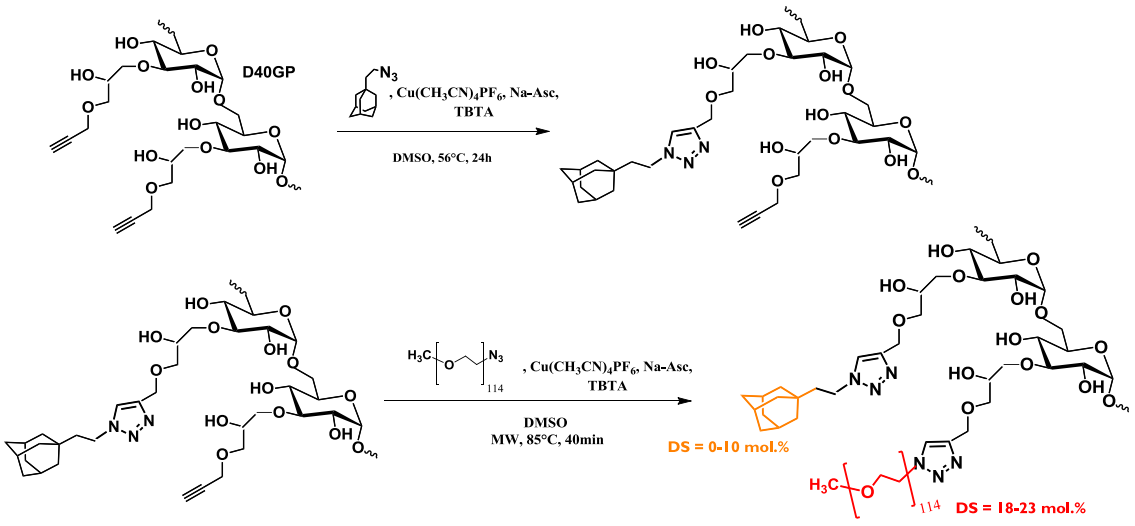

Scheme III.3: Reaction scheme for the MW-assisted one-pot CuAAC synthesis of D40-GP-Ada-PEG.

Typically, in the first step the aimed amount of Ada-N_3 was "clicked" quantitatively; then 1.6-1.8 equivalents of MeOPEG-N_3 were added to the reaction mixture to consume the residual alkynes. When performed under classical heating, due to the bulkiness of MeOPEG-N_3, the CuAAC required very long reaction times (3 days) for the second step completion. Microwave-assisted heating was reported to significantly increase the reaction rates of CuAAC, especially when the reactants are bulky or polymeric units[45, 46]. Indeed, when the same one-pot procedures were

performed under microwave irradiation, the reaction times reduced dramatically. Full conversion of the residual alkynes by the reaction with MeOPEG-N_3 was typically achieved within 40 min at 85 °C.

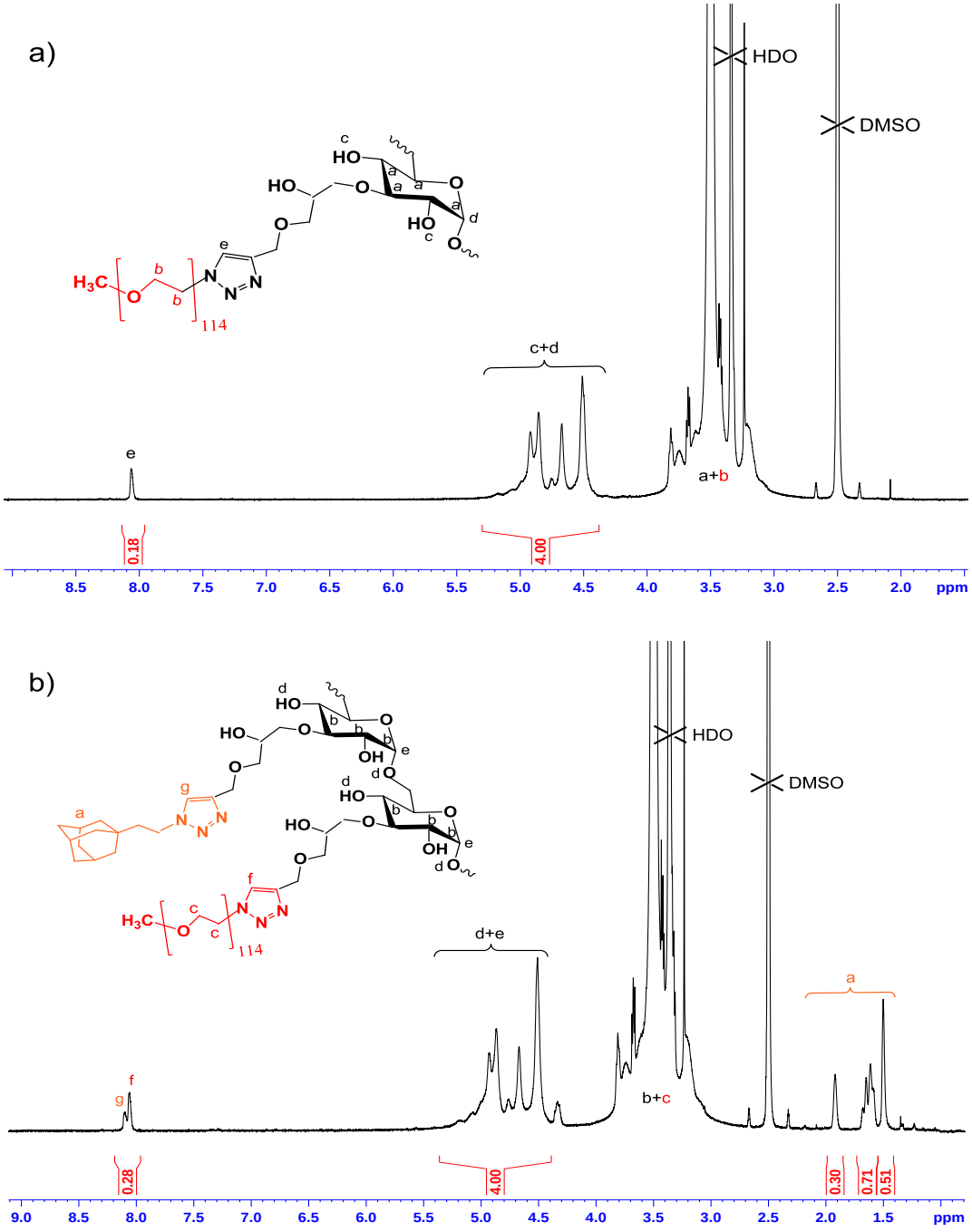

Figure III.2: ^{1}H-NMR spectra in DMSO-d_6 of: **a)** D40-18GP-18PEG, modified exclusively with 18 mol.% of 5000 g·mole^{-1} PEG chains. A single triazole proton is found at 8.06 ppm; **b)** D40-28GP-10Ada-18PEG, modified with 18 mol.% of PEG and 10 mol.% of adamantyl groups. Two partially overlapping triazole protons are observed at 8.06 and 8.10 ppm.

To evaluate binding properties of D40-GP-Ada-PEG polymers we studied their interaction in solution and on the surface with neutral epichlorhydrin-interconnected pβCD and positively charged pβCDN+, modified with quaternary ammonia, host polymers. The latter were prepared according to the previously reported by our scientific group procedure (described in the Experimental section).[47, 48] These polymers have branched structure where βCD moieties may be thought of as balls interlinked by poly(2-hydroxypropyl)ether sequences of different lengths (the structural formulas can be found in Chapter 2, **Figure II.17**). Due to the seven-time excess of epichlorohydrin with respect to βCD, a part of it is consumed on the formation of polytails along with polybridges. The sample used in this work has a cyclodextrin weight ratio (g/g) of 58.2%, as determined by ^{1}H-NMR, a molecular weight M_w of 208 kg·mole^{-1}, and a polydispersity index of 1.81, which were determined by size exclusion chromatography (SEC). To obtain positively charged host polymer, pβCD was modified with quaternary ammonia by reaction with 2,3-epoxypropyltrimethylammonium. The characteristics of all the host and guest polymers are reported in **Table III.1**.

Table III.1. Characteristics of D40-*X*GP-*Y*Ada-*Z*PEG (guest) and pβCD (host) polymers

Guest polymers	**GP, mol%**	**Ada, mol%**	**PEG, mol%**
D40-18GP-18PEG	18	0	18
D40-28GP-5Ada-23PEG	28	5	23
D40-28GP-10Ada-18PEG	28	10	18
Host Polymers	**CD, wt%**	**M_w, kg·mole^{-1}**	**N+/CD**
pβCD	67.0	208	0
pβCDN+[a]	58.2	-	1.62

[a] - prepared by modification of pβCD

2. Binding properties of D40-GP-Ada-PEG in solution. ITC studies

The ability of D40-GP-Ada-PEG to form inclusion complexes with βCD and βCD-polymers was examined by isothermal titration microcalorimetry (ITC). The interactions of the polymers with monomeric βCD are highly exothermic (**Table III.2**) as expected, given the perfect matching in size between grafted Ada and βCD-cavities, leading to strong van der Waals interactions between them. The experimental titration curves (**Figure III.3a**) were fitted to a simple 1:1

interaction model, which assumes that each of the Ada groups grafted on one chain (12 to 25 per chain) acts independently from the others. Basic thermodynamic parameters derived from these experiments are shown in **Table III.2**. The association constants are as high as 4.0-6.0 · 10^4 L/mole, which is superior to previously described dextrans modified with Ada-groups via simple esterification by 1-adamantanecarbonyl chloride.[33] It might be explained by the presence of relatively long and hydrophilic spacer in D40-GP-Ada-PEG, the latter making Ada groups more loosely attached and available for complexation. As in the work by Wintgens et al.,[33] a slight decrease of K_a is observed when the DS by Ada-groups is increased from 5 to 10 mol%, which could be attributed to a gradual loss of their accessibility due to sterical hindrance effects.

At the next stage we applied ITC to study the interpolymer interactions. The concentration of Ada groups in the solutions of D40-GP-Ada-PEGs was fixed at $5 \cdot 10^{-4}$ mole/L. The solution of D40-18GP-18PEG, bearing no adamantyl groups, was used at the mass concentration equal to that of D40-28GP-10Ada-18PEG with C(Ada) = $5 \cdot 10^{-4}$ mole/L. The enthalpograms, shown in **Figure III.3b,c** are plotted as a function of the βCD/Ada molar ratio. Except for the case of D40-18GP-18PEG (free of Ada groups) where no interaction could be detected (black circles in **Figure III.3b,c**), the guest polymers display highly exothermic interactions with both neutral pβCD and positively charged pβCDN+.

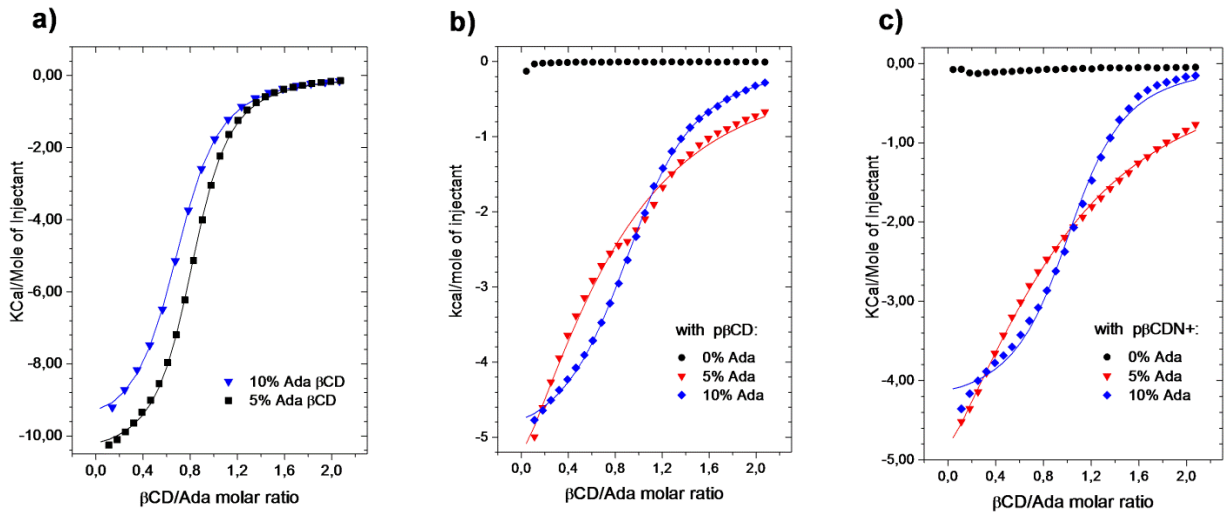

Figure III.3: Enthalpograms of the interaction of D40-GP-Ada-PEG polymers with monomeric βCD (**a**); pβCD (**b**) and pβCDN+ (**c**). The solid lines represent the fits of the data by One Set of Sites model (Origin 7.0 ITC custom version).

Likewise for monomeric βCD, the fits are done assuming a simple 1:1 interaction model. The imperfect matching between the experimental points and the fitting curves could be attributed to slight correlations between the interaction sites within a same chain. Nevertheless, the fits allowed us to estimate thermodynamic parameters of the interactions. The interactions strength is strongly dependent on the adamantyl content of the guest polymers. In the case of titration by pβCD, K_a becomes almost one order of magnitude higher in favor of D40-28GP-10Ada-18PEG – more densely substituted by Ada groups and less by PEG chains. Such behavior might be attributed to interplay between the cooperativity effects of neighboring adamantyl groups and steric hindrance arising from PEG grafts. One can suppose that D40-28GP-5Ada-23PEG is less likely to approach and form stable complexes with pβCD due to a lower number of linking points (5 mol. % Ada) and higher density of bulky PEG grafts. The evolution of the TΔS values is in agreement with this assumption: pronouncedly negative TΔS values at 5 mol.% Ada, which could correspond to anti-cooperative binding, switch to positive TΔS values at 10 mol. % Ada, giving an indication of more cooperative binding (**Table III.2**).

Table III.2. Thermodynamic parameters of interaction of the D40-GP-Ada-PEG polymers with monomeric βCD and βCD-polymers at 25°C

Titrant	Ada, mol.%	$K_a \cdot 10^{-3}$, L/mole	ΔH, kJ/mole	TΔS, kJ/mole	ΔG, kJ/mole
βCD	5	60.7	-44.4	-16.9	-27.4
	10	40.3	-41.6	-15.2	-26.3
pβCD	5	3.34	-40.0	-19.8	-20.2
	10	21.9	-21.7	3.0	-24.8
pβCDN+	5	3.02	-35.6	-15.7	-19.8
	10	35.4	-18.1	7.8	-26.0

The same tendency was observed in the case of titration by charged pβCDN+. Interestingly, the binding constants for the polymer bearing 5 mol.% of Ada groups are of the same order for pβCD and pβCDN+; on the other hand for the 10 mol.% polymer, K_a is pronouncedly higher when titrated by pβCDN+.

Given the results above, in the next step we were interested in evaluation and comparison of the binding properties of (PEG, adamantyl)-grafted dextrans on the surface by SPR.

3. Binding properties of D40-GP-Ada-PEG on the surface. SPR studies

To perform SPR binding experiments, βCD-polymers were deposited as a 1st layer on the golden surface of SPR sensor. When either pβCD or pβCDN+ solution is flowed over the sensor surface, the RI increases due to the physical adsorption of CD-polymers, driven by non-specific and electrostatic interactions between the polymers and the gold surface. In general, the experiment design was very similar to that used in Chapter 2 for the comparison of binding properties of guest polymers with and without PEG spacer, and is schematically illustrated in **Figure III.4**. Three injections of 2 g/L solutions were enough to reach the plateau in RI, indicating the surface saturation, as shown in the first part of the sensograms for neutral pβCD (**Figure III.5**). The resulting 1st layer obtained after equilibration for 20 min gives a quite stable ΔRI in both cases ($8.5 \cdot 10^{-4} \pm 0.8$ and $12.1 \cdot 10^{-4} \pm 0.7$ for pβCDN+ and pβCD respectively).

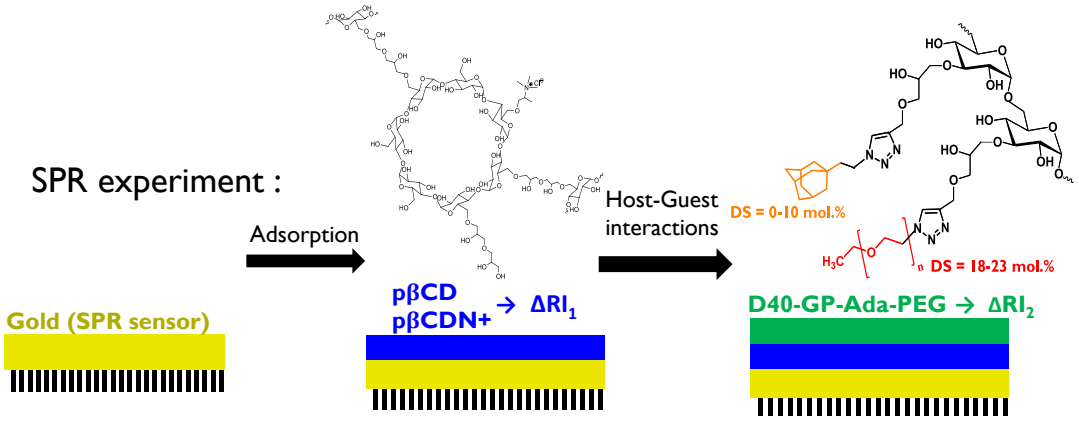

Figure III.4: Schematic representation of an SPR experiment for evaluation of D40-GP-Ada-PEG binding properties on the surface.

The adsorbed amounts of the polymers were estimated using the **Equation II.1** (described in Chapter 2 and Experimental Section). Calculations showed that the adsorbed amount is roughly 1.4 times higher for the neutral pβCD - 1.37 mg/m^2 – than for the charged pβCDN+ - 0.97 mg/m^2. Poorer adsorption characteristics of pβCDN+ might be related to strong hydration and spatial extension of the charged molecules, which prevents them from forming a strong linkage to the surface. In support of this, it should be noted that when pβCDN+ solution in pure H_2O is

used instead of 0.5M NaCl solution in the present case, electrostatic repulsions are not screened at all and only negligible amounts are adsorbed.

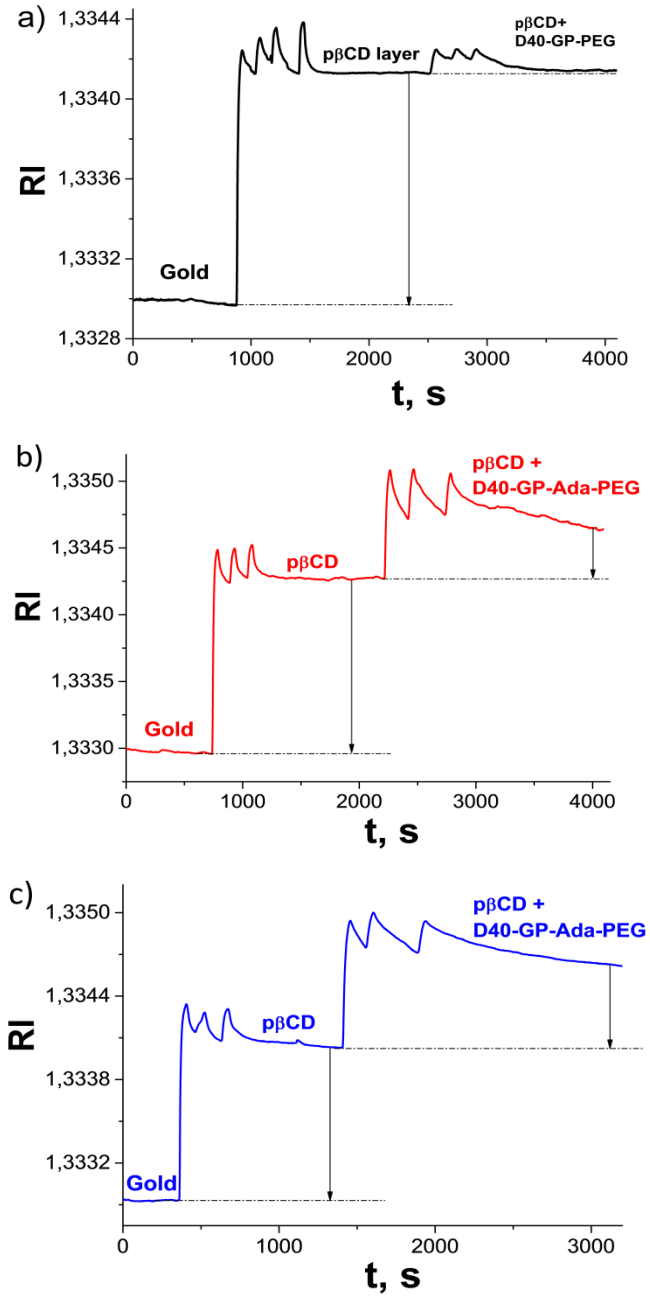

Figure III.5: Adsorption of D40-GP-Ada-PEG on neutral pβCD layer. DS(Ada): 0 (**a**), 5 (**b**), 10 (**c**) mol.%

The next step was to investigate the adsorption of the D40-GP-Ada-PEG polymers on the preformed pβCD-layer as a function of their DS(Ada). The results obtained in the case of neutral pβCD as the 1st layer are shown in **Figure III.5**. One can see that for the polymer bearing no Ada

groups there is no deposition of the 2nd layer with *Δ*RI going back to zero after the flow of water for ca. 15 min (**Figure III.5a**). This indicates that non-specific adsorption on the gold surface has been prevented by the first layer of neutral pβCD and that there is no detectable interaction between the pβCD layer and D40-18GP-18PEG. It correlates with the results obtained in solution by ITC (see previous section).

For the polymer bearing 5 mol.% of Ada groups, clear formation of the 2nd layer was observed after 3 successive injections. However, a gradual desorption takes place as water is flowed for ~30 min, indicating that the deposited polymer is rather loosely attached (**Figure III.5b**). When the DS(Ada) is raised to 10 mol.% the deposited D40-GP28-Ada10-PEG18 layer becomes more firmly anchored and equilibrated *Δ*RI value is increased by 30% (**Figure III.5c**). The content of PEG in all investigated polymers was at ca. 80-85 wt. %. Therefore we assumed them to have a dn/dc equal to that of pure MeOPEG-OH (0.135 mL/g) in order to calculate the adsorbed amounts (after 30 min of equilibration in water).

The obtained results (**Figure III.7**) show that the adsorption of the D40-GP-Ada-PEG polymers onto non-charged pβCD is predominantly driven by host-guest interactions. Moreover, higher adamantyl substitution degree appears to be responsible for the formation of thicker and more stable 2nd layer.

The situation is quite different when pβCDN+ is used as the 1st layer (**Figure III.6**). Even D40-18GP-18PEG with no Ada functions leads to formation of the 2nd layer with the adsorbed amount of 0.63 mg/m^2 (**Figure III.7**). It also shows no significant decrease in *Δ*RI during the equilibration period (20 min) in water, indicating strong binding between the layers (**Figure III.6a**). For D40-GP28-Ada5-PEG23 the adsorbed amount is ca. 3 times higher, but at the initial stage of equilibration a part of it is washed out (**Figure III.6b**). Finally, for the D40-GP28-Ada10-PEG18 the adsorbed amount is further increased and the layer gains in stability (**Figure III.6c**). Interestingly, the adsorption pattern on pβCDN+ is changed as well. No or little decrease in refractive index is observed straight after each consecutive injection. One can assume that due to the higher strength of interpolymer interaction with pβCDN+, there are less of loosely anchored D40-*X*GP-*Y*Ada-*Z*PEG molecules which are washed out after the deposition.

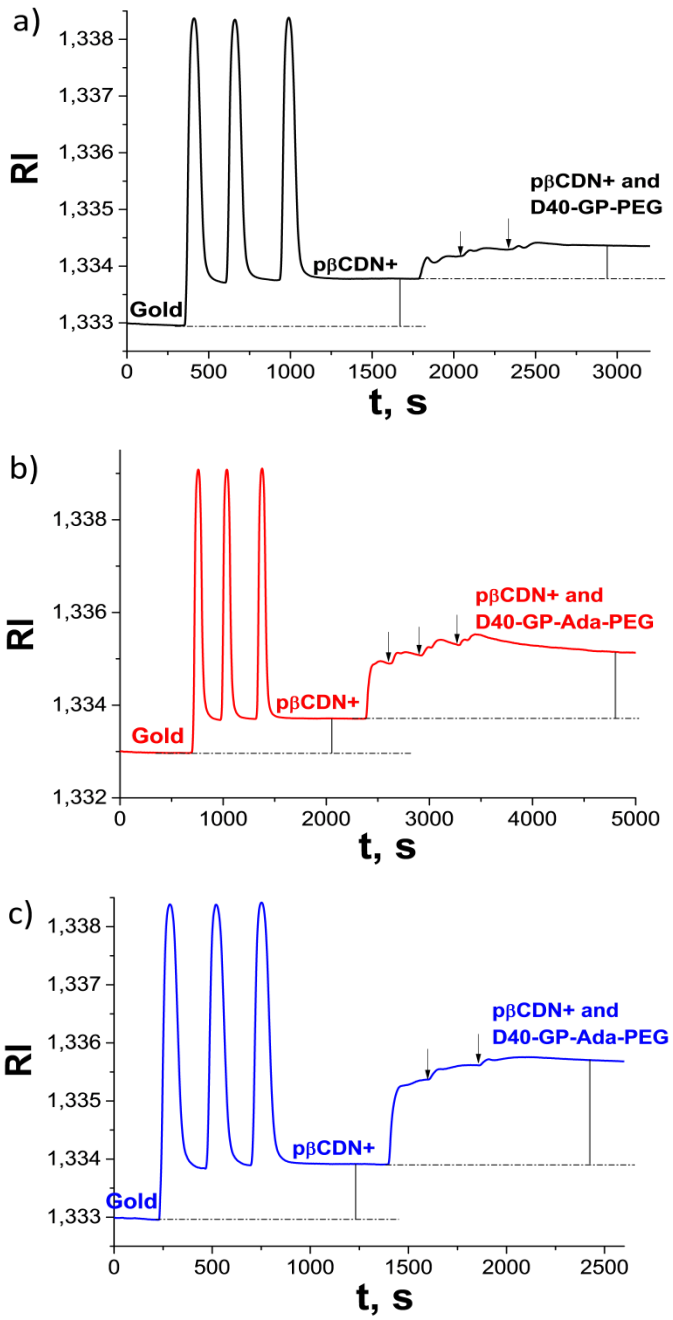

Figure III.6: Adsorption of D40-GP-Ada-PEG on pβCDN+ with 1.6 N^+ per CD. DS(Ada): 0 (**a**), 5 (**b**), 10 (**c**) mol.%. Consecutive injections are indicated by arrows.

Contrarily to the ITC study, where no interaction could be detected between D40-18GP-18PEG and pβCDN+ in solution, the same polymer (D40-18GP-18PEG) exhibits non-negligible interaction with the gold/pβCDN+ surface. It might be related to a contribution from the gold surface which is less saturated with pβCDN+ than with pβCD. However, this cannot fully explain quite large adsorbed amount of free from Ada-groups D40-18GP-18PEG. As polysaccharides and polysaccharide-based nanoassemblies are typically characterized by slightly negative values of

zeta potential[33], non-specific electrostatic interactions could also be at the origin of the enhanced interpolymer interaction. Given that, the adsorption behavior of D40-GP-Ada-PEG on the positively charged pβCDN+-layer might be related to interplay between the host-guest and reinforced non-specific interactions in the system. As a result, the adsorbed amounts of D40-GP-Ada-PEG on pβCDN+ are roughly 3 times higher compared to the neutral pβCD (**Figure III.7**).

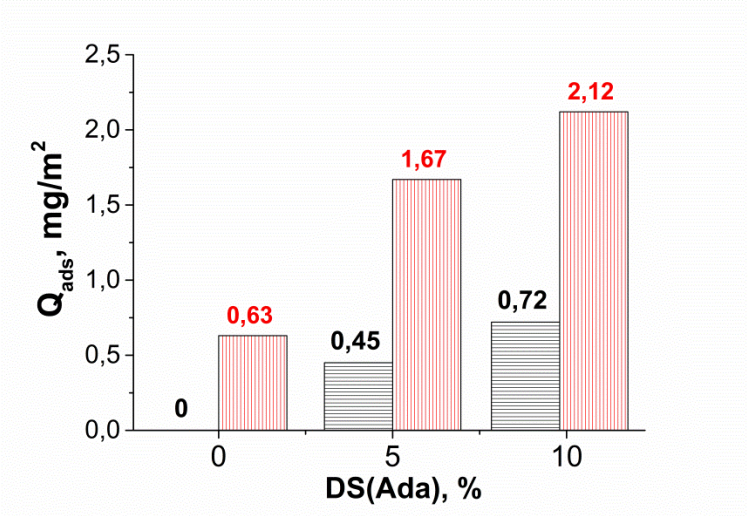

Figure III.7: The adsorbed amounts of D40-GP-Ada-PEG with various DS (Ada): on pβCD (black bars, horizontal pattern); on pβCDN+ (red bars, vertical pattern).

3.1. Adsorption kinetics by SPR

The kinetics of the interaction between the pβCDN+ adsorbed layer and D40-28GP-10Ada-18PEG was studied next, given that the latter demonstrated the most interesting SPR adsorption profile (**Figure III.6c, III.7**)**.** A modified version of SPR experiment was used. First, gold surface was saturated with pβCDN+, and then diluted D40-28GP-10Ada-18PEG solutions at various concentrations (0.01 – 0.20 g/L) were passed over the pβCDN+ layer. The results are represented in **Figure III.8**. At low concentrations (i.e. 0.01 g/L), the RI increases quasi-linearly with time, indicating that every polymer molecule reaching the surface should be adsorbed in this case. The adsorbed amount corresponding to the plateau (0.59 mg/m^2) is less than 30% of the saturation amount, obtained from the SPR adsorption experiment. The sensogram recorded at 0.025 g/L changes its character drastically. One observes a steep initial growth and 1.65 mg/m^2 of the deposited polymer at the plateau, which is already 78% of the saturation value. When increasing the concentration up to 0.1 g/L and higher, the initial exponential growth

becomes even steeper and the amount of adsorbed polymer at the plateau gradually approaches the saturation level from the experiment with multiple injections of the 1 g/L solution (**Figure III.7**). The above is an indication of strong affinity between the polymers. Indeed, at such low concentrations as 0.025 g/L one already observes a fast exponential saturation of the surface sites of pβCDN+.

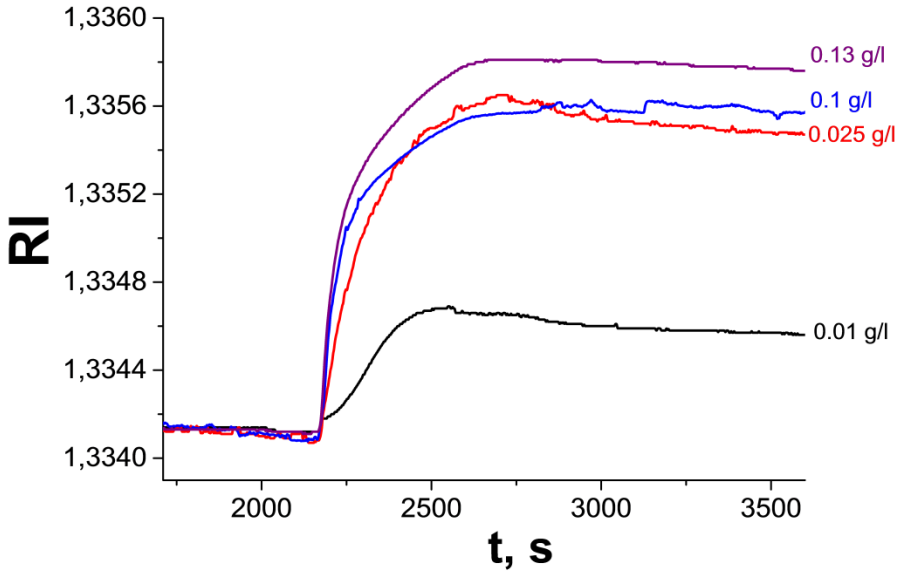

Figure III.8: The evolution of RI versus time for various D40-28GP-10Ada-18PEG concentrations flowed over a pβCDN+ layer.

Since the obtained sensograms contain continuous real-time data, one can extract information on the kinetics of interpolymer interaction from them. For the first part of the sensorgram (until RI_{max} is reached) the interaction might be schematically written as:

$$[\mathrm{R-Ada}]^{\mathrm{sol.}} + [\mathrm{R'-CD}]^{\mathrm{surf.}} \rightleftarrows [\mathrm{Complex}]^{\mathrm{surf.}} \qquad \textbf{(III.1)}$$

In this case the variation of RI versus time, due to complexation, is expressed by the following equation [49]:

$$d\mathrm{RI}/dt = k_a C_{Ada}(\mathrm{RI}_{max} - \mathrm{RI}) + k_d \qquad \textbf{(III.2)}$$

where C_{Ada} is the concentration of adamantyl groups in the injected solution. The k_a and k_d constants are obtained by fitting the experimental curves for the polymer concentrations $\geq$ 0.025 g/L to the integrated form of the dependence of RI versus time:

$$\mathrm{RI(t)} = \frac{C_{Ada} k_a [\mathrm{RI}_{max} - \mathrm{RI(0)}][1 - \exp(-C_{Ada} k_a + k_d t)]}{C_{Ada} k_a + k_d} + \mathrm{RI(0)} \qquad \textbf{(III.3)}$$

in which $\mathrm{RI(0)}$ is the refractive index in the moment of injection (t = 0). Examples of the obtained fits are shown in **Figure III.9**.

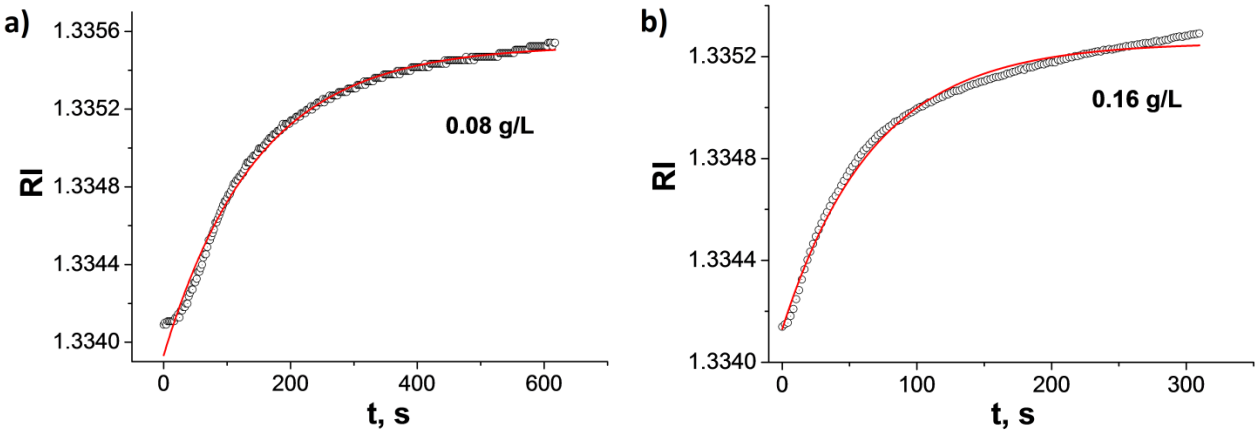

Figure III.9: Experimental response of RI versus time for the adsorption of D40-28GP-10Ada-18PEG on pβCDN+ layer (circles) with the corresponding first order exponential decay fits performed according to the **Equation III.3** (solid lines); C(D40-28GP-10Ada-18PEG) = 0.08 (**a**), 0.16 (**b**) g/L.

The average values of k_a and k_d obtained from the sensograms recorded at polymer concentrations varying in the range 0.08-0.20 g/L are of $7.0 \cdot 10^2$ $mol^{-1}s^{-1}$ and $1.1 \cdot 10^{-3}$ s^{-1} (**Table III.3**). From this one can calculate the association constants K_a using the following equation:

$$K_a = k_a / k_d \qquad \textbf{(III.4)}$$

Table III.3. Association (k_a) and dissociation (k_d) rates between D40-28GP-10Ada-18PEG and pβCDN+ layer on gold

C, g/l	k_a, $mol^{-1}s^{-1}$	k_d, s^{-1}
0.08	$8.6 \cdot 10^2$	$0.6 \cdot 10^{-3}$
0.10	$7.2 \cdot 10^2$	$0.8 \cdot 10^{-3}$
0.13	$8.6 \cdot 10^2$	$1.4 \cdot 10^{-3}$
0.16	$8.3 \cdot 10^2$	$2.0 \cdot 10^{-3}$
0.20	$2.5 \cdot 10^2$	$0.6 \cdot 10^{-3}$
Average	$(7.0 \pm 2.6) \cdot 10^2$	$(1.1 \pm 0.6) \cdot 10^{-3}$

The estimated average K_a = 6.4·10^5 L/mole is more than one order of magnitude higher than the one determined by ITC for the interaction in solution (K_a = 3.5·10^4 L/mole, **Table III.2**); it is also roughly 3 times higher than the K_a between native βCD and monomeric adamantane derivatives previously.[42] The phenomenon of substantial increase of K_a on the surface compared to the one in solution has been reported previously for polymeric guests and is attributed to increased cooperativity of interactions, the host moieties being constrained in close proximity on the surface. [50] Moreover, the K_a is one order of magnitude higher than that reported for the interaction between pβCD and Ada-substituted pNIPAm (pNIPAm-Ada) on gold surface[50], thus indicating an excellent affinity of D40-GP-Ada-PEG to pβCDN+. More specifically, association rate constants k_a (700 mol^{-1}s^{-1}) are around 3 times higher than the ones determined for PNIPAM-Ada/pβCD[50] or for adamantyl carboxylic acid/βCD systems.[51] At the same time, the dissociation rate constants k_d (1.1·10^{-3} s^{-1}) are more than one order of magnitude lower than those for monomeric host-guest interactions (adamantyl carboxylic acid/βCD) and 3 times lower than for PNIPAM-Ada/pβCD multivalent interactions case. The observed improvement of surface binding properties can be related to the previously mentioned additional non-specific interactions arising between D40-GP-Ada-PEG and pβCDN+ layers, leading to larger adsorption and slower desorption rates.

Conclusions

This study illustrates the potential of multivalent interpolymer host-guest interactions as a tool for efficient PEGylation of interfaces and colloidal particles.

A series of new (PEG, Ada)-grafted dextrans have been prepared by CuAAC click reaction, using alkyne modified dextrans and azide derivatives of adamantane and 5000 g·mole^{-1} PEG. These polymers have similar DS by PEG chains and the DS by Ada-groups varying from 0 to 10 mol.%. Due to the presence of longer and more flexible spacer between the Ada-groups and the dextran backbone, the polymers show significant improvement of their surface binding properties comparing to the previously described Ada-modified pNIPAm. Moreover, their ability to form inclusion complexes with monomeric βCD, neutral pβCD and cationic pβCDN+, both in solution and on the surface, proves to be strongly dependent on the degree of

substitution by Ada-groups. Thus, for the interaction with monomeric βCD the association constants K_a determined by ITC show similar values for D40-GP-Ada-PEG with different DS(Ada). However, in the case of interaction with neutral or positively charged βCD-polymers, one order of magnitude higher K_a is observed for more densely substituted by Ada D40-28GP-10Ada-18PEG. The latter gives an indication of strong cooperativity effects between the Ada-groups in synthesized polymers. SPR study of the adsorption kinetics by SPR showed that the D40-28GP-10Ada-18PEG affinity to pβCDN+ is further increased when the latter is surface-anchored.

Given the above, (PEG, Ada)-grafted dextrans should be auspicious candidates for applications, where fast and reversible PEGylation of surfaces or nanoparticulate carriers is required. Their potential will be illustrated on a practical example in Chapter 4, where D40-28GP-10Ada-18PEG is used for sterical stabilization of βCD-coated pNIPAm-based microgels.

Experimental section

Materials and reagents

Pyridine (99.9%, anhydrous), *N,N*'-dimethylformamide (DMF, 99.8%, anhydrous), tetrakis(acetonitrile)copper(I)tetrafluoroborate ($Cu(MeCN)_4PF_6$, 97%), thionyl chloride ($SOCl_2$, 99+%), 1-adamantaneethanol (98%) and glycidyl propargyl ether (GPE, 90+%) were purchased from Sigma-Aldrich (Saint Quentin Fallavier, France) and used as received. p-Toluenesulfonyl chloride (98%), sodium azide (99%), L-ascorbic acid sodium salt (Na-Asc, 99%) and dimethyl sulfoxide (DMSO, 99.8%, anhydrous) were purchased from Alfa Aesar and used as received. Sodium hydroxide (98+%, anhydrous pellets) were purchased from Acros Organics and used as received.

Dextran (DT40, M_w = $4.3 \cdot 10^4$ g mol^{-1}, PDI = 1.50, Amersham Pharmacia Sweden), lithium chloride (Alfa Aesar) and poly(ethylene glycol) methyl ether of 5000 Da (MeOPEG-OH, Sigma-Aldrich) were dried overnight in vacuum at 90 °C prior to use.

Tris[(1-benzyl-1H-1,2,3-triazol-4-yl)methyl]amine (TBTA)[52] was synthesized according to the literature data. Positively charged pβCDN+, modified with quaternary ammonia, was prepared from neutral epichlorohydrin-branched pβCD polymer available in the lab (208 kg·$mole^{-1}$, PDI = 1.82), according to the previously described procedures.[47, 48]

Methods and instrumentation

NMR spectroscopy: NMR measurements were performed in D_2O or DMSO-d_6, unless other is indicated, on a Bruker Avance II Ultrashield Plus 400 MHz NMR spectrometer. ^{1}H-NMR spectra were calibrated using the chemical shifts of the residual solvents signals according to the literature data [53].

Fourier-transform infrared spectroscopy (FT-IR): Fourier transform infrared spectroscopy (FT-IR) measurements were made on a Bruker Tensor 27 FT-IR spectrometer.

SEC: Size exclusion chromatography coupled to multi-angle laser light scattering (SEC-MALLS) was performed in deionized water with 0.1 mol·L^{-1} $LiNO_3$ (0.05% NaN_3) on TSK-gel type SW4000-3000 columns and detection by a Wyatt Dawn 8+ light scattering detector and a Wyatt Optilab

Rex refractive index detector. It was used to determine the molecular weight and PDI of epichlorohydrin-branched pβCD.

Isothermal titration microcalorimetry (ITC) measurements were performed using a MicroCal VPITC microcalorimeter. In each titration, injections of 10 µL of native βCD, pβCD or pβCDN+ solutions ($C_{\beta CD} = 5 \cdot 10^{-3}$ mol/L) were added from the computer controlled 295 µL microsyringe at an interval of 180 s into the cell (V = 1.4569 mL) containing the investigated polymer solution ($5 \cdot 10^{-4}$ mol/L of Ada-groups) while stirring at 450 rpm. The temperature was fixed at 25 °C. The raw experimental data were obtained as the amount of heat produced per second following each injection of a host solution as a function of time. Integration of the heat flow peaks by the instrument software (after taking into account heat of dilution) provides the amount of heat produced per injection. The experimental data were fitted with a theoretical titration curve using the instrument software with a model assuming a 1:1 stoichiometry for the adamantyl/βCD complex. The enthalpy change, $|\Delta H|$, the association constant, K_a, and the overall stoichiometry were adjustable parameters.

SPR: SPR measurements were carried out with a Spreeta SPR-EVM-BT from Texas Instruments. The light of an infrared light-emitting diode (LED; λ = 840 nm) reaches the sensor surface at a range of angles above the critical angle. A reflectivity-versus-angle spectrum is obtained, and an apparent refractive index (RI) is derived from it by the Spreeta software. The sensor surface is a gold layer (ca. 50 nm). In the case of adsorption on the golden surface the RI changes provide information on the adsorbed layer parameters. The sensor is integrated in a flow cell and the measurements were carried out at 23°C using a continuous water flow (3 mL/h) which was delivered by a syringe pump (Kd Scientific), and a Rheodyne injection valve to switch to the sample solution.

The sensor surface was cleaned with a 4 % CrO_3 solution in water and rinsed with MeOH before each experiment. After settling the sensor into the flow cell, an in-situ cleaning was performed with one injection (0.1 mL) of a solution of 0.1 M NaOH and 1 % Triton X-100 in water followed by 3 injections (0.1 mL) of 10 % EtOH in water. The sensor was calibrated in pure water, assuming a RI value of 1.33300, and the RI variations after the different polymer injections were monitored as a function of time.

Two types of experiments were run. In the first type, three consecutive injections of 0.1 mL of pβCD in water or pβCDN+ in 0.5 M NaCl (both at 2 g/L) were carried out to saturate the gold surface of the sensor, similarly to the way that was described in the Experimental section of Chapter 2. This was followed by 3-4 consecutive injections (0.1 mL) of one of the PEG-containing dextrans in water with various DS by adamantyls (1 g/L). Then the RI variation due to the 2nd layer deposition was measured 20 min after the first injection.

In the second type, 1 mL of pβCDN+ solution at 0.2 g/L was injected to saturate the gold surface of the sensor; then an injection of 1 mL of the D40-28GP-10Ada-18PEG solution at various concentrations (0.01-0.1 g/L) was performed, and the kinetics of the adsorption were recorded and analyzed.

The adsorbed amounts of the polymers were estimated from the values of ΔRI, using the **Equation II.1**; its derivation is described in the Experimental section of Chapter 2:

$$Q_{ads} = \frac{\Delta RI \cdot l_d}{2m \cdot (dn/dc)_{pol}} \qquad \textbf{(II.1)}$$

where l_d is the depth of penetration of the evanescent electromagnetic field (310.8 nm), m is the calibration coefficient of the sensor (m= 1) and $(dn/dc)_{pol}$ is the refractive index increment of the polymers. The latter was taken as 0.145 mL/g for pβCD and pβCDN+ host polymers.[50] The dn/dc of PEG-containing dextrans was considered to be equal to that of pure PEG, 0.135 mL/g (http://www.ampolymer.com/dn-dcValues.html). Given that D40-GP-Ada-PEG contain 80-85 wt% of PEG, this simplification appears to be fair.

Synthetic procedures

The syntheses under microwave irradiation (MW) were performed using a Monowave-300 reactor from Anton Paar. The microwave source was a magnetron with a 2.5 GHz frequency powered by a 900 W power generator, which could be operated at different power levels. The reaction mixtures were loaded inside quartz glass tubes; the tubes were closed with silicon caps using a pressure monitor unit, and placed into the reactor. The microwave reactor was programmed to maintain a constant temperature by adjusting the applied power; the desired temperature was reached gradually using an initial 3 min temperature ramp. After the end of the reaction, solutions were cooled to room temperature with compressed air. When necessary,

ultrafiltration was carried out under N_2 atmosphere using Amicon equipment and regenerated cellulose membranes with MWCO 30,000. Dialysis was done with Spectra/Por molecular porous tubing MWCO 6,000-8,000. The ultrafiltrated and dialyzed solutions were freeze-dried on CHRIST ALPHA 1-2 LD Plus lyophilizator.

Short names of the polymers were attributed using the following pattern: D40-*X*GP-*Y*Ada-*Z*PEG with X, Y and Z indicating the molar degree of substitution (DS) of anhydroglucosidic rings (further AHG) by different substituents.

1-Adamantaneethyltosylate: 1-Adamantaneethanol (4.80 g, 26.6 mmol) was dissolved in 25 mL of pyridine, cooled to 0 °C on ice bath and p-toluenesulfonyl chloride (8.37 g, 43.9 mmol) was added to the solution. The reaction mixture was allowed to warm and stirred overnight at room temperature. The solvent was evaporated under reduced pressure and the product was redissolved in 100 mL of EtOAc. The organic layer was washed once with saturated $NaHCO_3$ and twice with brine, dried over Na_2SO_4, filtered and evaporated under reduced pressure. The subsequent filtration through a silica pad (40 g, EtOAc/n-heptane = 1/25) yielded the final product as a white solid. Thin layer chromatography (TLC) was carried out using Silica gel 60 F_{254} TLC plates with 0.2 mm silica gel (EtOAc/heptane = 1/25). Yield: 89.4% (7.96 g). ^{1}H-NMR (DMSO-d_6) δ = 1.30-1.40 (m, 6H+2H, Ada overlapped with Ada-C*H*$_2$), 1.45-1.70 (m, 6H, Ada), 1.90 (s, 3H, Ada), 2.42 (s, 3H, -CH_3), 4.03 (t, 2H, C*H*$_2$-OTs), 7.49 (d, 2H, Ts), 7.78 (d, 2H, Ts).

1-Adamantaneethylazide (Ada-N_3): 1-Adamantaneethyltosylate (7.96 g, 23.8 mmol) was dissolved in 0.5 mol/L NaN_3 solution in DMSO (167 mL, 83.3 mmol) and stirred at 80°C for 50 h. 250 mL of water were added to quench the reaction, and after cooling down 800 mL of EtOAc were added. The organic phase was washed 3 times with water and one time with brine, dried over Na_2SO_4 and filtered. Concentration under reduced pressure and drying under vacuum gave yellowish oil. Yield: 74.6 % (3.64 g). The IR spectrum of the product showed a single -N_3 peak at 2094 cm^{-1}. ^{1}H-NMR ($CDCl_3$) δ = 1.38 (t, 2H, Ada-C*H*$_2$), 1.48 (s, 6H, Ada), 1.57-1.72 (m, 6H, Ada), 1.94 (s, 3H, Ada), 3.24 (t, 2H, C*H*$_2$$N_3$).

MeOPEG-Cl: MeOPEG-OH (10 g, 2 mmol) of 5000 g/mol was dissolved in 15 mL (206.5 mmol) of $SOCl_2$; the reaction mixture was heated to 85 °C and refluxed for 40 h. Excess $SOCl_2$ was removed by bubbling argon at 65°C. Then 100 mL of DCM were added and the obtained solution

was precipitated in 1 L of Et_2O, filtered and washed with Et_2O. The subsequent drying in vacuum at 40°C yielded the product as a white solid. Yield: 94.6 % (9.51 g).

MeOPEG-N_3: MeOPEG-Cl (9.40 g, 1.87 mmol) was dissolved in 100 mL of anhydrous DMF and treated with NaN_3 (3.30 g, 50 mmol). The reaction mixture was stirred at 80 °C for 60 h, precipitated in 1 L of Et_2O and filtered. The product was subsequently purified by dissolving it in 100 mL dichloromethane, washing with 200 mL of water, concentrating the organic layer to 50 mL under reduced pressure and its precipitation in 600 mL of 2-propanol. After filtration and drying in vacuum at 55 °C, the final product was obtained as white flakes. Yield: 70.9 % (6.68 g). The IR of the product confirmed the absence of residual NaN_3, showing a single -N_3 peak at 2117 cm^{-1}. ^{1}H-NMR (D_2O) δ = 3.38 (s, 3H, -OC*H*$_3$), 3.45-3.95 (m, PEG chain protons)

D40-18,28GP: Alkyne-substituted dextrans with ether bonds were synthesized according to the procedure described by Nielsen et al.[42] Dextran (1.5 g, 9.25 mmol AHG) was dissolved in 10 mL of 0.1M NaOH. It was followed by addition of glycidyl propargyl ether (0.55-0.85 mL, 5.09-7.86 mmol), increase of the reaction temperature to 35 °C and stirring for 16h. The product was precipitated in 220 mL of 2-PrOH, filtered on a sintered-glass funnel and washed with 100 mL of 2-PrOH. The product was then dissolved in ~50 mL of water, dialyzed against pure water for 48h and freeze-dried, yielding a white solid (1.27-1.56 g). ^{1}H-NMR (D_2O) δ = 2.93 (s, 1H, C ≡C*H*), 3.35-4.10 (m, 5H, dextran glucosidic protons), 4.23 (s, 2H, C*H*$_2$-C ≡C), 4.90-5.08 (s, 1H, dextran anomeric proton).

D40-18GP-18PEG: D40-18GP (0.150 g, 0.155 mmol alkynes) and MeOPEG-N_3 (1.32 g, 0.265 mmol) were dissolved in 16 mL of DMSO by warming at 50 °C. Subsequently TBTA (0.54 mL, 0.10 M in DMSO) and Na-Asc (0.17 mL, 0.28 M in water) were added to the solution, followed by bubbling with argon for 10 min. Finally, $Cu(MeCN)_4PF_6$ (23 mg, 0,062 mmol) was added to the reaction mixture, it was bubbled with argon for another 5 min and azide-alkyne cycloaddition (CuAAC) was performed under microwave irradiation (85 °C, 40 min). The reaction mixture was dialyzed against DMSO for 20 h, diluted with 250 mL of water and ultrafiltrated (MWCO 30,000). The product was obtained by freeze-drying as white solid (0.58 g). ^{1}H-NMR (DMSO-d_6) δ = 2.90-3.90 (m, dextran glucosidic and PEG protons, overlapped with HDO), 4.40-5.20 (m, 4H, dextran hydroxyl + anomeric), 8.06 (s, 1H, triazole).

D40-28GP-(5,10)Ada-(23,18)PEG: D40-28GP (0.160 g, 0.225 mmol alkyne) and Ada-N_3 (0.23-0.46 mL of a solution at 0.17 mol/L in DMSO) were dissolved in 17 mL of DMSO. TBTA (0.79 mL of a solution at 0.10 mole/L in DMSO) and Na-Asc (0.20 mL of a solution at 0.28 mole/L in water) were added, and the obtained solution was bubbled with argon for 10 min. Then, $Cu(MeCN)_4PF_6$ (50 mg, 0,132 mmol) was added, the reaction mixture was bubbled with argon for 5 min under sonication, followed by CuAAC, performed under microwave irradiation (70 °C, 20 min). Further, MeOPEG-N_3 (1.58-1.25 g, 0.32-0.25 mmol) was added to the reaction mixture and microwave irradiation was proceeded (85 °C, 40 min). The reaction mixture was dialyzed against DMSO for 20 h, diluted with 250 mL of water and ultrafiltrated (MWCO 30,000). The product was obtained by freeze-drying as white solid (0.69 g). ^{1}H-NMR (DMSO-d_6) δ = 1.50 (s, 6H, Ada), 1.57-1.72 (m, 6H, Ada), 1.92 (s, 3H, Ada), 2.90-3.90 (m, dextran glucosidic and PEG protons, overlapped with HDO), 4.40-5.20 (m, 4H, dextran hydroxyl + anomeric), 8.06 (s, 1H, triazole-PEG), 8.10 (s, 1H, triazole-Ada).

p*β*CDN+: To prepare a cationized p*β*CDN+, neutral epichlorohydrin crosslinked p*β*CD (208 kg·mole^{-1}, 67 wt% of *β*CD) prepared according to previously described procedure[47, 54] was modified with glycidyltrimethylammonium chloride. In a typical procedure, 4 g of p*β*CD was added to an alkaline solution containing 0.4 g of NaOH in 20 mL of water and mixed for 24 h at room temperature. It was followed by addition of 10 mL of aqueous solution of glycidyltrimethylammonium chloride (3.20 g, 18.95 mmol) and the reaction bath was heated at 50 °C for 24 h. The solution was then neutralized by addition of 6 N HCl to adjust the pH to 6. The polymer was purified by ultrafiltration on regenerated cellulose membrane with the MWCO of 30 000 Da. The final p*β*CDN+ product was obtained by freeze-drying (m = 3.85 g). The N+ content was determined by ^{1}H-NMR in D_2O by comparing the integral of three methyl groups of grafted quaternary ammonium groups (9H, 3.22 ppm) with the integral of anomeric protons of *β*CD (7H, 4.91-5.53 ppm). The result was 1.62N+ per CD cavity which corresponds to 58.2 wt% of *β*CD in the final product.

References

1. Knop, K.; Hoogenboom, R.; Fischer, D.; Schubert, U. S. Poly (ethylene glycol) in drug delivery: pros and cons as well as potential alternatives. *Angew. Chem., Int. Ed.* **2010,** *49* (36), 6288-6308.

2. Jokerst, J. V.; Lobovkina, T.; Zare, R. N.; Gambhir, S. S. Nanoparticle PEGylation for imaging and therapy. *Nanomedicine* **2011,** *6* (4), 715-728.
3. Abuchowski, A.; Van Es, T.; Palczuk, N.; Davis, F. Alteration of immunological properties of bovine serum albumin by covalent attachment of polyethylene glycol. *J. Biol. Chem.* **1977,** *252* (11), 3578-3581.
4. Alconcel, S. N.; Baas, A. S.; Maynard, H. D. FDA-approved poly (ethylene glycol)–protein conjugate drugs. *Polym. Chem.* **2011,** *2* (7), 1442-1448.
5. Owens, D. E.; Peppas, N. A. Opsonization, biodistribution, and pharmacokinetics of polymeric nanoparticles. *Int. J. Pharm.* **2006,** *307* (1), 93-102.
6. Oupicky, D.; Ogris, M.; Howard, K. A.; Dash, P. R.; Ulbrich, K.; Seymour, L. W. Importance of lateral and steric stabilization of polyelectrolyte gene delivery vectors for extended systemic circulation. *Molecular Therapy* **2002,** *5* (4), 463-472.
7. Vonarbourg, A.; Passirani, C.; Saulnier, P.; Benoit, J. P. Parameters influencing the stealthiness of colloidal drug delivery systems. *Biomaterials* **2006,** *27* (24), 4356-4373.
8. Nguyen, H.; Lemieux, P.; Vinogradov, S.; Gebhart, C.; Guerin, N.; Paradis, G.; Bronich, T.; Alakhov, V.; Kabanov, A. Evaluation of polyether-polyethyleneimine graft copolymers as gene transfer agents. *Gene therapy* **2000,** *7* (2).
9. Davis, M. E. The first targeted delivery of siRNA in humans via a self-assembling, cyclodextrin polymer-based nanoparticle: from concept to clinic. *Mol. Pharm.* **2009,** *6* (3), 659-668.
10. Klibanov, A. L.; Maruyama, K.; Torchilin, V. P.; Huang, L. Amphipathic polyethyleneglycols effectively prolong the circulation time of liposomes. *FEBS Lett.* **1990,** *268* (1), 235-237.
11. Gref, R.; Minamitake, Y.; Peracchia, M. T.; Trubetskoy, V.; Torchilin, V.; Langer, R. Biodegradable long-circulating polymeric nanospheres. *Science* **1994,** *263* (5153), 1600-1603.
12. Li, S. D.; Huang, L. Pharmacokinetics and biodistribution of nanoparticles. *Mol. Pharm.* **2008,** *5* (4), 496-504.
13. Gaucher, G.; Dufresne, M. H.; Sant, V. P.; Maysinger, D.; Leroux, J. C. Block copolymer micelles: preparation, characterization and application in drug delivery. *J. Controlled Release* **2005,** *109* (1-3), 169-188.
14. Schellekens, H.; Hennink, W. E.; Brinks, V. The immunogenicity of polyethylene glycol: facts and fiction. *Pharm. Res.* **2013,** *30* (7), 1729-1734.
15. Chanan-Khan, A.; Szebeni, J.; Savay, S.; Liebes, L.; Rafique, N.; Alving, C.; Muggia, F. Complement activation following first exposure to pegylated liposomal doxorubicin (Doxil®): possible role in hypersensitivity reactions. *Annals of Oncology* **2003,** *14* (9), 1430-1437.
16. Pasut, G.; Veronese, F. M. State of the art in PEGylation: the great versatility achieved after forty years of research. *J. Controlled Release* **2012,** *161* (2), 461-472.
17. Amoozgar, Z.; Yeo, Y. Recent advances in stealth coating of nanoparticle drug delivery systems. *Wiley Interdisciplinary Reviews: Nanomedicine and Nanobiotechnology* **2012,** *4* (2), 219-233.
18. Dams, E. T.; Laverman, P.; Oyen, W. J.; Storm, G.; Scherphof, G. L.; van der Meer, J. W.; Corstens, F. H.; Boerman, O. C. Accelerated blood clearance and altered biodistribution of repeated injections of sterically stabilized liposomes. *J. Pharmacol. Exp. Ther.* **2000,** *292* (3), 1071-1079.
19. Ishida, T.; Maeda, R.; Ichihara, M.; Irimura, K.; Kiwada, H. Accelerated clearance of PEGylated liposomes in rats after repeated injections. *J. Controlled Release* **2003,** *88* (1), 35-42.

20. Roberts, M. J.; Bentley, M. D.; Harris, J. M. Chemistry for peptide and protein PEGylation. *Adv. Drug Delivery Rev.* **2002,** *54* (4), 459-476.
21. Yoncheva, K.; Lizarraga, E.; Irache, J. M. Pegylated nanoparticles based on poly(methyl vinyl ether-co-maleic anhydride): preparation and evaluation of their bioadhesive properties. *Eur. J. Pharm. Sci.* **2005,** *24* (5), 411-419.
22. Liu, Z.; Davis, C.; Cai, W.; He, L.; Chen, X.; Dai, H. Circulation and long-term fate of functionalized, biocompatible single-walled carbon nanotubes in mice probed by Raman spectroscopy. *Proceedings of the National Academy of Sciences* **2008,** *105* (5), 1410-1415.
23. Goren, D.; Horowitz, A. T.; Tzemach, D.; Tarshish, M.; Zalipsky, S.; Gabizon, A. Nuclear delivery of doxorubicin via folate-targeted liposomes with bypass of multidrug-resistance efflux pump. *Clinical Cancer Research* **2000,** *6* (5), 1949-1957.
24. Mero, A.; Ishino, T.; Chaiken, I.; Veronese, F. M.; Pasut, G. Multivalent and flexible PEG-nitrilotriacetic acid derivatives for non-covalent protein pegylation. *Pharm. Res.* **2011,** *28* (10), 2412-2421.
25. David, C.; Millot, M. C.; Sebille, B.; Levy, Y. The reversible binding of hydrophobically end-capped poly(ethylene glycol)s to poly-beta-cyclodextrin-coated gold surfaces: a surface plasmon resonance investigation. *Sens. Actuator B-Chem.* **2003,** *90* (1-3), 286-295.
26. Pun, S. H.; Davis, M. E. Development of a nonviral gene delivery vehicle for systemic application. *Bioconjugate Chem.* **2002,** *13* (3), 630-639.
27. Volet, G.; Amiel, C. Polyoxazoline adsorption on silica nanoparticles mediated by host-guest interactions. *Colloid Surf. B-Biointerfaces* **2012,** *91*, 269-273.
28. Wu, L. F.; Brazel, C. S. Modifying the release of proxyphylline from PVA hydrogels using surface crosslinking. *Int. J. Pharm.* **2008,** *349* (1-2), 144-151.
29. Quaglia, F.; De Rosa, G.; Granata, E.; Ungaro, F.; Fattal, E.; La Rotonda, M. I. Feeding liquid, non-ionic surfactant and cyclodextrin affect the properties of insulin-loaded poly(lactide-co-glycolide) microspheres prepared by spray-drying. *J. Controlled Release* **2003,** *86* (2-3), 267-278.
30. El Fagui, A.; Amiel, C. PLA nanoparticles coated with a beta-cyclodextrin polymer shell: Preparation, characterization and release kinetics of a hydrophobic compound. *Int. J. Pharm.* **2012,** *436* (1-2), 644-651.
31. Versluis, F.; Voskuhl, J.; Vos, J.; Friedrich, H.; Ravoo, B. J.; Bomans, P. H. H.; Stuart, M. C. A.; Sommerdijk, N.; Kros, A. Coiled coil driven membrane fusion between cyclodextrin vesicles and liposomes. *Soft Matter* **2014,** *10* (48), 9746-9751.
32. Ren, S. D.; Chen, D. Y.; Jiang, M. Noncovalently Connected Micelles Based on a beta-Cyclodextrin-Containing Polymer and Adamantane End-Capped Poly(epsilon-caprolactone) via Host-Guest Interactions. *J. Polym. Sci., Part A: Polym. Chem.* **2009,** *47* (17), 4267-4278.
33. Wintgens, V.; Nielsen, T. T.; Larsen, K. L.; Amiel, C. Size-Controlled Nanoassemblies Based on Cyclodextrin-Modified Dextrans. *Macromolecular Bioscience* **2011,** *11* (9), 1254-1263.
34. Wintgens, V.; Layre, A. M.; Hourdet, D.; Amiel, C. Cyclodextrin Polymer Nanoassemblies: Strategies for Stability Improvement. *Biomacromolecules* **2012,** *13* (2), 528-534.
35. Dubacheva, G. V.; Dumy, P.; Auzély, R.; Schaaf, P.; Boulmedais, F.; Jierry, L.; Coche-Guerente, L.; Labbé, P. Unlimited growth of host–guest multilayer films based on functionalized neutral polymers. *Soft Matter* **2010,** *6* (16), 3747-3750.
36. Dubacheva, G. V.; Curk, T.; Mognetti, B. M.; Auzély-Velty, R.; Frenkel, D.; Richter, R. P. Superselective targeting using multivalent polymers. *J. Am. Chem. Soc.* **2014,** *136* (5), 1722-1725.

37. Antoniuk, I.; Wintgens, V.; Volet, G.; Nielsen, T. T.; Amiel, C. Bifunctionalized dextrans for surface PEGylation via multivalent host–guest interactions. *Carbohydr. Polym.* **2015,** *133*, 473-481.
38. Dedola, S.; Nepogodiev, S. A.; Field, R. A. Recent applications of the Cu-I-catalysed Huisgen azide-alkyne 1,3-dipolar cycloaddition reaction in carbohydrate chemistry. *Org. Biomol. Chem.* **2007,** *5* (7), 1006-1017.
39. Hein, C. D.; Liu, X. M.; Wang, D. Click chemistry, a powerful tool for pharmaceutical sciences. *Pharm. Res.* **2008,** *25* (10), 2216-2230.
40. Suzuki, T.; Ota, Y.; Kasuya, Y.; Mutsuga, M.; Kawamura, Y.; Tsumoto, H.; Nakagawa, H.; Finn, M. G.; Miyata, N. An Unexpected Example of Protein-Templated Click Chemistry. *Angew. Chem., Int. Ed.* **2010,** *49* (38), 6817-6820.
41. Greenwald, R. B.; Pendri, A.; Bolikal, D. Highly Water Soluble Taxol Derivatives: 7-Polyethylene Glycol Carbamates and Carbonates. *J. Org. Chem.* **1995,** *60* (2), 331-336.
42. Nielsen, T. T.; Wintgens, V.; Amiel, C.; Wimmer, R.; Larsen, K. L. Facile Synthesis of beta-Cyclodextrin-Dextran Polymers by "Click" Chemistry. *Biomacromolecules* **2010,** *11* (7), 1710-1715.
43. Siemsen, P.; Livingston, R. C.; Diederich, F. Acetylenic coupling: A powerful tool in molecular construction. *Angew. Chem., Int. Ed.* **2000,** *39* (15), 2633-2657.
44. Antoniuk, I.; Volet, G.; Wintgens, V.; Amiel, C. Synthesis of a new dextran-PEG-b-cyclodextrin host polymer using ‘‘Click’’ chemistry. *Journal of Inclusion Phenomena and Macrocyclic Chemistry* **2014,** *80*, 93-100.
45. Hoogenboom, R.; Moore, B. C.; Schubert, U. S. Synthesis of star-shaped poly(epsilon-caprolactone) via 'click' chemistry and 'supramolecular click' chemistry. *Chem. Commun.* **2006,** (38), 4010-4012.
46. Kappe, C. O.; Van der Eycken, E. Click chemistry under non-classical reaction conditions. *Chem. Soc. Rev.* **2010,** *39* (4), 1280-1290.
47. Renard, E.; Deratani, A.; Volet, G.; Sebille, B. Preparation and characterization of water soluble high molecular weight beta-cyclodextrin-epichlorohydrin polymers. *Eur. Polym. J.* **1997,** *33* (1), 49-57.
48. Blomberg, E.; Kumpulainen, A.; David, C.; Amiel, C. Polymer bilayer formation due to specific interactions between beta-cyclodextrin and adamantane: A surface force study. *Langmuir* **2004,** *20* (24), 10449-10454.
49. Oshannessy, D. J.; Brighamburke, M.; Soneson, K. K.; Hensley, P.; Brooks, I. Determination of rate and equilibrium binding constants for macromolecular interactions using surface plasmon resonance: use of nonlinear least squares analysis methods. *Anal. Biochem.* **1993,** *212* (2), 457-468.
50. Wintgens, V.; Amiel, C. Surface plasmon resonance study of the interaction of a beta-cyclodextrin polymer and hydrophobically modified poly(N-isopropylacrylamide). *Langmuir* **2005,** *21* (24), 11455-11461.
51. Busse, S.; DePaoli, M.; Wenz, G.; Mittler, S. An integrated optical Mach-Zehnder interferometer functionalized by beta-cyclodextrin to monitor binding reactions. *Sens. Actuator B-Chem.* **2001,** *80* (2), 116-124.
52. Chan, T. R.; Hilgraf, R.; Sharpless, K. B.; Fokin, V. V. Polytriazoles as copper(I)-stabilizing ligands in catalysis. *Org. Lett.* **2004,** *6* (17), 2853-2855.
53. Fulmer, G. R.; Miller, A. J. M.; Sherden, N. H.; Gottlieb, H. E.; Nudelman, A.; Stoltz, B. M.; Bercaw, J. E.; Goldberg, K. I. NMR Chemical Shifts of Trace Impurities: Common Laboratory

Solvents, Organics, and Gases in Deuterated Solvents Relevant to the Organometallic Chemist. *Organometallics* **2010,** *29* (9), 2176-2179.
54. Daoud-Mahammed, S.; Ringard-Lefebvre, C.; Razzouq, N.; Rosilio, V.; Gillet, B.; Couvreur, P.; Amiel, C.; Gref, R. Spontaneous association of hydrophobized dextran and poly-β-cyclodextrin into nanoassemblies.: Formation and interaction with a hydrophobic drug. *J. Colloid Interface Sci.* **2007,** *307* (1), 83-93.

Chapter 4

Poly(N-isopropylacrylamide)-based hierarchical microgels: sterical stabilization of the particles and supramolecular hydrogel formation *via* host-guest interactions

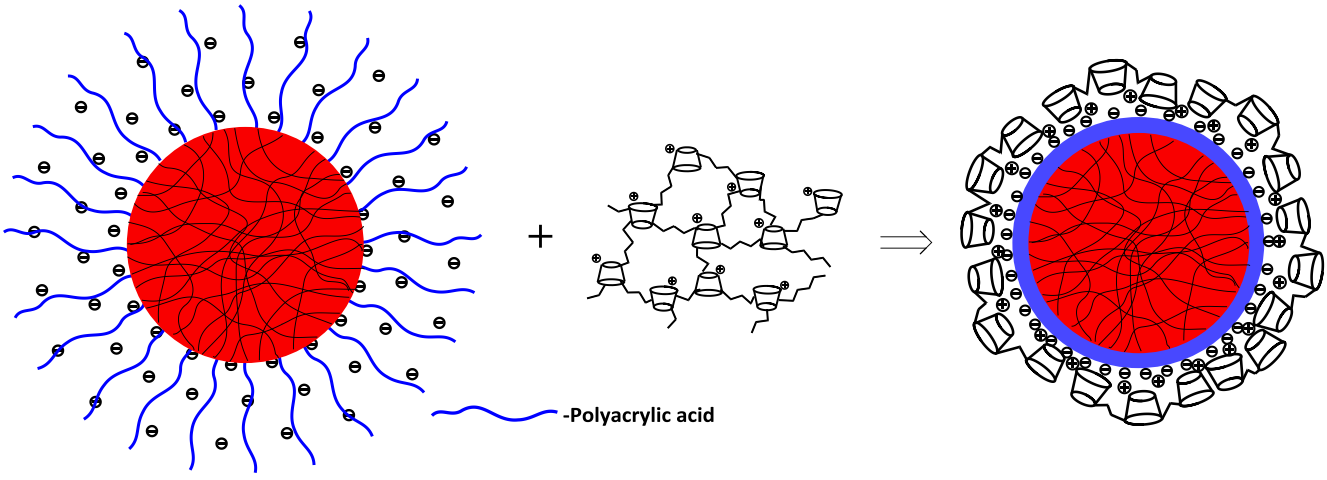

Table of contents

Introduction

The work described in the 4th chapter was done in collaboration with our colleagues from ELTE University (Budapest, HU) Daria Kaczmarek, Imre Varga and Attila Kardosh. We present a new approach to the synthesis and non-covalent sterical stabilization of hierarchically structured poly(*N*-isopropylacrylamide) (pNIPAm) microgels coated with positively charged poly-β-cyclodextrin. We also show the opportunity to prepare a supramolecular macrogel composed of hierarchical hydrogels interconnected via host-guest interactions.

Microgels are chemically cross-linked polymer networks with typical sizes in the range from 50 nm to 2 μm.[1] A special family of the microgel particles is stimuli responsive microgels that can undergo what is called volume phase transition (VPT) – non-linear, reversible change in their swelling degree in response to an external stimulus.[2, 3] One of the most well-known and widely employed polymers to produce responsive microgels is pNIPAm. Typically pNIPAm microgels are prepared by precipitation polymerization of N-isopropylacrylamide (NIPAm) with a bifunctional cross-linker comonomer, methylenbisacrylamide (BA), in the presence of sodium dodecyl sulfate (SDS).[3, 4] This method yields nanoparticles with low polydispersity and allows copolymerizing various hydrophobic and hydrophilic monomers, while microgel size can be tuned by adjusting the amount of SDS in the reaction mixture.[2] Due to the thermoresponsive character of pNIPAm the microgels show VPT triggered by increase of temperature, typically occurring at ~33°C (**Figure IV.1**).[2]

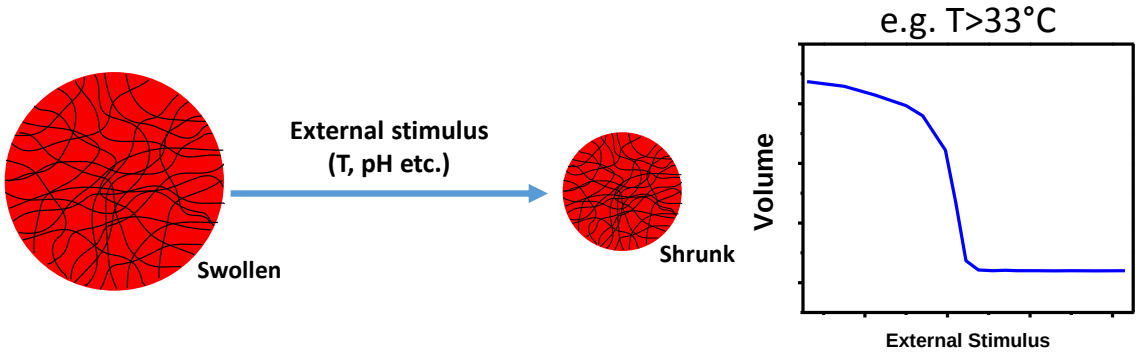

Figure IV.1: Schematic illustration showing the VPT process of a responsive cross-linked microgel particle triggered by an external stimulus, herein temperature.

Synthesis and characterization of pNIPAm-based responsive microgels have attracted a significant interest in the last decades. They are considered as promising candidates for various applications ranging from heavy metal scavenging and diagnostic applications, to controlled drug delivery systems.[2, 5] However, microgels composed of homopolymer pNIPAm are limited in their application in that their thermally induced VPT takes place at a fixed temperature of 33-34°C. This limitation might be overcome either by randomly introducing hydrophilic or polyelectrolyte comonomers in the structure of microgels or by preparing hydrophilic copolymer shells on top of pNIPAm core.[6] In addition to VPT temperature regulation opportunity, multiresponsive core-shell microgel architectures with complex phase transition behavior might be obtained when NIPAm is combined with another environmentally sensitive comonomer (e.g. pH-responsive AAc). However, with conventional precipitation polymerization the upper content of hydrophilic copolymers in such microgels is restricted by the necessity to satisfy the condition: VPT temperature < reaction temperature. Kardos et al. have recently developed a novel approach to prepare core-shell pNIPAm-g-pAAc microgels with unrestricted shell composition, containing up to 100% w/v of AAc (Unpublished results). Purely polyelectrolyte shell composition was aimed at facilitating post-modification of the particles with various cationic agents and at making pH-induced changes in phase transition behavior more pronounced. Hence, pNIPAm-g-100%pAAc were used in further described experiments. Further in the text we will always refer to microgels with 100% pAAc shell as pNIPAm-g-pAAc for simplicity reasons.

Due to the carboxylic groups being deprotonated at physiological pH, negatively charged pNIPAm-g-pAAc could be used as nanocarriers for oppositely charged molecules – surfactants, polymers, etc. However as stoichiometric binding is approached, the surface charge density of the microgel/oppositely charged molecule complexes diminishes resulting in a loss of their colloid stability. Furthermore, in the context of their potential usage as drug delivery carriers, a number of significant issues should be addressed, such as limited colloidal stability, poor biocompatibility resulting in fast opsonization by blood serum proteins[7] and burst release of actives after thermally triggered VPT.

A number of recent evidences in support of superficial functionalization of drug nanocarriers with CD-containing materials are found in literature. For instance, El Fagui et al. have reported

β-cyclodextrin polymer (pβCD) layer to play the role of a barrier slowing down the release kinetics of triclosane from hydrophobic PLA nanoparticles.[8, 9] Another way to exploit superficial CD shell consists in post-modification of drug delivery vehicles *via* reversible and competitor binding-responsive host-guest complexation of molecules of interest usually pre-functionalized with Ada-groups. Using this approach, various drug/gene nanocarriers could be non-covalently functionalized with fluorescent dies[10], targeting peptides[11] and sterically stabilizing hydrophilic polymers.[10, 12, 13]

a. Sterically stabilized pNIPAm-*g*-pAAc/pβCDN+ hierarchical microgels

Given the above, in this work we aimed to develop a reliable and straightforward approach to βCD-coated pNIPAm-g-pAAc microgels, which would allow preserving thermoresponsiveness of pNIPAm cores. To achieve this we use ionic self-assembly between the negatively charged at pH 7 pAAc shell and pβCDN+ (a neutral epichlorohydrin cross-linked pβCD modified with quaternary ammonia groups). This approach was chosen since it should provide an easy way to control the degree of coating and the overall charge of the resulting pNIPAm-g-pAAc/pβCD1.62N+ microgels (for simplicity reasons they will be mostly referred to as pNIPAm/βCD1.62N) by adjusting the +/- molar ratio during the mixing stage.

The pNIPAm/βCD1.62N have potential to be used as drug nanocarriers with improved release kinetics. However, for any biomedical application the particles are expected to have neutral overall charge, whereas in our case colloidal stability of pNIPAm/βCD1.62N is lost at zero-charge point (+/- = 1). Hence, there is a need to sterically stabilize them. Traditionally it is achieved via post-modification of the shell with non-charged hydrophilic polymer chains e.g. PEG, polyoxazolines, polysaccharides etc.; though tedious and time-consuming synthetic and purification steps are required in this case.[14, 15] Non-covalent supramolecular self-assembly appears to be a fast, facile and sustainable alternative. Therefore, we took advantage of a part of βCD-cavities from the pβCDN+ shell to attach a sterical stabilizer *via* inclusion complexation. It was achieved in 2 steps: **1)** formation of a supramolecular precursor between pβCDN+ and (PEG, Ada)-grafted dextrans described in Chapter 3; **2)** addition of negatively charged microgels to the precursor solution at stoichiometrical +/- = 1 ratio. This strategy allowed obtaining stable pNIPAm-g-pAAc/pβCDN+/DT40-28GP-10Ada-18PEG hierarchical microgels with neutral overall charge (for simplicity reasons they will be referred to as pNIPAm/βCD1.62N/PEG).

b. Supramolecular hydrogels based on pNIPAm/βCD1.62N hierarchical microgels

Hydrogels are cross-linked 3D-networks composed of hydrophilic polymeric chains or low molecular-mass gelators.[16] Due to their structural and functional resemblance to extracellular matrix, hydrogels find a lot of applications in biomedical industry as scaffolds in regenerative medicine and depos for sustained release of therapeutics.[17, 18, 19] Depending on the nature of cross-links two main classes of hydrogels are distinguished: covalently cross-linked *chemical hydrogels* and non-covalently constructed *physical hydrogels*. Comparing to their covalently cross-linked counterparts, physical hydrogels possess a number of advantages such as: immanent stimuli-responsive nature[20], reversibility[21, 22] and compositional flexibility. The ability of physical gels to reform themselves after damage, known as self-healing, emerges as a consequence of the reversible nature of physical cross-links. The reversibility, in turn, is due to common physical interactions exhibiting much lower bond energies (8-35 kJ·mol^{-1} for ionic interactions and hydrogen bonding) comparing to the dissociation energy of covalent C-C bond (347 kJ·mol^{-1}).[23]

Incorporation of particulate drug delivery vehicles, and thermoresponsive microgels in particular, in the hydrogels matrix might increase the pharmacological performance of both components.[19] The resulting composite or "plum pudding" hydrogels (**Figure IV.2**) often show better mechanical properties and the biocompatibility of microgels/nanoparticles is increased by "hiding" the latter in the biocompatible hydrogel network.

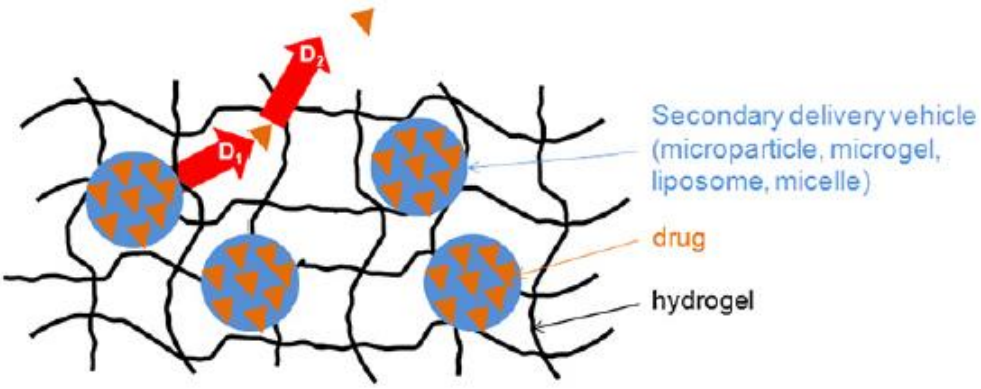

Figure IV.2: Illustration of a "plum pudding" hydrogel containing nanoscale delivery vehicle loaded with a drug. Such system is characterized by two diffusion coefficients: D_1 representing

diffusion of drug from nanovehicle; D_2 represents diffusion through the matrix. Reprinted from Hoare et al.[19]

Hydrogel matrix might play the role of a diffusion barrier able to diminish the "burst release" of drug issue observed for nanoscale carriers.[24] At the same time, fixation of the nanoparticles in the matrix prevents their migration or washing away from the site of action *in vivo*. Finally, multiple types of microgels carrying different payloads can be entrapped in the same gel matrix and simultaneously delivered.[25]

Richtering and Saunders distinguish three types of composite hydrogels containing microgels[23]: (i) microgel-filled hydrogels, (ii) microgels-reinforced hydrogels and (iii) doubly crosslinked microgels (DX microgels) (**Figure IV.3**). All these types of hydrogels exhibit structural hierarchy with two or more distinct length scales between the adjacent crosslinks represented by the correlation lengths ξ. In the first two cases microgels are either mechanically entrapped (**Figure IV.3, i**) or covalently linked (**Figure IV.3, ii**) with the bulk hydrogel matrix. In the case of DX microgels, however, the particles are directly interlinked and no additional hydrogel matrix is required (**Figure IV.3, iii**).

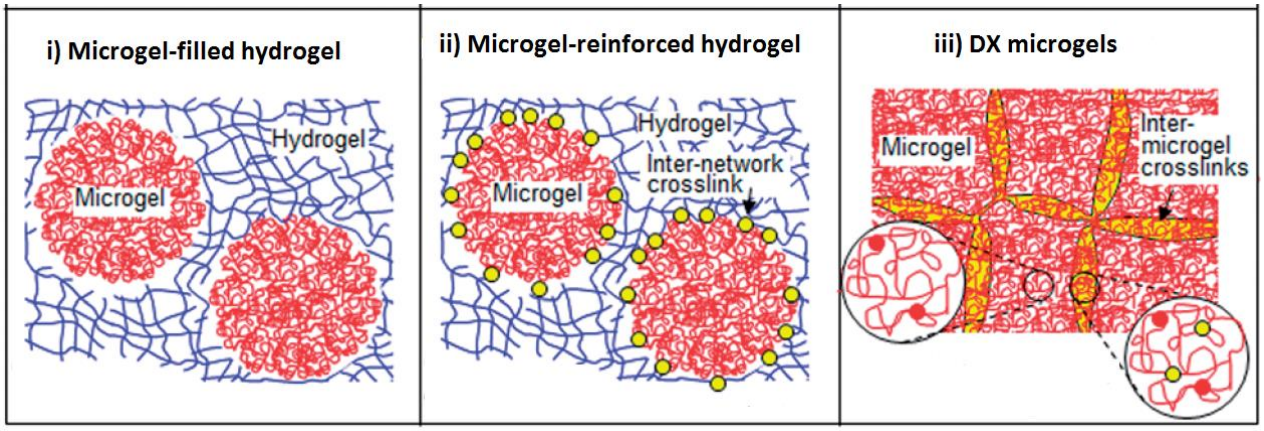

Figure IV.3: Schematic illustration of different types of microgel-containing hydrogels. Reprinted from Richtering and Saunders.[23]

Sivakumaran et al. have recently reported nanocomposite hydrogels composed of thermoresponsive pNIPAm-co-pAAc microgels either entrapped or covalently linked to inert carboxymethyl cellulose hydrogel.[26] The hydrogels showed capacity to facilitate temperature-triggered long-term release of bupivacaine hydrochloride, a cationic drug. Interestingly, both

increase of internal cross-link densities and covalent linking of microgels to the matrix led to lower overall rates of drug release, which was ascribed to reduced kinetics of microgel deswelling at higher temperatures (37°C). Similar microgel-reinforced systems were reported, composed of: hyaluronic acid-glycidyl methacrylate (HA-GMA) matrix and covalently linked ethylene-oxide (EO)-based microgels[27]; HA hydrogel network and covalently integrated surface-modified HA-microgels.[28, 29] However, mechanical properties of the hydrogels didn't benefit from the presence of microgels in these cases, which is apparently related to quite high distance between the embedded particles. Hence, their contribution to the overall network strength was rather disruptive.

Temperature-induced mechanical properties improvement was found for polyacrylamide (PAAm)-based composite hydrogels non-covalently filled with pNIPAm microgels.[30] At high temperatures (> VPT temperature of the microgels) the collapse of filler microgel particles led to a change in their nature from a soft to a hard filler. Incorporation of 25 $g \cdot L^{-1}$ of microgels in a hydrogel with total polymer concentration of 75 $g \cdot L^{-1}$ led to storage moduli twice as high at 20°C and ten times as high at 40°C comparing to the pure PAAm hydrogel with the same mass concentration (**Figure IV.4**).

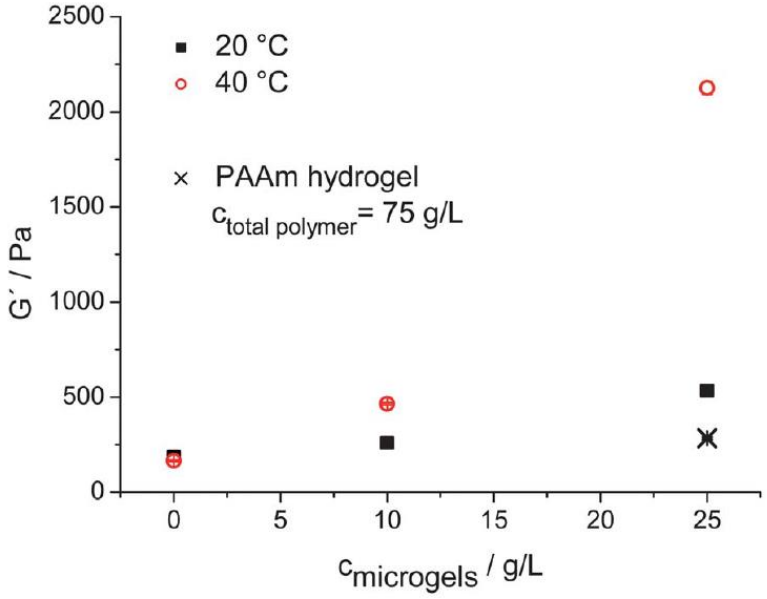

Figure IV.4: The storage modulus G' of pNIPAm microgel-filled PAAm hydrogels as a function of microgel concentration at two different temperatures. Reprinted from Meid et al.[30]

As mentioned above, DX microgels (**Figure IV.3, iii**) are formed *via* direct interaction between the microgel particles in a swollen state, provided that their surface groups and dangling polymer chains are close enough to establish a link.[23] DX microgels were first described in 2000 by Hu et al.[31] Their system was composed of epichlorhydrin crosslinked pNIPAm-g-pAAc microgels. In this case and in many later works, secondary crosslinking of the microgels was done covalently, by functionalizing them with vinyl groups and using free-radical chemistry.[32, 33] Such DX microgels were used as injectable formulations to reinforce degenerated intervertebral disc tissue.[33] The microgel cross-linking was performed directly *in vivo* and the resulting hydrogels had remarkably high toughness (G' = 0.7-1.3·10^5 Pa). However, because of the permanent character of secondary cross-linking such DX microgels lack reversibility and self-healing capacity.

The introduction of cyclodextrins as structural units of both chemical and physical hydrogels proved to be beneficial given the ease and versatility of CD functionalization (*via* multiple primary and secondary hydroxyls), their high biocompatibility and the opportunity to exploit the cyclodextrin-hydrophobic guest inclusion chemistry.[34] Over the last decade a large variety of complex supramolecular hydrogels containing CDs have been developed.[18] In some of recent examples βCD-Ada host-guest chemistry was used as a means to cross-link soft nanoscale objects into non-covalent 3D hydrogel networks. For instance, Himmelein et al. used hydrophobically self-assembled cyclodextrin vesicles (CDV) as multivalent 3D joints which were converted to a gel by addition of adamantane-modified hydroxyethylcellulose (HEC-Ad).[22] Due to its reversible nature their system showed shear-thinning/self-healing properties and was injectable through a syringe.

Given the above, in the second part of this work we had a goal to use pNIPAm/βCDN core-shell microgels as a building block for hierarchical DX microgels non-covalently cross-linked with Ada-substituted dextrans through host-guest interactions.

1. Sterically stabilized hierarchical pNIPAm-based microgels via host-guest interactions - pNIPAm/βCDN/PEG

1.1 Preparation of host polymer coated pNIPAm microgels – pNIPAm/βCDN

1.1.1 pNIPAm-g-pAAc microgels

PNIPAm microgels with unrestricted shell composition (up to 100% pAAc) were prepared by a two-step seeded precipitation polymerization technique. BA-crosslinked pNIPAm cores were synthesized in the first step (**Figure IV.5**). Then, using the pNIPAm cores as seeds, pAAc shell is introduced by the precipitation polymerization in the second stage. More details on the synthesis, purification and characterization of the pNIPAm-g-pAAc microgels is given in the Experimental section, however the information provided is not complete for confidentiality reasons (unpublished results by our colleagues from ELTE).

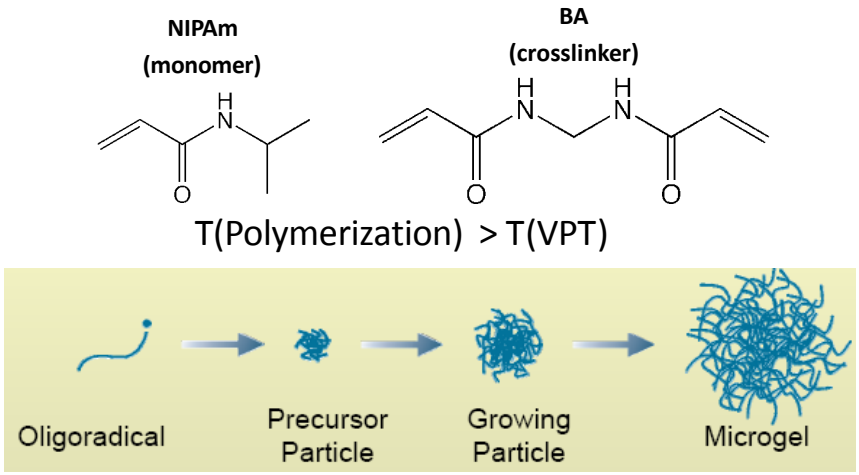

Figure IV.5: Schematic illustration of the pNIPAm microgel cores synthesis by precipitation polymerization technique.

If other is not indicated, the pNIPAm-g-pAAc microgels solutions were used at pH 7, which entails that most of the pAAc carboxylic groups are in the dissociated state (pK_a (AAc) = 4.25). Exact concentration of the pAAc-originating superficial negative charges, further denoted as C(AAc-) or simply C(-), was determined by titrations of microgel solutions at 4 different concentrations with cetyltrimethylammonium bromide (CTAB), while monitoring the electrophoretic mobility evolution. Details on the electrophoretic mobility titration and C(-) determination are given in the Experimental part. Then, a microgel stock solution with AAc (-)

concentration 0.29 mM (0.12 g·L^{-1}, **Table IV.1**) was prepared and used in further experiments. The dual (pH and temperature) responsiveness of pNIPAm-g-pAAc can be illustrated by thermo-DLS, i.e. measurements of hydrodynamic diameters of the particles at different temperatures, recorded at different pH (**Figure IV.6**).

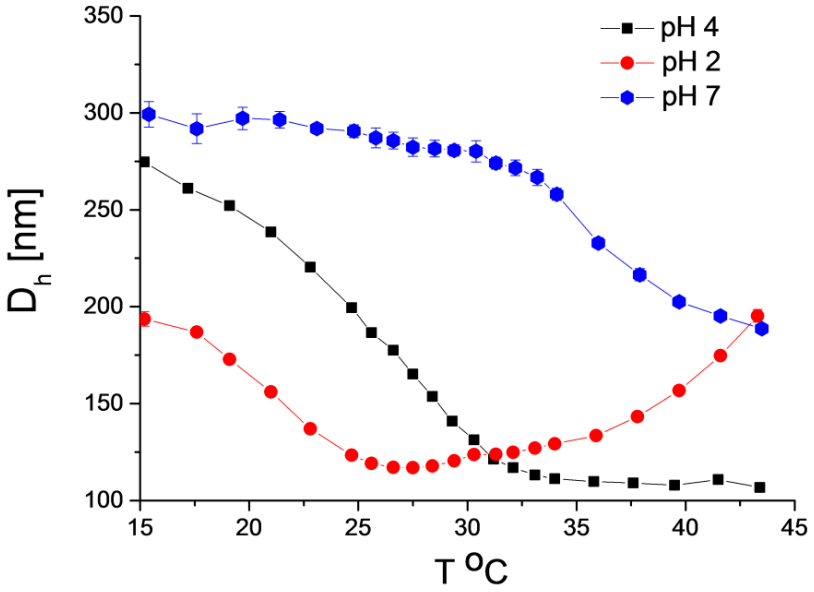

Figure IV.6: Evolution of hydrodynamic diameters of pNIPAm-g-100%pAAc microgels as a function of temperature at different pH. The pH was set with 10 mM phosphate buffer solutions.

One can see that at low temperatures (15-22°C) the degree of swelling of the microgels strongly depends on pH, i.e. their D_h increases from 190 to 300 nm when pH is increased from 2 to 7. Moreover, the temperature at which VPT occurs is shifted from 23°C to 36°C for pH 7 as compared to pH 2, indicating the synergetic effect of between the temperature and pH on the deswelling of pNIPAm-g-pAAc. The increase of D_h at pH 2 at T > 30°C can be explained by the low solvent quality for the protonated pAAc shell at these conditions. Indeed, the hydrogen bonding of non-dissociated carboxylic groups of pAAc with water is expected to be hampered at increased temperatures.

Table IV.1. Characteristics of the polymers and microgels used

Microgels	**C(AAc-), mM → C, g·L^{-1}**	**D_h, nm (pH 7)**		
pNIPAm-g-100%pAAc	1 mM → 0.40 g·L^{-1}	450		
Host polymers	**C(+), mM → C, g·L^{-1}**	**M_w, 10^{-3}g·mole^{-1}**	**CD, wt%**	**N+/CD**
pβCD1.62N+	1 mM → 1.20 g·L^{-1}	238	58.2	1.62
pβCD3.24N+	1 mM → 0.68 g·L^{-1}	268	51.8	3.24
pβCD5.00N+	1 mM → 0.49 g·L^{-1}	299	46.1	5.00
(PEG,Ada)-grafted dextrans	**C(Ada), mM → C, g·L^{-1}**	**M_w, 10^{-3}g·mole^{-1}**	**DS(Ada), mol.%**	**DS(PEG), mol.%**
D40-28GP-10Ada-18PEG	1 mM → 10.83 g·L^{-1}	267	10	18
D40-18GP-18PEG	-	262	0	18
Guest polymers	**C(Ada), mM → C, g·L^{-1}**	**M_w, 10^{-3}g·mole^{-1}**	**DS(Ada), mol.%**	
DT110Ada3	1 mM → 3.68 g·L^{-1}	115	4.7	
DT110Ada4	1 mM → 2.77 g·L^{-1}	117	6.2	
DT500Ada2	1 mM → 2.66 g·L^{-1}	533	6.5	

1.1.2 Host polymer coated pNIPAm/βCDN microgels

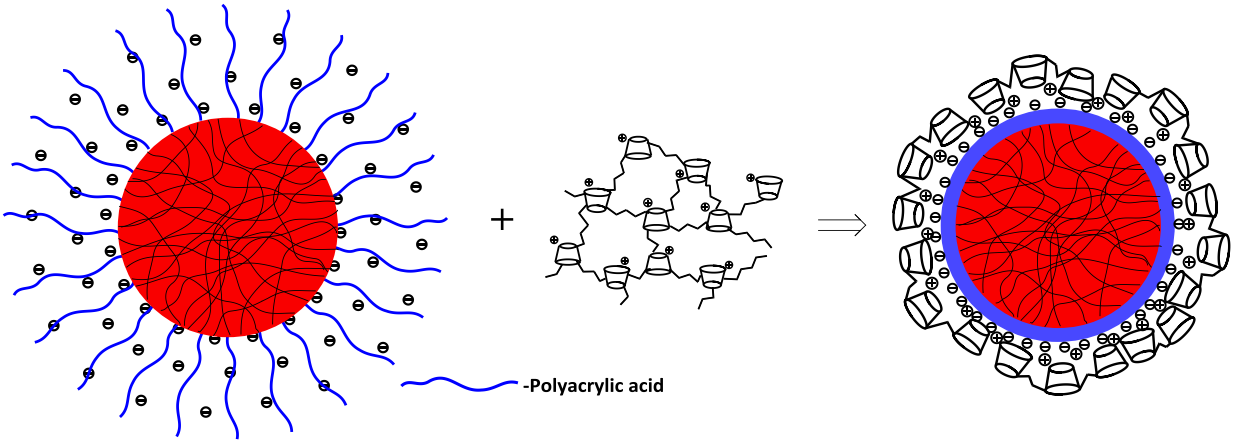

Figure IV.7: pNIPAm/βCDN host polymer coated microgels preparation strategy.

A positively charged pβCDN+ with 1.62 (+) charges per CD unit (**Table IV.1**) was used to form a host polymer shell around the microgels via multivalent electrostatic complexation with

dissociated AAc groups (**Figure IV.7**). Before the complexation the AAc groups were deprotonated by adding NaOH to the microgel solution and subsequent neutralization of excess of OH^- ions with HCl and readjusting the pH to 7.

1.1.3 Evidence of βCDN+ coating

The pNIPAm-g-pAAc microgel suspensions at 0.145 mM of (-) charges were mixed with pβCDN+ solutions with (+) charges concentrations in the range from 0.02 to 0.4 mM (if not indicated otherwise, concentrations are given for the final volume after mixing). The hydrodynamic diameters of the particles were gradually decreasing as more of cyclodextrin polymer was added (**Figure IV.8**) which might be explained by shrinking of the AAc external shell due to partial negative charge compensation. At roughly stoichiometrical +/- ratio electrophoretic mobility of the microgel/oppositely charged polymer complexes drops down to zero (**Figure IV.9**), leading to their aggregation at +/- = 0.7-1.3 (**Figure IV.8**). However, when excess of pβCDN+ is introduced (corresponding to +/- = 1.3-1.4) pNIPAm/βCD1.62N host microgels become positively overcharged and regain their colloidal stability. The excess of positive charges induces an increase in the osmotic pressure of the solvent in the shell, leading to a partial reswelling of the microgels (**Figure IV.8**). Moreover, the obtained overcharged complexes show good stability over time with their D_h only negligibly evolved after 8 days of storing in pure water at ambient temperature (**Figure IV.8**).

The electrostatic stabilization of overcharged pNIPAm/βCD1.62N was confirmed by cryo-transmission electron microscopy (cryo-TEM) experiments. In recent year cryo-TEM electronic microscopy has become an important tool for unveiling the structural details of soft matter nanostructures.[35, 36] In a typical cryo-TEM experiment, an aqueous solution of the sample is vitrified by instantaneous shock-freezing in liquid ethane prior to recording the TEM micrographs. As opposed to normal TEM, the artefacts associated with drying of the sample are avoided in cryo-TEM, making the obtained images more adequate representations of the microgel state in solution. Before vitrifying the samples, any non-bound with pβCD1.62N+ acrylic acid groups were protonated by creating pH = 2 with HCl. This results in shrinking of the shells and overall increase in the TEM contrast of the microgels.

Two microgel samples were compared: **a)** a sample from the middle of precipitation range, i.e. at C(+) = 0.16 mM; **b)** a sample from the positively overcharged range, at C(+) = 0.32 mM (**Figure IV.10b**). In the first case one clearly observes formation of non-well defined microgel aggregates in average composed of 6-8 coalesced particles (**Figure IV.10a**). On the other hand, the positively overcharged microgels show no signs of aggregation with well-separated individual particles even in an acidic medium (**Figure IV.10b**), which should be due to the cooperativity of binding between two oppositely charged polyelectrolytes. The average diameter of the particles determined from the micrograph is 92±11 nm, which is lower than the D_h obtained by DLS for the sample with +/- = 2.2 (308 nm, **Figure IV.8**). In part, it might be explained by a more complete shrinking of the pAAc shell at pH 2. However, the disparity in sizes is too sharp and might be explained by the inhomogeneous structure of the microgels used, with a dense core and more swollen periphery.[2]

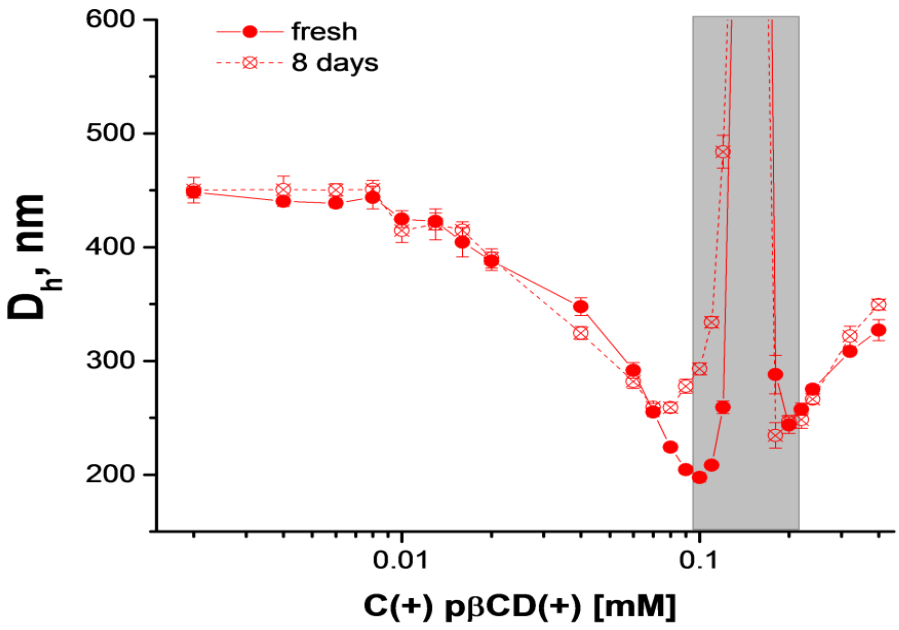

Figure IV.8: Evolution of hydrodynamic diameters (D_h) of pNIPAm/βCD1.62N host polymer coated microgels as a function of introduced (+)-charges concentration; stability of coated microgels after 8 days of storage at room temperature. C(AAc-) = 0.145 mM. The range of C(+) corresponding to colloidaly unstable particles is greyed out.

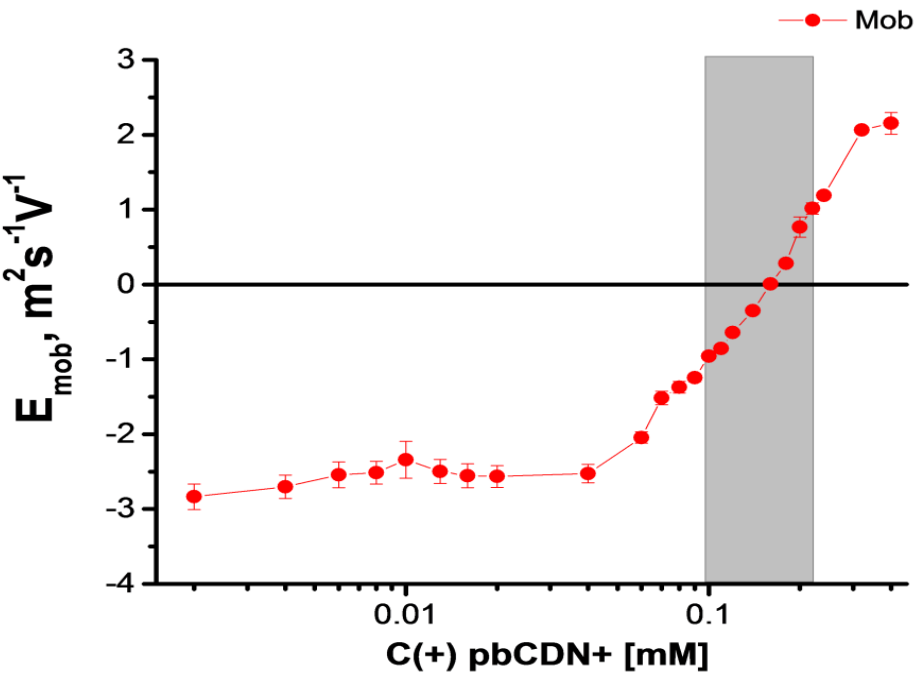

Figure IV.9: Electrophoretic mobilities (E_{mob}) of freshly prepared pNIPAm/βCD1.62N host polymer coated microgels as a function of introduced (+)-charges concentration. C(AAc-) = 0.145 mM. The range of C(+) corresponding to colloidaly unstable particles is greyed out.

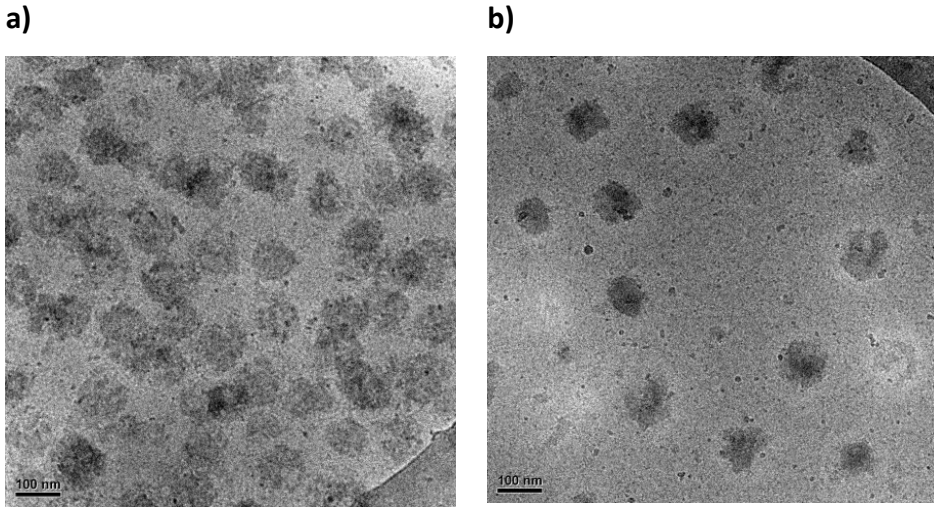

Figure IV.10: Cryo-TEM images of: **a)** pNIPAm/βCD1.62N microgels with close to stoichiometrical +/- ratio (C(AAc-) = 0.145 mM, C(+) = 0.16 mM); **b)** positively overcharged microgels (C(AAc-) = 0.145 mM, C(+) = 0.32 mM).

1.1.4 TC analysis of unbound βCDN+

To figure out the actual percentage of bound pβCDN+ we determined the total carbon (TC) amount in the supernatants of ultracentrifuged pNIPAm/βCD1.62N samples for all the investigated C(+) concentration range. The amount of TC is obtained through total combustion of the samples onto a platinum catalyst at 680°C. It leads to the catalytic oxidation of any carbon in the supernatant into carbon dioxide (CO_2). The concentration of the latter is then determined using a nondispersive infrared (NDIR) gas analyzer compared with the calibration curve recorded for a series of solutions with known TC concentrations. The procedure is described in more detail in the Experimental section.

Since we aimed to determine the TC amount corresponding to non-bound pβCDN+, it was important to minimize the signal from non-sedimented microgels. Acidifying of the samples to pH 2.5 prior to ultracentrifugation proved to increase the sedimentation efficiency *via* protonation of the residual AAc (-), shrinking of the shell and subsequent density increase in the case of uncoated microgels (**Figure IV.11a**). Higher particle concentrations also led to higher efficiency of bare microgels sedimentation. TC measurements on the initial samples before centrifuging and on the supernatants of a series with fixed C(AAc-) = 0.5 mM were performed at pH 2.5. The resulting TC(pβCDN+) – C(+)/C(-) dependency for the supernatants has two distinct regions with different slopes (blue curve in **Figure IV.11b**):

a) lower Slope 1 = 60, for C(+)/C(-) in the range 0 -2.0;

b) higher Slope 2 = 160, for the C(+)/C(-) in the range 2.0 - 2.8.

Slope 1 value is lower than that determined for the non-centrifuged samples - 162 (black curve in **Figure IV.11b**). This means that there is a continuous increase in the amount of bound pβCDN+ when the C(+)/C(-) ratio is varied from 0 to 2. The latter is coherent with the continuously increasing positive values of electrophoretic mobility observed for the overcharged microgels in the same C(+)/C(-) range (**Figure IV.9**). At C(+)/C(-) ratios larger than 2, the slope increases and reaches a value close to that of non-centrifuged samples. It means that no more pβCDN+ should bind to the microgels above this ratio.

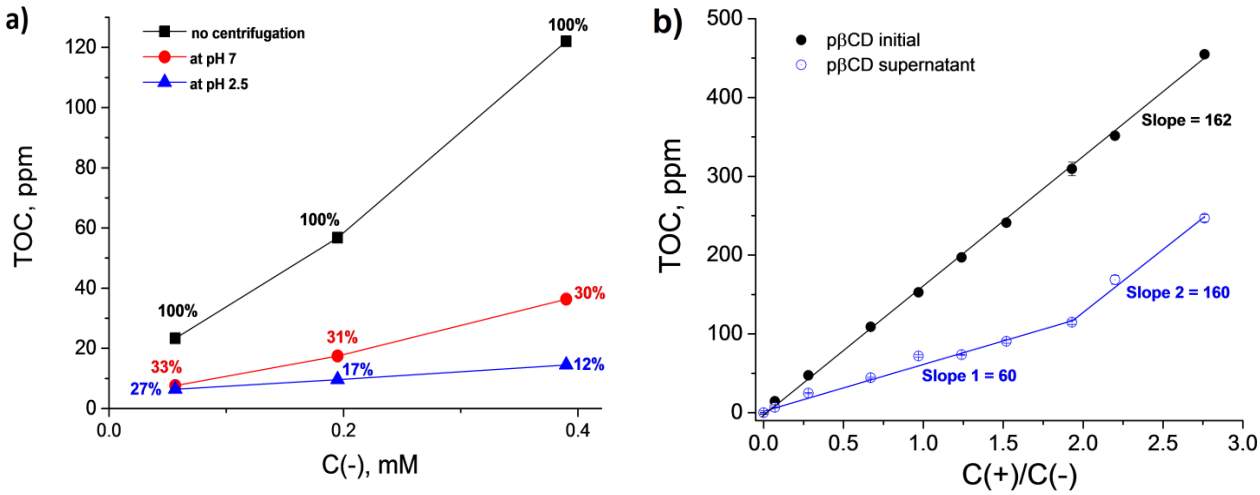

Figure IV.11: TC experiments for determination of non-bound pβCDN+ in the supernatants after binding with pNIPAm-g-pAAc microgels: **a)** bare pNIPAm-g-pAAc ultracentrifugation efficiency as a function of pH; **b)** TC corresponding to pβCDN+ in the mixture before ultracentrifugation (filled circles) and to non-bound pβCDN+ in the supernatants of pNIPAm/βCD1.62N complexes (empty circles) as a function of +/- charges ratio, pH = 2.5, C(AAc-) = 0.5 mM. Ultracentrifugation conditions: 62 400 × *g*, 40°C, 10h.

This result seems to be logical, given that cationic pβCDN+ molecules should approach already positively overcharged microgels and their adsorption should thus be less and less favorable. The relative amount of unbound pβCDN+ has been estimated at each C(+)/C(-) ratio from the TC measurements and reported in **Table IV.2**. In the C(+)/C(-) range 0 - 2.0, the unbound pβCDN+ fraction is of 40 % while it increases up to 54% for larger C(+)/C(-) ratio. Although these last results are rather qualitative, another important conclusion that can be drawn from the TC experiments is that for the whole C(+)/C(-) range we deal with samples containing significant amounts of non-bound pβCDN+ in the medium. At the same time, the interpretation of these data obtained for the samples at pH 2.5 should be done with caution. Partial desorption of pβCDN+ might occur during the centrifuging due to the protonation of AAc- groups (pH = 2.5), thus contributing to the TC signal of the supernatants.

Table IV.2. Percentage of non-bound pβCDN+ at different C(+)/C(-) ratios determined by TC analysis of the supernatants of the ultracentrifuged samples. Ultracentrifugation conditions: 62 400 × *g*, 40°C, 10h.

C(+), mM	C(+)/C(-)	pβCDN+$^{non\text{-}bound}$/ pβCDN+^{total}, %
0.34	0.67	40.6
0.48	0.97	47.1
0.62	1.24	37.4
0.76	1.52	37.6
0.96	1.93	37.2
1.10	2.2	48.0
1.38	2.76	54.3

40 ± 4

1.1.5 Influence of βCDN+ charge density

We also have studied the influence of the charge density of pβCDN+ with equal molecular weights (see **Table IV.1** for polymer characteristics) on the coating formation efficiency (**Figure IV.12**). For this purpose poly-β-cyclodextrins with 3.24 and 5.00 quaternary ammonia N+ per CD cavity were used. Electrophoretic mobility curves evolve in a remarkably similar way as functions of C(+) in the mixture for different polymers.

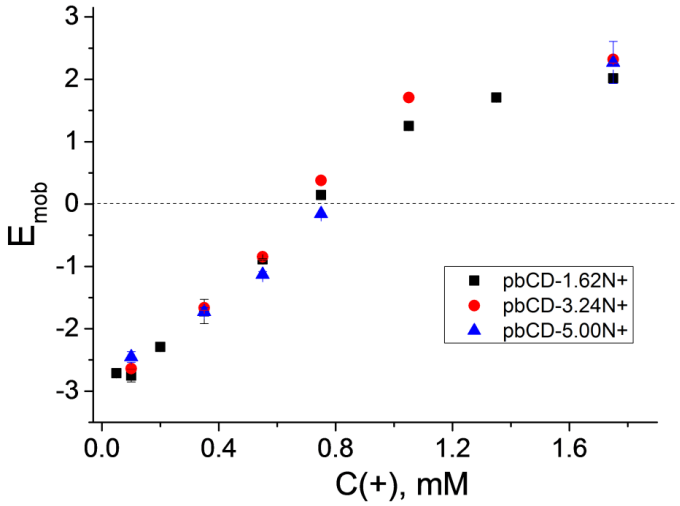

Figure IV.12: Electrophoretic mobilities (E_{mob}) of pNIPAm/βCDN coated with host polymers with different N+ charge density per βCD. C(AAc-) = 0.50 mM.

1.2 Stabilization of the neutral pNIPAm/βCDN microgels with DT40-GP-Ada-PEG

1.2.1 Strategy of steric stabilization

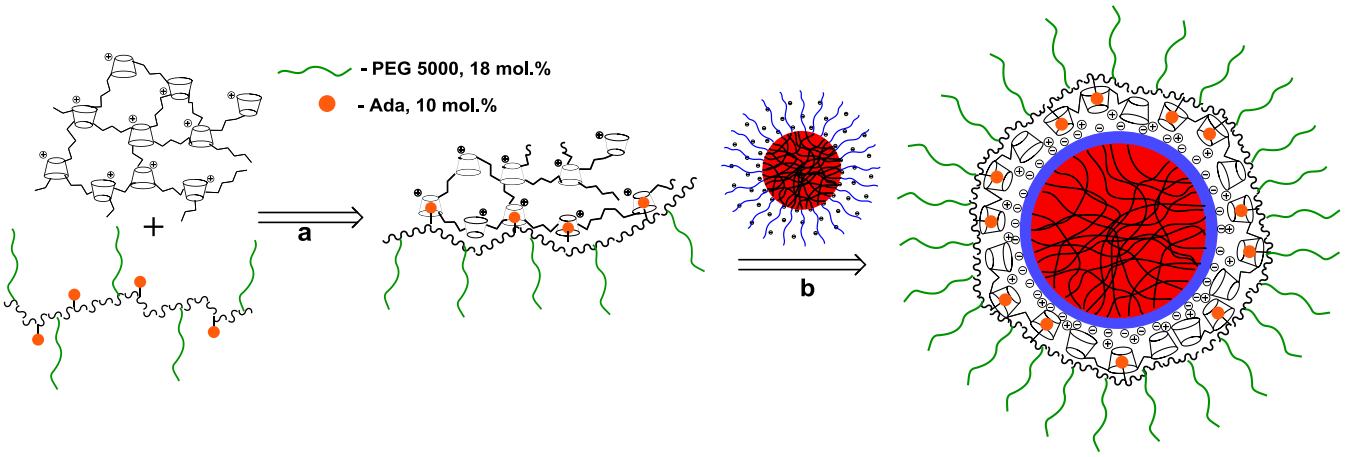

Figure IV.13: Strategy for host-guest driven sterical stabilization of pNIPAm/βCD1.62N core-shell microgels.

As it was shown, positive overcharging of pNIPAm-pAAc with pβCDN+ is needed to make the resulting pNIPAm/βCD1.62N colloidally stable. At the same time, for the majority of eventual biomedical applications microgels are required to have neutral or moderately negative overall charge. To overcome this drawback we used bifunctional (PEG, adamantane)-grafted dextrans (DT40-GP-Ada-PEG) for sterical stabilization of pNIPAm/βCD1.62N. The applied strategy consisted of 2 steps, namely: pre-mixing of required amount of pβCDN+ with DT40-28GP-10Ada-18PEG polymer bearing 10 mol % of adamantyls and 18 mol.% of 5000 Da PEG grafts[37] (described in detail in Chapter 3), followed by addition of microgel solution (**Figure IV.13**).

A pNIPAm/βCD1.62N sample from the middle of precipitation range with C(+) = 0.16mM and C(AAc-) = 0.145 mM was chosen to investigate its behavior as a function of Ada/CD molar ratio in the pβCDN+/DT40-28GP-10Ada-18PEG precursor complex. It turned out that already at Ada/CD = 0.3 precipitation was suppressed leading to stable microgels of around 200 nm (**Figure IV.14**).

To prove the host-guest driven origin of sterical stabilization we conducted a control experiment with DT40-18GP-18PEG, bearing exclusively 18 mol.% of PEG grafts (**Table IV.1**) and unable to form inclusion complexes with βCD. No considerable effect on the system behavior was

observed even at the DT40-18GP-18PEG weight concentrations corresponding to Ada/CD = 1 ratio in the DT40-28GP-10Ada-18PEG series (**Figure IV.14**).

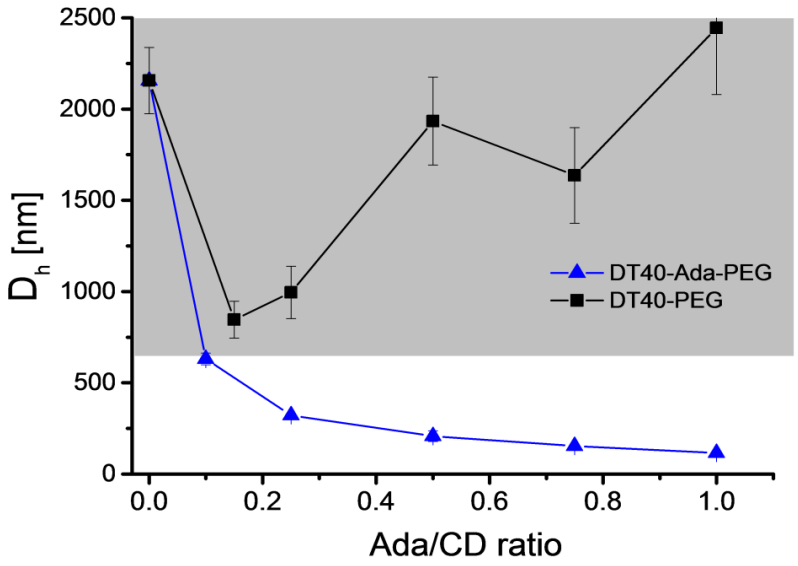

Figure IV.14: Efficiency of sterical stabilization of pNIPAm/βCD1.62N microgels from the middle of precipitation range by DT40-28GP-10Ada-18PEG (blue triangles) and DT40-18GP-18PEG (black squares) as a function of Ada/CD molar ratio (C(AAc-) = 0.145 mM, C(+) = 0.16mM). Greyed out area highlights the samples for which precipitation occurs.

Since Ada/CD = 0.3 molar ratio proved to be sufficient, its stabilizing effect on pNIPAm/βCD1.62N microgels was studied for the entire C(+) concentration range (**Figure IV.15**). One can see that the usage of DT40-28GP-10Ada-18PEG leads to a complete elimination of the precipitation region in the vicinity of zero charge point (**Figure IV.15a**). As a matter of fact, the smallest D_h are observed for sterically stabilized microgels with neutral overall charge. It might be explained by lower osmotic pressure of the solvent inside the shells with fully compensated superficial charges. This effect is, however, masked by aggregation in non-stabilized pNIPAm/βCD1.62N.

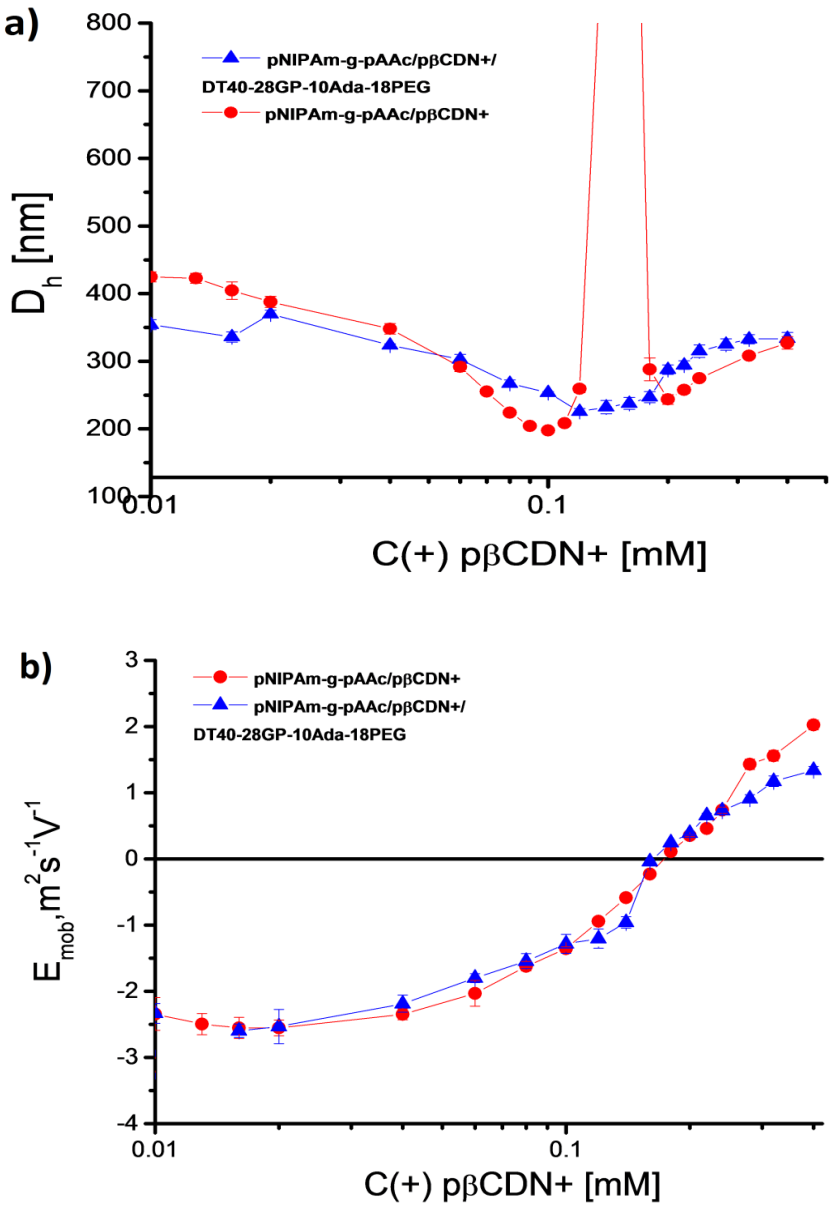

Figure IV.15: Comparison of hydrodynamic diameters (**a**) and electrophoretic mobilities (**b**) of pNIPAm/βCD1.62N and pNIPAm/βCD1.62N/PEG microgels prepared at equal +/- molar ratios (Ada/CD = 0.3, C(AAc-) = 0.145 mM).

1.2.2 Estimation of surface PEG chains conformation

We also tried to estimate the conformation of PEG chains in sterically stabilized pNIPAm/βCD1.62N/PEG microgel particles. De Gennes proposed the concept which distinguishes two main conformations of polymer chains anchored to surfaces, based on the grafting density: mushroom-like state and brush-like states.[38, 39] If the grafting density is low, the PEG chains are likely to be found in the mushroom-like conformation, when the polymer is

spread around the anchoring site into a compact structure. In contrast, if the grafting density is high, the chains are forced to be stretched out perpendicularly from the surface into a brush-like conformation. Quantitative criterion used to determine the conformational regime is based on the relation between the average distance between two adjacent PEG chains (D) and their Flory dimension (R_F). The chains are considered to be in the brush-like regime when $D < R_F$, whereas the polymer folds into a mushroom-like conformation when $D > R_F$, and intermediate structures are observed at $D \sim R_F$.

The Flory dimension of 5000 g/mole PEG in a good solvent (water) is given as:

$$R_F = b \cdot N^{0.6} = 0.35\ nm \cdot 114^{0.6} = 6.0\ nm \qquad \textbf{(IV.1)}$$

with $b = 0.35\ nm$ being the persistence length of the PEG monomer[39] and N corresponding to the number of monomers in the polymer chain.

The distance between the adjacent PEG chains on the surface of neutrally charged microgels may be estimated based on the set of known parameters, i.e. the hydrodynamic size of the particles (D_h= 270 nm), their molecular mass (M_w ~ 10^8 g·mole^{-1}), surface concentration of negative charges (C(-) = 0.145 mM), weight concentration of the microgels ($C_{\mu gel} = 0.145\ mM \cdot 0.4\ g \cdot L^{-1} = 0.058\ g \cdot L^{-1}$, see **Table IV.1**) and the Ada/CD molar ratio used (Ada/CD = 0.3).

Altogether it allows estimating the number of Ada groups and further – from the relation between the DS(Ada) and DS(PEG) in DT40-28GP-10Ada-18PEG, – the number of PEG chains per individual microgel particle. The latter was found to be $8.3 \cdot 10^4$ chains per particle. Further, assuming that each PEG chain occupies a square cell on the surface of microgels with the surface area A_{sph} =$2.3 \cdot 10^{-13}$ m^2, one can calculate the surface area corresponding to such a cell: $a = \frac{A_{sph}}{8.3 \cdot 10^4} = 2.8 \cdot 10^{-18}$ m^2 or 2.8 nm^2. Finally, one can derive the distance between two adjacent PEG chains (D) as the length of the side of the square cell as schematically illustrated in **Figure IV.16**. Thus obtained D (1.7 nm) is significantly lower than the R_F of individual PEG chains, indicating the brush-like conformation of the latter. It explains partly the origin of the achieved steric stabilization.

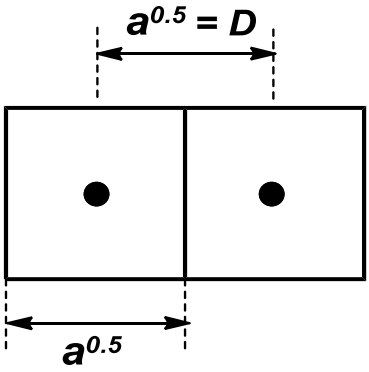

Figure IV.16: Schematic illustration of the approach used to estimate the distance (D) between the adjacent PEG chains on the surface of stabilized pNIPAm/βCD1.62N/PEG microgels. Black dots represent the anchor points of PEG grafts; a stands for the area of the square cell occupied by a PEG graft.

Since coating is formed *via* electrostatic interactions of pβCDN+ with pH-sensitive pAAc- groups, stability of pNIPAm/βCD1.62N/PEG in acidic environment was tested (**Figure IV.17a**). In freshly prepared complexes of pNIPAm-g-pAAc with different amounts of pβCDN+/DT40-28GP-10Ada-18PEG precursor (Ada/CD = 0.3) the pH was adjusted from 7 to 2 by addition of HCl. Microgels coated with lower amounts of pβCDN+/DT40-28GP-10Ada-18PEG (up to C(+) = 0.04mM, +/- = 0.28) undergo fast aggregation at pH 2 due to the protonation of AAc- groups non-bound with N+. At higher +/- ratios, the particles are stable even at pH 2 and their sizes are almost insensitive to the C(+) concentration. This could be due to the strong interpolyelectrolyte binding and PEG-corona, preventing the pAAc shell from being protonated. One might assume that at +/- < 0.28 the coating has a “patchy” character with significant regions of unprotected AAc- groups on the surface. Being protonated at pH 2, AAc should induce the interparticle aggregation through multiple H-bonding.

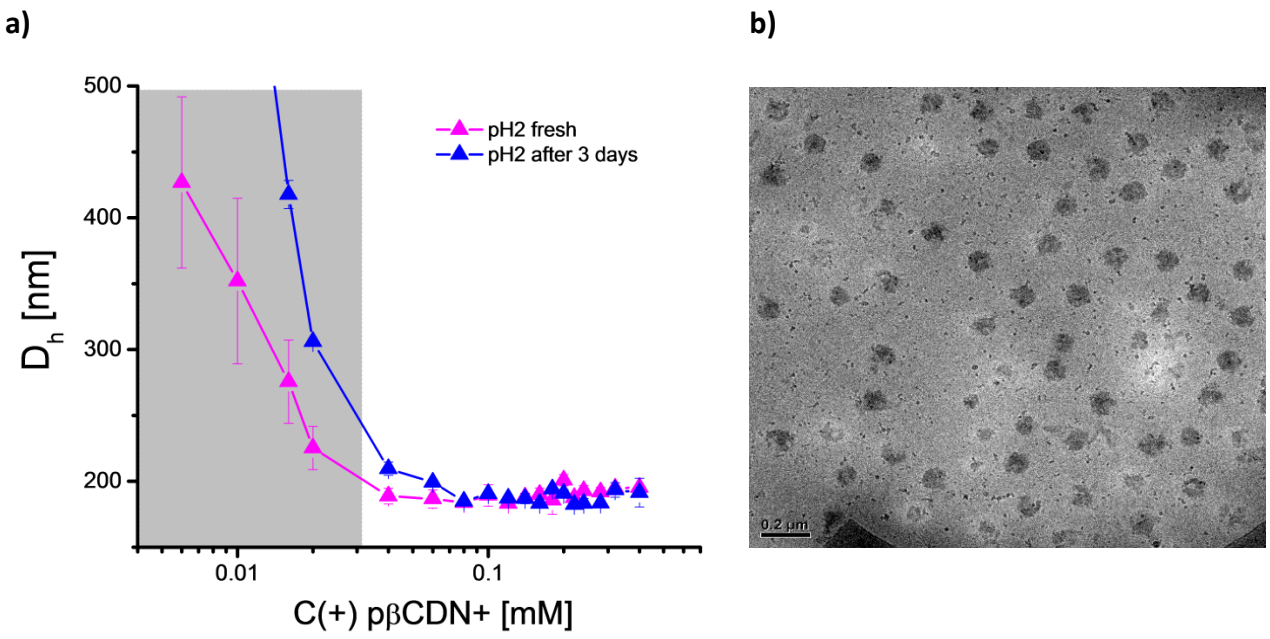

Figure IV.17: a) Colloidal stability of pNIPAm/βCD1.62N/PEG microgels in acidic environment as a function of coverage with pβCDN+/DT40-28GP-10Ada-18PEG precursor (pH = 2, Ada/CD = 0.3, C(AAc-) = 0.145 mM); **b)** Cryo-TEM image of pNIPAm/βCD1.62N/PEG frozen at pH = 2 (+/- = 1.1, Ada/CD = 0.3).

The time evolution of D_h of the microgels at pH 2 was studied. Even after 3 days no aggregation had occurred for the samples with +/- > 0.28, although a slight increase in D_h was observed in the 0.28 < +/- < 0.55 range (blue curve in **Figure IV.17a**). Cryo-TEM image of sterically stabilized neutral microgels (C(+) = 0.16 mM, +/- = 1.1) at pH 2 also showed the presence of well-defined non-aggregated particles (**Figure IV.17b**).

1.3 Thermoresponsive properties of pNIPAm/βCD1.62N and pNIPAm/βCD1.62N/PEG hierarchical microgels

In the next step we studied thermal behavior of CD-coated pNIPAm/βCD1.62N and sterically stabilized pNIPAm/βCD1.62N/PEG microgels by DLS at pH 7. The hydrodynamic diameters were measured as a function of temperature in the range from 25 to 62°C (**Figure IV.18**). The temperature was changed by 1.3-2.1°C steps and the samples were allowed to equilibrate until stable particle sizes were observed at each temperature (in average ca. 40 min per step).

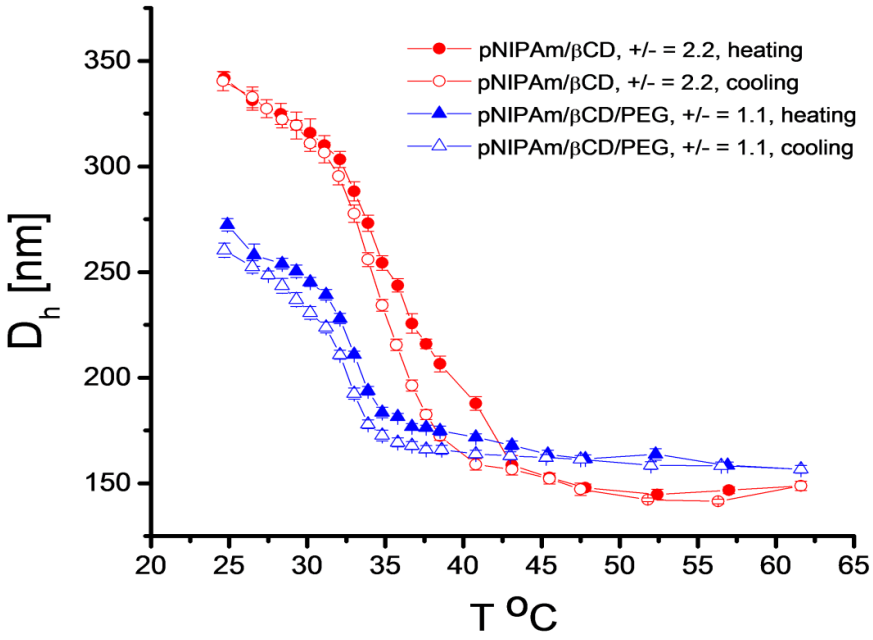

Figure IV.18: Hydrodynamic diameters as a function of temperature for positively overcharged pNIPAm/βCD1.62N (+/- = 2.2) and neutral, sterically stabilized pNIPAm/βCD1.62N/PEG (+/- = 1.10) microgels recorded at pH 7; the pH of the stock pNIPAm-g-pAAc solution was set with 0.1M NaOH. C(AAc-) = 0.145 mM.

Both overcharged pNIPAm/βCD1.62N (+/- = 2.2) and neutral pNIPAm/βCD1.62N/PEG (+/- = 1.10) experience well-defined reversible VPT, indicating the preservation of the pNIPAm cores thermoresponsive properties in their structure. Heating-cooling cycle didn't affect the E_{mob} value of neither pNIPAm/βCD1.62N nor pNIPAm/βCD1.62N/PEG, thereby confirming stability of the coatings. Interestingly, the VPT of pNIPAm/βCD1.62N/PEG occurs at lower temperature than that of pNIPAm/βCD1.62N (33.5°C vs. 35.9°C respectively determined from the heating curves). It is known that the lower critical solution temperature (LCST) of pNIPAm may be shifted to lower or higher values by copolymerizing it with more hydrophobic or hydrophilic co-monomers respectively.[40] Furthermore, when NIPAm is copolymerized with acid or basic co-monomers, such as acrylic acid, the overall hydrophilicity and LCST of the polymers can be tuned by adjusting pH of the medium or by counter-ion binding. The reported in **Figure IV.18** results are in good agreement with this. Indeed, at +/- = 1.1 due to the charge compensation the apparent hydrophilicity pNIPAm/βCD1.62N/PEG should be lower than that of overcharged pNIPAm/βCD1.62N at +/- = 2.2, leading to a decrease in VPT of the former.

2. Hierarchical hydrogels based on pNIPAm/βCDN through host-guest interactions

2.1 Hydrogels based on host-guest interactions between pβCD1.62N+ and DT110Ada

In the next step we aimed to exploit the superficial βCD groups in pNIPAm/βCDN and prepare a DX microgels network cross-linked via host-guest interactions. As it was recently demonstrated by Himmelein et al. on the example of βCD vesicles, the self-assembly of the latter into a supramolecular hydrogel can be directed by addition of Ada-modified hydroxyethylcellulose.[22] Being inspired by the success of their strategy, herein we will use Ada-substituted dextrans (DT-Ada) as multivalent cross-linkers, which are expected to establish interparticle connections between the microgels through the βCD-Ada inclusion complexation (**Figure IV.19**).

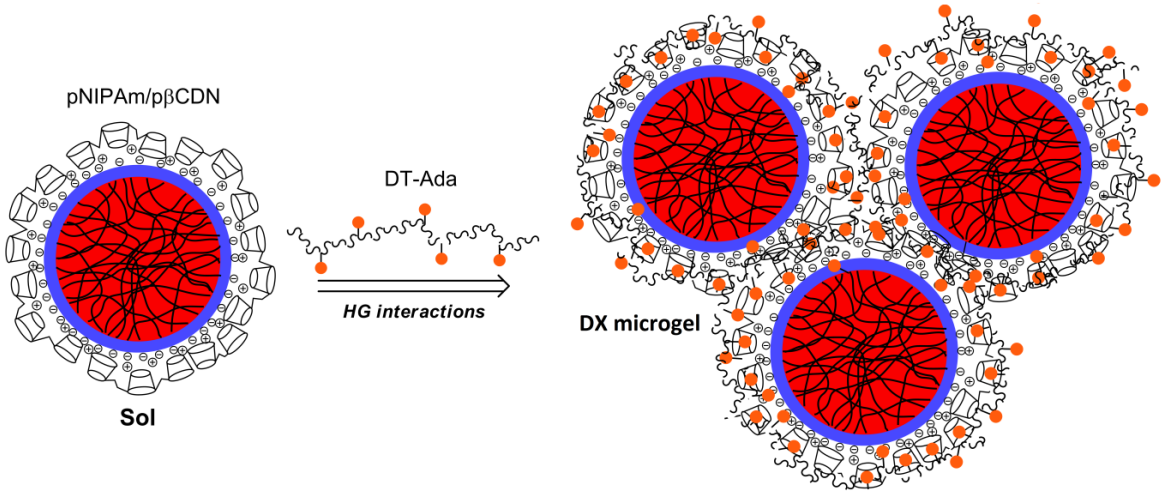

Figure IV.19: Schematic illustration of the strategy for host-guest driven cross-linking of pβCDN+-coated microgels into a DX microgel 3D network.

At first we attempted a direct gelation approach, i.e. by mixing positively overcharged pNIPAm/βCD1.62N at +/- = 2 with DT110-Ada3 (**Table IV.1**). However, an issue with pNIPAm/βCD1.62N colloidal stability at higher weight concentrations was encountered. Typically, precipitation of the microgels was observed at C(AAc-) > 8 mM (3.2 g·L^{-1}) and C(+) > 16 mM (19.2 g·L^{-1}) corresponding to a combined weight concentration of 2.25 wt% and, thus, limiting the possibility of direct hydrogel preparation.

To circumvent this limitation, an indirect gelation approach was used. In the first step, stable pNIPAm/βCD1.62N complexes at lower concentrations (typically C(AAc-) = 6 mM, C(+) = 4.8-12 mM) were prepared and mixed with DT110Ada at stoichiometrical Ada/CD molar ratios. The resulting mixtures were concentrated in 2.3-3.5 times under vacuum at 50°C. After cooling down to room temperature and reswelling of pNIPAm cores, transparent hydrogels with ~10-11 wt% dry weight of the components were formed. The characteristics of so prepared samples are given in **Table IV.3**. Two conclusions could be drawn from these data: 1) to avoid phase separation during concentrating one should use well-overcharged pNIPAm/βCD1.62N with +/- molar ratios far enough from the stoichiometrical ratio; 2) 11 wt% by dry weight of the components seems to be required to obtain stable non-flowing hydrogels. Lower than 0.8 +/- ratios were not tested since in this case the host polymer coverage of the particle surface is not full and the resulting microgels are less prone to be cross-linked *via* host-guest interactions.

The necessity for higher +/- molar ratios entails relatively low contributions of microgels (0.5-0.6 wt%) to the total dry weight concentration (11.6-11.9 wt%) in successful gel samples (**Table IV.3**). According to Senff and Richtering, rheological and phase behavior of BA-crosslinked pNIPAm microgel suspensions are strongly dependent of their effective volume fraction (ϕ_{ef}).[41] For instance, by measuring zero shear viscosity of microgels at different temperatures below LCST as a function of ϕ_{ef}, they observed a sharp increase in viscosity at $\phi_{ef} > 0.5$.[42] The phenomenon was ascribed to the microgel soft spheres being close to contact and interacting with each other at these concentration conditions. Hence, it was important to estimate the ϕ_{ef} of pNIPAm-g-pAAc microgels at $C_{\mu gel}$ = 0.6 wt% (6 g·L^{-1}) in order to understand the nature of the obtained hydrogels (*G3*, *G4*).

The molar weight of the used microgels $M_{\mu gel} \sim 10^8$ g·mole^{-1} was determined by static light scattering. From this, the number of particles per L, N_p, may be calculated as:

$$N_p = \frac{C_{\mu gel}}{M_{\mu gel}} \cdot N_A = 3.6 \cdot 10^{16}\ particles \cdot L^{-1}\ (\text{or } 3.6 \cdot 10^{19}\ particles \cdot m^{-3}) \qquad (\textbf{IV.2})$$

where N_A is the Avogadro number and $C_{\mu gel}$ is the concentration of microgels in g·L^{-1}. At +/- = 2 (molar ratio used in *G3* and *G4* samples) the R_h = 150 nm (1.5·10^{-7}m) for host polymer-coated microgels as determined by DLS. Hence, effective hydrodynamic volume of one particle of spherical shape is:

$$V_h = 4\pi R_h^3/3 = 1.4 \cdot 10^{-20} m^3 \quad \textbf{(IV.3)}$$

From this, the ϕ_{ef} can be estimated as:

$$\phi_{ef} = V_h \cdot N_p = 0.5 \quad \textbf{(IV.4)}$$

which coincides exactly with the threshold value required for the close contact of the microgels mentioned above.[42] From this one can assume that for *G3* and *G4* samples, the hydrogels exhibit structures rather similar to that of DX microgels than simply microgel-reinforced hydrogels.[23]

Table IV.3. Molar ratios and weight concentrations of the components in supramolecular gel samples prepared from pβCD1.62N+ and DT110Ada guest polymers

Components - *sample code*	**+/-**	**Ada/CD**	**C(microgel), wt%**	**C(pβCDN+), wt%**	**C(DT110Ada), wt%**	**C_{tot}, wt%**	**Observation**
pNIPAm/βCD1.62N/ DT110Ada3 - *G1*	0.8	1.3	0.6	1.4	3.4	5.4	phase separation
pNIPAm/βCD1.62N/ DT110Ada3 - *G2*	1.5	1.3	0.6	2.6	6.3	9.4	viscous liquid
pNIPAm/βCD1.62N/ DT110Ada3 - *G3*	2.0	1.3	0.5	3.3	8.1	11.9	gel
pNIPAm/βCD1.62N/ DT110Ada4 - *G4*	2.0	1.3	0.6	3.8	7.1	11.6	gel

2.1.1 Rheological properties

The viscoelastic properties of the *G3- G4* hydrogels were studied by oscillatory rheological measurements, which are described in greater detail in the Experimental section. Frequency sweep measurements of storage G' and loss G" moduli are shown in **Figure IV.20,a-c**. The G' and G" values prove to be frequency-dependent in all cases, which was previously reported as a typical behavior for physical gels.[43, 44, 45] At higher frequencies and shorter observation times materials show gel character with the elastic component G' dominating the viscous component G". At lower frequencies the system starts to behave as a viscous liquid with G" > G'. In a number of earlier studies on host-guest polymeric hydrogels such behavior is explained by

weakness and reversible character of the host-guest links, which are being broken and re-formed under applied stress.[44, 46, 47]

The finite lifetimes of the interpolymer cross-links are due to the fluctuations in the relative kinetic energy of the interacting Ada- and βCD-groups. These lifetimes (τ_{co}), also known as relaxation times, may be obtained as the inverse of the angular frequency ω_{co} ($\omega_{co}[rad \cdot s^{-1}] = 2\pi \cdot f_{co}[Hz]$) of the cross-over point of G' and G" in frequency sweeps:

$$\tau_{co} = (2\pi \cdot f_{co})^{-1} \quad \textbf{(IV.5)}$$

In our case the cross-over frequency ($f_{co}[Hz]$) can be correlated with the DX microgel network strength. Indeed, the *G2* sample which behaves as a viscous liquid (**Figure IV.20,a**) has the highest f_{co} value of 12.6 Hz (τ_{co}= 0.013 s), whereas in the case of *G3* which behaves as strong non-flowing gel the f_{co} is shifted down to 1.7 Hz (τ_{co}= 0.094 s) (**Figure IV.20,b**). The strength of hydrogel structures depending on their composition was also studied by strain-amplitude sweep performed at f= 10 Hz (**Figure IV.20,d**). The plateau G' moduli vary from 232 Pa for *G2* (+/- = 1.5, C_{tot} = 9.4 wt%), behaving as a viscous liquid, to 3257 Pa for *G3* hydrogel (+/- = 2.0, C_{tot} = 11.9 wt%). Similar values of elastic storage modulus were found for recently described cyclodextrin-based hierarchical hydrogels such as βCD-coated quantum dots cross-linked with azobenzene-modified thermoresponsive copolymers (G' = 2000 Pa, C_{tot} = 12.5 wt%)[20] or βCD vesicles interconnected with Ada-modified cellulose polymer (G' = 200-400 Pa, C_{tot} = 2-3 wt%)[22].

Interestingly, the *G4* hydrogel differs from *G3* only by higher DS(Ada) of the used DT110Ada macromolecular cross-linker (6.2 vs. 4.7 mol.% respectively), whereas the +/- ratio, Ada/CD ratio and total weight concentration of the components are equal. However, *G4* has significantly lower compared to *G3* gel network strength as evidenced from f_{co} and G'(10 Hz) values (**Figure IV.20,b-d**). One might expect the opposite effect for more highly substituted DT110Ada4, which is intended to provide higher cross-linking density between the microgels. At the same time, Wintgens et al. found that higher DS(alkyl) leads to associative phase separation instead of homogeneous 3D-network formation in the interaction between alkyl-substituted dextrans and neutral pβCD.[45] Increased number of hydrophobic groups per chain is thought to induce larger cooperativity of the interpolymer interaction. In the case of pNIPAm/βCD1.62N/DT110Ada4 system (*G4*) the latter might result in DT110Ada4 being tightly attached to the pβCD1.62N+-

shell of a single microgel, rather than connecting the neighboring particles. Both *G3* and *G4* exhibit quite high strain resistance and maintain their structure up to $\gamma \sim 100\%$ (**Figure IV.20,d**).

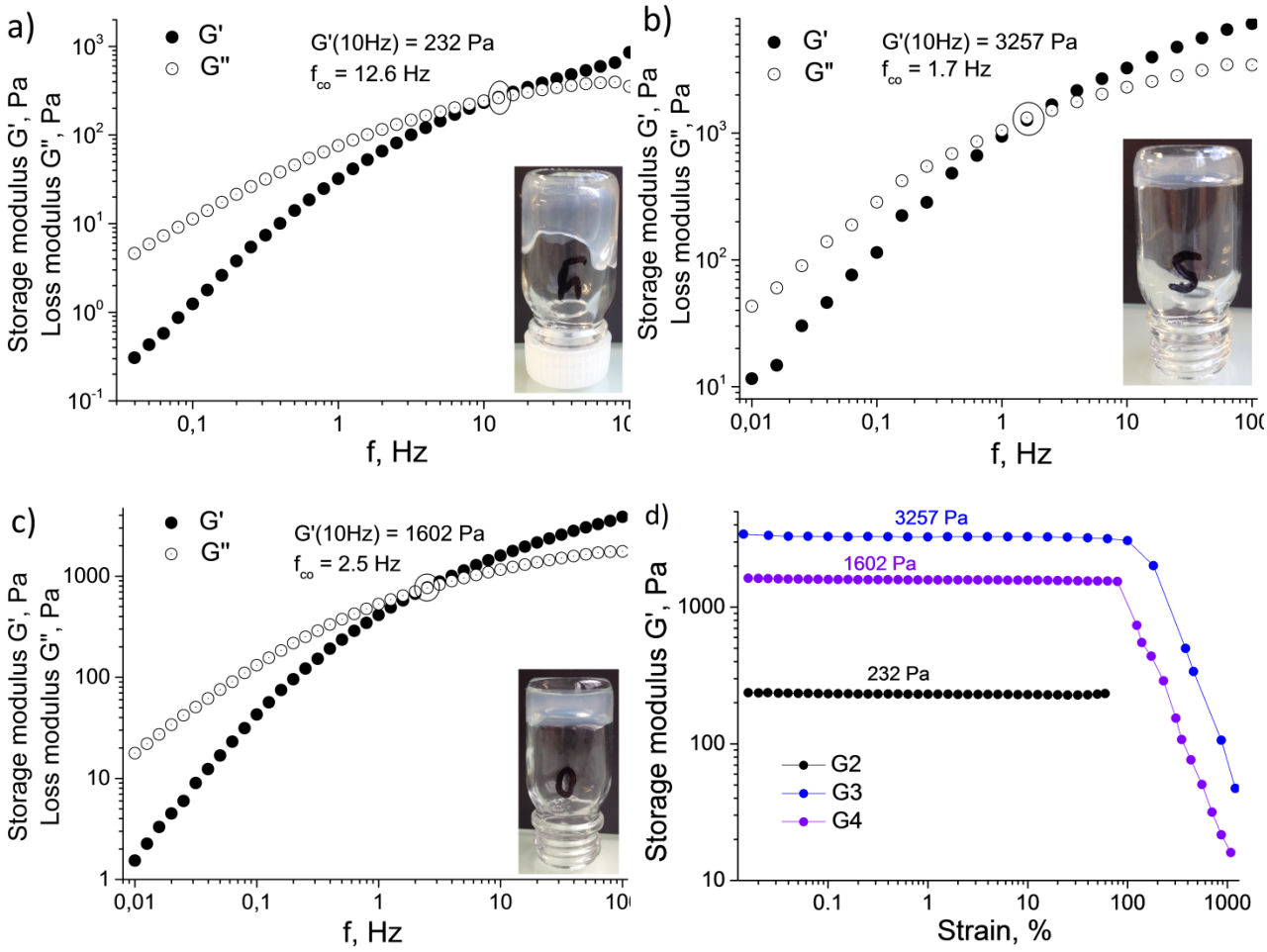

Figure IV.20: Oscillatory rheological measurements of hydrogel samples with varying +/- molar ratios and DS(Ada) of the guest polymer cross-linker. Storage G' and loss G" moduli obtained from frequency sweep performed at 0.1% strain for (**Table IV.2**): **a)** *G2*, **b)** *G3*, **c)** *G4*. Storage modulus G' (**d**) of *G2*, *G3*, and *G4* samples obtained from amplitude-strain sweep performed at f = 10 Hz. All measurements were performed at 25°C.

In order to confirm that the 3D-network is actually formed through the host-guest interactions two control samples containing no guest polymer cross-linker were prepared (**Table IV.4**). The concentration of the *G5* sample composed of pβCDN+ -coated microgels to 11.7 wt% expectedly resulted in a loss of colloidal stability and phase separation.

Uniform pNIPAm microgel dispersions with concentrations corresponding to close-packing (~ 5 wt%) were reported to undergo sol-gel transition at temperatures below LCST.[48] Uncoated

pNIPAm-g-pAAc microgels don't form gels even at concentrations as high as 10.1 wt% (*G6* sample). It should be related to the difficulty of achieving the close-packing due to the repulsive forces between the negatively charged particles.

Table IV.4. Characteristics of the control samples containing no DT110Ada guest polymer cross-linker.

Components - *sample code*	**+/-**	**C(microgel), wt%**	**C(pβCDN+), wt%**	**C(DT110Ada), wt%**	**C_{tot}, wt%**	**Observation**
pNIPAm/βCD1.62N - *G5*	2.0	2.7	16.0	0	11.7	phase separation
pNIPAm - *G6*	-	10.1	0	0	10.1	liquid

The frequency sweep data for the *G* samples were attempted to fit to the Maxwell model. This basic viscoelasticity model was widely used for describing the behavior of entangled physically bonded polymer networks[49, 50] and polymeric host-guest hydrogels.[47] The Maxwell model implies that storage G' and loss G'' moduli of a viscoelastic body vary as a function of the strain angular frequency ω according to the following equations:

$$G'(\omega) = \frac{G_0(\omega\tau)^2}{1+(\omega\tau)^2} \quad \textbf{(IV.6)}$$

$$G''(\omega) = \frac{G_0\omega\tau}{1+(\omega\tau)^2} \quad \textbf{(IV.7)}$$

where ω is the angular frequency [rad·s^{-1}], τ – is the relaxation time and G_0 is the G' at high frequencies where it typically reaches a stable plateau value. From the equations above it also follows that $G'/G'' = \omega\tau$. In our case τ was obtained from the G' and G'' cross-over frequency value and was set as a fixed parameter during the fitting. Since the G' didn't reach the plateau in the available range of angular frequencies, G_0 was set as a free optimized parameter. Despite the evidenced by the frequency sweep data viscoelastic character of the *G* samples (**Figure IV.20**), rather poor fits to the Maxwell model were obtained. An example of such fits for the *G3* sample is illustrated in **Figure IV.21**. Only the loss modulus G'' measured data for low frequencies (0.1-1.6 rad·s^{-1}) is somewhat coherent with corresponding fit (dashed line).

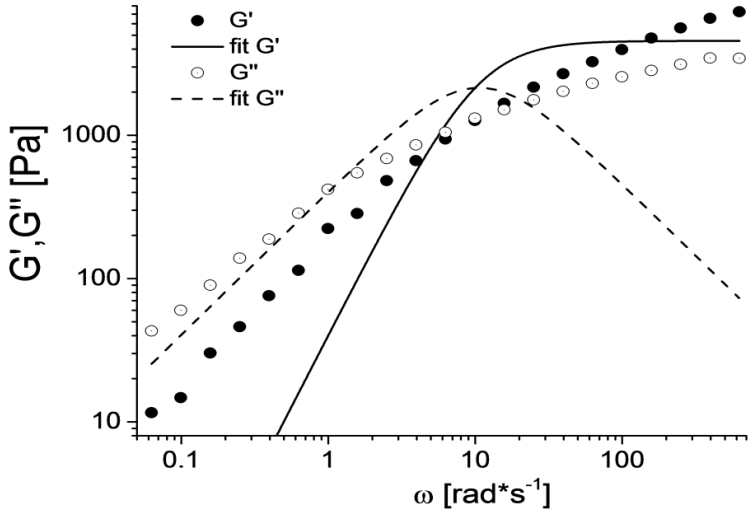

Figure IV.21: Storage G' and loss G" moduli as a function of angular frequency ω for the *G3* hydrogel sample and non-linear fits of G' (solid line) and G" (dashed line) to the Maxwell model performed based on the equations **IV.6** and **IV.7** respectively (25°C, γ = 0.1%).

Failure of the fitting might be due to the simplistic character of the Maxwell model, which is appropriate for the description of viscoelastic materials with a single and well-defined relaxation time τ. For instance, van de Manakker et al. obtained relatively good fits for the host-guest hydrogel networks composed of linear and 4-arm star PEG polymers end-functionalized with βCD- and cholesterol-groups.[47] However, they found that the fitting to Maxwell model was no longer possible for more structurally complex hydrogels composed of 8-arm PEGs with the same end-functionalities. They ascribed it to the presence of broader range of relaxation mechanisms with different relaxation times involved in the stress relaxation in the latter case. We assume that the same argumentation holds for the rather structurally complex pNIPAm/βCD1.62N/DT110Ada3 doubly cross-linked microgels.

Since the obtained hydrogels are composed of cross-linked thermoresponsive pNIPAm beads, their mechanical properties are expected to be temperature-dependent. The evolution of storage G' and loss G" moduli of *G3* sample as a function of temperature was studied in the range of 25-60°C (**Figure IV.22,a**).

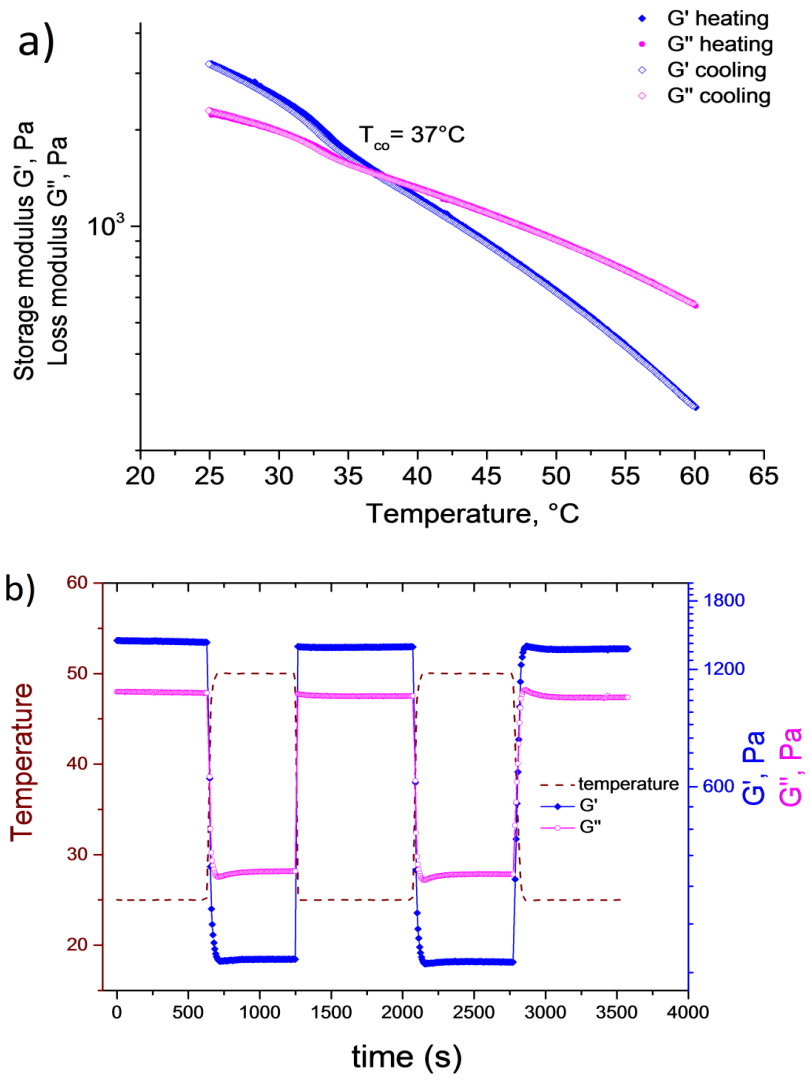

Figure IV.22: Oscillatory rheological measurements of the pNIPAm/βCD1.62N/DT110Ada3-*G3* hydrogel temperature-induced phase transitions: **a)** G', G" evolution under temperature ramps (temperature change rate = 2°C/min, f = 10 Hz, γ = 0.1%); **b)** dynamics of G', G" recovery under instantaneous switching of temperature between 25 and 50°C (f = 10 Hz, γ = 0.1%).

Both storage and elastic moduli decrease with temperature; however, the decrease of G' occurs at higher rate and upon reaching 37°C (T_{co}) G" starts exceeding G', accompanied by gel-to-sol phase transition. The transition temperature is in a good agreement with the VPT temperature of pNIPAm/βCD1.62N microgels found by thermo-DLS (35.9°C, **Figure IV.18**). The gradual cooling back from 60 to 25°C leads to the full restoration of the initial moduli values; no hysteresis was observed neither for G' nor for G".

In the next step we wanted to figure out whether the mechanical properties of *G3* can be preserved in the course of several heating-cooling cycles. The temperature was raised to 50°C instantaneously, maintained constant for 10 min and lowered back to 25°C straight away (**Figure IV.22,b**). The cycle was repeated twice and the initial G', G" values were fully restored proving the reversibility of the temperature-induced phase transition. Remarkably, the restoration of the mechanical properties occurs within a few seconds, showing almost no retardation with respect to the temperature change.

2.2 Hydrogels based on host-guest interactions between pβCD3.24N+ and DT500Ada

Analyzing the composition of the successful hydrogel samples prepared from pβCD1.62N+ and DT110Ada (**Table IV.3**), it becomes obvious that, despite their volume fraction being ~ 0.5, the pNIPAm-g-pAAc microgels contribution to the total weight concentration of the samples is fairly low (4.2 and 5.2% for *G3* and *G4* respectively). Hence, the properties of thermoresponsive microgel "bricks" in such gels are likely to be dominated by the properties of the host-guest polymers "mortar". One way to increase the weight contribution from microgels while using the same +/- and Ada/CD molar ratios during the formulation of the samples consists in increasing the positive charge density of the host polymers.

As showed in **Figure IV.12** pβCD3.24N+ with doubled number of N+ per CD cavity work as efficiently as pβCD1.62N+ for coating and electrostatic stabilization of pNIPAm-g-pAAc. Thus, in the next step we tried to cross-link pβCD3.24N+-coated microgels (+/- = 2.0) with DT110Ada3. It turned out that pNIPAm/βCD3.24N/DT110Ada3 continue to remain in a viscous liquid state even at C_{tot} as high as 14.8 wt%. Decreased host-guest cross-linking efficiency in this case should be related to a lower concentration of βCDs in the external shell of the overcharged pNIPAm/βCD3.24N particles.

In an attempt to overcome this problem we used a guest polymer with an increased molecular weight (DT500Ada2 in **Table IV.1**) as a cross-linker. This approach proved successful: a stable transparent gel was formed at C_{tot} = 11.0 wt% (*E1* in **Table IV.5**). Positive impact of higher M_w of the guest polymer is apparently related to the higher number of Ada groups attached to a single polymer chain in this case (200 vs. 32 Ada per chain for DT500Ada2 and DT110Ada3 respectively). As a result, a DT500Ada2 molecule has a potential to form a higher number of host-guest cross-links between the neighboring microgel particles.

Table IV.5. Molar ratios and weight concentrations of the components in supramolecular gel samples prepared from pβCD3.24N+ and DT500Ada2 guest polymer; the *FR1* hydrogel was prepared through a freeze-drying pathway (described in the sub-section 2.2.1)

Components - *sample code*	**+/-**	**Ada/CD**	**C(microgel), wt%**	**C(pβCDN+), wt%**	**C(DT500Ada), wt%**	**C_{tot}, wt%**	**Observation**
pNIPAm/βCD3.24N/ DT500Ada2 - *E1*	2.0	1.0	1.3	4.4	5.3	11.0	gel
βCD3.24N/ DT500Ada2 - *E2*	-	1.0	0	4.3	5.2	9.5	gel
pNIPAm/βCD3.24N/ DT500Ada2 – *FR1*	2.0	1.0	1.3	4.3	5.3	10.9	gel

2.2.1 Rheological properties

Frequency sweep rheological measurements (**Figure IV.23,a**) indicate that the interpolymer cross-links in *E1* have longer lifetimes than those in *G3* prepared from DT110Ada3 (f_{co}= 1.1 Hz, τ_{co}= 0.145 s) due to the increased cooperativity of the interactions. Furthermore, comparing to the *G3* hydrogel, the contribution from microgels to the C_{tot} is increased more than two times for *E1* – from 4.2 to 11.8%.

The gelation process was confirmed to be driven by the βCD-Ada inclusion complexation (**Table IV.4**). In order to understand the impact of microgels on the mechanical properties of the hydrogels a blank sample *E2*, containing only pβCD3.24N+ and DT500Ada2, was prepared, so that its C_{tot} was equal to the sum of C(pβCD3.24N+) and C(DT500Ada) in the *E1* hydrogel (**Table IV.5**). It forms a stable non-flowing hydrogel with reversible character at C_{tot} = 9.5 wt% (**Figure IV.23,b**). In a strain-amplitude sweep experiment the *E2* hydrogel reveals slightly lower G' plateau values comparing to *E1* (**Figure IV.23,d**)., which can be in part related to the higher total concentration of the latter. On the other hand, the extent of the linear viscoelastic region is significantly higher for microgel-free *E2*, i.e. the hydrogel maintains its structure up to 250% strain, while in the case of *E1* a breakdown is observed already at 100% strain. These results indicate that despite having a high volume fraction and being in close contact pNIPAm-g-pAAc microgels do not mechanically reinforce the resulting hydrogels network. Being highly swollen in water below the VPT temperature, they should behave rather as soft disruptive regions, i.e. the

volume of hydrogel occupied by microgels is depleted of host-guest cross-links constituting the 3D-network.

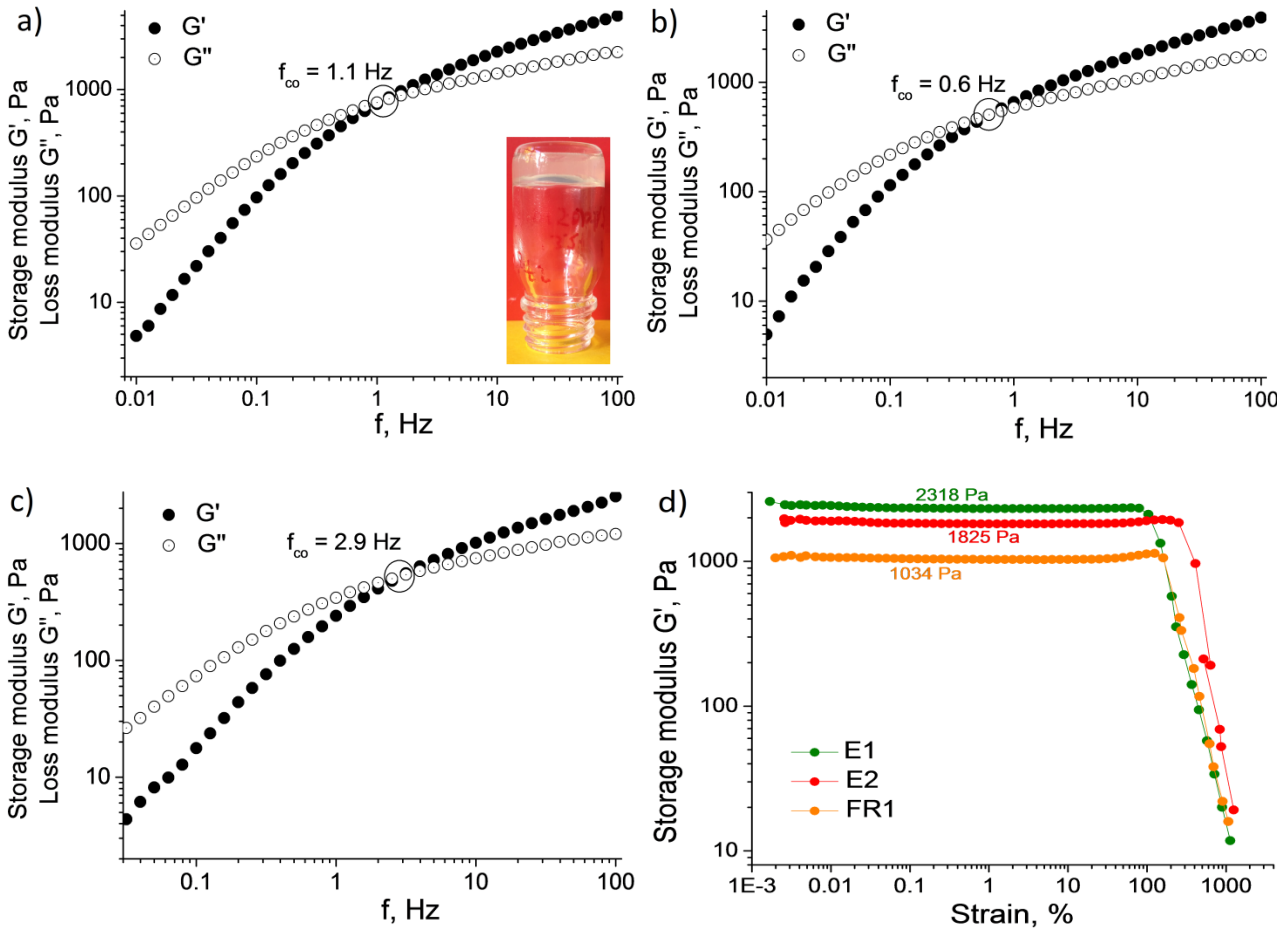

Figure IV.23: Oscillatory rheological measurements of hydrogels prepared using pβCD3.24N+ host and DT500Ada2 guest polymers. Storage G' and loss G" moduli obtained from frequency sweep performed at 0.1% strain for (**Table IV.4**): **a)** *E1*, **b)** *E2*, **c)** *FR1*. Storage modulus G' (**d**) of *E1*, *E2*, and *FR1* samples obtained from amplitude-strain sweep performed at f = 10 Hz. All measurements were performed at 25°C.

The behavior of G' and G" of the hydrogels at various temperatures was studied by heating-cooling cycles[44] in the range 25-60°C (**Figure IV.24**). Both microgel-containing *E1* and microgel-free *E2* exhibit thermoresponsiveness and gel-to-sol phase transition upon heating. However, the patterns of G', G" evolution, as well as the cross-over temperature T_{co}, differ significantly. The *E1* behaves in a way similar to that of its counterpart *G3* described in previous section (**Figure IV.22**), i.e. along with the gradual decrease of the moduli with increasing the temperature one observes an abrupt flexure in both storage and loss moduli curves at 33-34°C,

corresponding to the VPT of microgels (**Figure IV.24,a**). Also, *G3* and *E1* have close T_{co} values (37 and 41°C respectively). In the case of *E2* the moduli values decrease in a less steep way, which results in a significantly higher gel-to-sol transition temperature (T_{co} = 51°C, **Figure IV.24,a**). This is in a good agreement with the literature data for host-guest mediated polymer networks.[44] Given the enthalpy-driven nature of the βCD-Ada inclusion complexes, the number of cross-links gradually decreases as the temperature is raised.

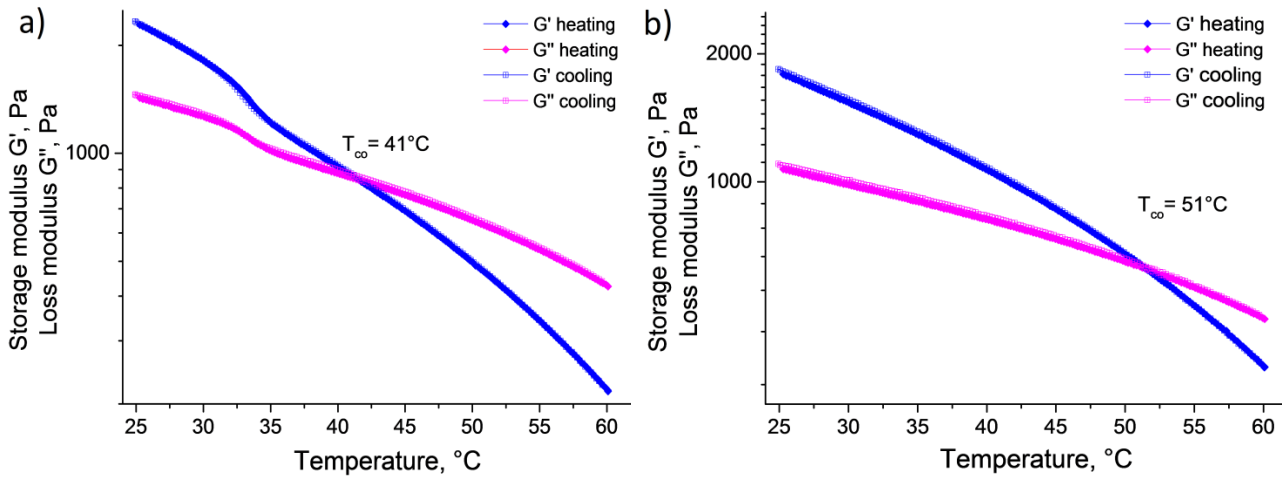

Figure IV.24: Evolution of storage G' and loss G" moduli under heating and cooling temperature ramps (temperature change rate = 2°C/min, f = 10 Hz, γ = 0.1%) for **a)** *E1* and **b)** *E2* hydrogel samples (**Table IV.4**).

The decrease of the gel-to-sol transition down to the physiological temperature range (37-41°C) due to the presence of pNIPAm-g-pAAc microgels opens up attractive prospects for their use in biomedical applications.

As it was mentioned above, for viscoelastic materials and according to the simplest model involving a single relaxation time τ, the following relationship holds: $G'/G'' = \omega\tau$. Thus, from the temperature sweep of storage G' and loss G" moduli recorded at a constant frequency (**Figure IV.22a, 24**), one can also calculate the relaxation times τ at different temperatures. Considering that the hydrogel network is formed primarily *via* host-guest interactions, the relaxation time of the network τ is a function of reaction (reversible breaking of the interchain host-guest links) rate constant, k. Since the considered reaction should be a first-order, k equals τ^{-1}. According to the Arrhenius equations, k and τ depend on the temperature in the following way:

$$k = A \cdot e^{-E_a/RT} \quad \textbf{(IV.8)}$$

$$\tau = A^{-1} \cdot e^{E_a/RT} \quad \textbf{(IV.9)}$$

where A is the pre-exponential factor, T[K] is the temperature and R= 8.3144598 J·mole^{-1}·K^{-1} is the universal gas constant. Hence, from the k or τ values at different temperatures one might estimate the activation energies E_a of the interchain links breaking by plotting $\ln k$ as a function of $1/T$, the slope of such a graph being equal to $-E_a/R$.[51]

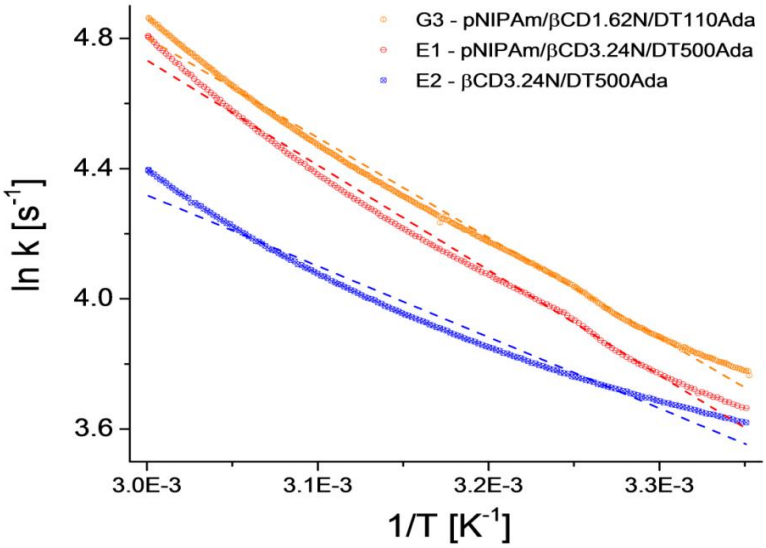

Figure IV.25: Arrhenius plots for the determination of E_a of the host-guest supramolecular hydrogels with different compositions (**Tables IV.3, IV.5**) constructed according to the **equation IV.4**. The linear fits of the curves are represented by dash lines.

As shown in **Figure IV.25**, the Arrhenius plots are not really linear. This is certainly a limit of the use of a Maxwell model with single relaxation time at each temperature. Given this, average activation energies have been extracted from the plots. The slopes are very similar for the microgel-containing hydrogels (*G3*, *E1*), whereas the curve for microgel-free hydrogel (*E1*) differs from them, showing a lower $-E_a/R$ value.

Table IV.6. Activation energies E_a of pNIPAm microgel-containing and microgel-free host-guest supramolecular hydrogels

Sample	Composition	C(pβCDN+DT-Ada), wt%	E_a, kJ·mole^{-1}
G3	pNIPAm/pβCD1.62N/DT110Ada	11.4	25.5
E1	pNIPAm/pβCD3.24N/DT500Ada	9.7	26.8
E2	pβCD3.24N/DT500Ada	9.5	18.1

The activation energies found for all three samples (**Table IV.6**) lie in the range reported in literature for reversible polymeric networks interconnected through βCD-Ada cross-links (18-41 kJ·mole^{-1}). [45, 52] As expected from the appearance of the Arrhenius plots, pNIPAm microgel-containing hydrogels (*G3*, *E1*) exhibit very close values of E_a, although they differ significantly in the sum of network forming host and guest polymers concentrations, C(pβCDN+DT-Ada) (**Table IV.6**). At the same time, the "blank" hydrogel sample *E2*, having the same as *E1* C(pβCDN+DT-Ada), exhibits a substantial drop of E_a, i.e. from 26 to 18 kJ·mole^{-1}. Such a change in the network breaking kinetic parameters wouldn't be expected in the case simple microgel-filled hydrogels, where the microgel particles are randomly dispersed without any chemical or strong physical bonding with the network and/or the other particles.[23] Indeed, in the latter case the microgels presence would act in a similar way as a decrease in network forming polymers concentration, without strongly affecting the k and E_a values. Thus, the obtained results might indicate that the pNIPAm-g-pAAc microgels embedded in the hydrogel preserve their pβCDN+ coating. The latter makes microgels firmly connected with the rest of the network and between each other through the combination of electrostatic and host-guest interactions. Furthermore, as showed by the ϕ_{ef} calculations, microgels are expected to be in close contact, thus indicating their DX microgels-like character.

2.2.1. Freeze-drying pathway for the preparation of pNIPAm/βCD3.24N/DT500Ada2 hydrogels

The hydrogel samples described so far were prepared by concentrating the mixtures of βCDN+ -coated microgels with guest polymers under vacuum at 55°C. Given the rather tedious character and not always good reproducibility of this procedure we were looking for an alternative indirect gelation approach.

A full analogue of the *E1* hydrogel in terms of the weight concentrations and molar ratios of the components was prepared using a freeze-drying pathway. Stable pNIPAm/βCD3.24N coated microgels at low concentration (C(AAc-) = 3 mM, C(+) = 6 mM) were freeze-dried and redissolved in DT500Ada2 solution in water (Ada/CD = 1). The strategy proved successful (*FR1* in **Table IV.4**). However, it should be noted that at equal C_{tot} the *FR1* hydrogel has a somewhat weaker mechanical properties comparing to *E1* (**Figure IV.19, c-d**). It may be related to aggregation between the relatively densely packed pNIPAm/βCD3.24N microgels in a freeze-dried state. Further, such aggregates might not be fully disrupted during the interaction with DT500Ada2 solution resulting in the lower strength of the gel network.

Conclusions

This study demonstrates the versatility of core-shell pNIPAm microgels non-covalently coated with βCD polymer as potential drug delivery vehicles and building blocks for hierarchically structured hydrogels with multi-responsiveness profile.

The microgels used are composed of crosslinked thermoresponsive pNIPAm core and shell with unrestricted composition, containing up to 100% w/v of pAAc in the form of non-crosslinked densely grafted chains. We have taken advantage of the negative surface charge of the microgels at pH 7 to coat them with positively charged pβCDN+ host polymers *via* electrostatic self-assembly. The overall charge of the resulting pNIPAm/βCDN microgels can be tuned from negative to positive and the βCD content in the shell at a fixed +/- ratio can be varied by simply using pβCDN+ with different quaternary ammonia N+ modification levels. Positively overcharged pNIPAm/βCDN suspensions were stable in water over long periods of time. However, the overall neutral microgels, which represent the highest interest for potential biomedical applications, proved to have poor colloidal stability. Thus, a pathway to remove this limitation relying on the host-guest chemistry of the pβCDN+ coating was proposed. Neutral pNIPAm/βCDN were successfully sterically stabilized with prepared by CuAAC bifunctionalized (PEG, Ada)-grafted dextrans. Both in the case of pNIPAm/βCDN and pNIPAm/βCDN/PEG microgels, a full preservation of temperature-triggered VPT of pNIPAm core was observed. The developed systems attractiveness for potential drug delivery applications is determined by three main factors: a) pNIPAm core for a temperature-induced release of hydrophobic actives

upon shrinking; b) βCD-containing shell intended to slow down the initial "burst release" phenomenon; c) hydrophilic PEG corona known for providing the nanoscale drug carriers with "stealth" properties and longer blood circulation times.

In the second part of this work we studied another way of exploiting the surface host-guest chemistry of pNIPAm/βCDN. It involves non-covalent crosslinking of individual microgels with Ada-modified dextrans to yield hierarchical 3D networks. Depending on the total weight concentrations and molar ratios of the components, we observed phase separation, formation of viscous liquids or formation of hydrogels. The elastic storage moduli of the hydrogels with C_{tot} of 10-11 wt% (G' = 1-3·10^3 Pa) are comparable with those reported for cyclodextrin-based supramolecular hydrogels with various architectures. Regarding the poor colloidal stability of pNIPAm/βCDN at high concentrations, the hydrogels can be formulated in two indirect ways: a) by concentrating the mixtures of starting components at lower than gelation point concentrations under vacuum at 55°C; b) by freeze-drying the pNIPAm/βCDN and their subsequent rehydration with a guest polymer solution.

The host-guest interactions prove to be at the origin of the gel formation as evidenced by the "blank" experiments with the samples non-containing microgels. However, the activation energies E_a of the network breaking are strongly influenced by the presence of pNIPAm-g-pAAc. Moreover, calculations of the effective volume fraction ϕ_{ef} of microgels show that the latter are expected to be at a close contact in the successful hydrogel samples. This indicates that the pβCDN+ coating is preserved and the structure of the hydrogels is close to that of doubly-crosslinked microgels. To the best of our knowledge, this is the first example of DX microgels non-covalently crosslinked *via* host-guest interactions. Furthermore, the hydrogels exhibit fully reversible temperature-induced gel-sol transition due to the synergetic effect between shrinking of the microgels and dissociation of βCD-Ada crosslinks at higher temperatures. Due to the presence of microgels the gel-sol transition temperature of pNIPAm/pβCDN/DT-Ada is significantly shifted down to the physiological temperature range (37-41°C) as compared to uniform pβCDN/DT-Ada host-guest hydrogels (51°C). It opens up attractive prospects of their potential use in biomedical applications.

Experimental section

Materials and reagents

Microgels composed of cross-linked poly(*N*-isopropylacrylamide) (pNIPAm) core and 100% poly(acrylic acid) (pAAc) shell were prepared using precipitation polymerization technique developed by Kardos et al. (Unpublished data). N-isopropylacrylamide (NIPAm), methylenbisacrylamide (BA), ammonium persulfate (APS), acrylic acid (AAc) and sodium dodecyl sulfate (SDS) were purchased from Sigma-Aldrich and used as received. All solutions were prepared in ultraclean Milli-Q water (total organic content = 4 ppb; resistivity = 18 mΩ.cm, filtered through a 0.2 μm membrane filter to remove particulate impurities).

In a typical polymerization procedure, calculated amounts of NIPAm together with BA cross-linker and SDS were dissolved in distilled water, introduced in a double-wall Pirex glass reactor and put under vigorous stirring.[1] To keep the temperature of the reaction mixture constant at 80°C, the outer shell of the reactor was connected to a thermostat and controlled temperature water was circulated in it. The reaction mixture was degassed by purging it with nitrogen for 60 min. Then, the reaction was initiated by adding an aqueous solution of APS to the reactor followed by 4h under vigorous stirring at 80°C. After reaching 95% conversion of the NIPAm monomer, AAc monomer was fed into the reaction mixture to form the shell consisting of 100% grafted pAAc chains. The final product, pNIPAm-g-100%pAAc microgels, was purified from unreacted monomers and polymeric byproducts by centrifugation (Hettich 220R centrifuge, 16 000 rpm), decantation, and redispersion. The centrifuged microgels were redispersed in Milli-Q water and the cycle was repeated up to 5 times. Purified microgels were characterized by DLS, UV/Vis spectroscopy and surface tension measurements.

Synthesis of "host" polymers, neutral epichlorhydrin-interconnected pβCD and positively charged pβCDN+, modified with quaternary ammonia, is described in the Experimental section of Chapter 3.[53, 54] Synthesis and binding properties of bifunctional (PEG, adamantane)-grafted dextrans (DT40-GP-Ada-PEG) are described in detail in Chapter 3.[37]

[1] As mentioned before, amounts of the reagents taken, as well as exact details on the synthetic procedure cannot be unveiled herein for confidentiality reasons (Unpublished data by Kardosh et al.)

Methods and instrumentation

Coated microgels preparation: *1. pNIPAm/βCDN core-shell microgels:* In a typical procedure 2 mL of pNIPAm-g-pAAc microgels solution at 0.145 or 0.29 mM of (-) charges were mixed with pbCDN+ solutions with increasing concentrations of (+) charges (V = 2mL). The mixing was performed for 2 minutes at 600 rpm and at room temperature (pH = 7.0). Sizes and E_{mob} of the resulting pNIPAm-g-pAAc/pβCDN+ complexes were monitored by DLS and electrophoretic mobility measurements respectively.

2. pNIPAm/βCDN/PEG sterically stabilized core-shell microgels: At the first stage, to determine the required conditions to sterically stabilize neutrally charged pNIPAm/βCDN microgels (C(AAc-) = 0.145 mM, C(+) = 0.16mM), precursor host-guest supramolecular precursors between pbCDN+ and PEGylated guest polymer, DT40-28GP-10Ada-18PEG, were formed by vigorous mixing of aqueous solutions of individual polymers for 2 min at different Ada/CD molar ratios (pH 7). Typically, 0.54 ml of pβCD1.62N+ stock solution (C(+) = 1mM) were mixed with various volumes of DT40-28GP-10Ada-18PEG stock solution in water (C(Ada) = 0.78 mM). The volume was adjusted to 1.5 mL with water and the precursor solutions were left under stirring for 3 min followed by addition of 1.5 mL of pNIPAm-g-pAAc solution with C(AAc-) = 0.29 mM. Then, increasing amounts of a βCDN/PEG precursor stock solution with Ada/CD = 0.3, found to be appropriate for efficient sterical stabilization, were mixed with microgels at C(AAc-) = 0.29 mM to investigate the impact of non-covalent PEGylation on the whole range of +/- molar ratios. The resulting pNIPAm/βCDN/PEG particles were characterized by DLS and electrophoretic mobility measurements.

Dynamic light scattering: Particle size and polydispersity were determined by DLS. The measurements were performed with a Brookhaven Instruments device, which consists of a BI-200SM goniometer and a BI-9000AT digital autocorrelator. An Argon-ion laser, Omnichrome, model 543AP, was used as a light source. The laser was used at a wavelength of 488.0 nm and emitted vertically polarized light. The autocorrelator was set in a "multi τ" mode; i.e., the time axis was logarithmically spaced to span the required correlation time range. The autocorrelation functions were measured at a detection angle of 90° with a 100 µm pinhole size. The obtained autocorrelation functions were then analyzed by a second-order cumulant and the CONTIN methods. The extracted diffusion coefficients D data were then converted into hydrodynamic

diameters D_h using Stokes-Einstein equation (**Equation II.5** in the Experimental section of Chapter 2).

Zeta potential: A Zetasizer Nano ZS from Malvern Instruments was used to measure the electrophoretic mobility of pNIPAm-g-pAAc/pβCD and pNIPAm-g-pAAc/pβCD/DT40-GP-Ada-PEG complexes. The instrument uses a combination of laser Doppler velocimetry and phase analysis light scattering (PALS) in a technique called M3-PALS. Prior to the measurements the instrument was always tested with Malvern Zeta Potential Transfer Standard. All the measurements were performed at 25°C. The standard error in the values of the electrophoretic mobility was found to be around 10%. The measurements were performed at well-defined ionic strengths of $1 \cdot 10^{-3}$M adjusted by NaCl solution. The electrophoretic mobility of non-modified pNIPAm-g-100%pAAc was found to be ca. -2.75 $m^2 \cdot s^{-1} \cdot V^{-1}$ with slight variations depending on the weight concentrations of the sample.

Determination of AAc (-) charges concentration by titration with CTAB: Series of microgels with the estimated concentrations of AAc (-)-charges of 0.0125mM, 0.05mM , 0.1mM were titrated with CTAB solution while recording the E_{mob} changes. The concentration of CTAB needed to neutralize the microgels (C_0 where $E_{mob} = 0$) was determined from the titration curves (**Figure IV.26**). Assumption was made that non-bound amount of CTAB was constant in all titration experiments. If this holds, the increase in C_0 when going from a lower to a higher microgel concentration corresponds exclusively to the increase of bound amount of CTAB. In **Figure IV.26** B stands for bound amount of CTAB required to reach $E_{mob} = 0$ for the lowest estimated AAc (-)-charges concentration. The B equals to actual concentration of AAc (-) aimed to be found. This value cannot be determined directly. However, the difference between $C_0(0.05)$ and $C_0(0.0125)$ should be equal to $3B$, the former solutions being 4 times more concentrated. Following the same logic, the difference between the $C_0(0.1)$ and $C_0(0.05)$ should be equal to $4B$. From this one can derive the B value.

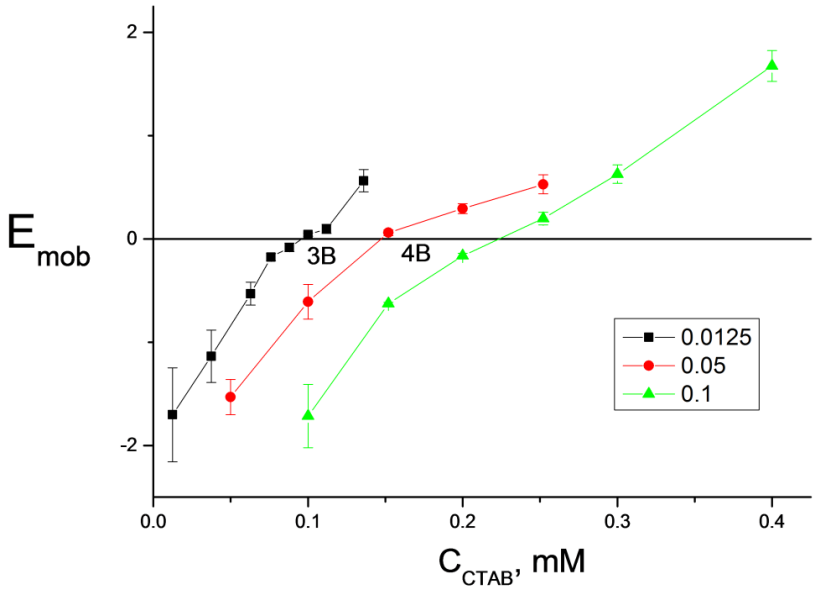

Figure IV.26: E_{mob} – f(C_{CTAB}) titration curves for the determination of exact concentration of AAc (-) in pNIPAm-g-pAAc solutions.

The data extracted from the titration curves shown in **Figure IV.26** are as follows:

$C_0(0.0125) = 0.096$ mM

$C_0(0.05) = 0.148$ mM

$C_0(0.1) = 0.223$ mM

1. $C_0(0.05) - C_0(0.0125) = 0.052$ mM = 3B → $B_1 = 0.052/3 = 0.017$ mM

2. $C_0(0.1) - C_0(0.05) = 0.076$ = 4B → $B_2 = 0.076/4 = 0.019$

Hence, $\mathbf{B_{average} = 0.018\ mM}$.

CryoTEM: Cryo-TEM experiments were performed in the Pierre and Marie Curie University (UPMC) with a kind assistance by Jean-Michel Guigner. The images were recorded on an Ultrascan 2k CCD camera (Gatan, U.S.), using a LaB6 JEOL JEM 2100 (JEOL, Japan) cryomicroscope operating at 200 kV with a JEOL low dose system (Minimum Dose System, MDS) to protect the thin ice film from any irradiation before imaging and to reduce the irradiation during the image capture. The images were recorded at 93K. The samples were prepared as follows. A drop of the microgel complexes solution at pH 2 was deposited on a Quantifoil grid

(Micro Tools GmbH, Germany). The grids were previously treated by glow-discharge in the presence of argon to increase their surface hydrophilicity. The excess of solution was then blotted out with a filter paper, and before evaporation the grid was quench-frozen in liquid ethane to form a thin vitreous ice film. The grid was mounted in a Gatan 626 cryo-holder cooled with liquid nitrogen and transferred in the microscope.

Ultracentrifugation: An ultracentrifuge from Beckman Coulter (Optima Max-XP, type TLA 110 rotor) was used to separate the microgel particles from the liquid phase. The centrifugations were performed at a relative centrifugal force (RCF) 62 400 × *g* for at least 10h, while heating the solutions to 40°C.

Total Carbon measurements: TC measurements were performed on a Shimadzu TOC-L CSN instrument. A potassium hydrogen phthalate solution in ultrapure water (2.125 $g \cdot dm^{-3}$ corresponding to 1000 $mgC \cdot dm^{-3}$) was used to establish a calibration curve in the 10−200 $mgC \cdot dm^{-3}$ range. The samples under investigation were transferred inside TC combustion tubes filled with platinum catalyst at 680°C in oxygen-rich atmosphere. The CO_2 generated due to the total combustion of the samples (required sample V = 8 mL) was then measured using an integrated NDIR gas analyzer and compared with the calibration curve to determine the TC concentration.

Supramolecular hydrogel preparation: *1. Vacuum concentration pathway:* Aqueous dispersions of colloidally stable pNIPAm/*β*CD1.62N (C(AAc-) = 6 mM, +/- = 0.8-2.0) or pNIPAm/*β*CD3.24N (C(AAc-) = 6 mM, +/- = 2.0) coated microgels were mixed with aqueous solutions of DT110Ada (Ada/CD = 1.3) or DT500Ada (Ada/CD = 1.0) respectively at pH 7 and room temperature. The obtained mixtures were then concentrated to the required weight concentrations for gelation under vacuum at 55°C. Transition from turbid liquids to transparent gels occurred upon cooling the concentrated samples back to 25°C.

1. Freeze-drying pathway: Stable solution of pNIPAm/*β*CD3.24N microgels (C(AAc-) = 3 mM, C(+) = 6 mM) was freeze-dried and a hydrogel (*FR1*, 10.9 wt%) was obtained by rehydrating the freeze-dried sample (70 mg) with 1.30 mL of DT500Ada2 guest polymer water solution (C(Ada) = 20mM, Ada/CD = 1.0) for 24h at room temperature.

Rheological measurements: Rheological characterization of the hydrogels was performed with a DHR-2 Rheometer (TA Instruments), equipped with a 1° cone geometry of 40 mm diameter. An insulated ring was placed around the geometry to prevent water evaporation. The hydrogel samples under investigation (V= 400-500 μm) were placed between the geometry and the Peltier plate with a spatula or with a pipette (in the case of weak gels or viscous liquids). Oscillatory frequency sweep measurements at 20 °C and 0.1% strain were performed in order to evaluate basic rheological characteristics of the samples such as storage G' and loss G" moduli cross-over frequency, f_{co}[Hz]. Covered frequencies vary in the range from 0.01 to 100 Hz. Limits of linear viscoelasticity regime were studied by strain amplitude sweep experiments with the strain amplitudes varying from 0.001 to 1000% (f= 10 Hz). Temperature sweep experiments from 25 to 62°C were performed at a heating rate of 2°C/min (f= 10 Hz, γ= 0.1%). In heating-cooling cycles experiment (*G3* sample) G' and G" were monitored as a function of time at two alternately changing temperatures, 25 and 50°C, for 10 min (f= 10 Hz, γ= 0.1%). The switch between two temperatures was set to happen in a rapid way (~ 15 seconds).

References

1. Islam, M. R.; Serpe, M. J. Penetration of polyelectrolytes into charged poly (N-isopropylacrylamide) microgel layers confined between two surfaces. *Macromolecules* **2013,** *46* (4), 1599-1606.
2. Acciaro, R.; Gilanyi, T.; Varga, I. Preparation of Monodisperse Poly(N-isopropylacrylamide) Microgel Particles with Homogenous Cross-Link Density Distribution. *Langmuir* **2011,** *27* (12), 7917-7925.
3. Pelton, R. Temperature-sensitive aqueous microgels. *Adv. Colloid Interface Sci.* **2000,** *85* (1), 1-33.
4. Destribats, M.; Eyharts, M.; Lapeyre, V.; Sellier, E.; Varga, I.; Ravaine, V.; Schmitt, V. Impact of pNIPAM microgel size on its ability to stabilize Pickering emulsions. *Langmuir* **2014,** *30* (7), 1768-1777.
5. Nayak, S.; Lee, H.; Chmielewski, J.; Lyon, L. A. Folate-mediated cell targeting and cytotoxicity using thermoresponsive microgels. *J. Am. Chem. Soc.* **2004,** *126* (33), 10258-10259.
6. Jones, C. D.; Lyon, L. A. Synthesis and characterization of multiresponsive core-shell microgels. *Macromolecules* **2000,** *33* (22), 8301-8306.
7. Owens, D. E.; Peppas, N. A. Opsonization, biodistribution, and pharmacokinetics of polymeric nanoparticles. *Int. J. Pharm.* **2006,** *307* (1), 93-102.
8. El Fagui, A.; Amiel, C. PLA nanoparticles coated with a β-cyclodextrin polymer shell: preparation, characterization and release kinetics of a hydrophobic compound. *Int. J. Pharm.* **2012,** *436* (1), 644-651.
9. El Fagui, A.; Dalmas, F.; Lorthioir, C.; Wintgens, V.; Volet, G.; Amiel, C. Well-defined core-shell nanoparticles containing cyclodextrin in the shell: A comprehensive study. *Polymer* **2011,** *52* (17), 3752-3761.
10. Agostoni, V.; Horcajada, P.; Noiray, M.; Malanga, M.; Aykaç, A.; Jicsinszky, L.; Vargas-Berenguel, A.; Semiramoth, N.; Daoud-Mahammed, S.; Nicolas, V. A “green” strategy to construct non-covalent, stable and bioactive coatings on porous MOF nanoparticles. *Scientific reports* **2015,** *5*.
11. Davis, M. E. The first targeted delivery of siRNA in humans via a self-assembling, cyclodextrin polymer-based nanoparticle: from concept to clinic. *Mol. Pharm.* **2009,** *6* (3), 659-668.
12. Davis, M. E.; Zuckerman, J. E.; Choi, C. H. J.; Seligson, D.; Tolcher, A.; Alabi, C. A.; Yen, Y.; Heidel, J. D.; Ribas, A. Evidence of RNAi in humans from systemically administered siRNA via targeted nanoparticles. *Nature* **2010,** *464* (7291), 1067-1070.
13. Wintgens, V.; Layre, A. M.; Hourdet, D.; Amiel, C. Cyclodextrin Polymer Nanoassemblies: Strategies for Stability Improvement. *Biomacromolecules* **2012,** *13* (2), 528-534.
14. Gref, R.; Minamitake, Y.; Peracchia, M. T.; Trubetskoy, V.; Torchilin, V.; Langer, R. Biodegradable long-circulating polymeric nanospheres. *Science* **1994,** *263* (5153), 1600-1603.
15. Devadasu, V. R.; Bhardwaj, V.; Kumar, M. R. Can controversial nanotechnology promise drug delivery? *Chem. Rev.* **2012,** *113* (3), 1686-1735.
16. Lee, K. Y.; Mooney, D. J. Hydrogels for tissue engineering. *Chem. Rev.* **2001,** *101* (7), 1869-1880.
17. Balakrishnan, B.; Banerjee, R. Biopolymer-based hydrogels for cartilage tissue engineering. *Chem. Rev.* **2011,** *111* (8), 4453-4474.

18. Tan, S.; Ladewig, K.; Fu, Q.; Blencowe, A.; Qiao, G. G. Cyclodextrin-Based Supramolecular Assemblies and Hydrogels: Recent Advances and Future Perspectives. *Macromol. Rapid Commun.* **2014,** *35* (13), 1166-1184.
19. Hoare, T. R.; Kohane, D. S. Hydrogels in drug delivery: progress and challenges. *Polymer* **2008,** *49* (8), 1993-2007.
20. Liu, J.; Chen, G.; Guo, M.; Jiang, M. Dual stimuli-responsive supramolecular hydrogel based on hybrid inclusion complex (HIC). *Macromolecules* **2010,** *43* (19), 8086-8093.
21. Deng, W.; Yamaguchi, H.; Takashima, Y.; Harada, A. A Chemical-Responsive Supramolecular Hydrogel from Modified Cyclodextrins. *Angew. Chem.* **2007,** *119* (27), 5236-5239.
22. Himmelein, S.; Lewe, V.; Stuart, M. C.; Ravoo, B. J. A carbohydrate-based hydrogel containing vesicles as responsive non-covalent cross-linkers. *Chem. Sci.* **2014,** *5* (3), 1054-1058.
23. Richtering, W.; Saunders, B. R. Gel architectures and their complexity. *Soft Matter* **2014,** *10* (21), 3695-3702.
24. Chen, P. C.; Kohane, D. S.; Park, Y. J.; Bartlett, R. H.; Langer, R.; Yang, V. C. Injectable microparticle–gel system for prolonged and localized lidocaine release. II. In vivo anesthetic effects. *Journal of Biomedical Materials Research Part A* **2004,** *70* (3), 459-466.
25. Lynch, I.; de Gregorio, P.; Dawson, K. Simultaneous release of hydrophobic and cationic solutes from thin-film "plum-pudding" gels: a multifunctional platform for surface drug delivery? *The Journal of Physical Chemistry B* **2005,** *109* (13), 6257-6261.
26. Sivakumaran, D.; Maitland, D.; Oszustowicz, T.; Hoare, T. Tuning drug release from smart microgel–hydrogel composites via cross-linking. *J. Colloid Interface Sci.* **2013,** *392*, 422-430.
27. Bencherif, S. A.; Siegwart, D. J.; Srinivasan, A.; Horkay, F.; Hollinger, J. O.; Washburn, N. R.; Matyjaszewski, K. Nanostructured hybrid hydrogels prepared by a combination of atom transfer radical polymerization and free radical polymerization. *Biomaterials* **2009,** *30* (29), 5270-5278.
28. Jha, A. K.; Malik, M. S.; Farach-Carson, M. C.; Duncan, R. L.; Jia, X. Hierarchically structured, hyaluronic acid-based hydrogel matrices via the covalent integration of microgels into macroscopic networks. *Soft Matter* **2010,** *6* (20), 5045-5055.
29. Jia, X.; Yeo, Y.; Clifton, R. J.; Jiao, T.; Kohane, D. S.; Kobler, J. B.; Zeitels, S. M.; Langer, R. Hyaluronic acid-based microgels and microgel networks for vocal fold regeneration. *Biomacromolecules* **2006,** *7* (12), 3336-3344.
30. Meid, J.; Dierkes, F.; Cui, J.; Messing, R.; Crosby, A. J.; Schmidt, A.; Richtering, W. Mechanical properties of temperature sensitive microgel/polyacrylamide composite hydrogels—from soft to hard fillers. *Soft Matter* **2012,** *8* (15), 4254-4263.
31. Hu, Z.; Lu, X.; Gao, J.; Wang, C. Polymer gel nanoparticle networks. *Adv. Mater.* **2000,** *12* (16), 1173-1176.
32. Liu, R.; Milani, A. H.; Freemont, T. J.; Saunders, B. R. Doubly crosslinked pH-responsive microgels prepared by particle inter-penetration: swelling and mechanical properties. *Soft Matter* **2011,** *7* (10), 4696-4704.
33. Milani, A. H.; Freemont, A. J.; Hoyland, J. A.; Adlam, D. J.; Saunders, B. R. Injectable doubly cross-linked microgels for improving the mechanical properties of degenerated intervertebral discs. *Biomacromolecules* **2012,** *13* (9), 2793-2801.
34. Liao, X.; Chen, G.; Liu, X.; Chen, W.; Chen, F.; Jiang, M. Photoresponsive pseudopolyrotaxane hydrogels based on competition of host–guest interactions. *Angew. Chem.* **2010,** *122* (26), 4511-4515.

35. Crassous, J. J.; Rochette, C. N.; Wittemann, A.; Schrinner, M.; Ballauff, M.; Drechsler, M. Quantitative analysis of polymer colloids by cryo-transmission electron microscopy. *Langmuir* **2009,** *25* (14), 7862-7871.
36. Crassous, J. J.; Wittemann, A.; Siebenbürger, M.; Schrinner, M.; Drechsler, M.; Ballauff, M. Direct imaging of temperature-sensitive core-shell latexes by cryogenic transmission electron microscopy. *Colloid. Polym. Sci.* **2008,** *286* (6-7), 805-812.
37. Antoniuk, I.; Wintgens, V.; Volet, G.; Nielsen, T. T.; Amiel, C. Bifunctionalized dextrans for surface PEGylation via multivalent host–guest interactions. *Carbohydr. Polym.* **2015,** *133*, 473-481.
38. De Gennes, P. Polymers at an interface; a simplified view. *Adv. Colloid Interface Sci.* **1987,** *27* (3-4), 189-209.
39. Steinmetz, N. F.; Manchester, M. PEGylated viral nanoparticles for biomedicine: the impact of PEG chain length on VNP cell interactions in vitro and ex vivo. *Biomacromolecules* **2009,** *10* (4), 784-792.
40. Liu, R.; Fraylich, M.; Saunders, B. R. Thermoresponsive copolymers: from fundamental studies to applications. *Colloid. Polym. Sci.* **2009,** *287* (6), 627-643.
41. Senff, H.; Richtering, W. Influence of cross-link density on rheological properties of temperature-sensitive microgel suspensions. *Colloid. Polym. Sci.* **2000,** *278* (9), 830-840.
42. Senff, H.; Richtering, W. Temperature sensitive microgel suspensions: Colloidal phase behavior and rheology of soft spheres. *The Journal of chemical physics* **1999,** *111* (4), 1705-1711.
43. Charbonneau, C.; Chassenieux, C.; Colombani, O.; Nicolai, T. Controlling the dynamics of self-assembled triblock copolymer networks via the pH. *Macromolecules* **2011,** *44* (11), 4487-4495.
44. Charlot, A.; Auzely-Velty, R.; Rinaudo, M. Specific interactions in model charged polysaccharide systems. *J. Phys. Chem. B* **2003,** *107* (32), 8248-8254.
45. Wintgens, V.; Daoud-Mahammed, S.; Gref, R.; Bouteiller, L.; Amiel, C. Aqueous polysaccharide associations mediated by β-cyclodextrin polymers. *Biomacromolecules* **2008,** *9* (5), 1434-1442.
46. Li, L.; Guo, X.; Wang, J.; Liu, P.; Prud'homme, R. K.; May, B. L.; Lincoln, S. F. Polymer networks assembled by host− guest inclusion between adamantyl and β-cyclodextrin substituents on poly (acrylic acid) in aqueous solution. *Macromolecules* **2008,** *41* (22), 8677-8681.
47. van de Manakker, F.; Vermonden, T.; el Morabit, N.; van Nostrum, C. F.; Hennink, W. E. Rheological behavior of self-assembling PEG-β-cyclodextrin/PEG-cholesterol hydrogels. *Langmuir* **2008,** *24* (21), 12559-12567.
48. Zhao, Y.; Cao, Y.; Yang, Y.; Wu, C. Rheological study of the sol-gel transition of hybrid gels. *Macromolecules* **2003,** *36* (3), 855-859.
49. Cates, M. Reptation of living polymers: dynamics of entangled polymers in the presence of reversible chain-scission reactions. *Macromolecules* **1987,** *20* (9), 2289-2296.
50. Vermonden, T.; van Steenbergen, M. J.; Besseling, N. A.; Marcelis, A. T.; Hennink, W. E.; Sudhölter, E. J.; Cohen Stuart, M. A. Linear rheology of water-soluble reversible neodymium (III) coordination polymers. *J. Am. Chem. Soc.* **2004,** *126* (48), 15802-15808.
51. Atkins, P.; De Paula, J. *Elements of physical chemistry*; Oxford University Press, USA2013.
52. Sandier, A.; Brown, W.; Mays, H.; Amiel, C. Interaction between an adamantane end-capped poly (ethylene oxide) and a β-cyclodextrin polymer. *Langmuir* **2000,** *16* (4), 1634-1642.

53. Blomberg, E.; Kumpulainen, A.; David, C.; Amiel, C. Polymer bilayer formation due to specific interactions between beta-cyclodextrin and adamantane: A surface force study. *Langmuir* **2004,** *20* (24), 10449-10454.
54. Renard, E.; Deratani, A.; Volet, G.; Sebille, B. Preparation and characterization of water soluble high molecular weight beta-cyclodextrin-epichlorohydrin polymers. *Eur. Polym. J.* **1997,** *33* (1), 49-57.

General conclusions and perspectives

The goal of this PhD project was to elaborate new polysaccharide-based host (β-cyclodextrin modified) and guest (adamantyl modified) polymer architectures with improved binding characteristics, as well as to integrate such polymers as structural elements of complex hierarchical systems with stimuli-responsiveness properties, e.g. sterically stabilized pNIPAm-based microgels and supramolecular hydrogels composed of pNIPAm-based microgels interconnected *via* host-guest interactions. In view of their potential biomedical applications, the presence of β-cyclodextrin (βCD)-polymers in such systems was aimed to endow them with bioavailability, reversibility and controlled kinetics of drug release.

First, host and guest dextrans with hydrophilic poly(ethylene glycol) (PEG) spacers were prepared using a combination of "click" chemistry synthetic tools, i.e. nucleophile-mediated thiol-ene Michael addition and copper(I)-catalyzed azide-alkyne cycloaddition (CuAAC). They are composed of either βCD (DT40-gPEG-βCD) or adamantyl groups (DT40-gPEG-Ada) linked to the dextran backbone by the means of short ($M_w \sim 360$ g·mole^{-1}) PEG spacer. The polymers were characterized by NMR, light scattering techniques and SAXS. Modelling of the SAXS data revealed that while DT40-gPEG-Ada shows a comb-like structure in water solutions, its host counterpart DT40-gPEG-βCD has a star-like structure composed of at least 4 comb-like branches. The latter was interpreted as an indication that cross-linking of the alkyne-modified dextran scaffolds takes place during the CuAAC stage of the synthesis. It can be related to the fact that alkynes in DT40-g-PEG-hex-5-ynoate precursor of DT40-gPEG-βCD are located at the ends of flexible PEG chains and thus are more likely to approach each other and undergo acetylenic cross-coupling.

The binding properties of the polymers in solution and on solid surface were studied by ITC and SPR respectively and compared to those of previously reported βCD- and Ada-substituted dextrans with short hydrophobic spacers. The presence of flexible PEG spacer proved to enhance the availability of Ada groups in DT40-gPEG-Ada, which resulted in a 5-fold increase of its affinity constant (K_a) to monomeric βCD in solution and improved adsorption on the surficial pβCD layers. However, the presence of PEG spacer proved to be less beneficial in the case of

host polymers, where DT40-gPEG-βCD showed in average 4 times lower K_a than those of the host polymer with a sort hydrophobic spacer (DT70GPβCD).

In the next step we used a combination of SAXS and light scattering to study the host-guest driven formation of the nanoassemblies between the aforementioned polymers with various architectures. Such nanoassemblies were formed spontaneously upon mixing the host and guest polymer aqueous solutions at βCD/Ada =1 molar ratio. The nature of individual polymers was found to have a significant influence on the size and internal organization of the nanoassemblies. In general, particles containing DT40-gPEG-βCD are smaller and have less compact structure than those containing DT70GPβCD. The same effect, though to a lesser extent, was observed for the particles composed of DT40-gPEG-Ada as a guest polymer. The obtained results contribute to design of host-guest polymers with improved properties, i.e. polymers capable of self-assembling into more stable, biodegradable nanoparticles with more attractive drug delivery profiles.

In the second part of this work, a series of new (PEG, Ada)-grafted dextrans (denoted as D40-GP-Ada-PEG) were prepared by CuAAC click reaction, using alkyne modified dextrans and azide derivatives of adamantane and 5000 g·mole^{-1} PEG. The degree of substitution (DS) by PEG grafts was kept similar (18-23 mol.%) while the level of substitution by hydrophobic Ada groups was varied from 0 to 10 mol.%. It was shown that due to the relatively long triazole-ether spacer between the Ada-groups and dextran backbone, D40-GP-Ada-PEG have higher K_a with monomeric βCD in solution as compared to previously described Ada-modified dextrans and pNIPAm with Ada-groups rigidly attached to the polymers through short ester and amide bonds respectively.

Furthermore, in the case of interaction with neutral or positively charged βCD-polymers, both in solution and on the surface, the interpolymer affinity proved to be strongly dependent on the DS(Ada), i.e. the K_a for more densely substituted D40-28GP-10Ada-18PEG (10 mol.% Ada) is one order of magnitude higher than that for D40-28GP-5Ada-23PEG (5 mol.% Ada). Such non-linear increase in K_a is an indication of strong cooperativity effects between the Ada-groups in synthesized polymers. Given the above, (PEG, Ada)-grafted dextrans should be auspicious candidates for applications, where fast and reversible PEGylation of surfaces or nanoparticulate carriers is required.

In the last park of the presented work our goal was to develop an approach to the synthesis and non-covalent sterical stabilization of poly(*N*-isopropylacrylamide)-g-100%poly(acrylic acid) (pNIPAm-g-pAAc) core-shell microgels coated with positively charged β-cyclodextrin polymer (denoted as pNIPAm/βCDN). Furthermore, we showed that pNIPAm/βCDN can be used as building blocks of thermo-reversible hierarchical hydrogels non-covalently crosslinked *via* host-guest interactions.

First, we used electrostatic self-assembly to attach the β-cyclodextrin polymer bearing quaternary ammonia groups (pβCDN+) to the surface of negatively charged at pH 7 microgels. This approach provided an easy way to control the degree of coating and the overall charge of the resulting pNIPAm/βCDN complexes by simply adjusting the +/- molar ratio during the mixing stage, while the βCD content in the shell at a fixed +/- ratio can be varied by using pβCDN+ with different quaternary ammonia N+ substitution levels. The pNIPAm/βCDN aqueous suspensions proved colloidally stable when positively overcharged with pβCDN+ but aggregated at neutral overall charge, which would be a serious limitation for any potential biomedical use. This problem could be solved by exploiting the host-guest chemistry of pβCDN+. Neutral pNIPAm/βCDN were sterically stabilized through a simple 2-step procedure involving: 1) preparation of supramolecular precursor between pβCDN+ and D40-GP-Ada-PEG described above; 2) electrostatic self-assembly of the precursor with pNIPAm-g-pAAc yielding pNIPAm/βCDN/PEG hierarchical microgels. Both positively overcharged pNIPAm/βCDN and neutral pNIPAm/βCDN/PEG microgels show a full preservation of temperature-induced volume-phase transition (VPT) of the pNIPAm core.

We also elaborated hierarchically structured hydrogels based on positively overcharged pNIPAm/βCDN by non-covalently crosslinking them with Ada-modified dextrans (DT-Ada). Rheological measurements and calculations of the effective volume fraction ϕ_{ef} of the microgels in such hydrogels (at 10-11 wt%) suggest that the individual microgels are at a close contact, thus making their architecture similar to that of so-called doubly-crosslinked microgels (DX microgels). To the best of our knowledge, this is the first example of DX microgels non-covalently crosslinked *via* host-guest interactions. Furthermore, the hydrogels exhibit fully reversible temperature-induced gel-sol transition due to the synergetic effect between shrinking of the microgels and dissociation of βCD-Ada crosslinks at higher temperatures. Due to

the presence of microgels the gel-sol transition temperature of pNIPAm/pβCDN/DT-Ada is significantly shifted down to the physiological temperature range (37-41°C) as compared to uniform pβCDN/DT-Ada host-guest hydrogels (51°C).

The obtained results may be extended over a multitude of promising directions.

With regard to the first part our work, the DT40-gPEG-βCD synthesis procedure needs to be optimized in order to avoid the alkyne crosslinking issues at the CuAAC stage. It would also be interesting to replace the PEG spacer with a one responsive to external stimuli, e.g. pNIPAm. It would allow temperature-triggered assembly and dissociation of the resulting host-guest nanoparticles. In collaboration with colleagues from Bristol University (Kathrin Lange, Wuge Briscoe) we began the study of the surface properties of the host-guest nanoassemblies, and the initial surface-force apparatus (SFA) and atomic force microscopy (AFM) results show their high potential as lubrication agents. Finally, we plan to study the entrapment and release of model hydrophobic drugs into the nanoassemblies prepared from the DT40-gPEG-βCD and DT40-gPEG-Ada.

Besides the sterical stabilization of pβCDN+ - coated thermoresponsive microgels, (PEG, Ada)-grafted dextrans described in Chapter 3 of this manuscript can find a number of interesting applications. Namely, we envisage using D40-GP-Ada-PEG for the PEGylation of hydrophilic drug loaded metal-organic framework (MOF) nanoparticles coated with phosphated βCD. In this case the bulkiness and superior binding properties of D40-GP-Ada-PEG would allow outperforming simple Ada-substituted linear PEGs which tend to penetrate into the crystalline structure of nano-MOF and hamper their drug-loading capacity.

There is a high potential to go towards the usage of hierarchical pNIPAm/βCDN/PEG microgels as thermoresponsive smart drug delivery vectors. The presence of the host polymer external shell and PEG corona in their structure are expected to provide better control over the loaded drugs release kinetics and to address the issue of pNIPAm low biocompatibility respectively.

Last but not least, the pNIPAm/pβCDN/DT-Ada hierarchical hydrogels might be used as a medium for the differentiation of pluripotent stem cells. Indeed, after completion of the

differentiation process the differentiated cells would be collected by increasing the temperature to 37-41°C and inducing the gel-sol transition of the network. However, such applications would require some modifications in the design of the system. First of all, as it was shown by total carbon (TC) measurements the N+ -overcharged pNIPAm/pβCDN contain significant amounts of non-bound pβCDN+. Polymeric materials containing permanent positive charges are known to be less biocompatible than their neutral or negatively charged analogues. Given this we envisage replacing pβCDN+ coating with the one based on neutral βCDs as a future extension of this work. This might be achieved by copolymerizing NIPAm with NH_2 - or alkyne-containing monomers in the external shell. The latter would allow modifying the surface of the microgels with either βCD tosylate (βCD-OTs) βCD azide (βCD-N_3) derivatives using nucleophilic substitutions or CuAAC reactions respectively. Hierarchical hydrogels built of such βCD-grafted microgels are expected to be less toxic and less sensible to variations of pH and ionic force in the cell culture media.

Abstract

This PhD work is based on the development of new architectures of polysaccharide-based host and guest polymers and their application in the design of hierarchically structured soft nanoparticles and supramolecular hydrogels with interesting drug delivery profiles. In the first section of the manuscript we describe a synthetic pathway to host and guest polymers with hydrophilic poly(ethylene glycol) PEG spacer between the dextran backbone and either β-cyclodextrin (βCD) host or adamantane (Ada) guest grafted groups. The presence of the PEG spacer led to a substantial improvement of the availability of Ada groups of the guest polymer as compared to its counterpart, where Ada are linked to the backbone with a short hydrophobic spacer. This was followed by the study of nanoassemblies formation between the different types of host and guest polymers. Once again, PEG spacer had a significant impact on the size and internal structure of the resulting nanoassemblies. The second part of this work describes synthesis of a series of new (PEG, Ada)-grafted dextrans prepared by copper(I)-catalyzed azide-alkyne cycloaddition (CuAAC). The degrees of substitution (DS) by PEG grafts (5000 g/mole) are close to 20 mol% while the DS by Ada-groups are varied from 0 to 10 mol.%. The affinity of these polymers to monomeric βCD, as well as their ability to form superficial layers with β-cyclodextrin polymers (pβCD, pβCDN+), are strongly dependent on the DS by Ada, giving an indication of cooperativity effects between them. In the last part we described a strategy to a non-covalent modification of thermoresponsive poly(*N*-isopropylacrylamide) (pNIPAm)-based microgels with a pβCDN+ host polymer shell. It uses on electrostatic self-assembly between pβCDN+ and negatively charged poly(acrylic acid) (pAAc) chains grafted to the surface of microgels. The resulting pNIPAm/βCDN microgels with neutral overall charge could be colloidally stabilized with (PEG, Ada)-grafted dextrans *via* a hierarchical self-assembly procedure. Finally, using Ada-modified dextrans (DT-Ada), pNIPAm/βCDN microgels could be physically cross-linked to yield hierarchical 3D hydrogels (at 10 wt%). Their gel-sol transition temperature is shifted down to the physiological temperature range (37-41°C) as compared to uniform pβCDN/DT-Ada host-guest hydrogels (51°C).

Keywords: soft matter, host-guest interactions, cyclodextrins, hierarchical self-assembly

Résumé

Ce travail de thèse concerne le développement de nouvelles architectures de polymères hôte et invité à base de polysaccharide et leur application dans la conception de nanoparticules molles à structure hiérarchique et d'hydrogels supramoléculaires pour l'encapsulation et la libération de médicaments. Dans la première partie du manuscrit, nous décrivons une voie de synthèse de polymères hôtes et invités comprenant des chaînons espaceurs poly(éthylène glycol) hydrophile (PEG) entre le squelette de dextrane et soit le groupement β-cyclodextrine (βCD)(polymère hôte) ou le groupement adamantane (Ada) (polymère invité). La présence des bras espaceurs PEG a conduit à une amélioration substantielle de la disponibilité des groupes Ada du polymère invité par rapport à la situation avec un bras espaceur court et hydrophobe. Nous avons ensuite étudié la formation de nanoassemblages entre les différents types de polymères hôtes et invités. Une fois de plus, les espaceurs PEG ont eu un impact significatif sur la taille et la structure interne des nanoassemblages. La deuxième partie de ce travail décrit la synthèse d'une nouvelle série de dextranes greffés par des chaînons PEG et Ada, préparés par réactions de cycloaddition d'azoture-alcyne catalysées le cuivre (I) (CuAAC). Les degrés substitution (DS) en chaînons PEG greffés (5000 g/mole) sont de l'ordre de 20 mol.% tandis que les DS par les groupements Ada sont variés de 0 à 10 mol.%. L'affinité de ces polymères pour la βCD native, ainsi que leur capacité à former des couches superficielles avec des polymères de β-cyclodextrine (pβCD et pβCDN+), s'avérent dépendre fortement du DS en groupements Ada, ce qui résulte de la coopérativité des interactions impliquées. Dans la dernière partie, nous avons décrit une stratégie de modification non covalente de microgels sensibles à la temperature à base de poly (*N*- isopropylacrylamide) (pNIPAm), pour les recouvrir d'une couronne de pβCDN+. Cette stratégie s'appuie sur l'auto-assemblage électrostatique entre pβCDN+ et les chaînes de poly(acide acrylique) chargés négativement (pAAc) et greffées à la surface des microgels. Dans le cas d'une charge globalement neutre des microgels pNIPAm/βCDN, la stabilisation colloïdale a pu être réalisée à l'aide de dextranes greffés (PEG, Ada) en utilisant une procédure d'assemblage hiérarchique. Enfin, à l'aide de dextrane modifé par des groupements Ada (DT-Ada), les microgels pNIPAm/βCDN ont pu être associés pour produire des hydrogels 3D hiérarchiques (10wt %). Leur température de transition sol-gel est décalée vers le bas pour atteindre la gamme des températures physiologiques (37-41°C) par rapport à celle observée dans un hydrogel hôte-invité uniforme βCDN/DT-Ada (51°C).

Mots clés**:** matière molle, interactions hôte-invité, cyclodextrins, auto-assemblage hiérarchique